Anti-windup Synthesis using Riccati equations

Thesis Submitted for the degree of
Doctor of Philosophy
at the University of Leicester

by

Jorge Sofrony Esmeral
Department of Engineering
University of Leicester

September 2007

ProQuest LLC
789 East Eisenhower Parkway
P.O. Box 1346
Ann Arbor, MI 48106-1346

Abstract

This thesis studies the design and implementation of anti-windup compensators for systems with magnitude and rate-limited actuators; the thesis contains four main contributions. The first is the development of a new method for anti-windup compensator design, based on the solution of a single Riccati equation, for systems with magnitude saturated actuators. The second contribution shows how this new method can be adapted to systems with rate saturation. The third contribution describes the application of the anti-windup techniques developed to a complex experimental aircraft model in order to reduce the susceptibility to pilot-induced-osicalltions. The thesis culminates with a description and analysis of the implementation of these anti-windup compensators on a real aircraft and the subsequent flight tests. The flight test results clearly illustrate the advantages of employing anti-windup compensation in terms of improved handling qualities and reduced susceptibility pilot-induced-oscillations.

Acknowledgements

First of all I would like to thank Dr. Matthew Turner and Professor Ian Postlethwaite for their unconditional support; I could have not done most of the work here presented without them. Secondly, I would like to thank my wife Jennifer Mojica for being with me all this time and withstanding the sufferings of someone else's PhD. journey, and from where a lovely person sprouted, Martin Sofrony Mojica. Without him things would have been less time consuming but not quite as enjoyable. As usual, I would like to thank my mother and father for I am thanks to them. Finally, I would like to thank the DLR crew that allowed the ATTAS flight tests to be a reality. Within the people involved, special acknowledgements must be given to Oliver Brieger, Dirk Leiβling, Lt.Col. "Q" Rudinger and Lt.Col. Markus Ritter.

Jorge Sofrony

September 2007

Contents

Chapter 1

Anti-Windup: Overview

Most practical control design methodologies are concerned with the design of *linear* controllers for systems where the plant is normally assumed to be *linear* or approximately linear. Although the assumption of linearity is well-known to be a gross approximation, such controller design methodologies have found favour in both industry and academia due to their typical effectiveness and their transparency. In addition, the subject of linear systems theory which enables the design of such controllers is mature and a great deal of commercial software is available to assist. Unfortunately, in reality, there are some nonlinearities which are difficult to ignore completely. One such nonlinearity is the so-called "saturation " nonlinearity which models the fact that all actuators, which are often mechanical systems, have limits of some type. For example, in aircraft the control surface deflections are constrained to lie within a certain range; in motors, the supply current and voltage is limited; in industrial processes flow rate through valves cannot be less than zero. When these nonlinearities are introduced into control loops which are otherwise largely linear, the effects can be surprising, sometimes catastrophic and often unpredictable.

The main effect that input saturation (and input constraints in general) has on the closed-loop system is that the output of the controller differs from the input to the plant. In other words, the *desired* control signal differs from the actual signal delivered to the plant. When the control signal's magnitude is large enough as to be outside saturation limits, the effective gain of the system is lowered (in a nonlinear manner), reducing the influence of the controller

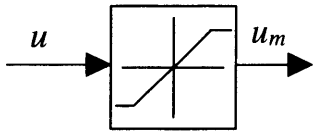

Figure 1.1: Block representation of the saturation function

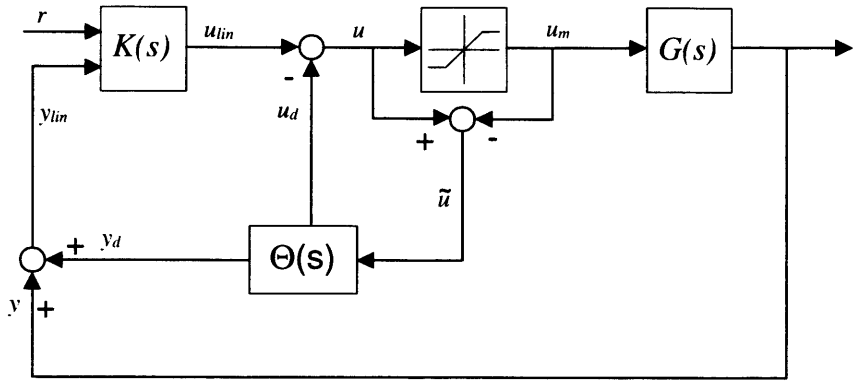

Figure 1.2: Generic Anti-Windup scheme

on the system and making the system appear "pseudo" open-loop. The undesirable effects of input saturation began to be studied in the context of proportional integral derivative (PID) control many years ago ([23, 58, 3, 5]) and, indeed, these studies led to the term "windup". Roughly speaking, the term "windup" was traditionally associated with the excessive values to which the integrator state of the PID controller could "windup" to, if the plant input was saturated. Control signal saturation would lead to a larger error signal which the integrator would keep integrating, leading to larger control signals, perhaps keeping the system "locked" in saturation. These large integrator states manifested themselves as large overshoots and long settling times as the integrator dissipated its "energy" into the system. Although now the term "windup" is taken to mean a general degradation in performance due to input saturation, the term originates from early experiences of practitioners of PID control.

Not surprisingly, attempts to alleviate these negative effects of saturation soon began ([3, 19, 40]), normally as *ad hoc* modifications to the controller. Following on from their association with PID windup, these saturation alleviation methods were termed "anti-windup" compensators. However, today, as with the term "windup", *anti-windup compensation* typically means a way of modifying a controller to account for actuator saturation. Anti-windup (AW), also known as *linear conditioning*, is now taken to mean the augmentation of (normally linear) controllers with (normally linear) elements to assist their behaviour during and immediately after saturation has occurred. The standard design procedure has two steps: first, a linear controller for the nominal system without saturation is designed. Then, AW compensation is implemented to help the system during saturation periods. The AW compensator is designed in such a way that it is active only when the system undergoes saturation, modifying its behaviour and helping it return to normal *linear* dynamics as soon as possible.

Figure 1.2 shows a fairly general representation of an anti-windup scheme (and one which

will be used throughout this thesis). Here $G(s)$ is the linear plant and $K(s)$ is the nominal controller. The input to the plant $u_m(t)$ may differ from the control signal $u(t)$ due to the saturation function. $\Theta(s)$ is the anti-windup compensator which becomes active during periods of saturation. In general terms, an AW compensator is a linear transfer function which is designed with the aim of improving the closed-loop performance (in some sense) during and immediately after saturation.

One of the main advantages of AW schemes is that nominal performance is not directly restricted by the conditioning method, giving full freedom in the design of the initial linear controller. This is one of the most attractive features of AW compensation, enabling an engineer to retain the properties of the baseline controller except during periods of saturation. It is important to note that AW conditioning is only intended as a precaution for systems that enter saturation occasionally and should not be implemented on systems that are outside the control constraints most of the time.

To illustrate the unpredictable effects of saturation consider the simple mass-spring-damper example used in [107, 26] amongst others. The nominal plant $G(s)$ is given by a two state single-input-single-output (SISO) system:

$$A = \begin{bmatrix} 0 & 1 \\ -10 & -10 \end{bmatrix}; B = \begin{bmatrix} 0 \\ 10 \end{bmatrix}; C = \begin{bmatrix} 1 & 0 \end{bmatrix}; D = \begin{bmatrix} 0 \end{bmatrix} \tag{1.1}$$

A two-degree-of-freedom (2-D.o.F.) linear controller is designed with some performance specifications in mind; good response time, negligible steady-state error and well damped dynamics of the closed-loop system. Such controller has the following structure.

$$K(s) = [K_1(s), K_2(s)] = \left[\begin{array}{c|cc} A_c & B_{cr} & B_c \\ \hline C_c & D_{cr} & D_c \end{array}\right] \tag{1.2}$$

where,

$$A_c = \begin{bmatrix} -80 & 0 & 2.5 \\ 1 & 0 & 0 \\ 0 & 0 & -2.5 \end{bmatrix} \quad B_{cr} = \begin{bmatrix} 0 \\ 0 \\ 1 \end{bmatrix} \quad B_c = \begin{bmatrix} -1 \\ 0 \\ 0 \end{bmatrix}$$
$$C_c = \begin{bmatrix} -9450 & 3375 & 33.75 \end{bmatrix} \quad D_{cr} = \begin{bmatrix} 0 \end{bmatrix} \quad D_{cr} = \begin{bmatrix} -135 \end{bmatrix} \tag{1.3}$$

In order to highlight the effects that actuator saturation has on the closed-loop system and the possible advantages of using AW conditioning schemes, the system is assumed to have input saturation constrains of ± 1. In the absence of saturation, that is when we consider the

saturation block in Figure 1.2 as the identity operator, the nominal linear closed-loop system has good robustness properties and well-damped time responses. To demonstrate the effectiveness of anti-windup compensation when saturation is present, full-order AW compensation, as proposed in [88, 107], is considered. The system is simulated for both the conditioned and the unconditioned nonlinear scenario and compared against the linear response. Notice from the top-left hand side of Figure 1.3 that the linear closed-loop system, i.e. no saturation present, has excellent time and frequency responses with satisfactory tracking properties. Unfortunately, the system's control effort exceeds the saturation constraints during the transient behaviour, meaning that performance degradation and stability issues *may* arise when these limits are imposed.

The plot for the saturated closed-loop system without AW is shown in the middle of Figure 1.3 (dotted line). The detrimental effects of saturation have been revealed with a clear phase shift between reference and response; although not catastrophic in this case, phase shifts of this sort have been associated with many aircraft related accidents (see Chapter 6 for more detail). Also notice how the controller output (control signal before saturation) has an excess of magnitude which will tend to keep the system locked in saturation for longer periods of time. The saturated closed-loop response with AW (bottom of Figure 1.3, solid line) shows how performance is partially recovered when using AW compensation; although the system still cannot track the magnitude of the reference (the demand is actually infeasible), the phase shift has been eliminated and better tracking properties result. Probably the most noticeable consequence of using AW compensation is the reduction of system saturation. Notice how the controller output tries to follow *linear dynamics*, reducing the effects of saturation, but most importantly, reducing system deviation from these linear dynamics.

The above example shows that even a well-designed linear control system can behave in an unforeseen (sometimes disastrous) manner due to saturation. In the case considered above, saturation only caused a mild loss in performance, but for less benign examples, internal stability of the closed-loop system may be severely compromised. It has been shown that a well-designed AW compensator can help the system retain stability and enhance performance despite the presence of saturation. Unfortunately, the design of AW compensators is not a trivial task and until the mid-1990's very little attention had been devoted to the systematic design of such compensation schemes. In fact, many of the early schemes (including popular ones such as the Hanus conditioning technique [40] and the high-gain AW [34] technique) do not explicitly account for closed-loop stability and their design is guided by intuitive, but rather vague, reasoning. Furthermore, their application is often restricted to simple single-loop

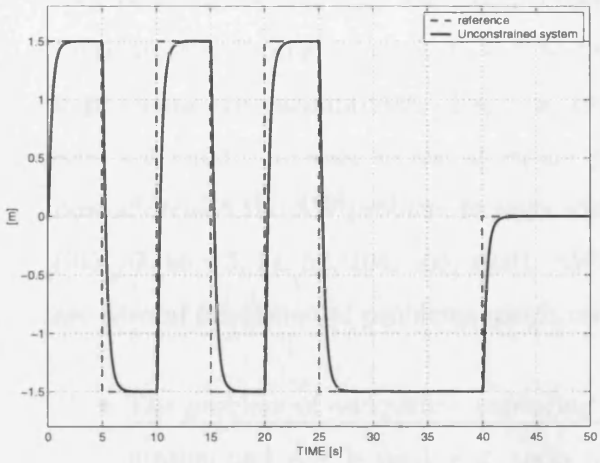

unconstrained output $y(t)$

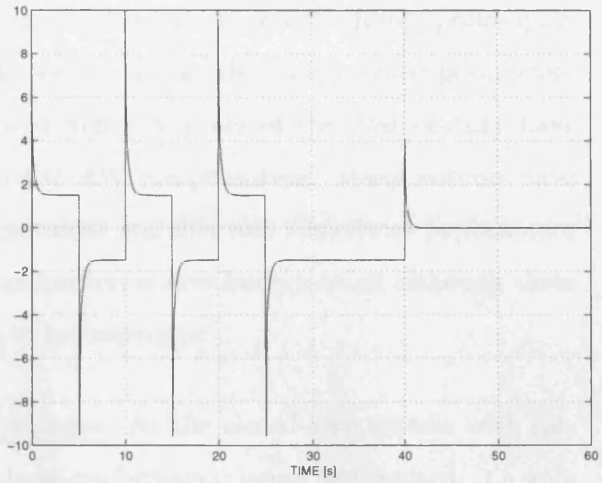

unconstrained control signal

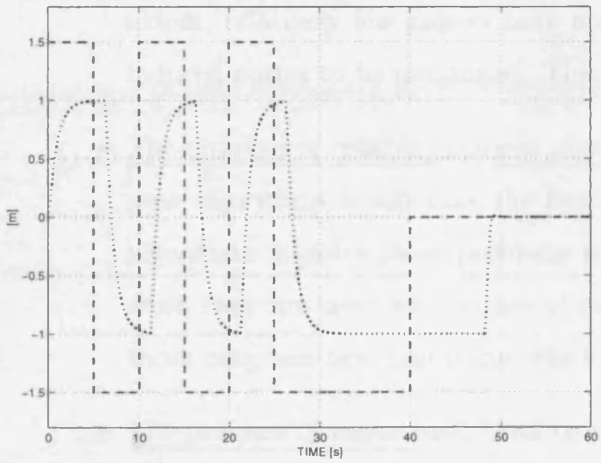

constrained output $y(t)$, no AW

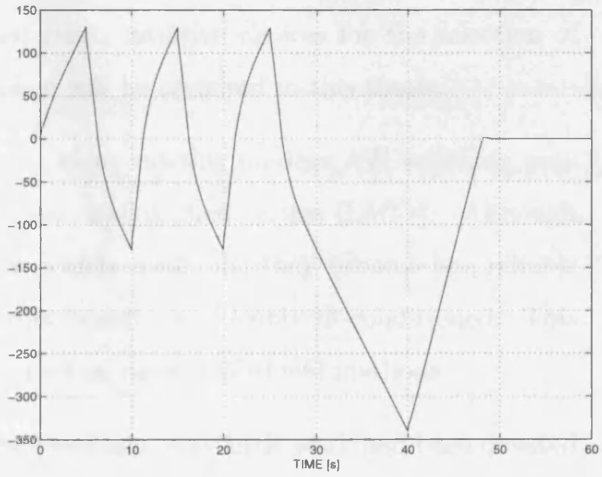

constrained control signal before saturation, no AW

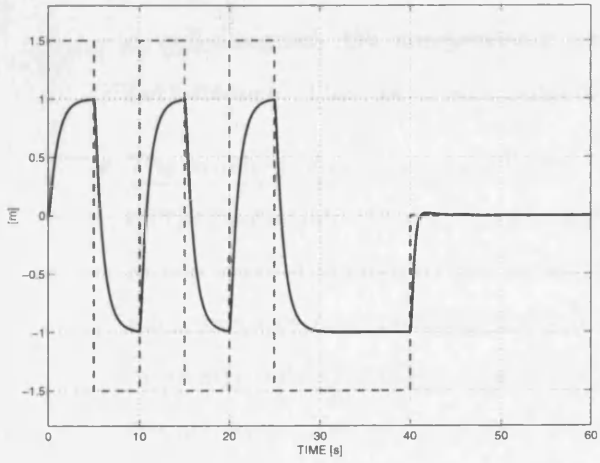

constrained output $y(t)$, AW

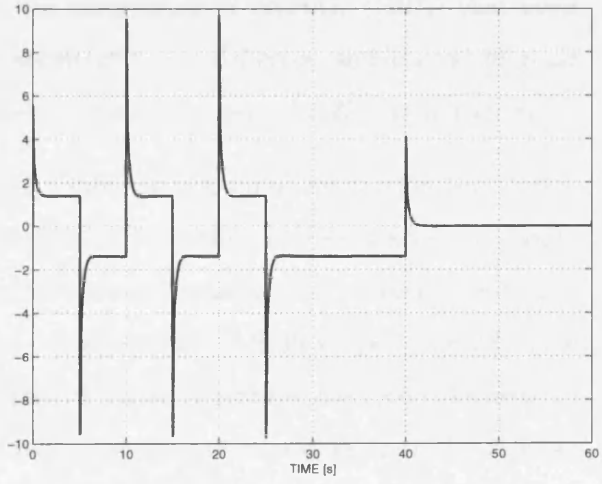

constrained control signal before saturation, AW

Figure 1.3: Mass-spring-damper Example: Closed-Loop System Response - reference (thick dashed)

control problems and they are characterised by an "if it works, it works" design philosophy; there are few tuning rules which enable the engineer to adjust the compensator parameters if problems are encountered. The late 1990's and first few years of the 21st century have seen a dramatic increase in the attention devoted to AW compensation. Many authors have now addressed the AW problem in ways which guarantee stability and sometimes performance ([65, 37, 66, 73, 21, 52, 104, 105, 103]). AW compensation is now fairly mature although there are several fundamental problems which remain to be overcome:

- The problem of adequately capturing performance. As the closed-loop system with saturation and AW is nonlinear, tools to address performance issues are limited. $\mathcal{L}_2$ gain approaches have dominated the literature and while these have been successful to some extent, relatively few papers have proposed clear, intuitive choices for the selection of induced norms to be minimised. This problem will be revisited in this thesis.

- The problem of reliable synthesis algorithms. Many existing modern AW solutions, propose algorithms which take the form of linear matrix inequalities (LMI's). Although algorithms to solve these problems are now widely available, they become less reliable when they are used with plants of high-order which are possibly ill-conditioned. This thesis proposes new algorithms which are based on more traditional methods.

- The problem of robustness. Until only a few years ago, very little work had been devoted to assessing the robustness of AW designs and very few algorithms were available for the synthesis of robust compensators. It was demonstrated recently ([107]) that even a well-designed AW compensator can be sensitive to model-error and can yield poor performance. This thesis will explicitly consider the robustness of AW compensators.

- The problem of actuator rate-limits. In many applications, input saturation (i.e. limits on the magnitude of the control signal) is less problematic than rate-saturation i.e. limits on the rate of change of the control signal). This is particularly important for highly manoeuvrable modern aircraft where several crashes (e.g. JAS 39 Gripen, YF-22) have been attributed to this phenomenon. Although some attention has been devoted to the actuator rate-limit problem, there are few intuitive, systematic, numerically reliable algorithms available which tackle this problem. This thesis will also make a contribution here.

Thus, while considerable advances have been achieved in the AW literature, many important problems remain to be addressed. This thesis will attempt to tackle some of them, solving and

describing different parts of the actuator constraint problem. Chapter 3 is a brief description of existing AW schemes, giving the reader more insight into the general problem formulation and its solution. The AW architecture used throughout and the closed-loop system are described, followed by a discussion on the *M conditioning scheme* and its resulting decoupled structure. This is later compared with *a* generic AW architecture in order to try and unify different existing design techniques using the M parametrisation.

Chapter 4 states some of the main theoretical results of this thesis and concentrates on position saturating actuators exclusively. It starts by describing in detail what may be termed the *Performance AW Problem* and by using the decoupled structure mentioned earlier, the problem is posed formally and solved using "simple" linear algebra arguments and manipulations. The chapter proceeds by describing the problem of *Robust AW Compensation* and the implications of having plant uncertainty. As before, the problem is posed and solved using similar arguments to those of the performance AW problem. In order to demonstrate the results obtained an academic example, that of a missile auto-pilot, is used to show the benefits of AW compensation in general and the advantages of the design schemes proposed here.

In Chapter 5 the problem of actuator rate-limiting is tackled by using AW conditioning. The general problem setup and AW architecture are described, obtaining a decoupled structure of an augmented system which consists of both the plant and the modeled rate-limit dynamics. This allows the use of AW techniques at the expense of having to solve a *local stability* problem. After a formal description of the *Rate-limit AW problem*, the solution yields an LQR-type equation as one of the sufficient conditions. As the interplay between free parameters is somewhat complicated, two tuning algorithms are proposed where a clear trade-off between region of stability and performance is portrayed. This is followed by an example and some conclusions.

During the research phase of this thesis, the University of Leicester (UoL) was part of the GARTEUR AG-15 group - an alliance of European industrial and academic institutions collaborating to address some of the issues associated with pilot-induced-oscillations. Certain types of these pilot-induced-oscillation events are associated with position and rate-limited actuators and there was a natural interest in methods, such as anti-windup compensation, which could be used to help prevent the occurrence of such phenomena. The GARTEUR collaboration provided an opportunity to test the techniques developed in Chapter 5 on a fly-by-wire aircraft. Chapter 6 thus consists of a description and a simulation analysis of the effects the pilot has on the closed-loop behaviour of the aircraft and the subsequent PIO's (pilot-induced-oscillations) that may develop when rate-limits are encountered. The chapter discusses the

OLOP (open-loop onset point) criterion, a tool often used in the prediction of PIO's and the selection of the modelled pilot gains. The main contribution made here is the application of the results of Chapter 5 to a realistic, high-order nonlinear model of a fly-by-wire aircraft and the analysis of the corresponding simulation results.

Chapter 7 describes the flight tests which were conducted following the simulation work described in Chapter 6. The chapter shows how the anti-windup compensators were adapted for in-flight testing and the flight test results are fully described - including AW design parameters, trim points, flight plan, pilot comments and flight-test data analysis. The highlight of this chapter, and probably this thesis, is the assessment of the AW compensation scheme proposed herein via pilot ratings and real flight data.

Chapter 2

Preliminaries

This chapter introduces several concepts which are needed and used throughout the remainder of the thesis. For the most part, the chapter serves as a short review of key definitions, notation and existing results in the control literature. It should be noted that the chapter is not intended to be a comprehensive account of signals and systems or feedback control theory; the references herein (particularly [88, 34]) should be consulted for more details.

2.1 Signals and systems

In this thesis, a signal is a function of time which maps the time variable "t" to a vector space. More specifically, $f(t)$ is taken as a map from the real half-line to the n-dimensional vector space, $\mathbb{R}^n$.

$$f(.) : [0, \infty) \mapsto \mathbb{R}^n \tag{2.1}$$

The *distance* between a vector $y(t)$ and a compact set $\mathcal{Y}$ is denoted by

$$\text{dist}(y, \mathcal{Y}) := \inf_{w \in \mathcal{Y}} \|y - w\| \tag{2.2}$$

where $\|.\|$ denotes the standard Euclidean norm

$$\|x\| = \sqrt{x'x} \tag{2.3}$$

and x' denotes the transpose of x.

For any vector x, the element-wise operator $x \succeq 0$ means that all the components x_i are non-negative. For two vectors x, $y \in \mathbb{R}^n$, $x \succeq y$ means that $x_i - y_i \geq 0, \forall i \in \{1, \ldots, n\}$. The set $\mathcal{S}(d, d_0) = \{d : -d_0 \preceq d \preceq d_0\}$ (it is a more compact way of defining a hypercuboid in the dimensions of d, see [32]) is defined as it will be useful in the local version of the AW compensation scheme.

The size of a signal is measured through an appropriate norm. The norms of interest in this thesis are the so-called $\mathcal{L}_p$ norms which, for a Lebesque measurable signal $x(t)$ and integers $p \in [1, \infty)$, are defined as

$$\|x\|_p = \left\{ \int_0^\infty \|x(t)\|^p dt \right\}^{\frac{1}{p}} \tag{2.4}$$

The space of signals for which the norm $\|x\|_p$ is finite is known as the $\mathcal{L}_p$ space . Alternatively, the space $\mathcal{L}_p$ can be defined as

$$\mathcal{L}_p = \{x \in \mathbb{R}^n : \quad \|x\|_p < \infty\} \tag{2.5}$$

The signal space $\mathcal{L}_2$ is of direct relevance to the results in Chapters 4 and 5, and is prevalent throughout optimal and robust control literature. It is defined as

$$\mathcal{L}_2 = \{x \in \mathbb{R}^n : \quad \|x\|_2 < \infty\} \tag{2.6}$$

where the $\mathcal{L}_2$ norm is given by

$$\|x\|_2 = \left\{ \int_0^\infty \|x(t)\|^2 dt \right\}^{\frac{1}{2}} \tag{2.7}$$

Interestingly the $\mathcal{L}_2$ norm has a frequency domain interpretation. Let $\hat{x}(j\omega)$ be the Fourier transform of $x(t)$ and let $\hat{x}^\star(j\omega)$ be its complex conjugate transpose, then the $\mathcal{L}_2$ norm, in the frequency domain, can be defined as

$$\|\hat{x}\|_2 = \frac{1}{2\pi} \left\{ \int_{-\infty}^\infty \hat{x}^\star(j\omega)\hat{x}(j\omega) d\omega \right\}^{\frac{1}{2}} \tag{2.8}$$

Due to Parseval's theorem (see for example [70, 8, 80]), it transpires that the $\mathcal{L}_2$ norm in the time and frequency domains are actually equal, viz

$$\|\hat{x}\|_2 = \|x\|_2$$

and thus we do not distinguish between the two. This fact is crucial for measuring the size of (linear) systems by an induced $\mathcal{L}_2$ norm.

A (possibly nonlinear) system, $\mathcal{G}$ is a mapping from one signal space, D_u to another D_y. It is denoted

$$\mathcal{G}(.) : D_u \mapsto D_y \tag{2.9}$$

Thus, given the input $u(t) \in D_u$, the output $y(t) \in D_y$ is written $y = \mathcal{G}(u)$, where the time argument has been dropped for convenience.

A system is said to be *time-invariant* if a time-shift in the input produces the same output as would be expected, but time shifted i.e.

$$y(t-\tau) = \mathcal{G}(u(t-\tau)) \tag{2.10}$$

2.1.1 Linear systems

Linear systems are systems which satisfy the superposition and homogeneity properties. A system $\mathcal{G}$ is linear if, for all $u, v \in D_u$ and positive real scalar α, it follows that

$$\mathcal{G}(u+v) = \mathcal{G}u + \mathcal{G}v \tag{2.11}$$

$$\mathcal{G}(\alpha u) = \alpha\mathcal{G}(u) \tag{2.12}$$

This thesis assumes systems are causal, and this being the case, the output $y \in \mathcal{D}_y$ of a linear system can be written as $y = \mathcal{G}(t) * u(t)$ where the linear operation "$*$" represents the convolution operation

$$y(t) = \int_0^t g(t-\tau)u(\tau)d\tau \tag{2.13}$$

where $g(t-\tau)$ is the time-shifted impulse response of $\mathcal{G}$. Taking the Laplace transform of (2.13), it is possible to obtain the so-called "transfer function matrix" of $\mathcal{G}$ as

$$y(s) = \mathcal{G}(s)u(s)$$

where $\mathcal{G}(s)$ is the Laplace transform of the impulse response $g(t)$. For single-input-single-output (SISO) systems, the transfer function is then defined as

$$\mathcal{G}(s) = \frac{y(s)}{u(s)}$$

where $u(s)$ and $y(s)$ are Laplace transforms of $u(t)$ and $y(t)$ respectively and $\mathcal{G}(s)$ is a rational function in the Laplace variable s.

Linear time invariant (LTI) systems, described by linear differential equations, are often represented in state-space form as:

$$\mathcal{G} \sim \begin{cases} \dot{x} = Ax + Bu \\ y = Cx + Du \end{cases} \tag{2.14}$$

As shorthand, the following notation is often adopted in the thesis.

$$\mathcal{G} = \left[\begin{array}{c|c} A & B \\ \hline C & D \end{array}\right] \tag{2.15}$$

In general, the matrices A, B, C, D can be time varying. If $\mathcal{G}$ is assumed *linear time-invariant* (LTI), the matrices A, B, C, D are constant and the transfer function of the systems is obtained by calculating

$$\mathcal{G}(s) = D + C(Is - A)^{-1}B$$

In this thesis, no distinction is made between the time-domain description of $\mathcal{G}$ and its transfer function, and their arguments are often omitted for compactness; it should be clear from the context which is meant. One of the convenient aspects of LTI systems theory is that stability is completely determined by the eigenvalues of the matrix A, denoted by $\mathbf{spec(A)}$, and makes it trivial for the designer to check for stability of the system (the design task is less trivial). It is worth stressing the importance of linear systems in control theory as most classical control literature is concerned with the problem of linear feedback systems. Consequently, a wide range of tools and theory is available, some key to the development of ideas proposed here.

2.1.2 Nonlinear systems

In real control applications systems can rarely be represented as linear; "life" is generally highly nonlinear. A *nonlinear* system is a system $\mathcal{G} : D_u \mapsto D_y$, which does not satisfy either the superposition or the homogeneity principles, that is

$$\mathcal{G}(\alpha u + \beta v) \neq \alpha\mathcal{G}(u) + \beta\mathcal{G}(v) \quad \forall \alpha, \beta \quad scalar \quad and \quad x, v \in D_u \tag{2.16}$$

Many physical nonlinear systems can be represented as a set of state-space differential equations which are a generalisation of the linear state-space description above

$$\mathcal{G} \sim \begin{cases} \dot{x} &= f(x, u, t) \\ y &= h(x, u, t) \end{cases} \tag{2.17}$$

The system is said to be linear if $f(x, u, t) = Ax(t) + Bu(t)$ and $h(x, u, t) = Cx(t) + Du(t)$. Otherwise the system is said to be non-linear.

Stability analysis of such systems is rather more complicated as no transfer function can be defined. Instead, techniques such as the Small Gain Theorem, Lyapunov stability theory or absolute stability theory (Circle and Popov criteria) are often employed for stability analysis of such systems. Another consideration when dealing with non-linear systems is that global stability cannot always be guaranteed; in such cases *local stability* may be achieved within a given region of attraction.

Nonlinear systems can generally be *linearised* around some equilibrium point x_e (i.e. $\dot{x}_e = 0$) in the state space. This allows for the design and analysis of control systems using linear control techniques. While such technique only guarantees that the properties inferred from the linearised system apply exclusively in the vicinity of a given equilibrium point of the nonlinear system, linearisation is a very common practice amongst control engineers and is often the only tractable way of designing suitable controllers.

2.2 Measure of system size

The "size" of a system is rather difficult to define, particularly if that system is multivariable (i.e. either D_u of D_y has a higher dimension than unity). The consensus of opinion in control theory, and that used in this thesis, is to measure the size of systems using norms which are induced by signal norms. In particular, for a given $p \in [1, \infty)$, the $\mathcal{L}_p$ induced norm is defined as

$$\|\mathcal{G}\|_{i,p} = \sup_{0 \neq u \in \mathcal{L}_p} \frac{\|\mathcal{G}(u)\|_p}{\|u\|_p} \tag{2.18}$$

An important special case is the induced $\mathcal{L}_2$ norm which can be defined as

$$\|\mathcal{G}\|_{i,2} = \sup_{0 \neq u \in \mathcal{L}_2} \frac{\|\mathcal{G}(u)\|_2}{\|u\|_2} \tag{2.19}$$

In the special case that $\mathcal{G}$ is a linear system, the induced $\mathcal{L}_2$ norm can also be defined as

$$\|\mathcal{G}\|_{i,2} = \|\mathcal{G}\|_\infty := \sup_{\omega \in [0,\infty]} \bar{\sigma}[\mathcal{G}(j\omega)] \tag{2.20}$$

where $\bar{\sigma}(.)$ represents the maximum singular value of a matrix and with some abuse of notation, $\mathcal{G}(j\omega)$ represents the Fourier transform of $\mathcal{G}$. The notation $\|\mathcal{G}\|_\infty$ represents the $\mathcal{H}^\infty$ norm of a linear system. The induced $\mathcal{L}_2$ norm of a system $\mathcal{G}$ is also termed the $\mathcal{L}_2$ *gain* of a system. It is commonly used in control theory because it can also be interpreted as the root-mean-square energy gain of a system and its form makes it numerically tractable. In particular, if the induced $\mathcal{L}_2$ norm is well-defined, the system is said to be *finite* $\mathcal{L}_2$ *gain* stable.

In later chapters it will be necessary to use a *local* version of the induced $\mathcal{L}_2$ norm. In particular, if the input $u \in \mathcal{W} \subset \mathcal{L}_2$ (the input signal u is in $\mathcal{L}_2$) and the output $y \in \mathcal{D}_y$, the *local* $\mathcal{L}_2$ gain is defined as

$$\|\mathcal{G}\|_{i,2,\mathcal{W}} := \sup_{0 \neq u \in \mathcal{L}_2, u \in \mathcal{W}} \frac{\|\mathcal{G}(u)\|_2}{\|u\|_2} \tag{2.21}$$

Note that as $\mathcal{W} \subset \mathcal{L}_2$ it follows that

$$\sup_{0 \neq u \in \mathcal{L}_2, u \in \mathcal{W}} \frac{\|\mathcal{G}(u)\|_2}{\|u\|_2} \leq \sup_{0 \neq u \in \mathcal{L}_2} \frac{\|\mathcal{G}(u)\|_2}{|u\|_2} \tag{2.22}$$

so in general $\|\mathcal{G}\|_{i,2,\mathcal{W}} \leq \|\mathcal{G}\|_{i,2}$. We say the operator $\mathcal{G}$ is small-signal finite-gain $\mathcal{L}_2$ stable if equation (2.21) holds (see [48]).

2.3 Stability

This section will start by giving a general definition of stability. Consider the time-invariant system

$$\dot{x} = f(x), \quad f(.) : \mathbb{R}^n \mapsto \mathbb{R}^n$$

where $f(x)$ can be non-linear and $x \in \mathbb{R}^n$. An equilibrium point for such a system is defined as the point where all the time derivatives are exactly equal to zero, i.e. $f(x_e) = 0$. Equilibrium points can be stable, unstable or saddle points. Linear systems only have one equilibrium point, while nonlinear systems may have several. Stable equilibrium are desirable states and without any loss of generality, can be assumed to be the origin, i.e. $x_e = 0$.

Definition 2.1 *[48] An equilibrium state x_e is said to be stable if and only if for all $\alpha > 0$, there exists a $\delta(\alpha)$ such that*

$$\|x_0 - x_e\| < \delta(\alpha) \Leftrightarrow \|x(t) - x_e\| < \alpha, \; \forall t > t_0$$

where x_0 is said to be the initial condition at time t_0. □

The basic idea behind this definition is graphically simple to interpret: a system is stable if there exist a ball $\mathcal{B}(x_e, \delta) := \{x \in \mathbb{R}^n : \|x - x_e\| \leq \delta\}$ centred at x_e with radius δ such that for any initial state, $x(0) \in \mathcal{B}(x_e, \delta)$, the states of the system will remain within a ball centred at x_e wit h radius α forever, i.e.

$$x(0) \in \mathcal{B}(x_e, \delta) \Rightarrow x(t) \in \mathcal{B}(x_e, \alpha), \quad \forall t > 0$$

The above is a standard but fairly weak definition of stability which effectively calls a system locally stable if its state is locally bounded. In this thesis we shall require some more specific definitions of stability as given below.

Definition 2.2 *(Asymptotic Stability) Consider the system*

$$\dot{x} = f(x) \tag{2.23}$$

where $x \in \mathbb{R}^n$ and $x = 0$ is an equilibrium point. The system is said to be locally asymptotically stable *(LAS) with* basin of attraction $\mathcal{X}$ *if*

$$lim_{t \to \infty} x(t) = 0 \quad \forall x(0) \in \mathcal{X} \subset \mathbb{R}^n \tag{2.24}$$

Furthermore, if $\mathcal{X} = \mathbb{R}^n$, the system is said to be globally asymptotically stable (GAS). □

Definition 2.3 *The autonomous system*

$$\dot{x} = f(x, u)$$

is said to be Locally Asymptotically Stabilisable *with basin of attraction $\mathcal{X}$ if there exists a control strategy $u(x)$ and a set $\mathcal{X}$ such that the resulting system is LAS within this set. Furthermore, if there exists a control strategy $u(x)$ such that $\mathcal{X}$ can be chosen to be an arbitrarily large, but bounded, set, the system is said to be* Semi-globally Asymptotically Stabilisable.

Finally, if there exists a control strategy $u(x)$ such that $\mathcal{X} = \mathbb{R}^n$, the system is said to be globally asymptotically stablisable. □

Note that for linear systems, local stabilisability implies that the system is globally stabilisable and thus linear systems are often just described as "stabilisable" (which can be characterised by well-known conditions on the pair (A, B)) [34, 88]; for nonlinear systems, in general, local stabilisability does not imply global stabilisability.

2.4 Nonlinear stability tools

Establishing the stability of nonlinear systems is much more difficult than doing so for linear systems, and, as mentioned above, stability generally can only be obtained with respect to certain regions of attraction for each equilibrium point. This section will give a brief account of nonlinear stability tools used in later chapters. It should be understood that this section does not try to give an exhaustive treatment of nonlinear stability in general; rather the main features of the stability criteria used hereafter are elucidated.

2.4.1 Lyapunov stability theory

Lyapunov stability theory, or more accurately, *Lyapunov's Second Method*, is perhaps the most common nonlinear stability tool used in the control literature. Its appeal stems from its intuitive interpretation and that for systems with a strong linear component to them, it is often easy to choose a dissipative function which guarantees stability. In essence, Lyapunov stability theory involves picking a positive definite candidate function,

$$V(x) > 0 \quad \forall x \neq 0$$

and ensuring that its time-derivative decreases along the trajectories of the system, which for autonomous systems can be written as

$$\dot{V}(x) = \frac{\partial V}{\partial x} f(x) \leq 0$$

If this is the case, i.e. $V(x) > 0$ and $\dot{V}(x) \leq 0$, then we say that $V(x)$ is a *Lyapunov function.* The Lyapunov function $V(x)$ can be thought of as an "energy" function and requiring that its derivative decreases with time, can be thought of as ensuring that the energy of the system decreases over time, and thus settling down to an equilibrium. This can be stated formally as follows

Theorem 2.1 *[48] Let $x = 0$ be an equilibrium point for the system (2.23) and let $\mathcal{X} \subset \mathbb{R}^n$ be a domain containing $x = 0$. Let $V(x)$ be a continuously differentiable function $V(.) : \mathcal{X} \mapsto \mathbb{R}$ such that*

$$V(0) = 0 \quad \text{and} \quad V(x) > 0 \quad \forall x \in \mathcal{X} - \{0\} \tag{2.25}$$

Then if

i) $\dot{V}(x) \leq 0 \; \forall x \in \mathcal{X}$, then the trajectories of x remain within $\mathcal{X}$.

ii) $\dot{V}(x) < 0 \; \forall x \in \mathcal{X} - \{0\}$, then $x = 0$ is locally asymptotically stable.

Furthermore if $\mathcal{X} = \mathbb{R}^n$ in either of the above statements and $V(x)$ is radially unbounded ($\|x\| \to \infty \Rightarrow V(x) \to \infty$), then these properties are said to hold globally. □

Thus, when establishing stability via this method, it is normally the case that a candidate Lyapunov function is picked and one tries to establish that its derivative decreases over time. Note that it is generally a *trial and error* method as a Lyapunov function, or at least its structure, must be chosen *a priori.* However for given types of system, various structures of Lyapunov functions are now well known and it is often not too difficult to choose one for these systems.

Although Lyapunov stability theory is applicable to general nonlinear systems, it is particularly convenient for linear systems and has a strong relationship to many well-known results. For instance if we consider the linear system

$$G = \left[\begin{array}{c|c} A & B \\ \hline C & D \end{array}\right] \tag{2.26}$$

it transpires that a *necessary and sufficient* condition for this system to be asymptotically stable is that there exist a positive definite matrix, $P > 0$, which satisfies the following equation

$$A'P + PA = -Q < 0$$

If this is the case, it can easily be verified that $V(x) = x'Px$ is a Lyapunov function for the system. The above equation is often called a *Lyapunov equation* due to this. This implies that for linear systems, quadratic Lyapunov functions are both necessary and sufficient to predict stability. For nonlinear systems the task of proving stability is not as straightforward, but often, if a nonlinear system has a significant linear portion to it, quadratic Lyapunov functions $V(x) = x'Px > 0$ are usually chosen due to their simplicity and tractability. In this case, however, failure to establish stability using a given Lyapunov function does not mean the system is *unstable*, it simply means that stability cannot be established with that particular choice of Lyapunov function candidate.

Quadratic Lyapunov functions have played an important role in linear systems theory, particular in the development of the linear optimal control theory. In particular it is well known that the system (2.26) can be stabilised by applying a state-feedback control law of the form

$$u = -R^{-1}B'Px$$

where $P > 0$ is computed from the Riccati equation

$$A'P + PA - PBR^{-1}B'P + Q = 0 \tag{2.27}$$

where $R > 0$ and $Q > 0$ (for simplicity). In this case the closed-loop "A" matrix which governs the system has the form $A_{cl} = A - BR^{-1}B'P$. To guarantee asymptotically stable, note it suffices to choose $V(x) = x'Px > 0$, where the Riccati equation in (2.27) can be re-written as

$$(A - BR^{-1}B'P)'P + P(A - BR^{-1}B'P) + PBR^{-1}B'P + Q = 0 \tag{2.28}$$

$$(A - BR^{-1}B'P)'P + P(A - BR^{-1}B'P) = -Q - PBR^{-1}B'P < 0 \tag{2.29}$$

We conclude that the closed-loop system is stable and that $\mathbf{spec}(A_{cl}) \in \mathcal{C}^-$, where the notation $\mathbf{spec}(M)$ indicates the set of eigenvalues, or spectrum of matrix M.

Similarly, the system in equation (2.26) (assuming $D = 0$ for simplicity) is said to be *bounded real* if $\|G\|_\infty < \gamma$ for some $\gamma > 0$. It transpires that this is the case if there exists a matrix $P > 0$ such that the following Riccati equation is satisfied

$$A'P + PA + \gamma^{-2}PBB'P + C'C = 0$$

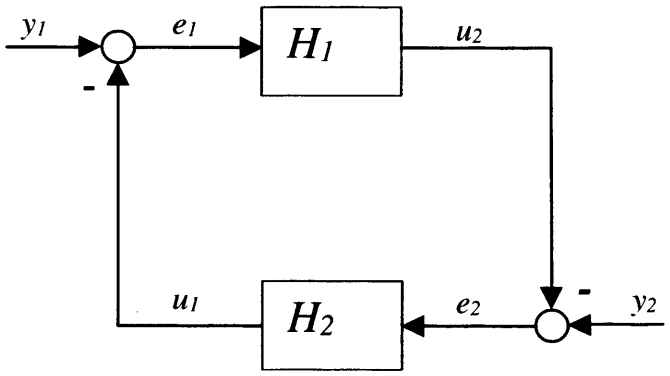

Figure 2.1: General block structure of feedback systems

Again it can be verified that choosing a Lyapunov function $V(x) = x'Px$ allows one to conclude that such a system is asymptotically stable.

Although this section has only given a brief, superficial overview of the interplay between results from linear systems theory and Lyapunov stability, it is important to emphasise that there is often a strong relationship between the two. In fact, the relationship between bounded-realness of a linear system and Lyapunov stability will be exploited in subsequent chapters of the thesis.

2.4.2 Small Gain Theorem

Lyapunov stability analysis is built upon the state-space representation of systems; we must have a set of differential equations describing of the system. Another approach which is arguably more convenient, particularly for large systems, is that of input-output stability: *when does a system produce a bounded output given a bounded input?* There are several approaches to answering this question, including the popular passivity approach, but the one we advocate here is the Small Gain Theorem (SGT).

Consider the system shown in Figure 2.1 which depicts a feedback interconnection of two (nonlinear in principle) systems, H_1 and H_2. This feedback system is considered to be stable if the map from the inputs $y = [y_1' \; y_2']'$ to the outputs $u = [u_1' \; u_2']'$ (or equivalently $e = [e_1' \; e_2']'$) is finite-gain $\mathcal{L}_p$ stable. In other words, conditions which ensure that $\|u\|_p \leq \gamma \|y\|_p$ are sought. Note that most, if not all, control problems consider input-output stability and so the above problem is a central aspect of control theory. It has become particularly important in robust control, most notably $\mathcal{H}^\infty$ theory as only the "gains" of systems are required, not detailed descriptions.

The SGT relies only on an input-output description of each of the subsystems. In particular

we assume that H_1 and H_2 are finite-gain $\mathcal{L}_p$ stable operators [1], i. e.

$$u_2 = H_1(e_1) \quad u_1 = H_2(e_2) \tag{2.30}$$

$$\|H_1\|_{i,p} = \gamma_1 \quad \|H_2\|_{i,p} = \gamma_2 \tag{2.31}$$

The small gain theorem can be formally stated as

Theorem 2.2 *(*Small Gain Theorem*) [48] Consider the feedback system portrayed in Figure 2.1 and assume $y \in \mathcal{L}_p$ and that the interconnecting systems are finite gain $\mathcal{L}_p$ stable. Then if $\gamma_1\gamma_2 < 1$, the feedback system is finite gain $\mathcal{L}_p$ stable i.e. there exists a $\gamma > 0$ such that*

$$\|u\|_p \leq \gamma\|y\|_p$$

□

One of the main attractions of the SGT, as alluded to above, is that detailed descriptions of the two feedback components are not necessary - only bounds on the systems' norms are required. This explains its prevalence in the robust control literature where it is used to analyse systems with plant uncertainty in which one part of the system (the nominal part) is known well and the other part of the system (the uncertain part) is not very well known, but a bound on its norm is given. Most uncertain control systems can be massaged into the block structure of Figure 2.1, where H_2 represents the uncertainty block Δ and H_1 is given by the remaining system dynamics; this representation generally being called the "$M - \Delta$" structure (see [34] for more detail). $\mathcal{H}^\infty$ control theory is devoted to the computation of controllers which ensure that the $\mathcal{H}^\infty$ norm (which is identical to the induced $\mathcal{L}_2$ norm) of the closed-loop system is small, hence making the closed-loop system robust to as much uncertainty as possible, in a *small gain sense.*

Thus, the SGT provides a convenient environment for the analysis of many feedback systems of practical interest, particularly those containing uncertain or nonlinear elements whose exact mathematical description is unknown. The main deficiency of the SGT is its conservatism; in general it only provides sufficient conditions for stability, not necessary.

2.4.3 The Circle Criterion

The Small Gain Theorem is particularly useful in robust control theory because it allows one to conduct stability analysis of systems where only the induced $\mathcal{L}_p$ norm of the uncertain

[1] For simplicity and compactness the bias term β existing in the general induced norm formulation (see [48]) is omitted as it is assumed that $Hu = 0$ if $u = 0$

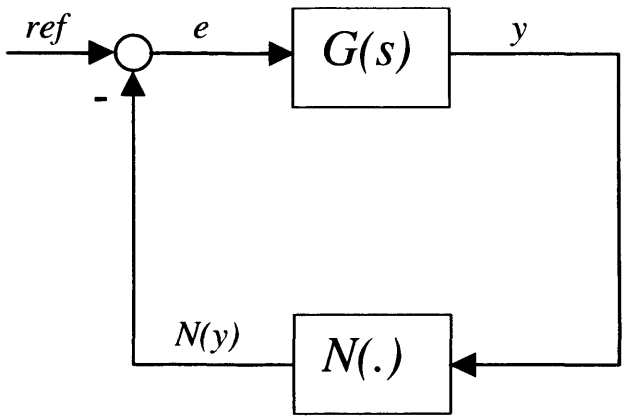

Figure 2.2: Block structure of some type of feedback systems

component is known. However in many systems, more information about the "uncertain" or nonlinear element is known, not just its induced norm. In fact, many systems can be represented as a feedback combination of a linear system and a *static* nonlinear element. Examples of these would be systems containing saturation or dead-zone elements, which are the type of system under consideration. Such systems can be represented, after appropriate manipulations, as in Figure 2.2, where $G(s)$ represents the linear part of the system and $\mathcal{N}(.) : \mathbb{R}^m \mapsto \mathbb{R}^m$ represents the static (but possibly time-varying) nonlinear element. It is assumed that the system is *well-posed*; that is the solution to the feedback equations always exists and is unique. For this class of systems it is often possible to prove stability of the nonlinear closed-loop, based largely, on information about the linear system $G(s)$ and some approximate information about $\mathcal{N}(.)$.

The classical topic of "absolute stability" theory is devoted to this class of systems [48]. The standard assumption is to assume that the nonlinear element $\mathcal{N}(.)$ belongs to a certain sector (introduced shortly). The system is said to be "absolutely" stable if it has a globally asymptotically stable equilibrium point at the origin for all nonlinearities within a given sector; it is said to be absolutely stable with a finite domain if it is locally asymptotically stable for all nonlinearities within a given sector. Absolute stability theory has occupied the minds of control theorists for many years and it has a rich history (including several fallacious conjectures - the Aizermann and Kalman conjectures being perhaps the most notorious) and is still being developed today within the context of integral-quadratic-constraints (IQC's).

For this thesis we are content to study only the Circle Criterion which is perhaps the most well-known method in absolute stability theory. Although it is one of the more conservative methods, its key advantage is that it leads to tractable *synthesis* schemes. Other absolute stability theory, such as the Popov Criterion, may be useful for analysis but typically tend to result in complex, intractable synthesis routines. The main requirement of the Circle Criterion

is that the nonlinearity $\mathcal{N}(.)$ is *sector bounded*; the definition below is adapted from [48]

Definition 2.4 *A memoryless nonlinearity* $\mathcal{N}(.) : \mathbb{R}^m \mapsto \mathbb{R}^m$ *is said to belong to* Sector$[\mathcal{K}_1, \mathcal{K}_2]$ *where*

$$\mathcal{K}_1 = \text{diag}(\mathcal{K}_{1,1}, \mathcal{K}_{1,2}, \ldots, \mathcal{K}_{1,m}) > 0, \quad \mathcal{K}_2 = \text{diag}(\mathcal{K}_{2,1}, \mathcal{K}_{2,1}, \ldots, \mathcal{K}_{2,m}) > 0, \tag{2.32}$$

if $\mathcal{K}_2 - \mathcal{K}_1 > 0$ *and the following inequality holds for all* $y(t)$

$$[\mathcal{N}(y) - \mathcal{K}_1 y]'[\mathcal{N}(y) - \mathcal{K}_2 y] \leq 0 \tag{2.33}$$

□

Without loss of generality, the feedback system in Figure 2.2 can be manipulated into a form in which the nonlinearity $\mathcal{N}$ inhabits a slightly different sector, the Sector$[0, \mathcal{K}]$, where $\mathcal{K}$ is again some positive definite diagonal matrix. Such a transformation makes the sector-based results less tedious to state. Another concept which is useful for the statement of the Circle Criterion is the concept of *strict positive realness*(SPR).

Definition 2.5 *[48] Let* $Z(s)$ *be a real rational proper transfer function matrix and suppose that* $\det[Z(s) + Z'(-s)]$ *is not identically zero. Then* $Z(s)$ *is strictly positive real (SPR) if and only if*

1. $Z(s)$ *is Hurwitz*
2. $Z(j\omega) + Z'(-j\omega) > 0 \quad \forall \omega \in \mathbb{R}$
3. *and either*
   a) $Z(\infty) + Z'(\infty) > 0$;
   b) $Z(\infty) + Z'(\infty) = 0$ *and* $\lim_{\omega \to \infty}[Z(j\omega) + Z'(-j\omega)] > 0$;
   c) $Z(\infty) + Z'(\infty) \geq 0$ *and there exist positive constants* σ_0 *and* ω_0 *such that*

$$\omega^2 \sigma_{min}[Z(j\omega) + Z'(-j\omega)] \geq \sigma_0, \quad \forall |\omega| \geq \omega_0$$

□

The Circle Criterion can now be stated as

Theorem 2.3 (Circle Criterion) *Consider the feedback interconnected system in Figure 2.2 where* $G(s)$ *has minimal state-space realisation as given in equation (2.26) and has states denoted by* x *and output denoted by* y. $\mathcal{N}(.) \in$ Sector$[0, \mathcal{K}]$ *and assume all dimensions are compatible. Then the following are statements are equivalent*

i) The interconnection in Figure 2.2 is absolutely stable for all $\mathcal{N}(.) \in \text{Sector}[0, \mathcal{K}]$.

ii) $I + \mathcal{K}G(s)$ *is strictly positive real.*

iii) There exists a positive definite function $V(x) \geq 0$ *and a diagonal positive definite matrix* $W > 0$ *such that*

$$\dot{V}(x) + \mathcal{N}'(y)W[y - \mathcal{N}(y)] + [y - \mathcal{N}(y)]'W\mathcal{N}(y) < 0 \quad \forall x \neq 0$$

i.e. $V(x)$ *is a Lyapunov function.*

□

The second item is the traditional way of stating the Circle Criterion and, for single-input-single-output systems has an attractive graphical interpretation in the frequency domain. This graphical interpretation of the Circle Criterion will be used later when looking at the PIO problem, but it should be noted that it is not particularly useful for multi-input-multi- output (MIMO) systems. The third item is the most central to this thesis and it effectively provides a Lyapunov argument for the Circle Criterion. This formulation is appealing because it allows one to pose tractable synthesis routines for systems with saturation nonlinearities . The relationship between statements i) and iii) is easy to see via a Lyapunov argument. The relationship between statements ii) and iii) is nontrivial and requires the evocation of the Kalman-Yakubovich-Popov (KYP) Lemma which essentially provides a connection between positive realness and passivity. The Circle Criterion will be used extensively throughout the remainder of the thesis.

Chapter 3

Representation of Anti-windup schemes

Anti-windup techniques probably have their roots in industry, where early compensation attempts were developed before the academic research community began to study them. They were used traditionally to solve problems of integrator windup in electric motor and boiler control systems [31]; essentially they were practical solutions to simple practical problems. When the academic community began to study them in the 1980's, it became apparent that, due to the diversity of the techniques, there was little common framework uniting the different approaches. Hence authors such as [3], [52], [21] and [118] began to develop ways of unifying the various schemes available. This gave insight into the different design structures and philosophies, allowing different techniques to be compared closely within a common framework.

In this thesis we largely follow the architecture proposed in [118] as we think it gives a transparent and easy-to-analyse scheme. The aim of this chapter is to discuss the different frameworks in which AW could be interpreted and also to interpret some of the existing AW schemes within these various architectures. This chapter will form a theoretical framework on which subsequent chapters are constructed.

3.1 General AW Setup

Consider the block diagram of Figure 3.1 which represents a general AW setup. $G(s)$ represents the plant driven by the saturated control signal $u_m \in \mathbb{R}^m$; $K(s)$ is the nominal controller driven by a reference signal within $\mathbb{R}^{n_r}$ and by the plant output $y \in \mathbb{R}^{n_p}$. These two elements are interconnected through the static nonlinear saturation function $\text{sat}(.) : \mathbb{R}^m \mapsto \mathbb{R}^m$ which is

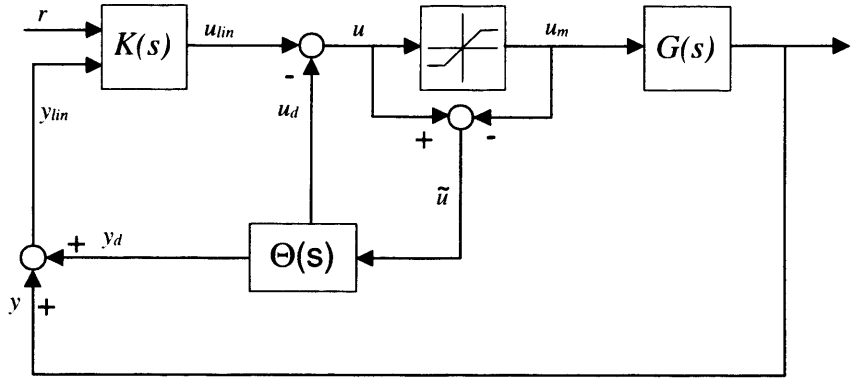

Figure 3.1: Generic Anti-Windup scheme

defined as follows.

$$\text{sat}(u) := \begin{bmatrix} \text{sat}_1(u_1) \\ \text{sat}_2(u_2) \\ \vdots \\ \text{sat}_m(u_m) \end{bmatrix} \tag{3.1}$$

where

$$\text{sat}_i(u_i) := \text{sign}(\text{u}_\text{i}) \times \max\{|\text{u}_\text{i}|, \bar{\text{u}}_\text{i}\} \tag{3.2}$$

Observe that the saturation nonlinearity limits the magnitude of the effective control signal u_m, to a hyper-cuboid

$$\mathcal{U} := [-\bar{u}_1, \bar{u}_1] \times [-\bar{u}_2, \bar{u}_2] \times \ldots \times [-\bar{u}_m, \bar{u}_m] \tag{3.3}$$

Thus, for large inputs it is clear that the effective control signal $u_m \in \mathcal{U} \subset \mathbb{R}^m$ may differ from the unconstrained control signal, $u \in \mathbb{R}^m$. It is this difference which is responsible for the unpredictable effects in an otherwise linear control loop. To overcome the effects of actuator saturation, the anti-windup compensator $\Theta(s) = [\Theta_1'(s)\ \Theta_2'(s)]'$ is introduced. This AW compensator is either a static gain or a transfer function matrix which is responsible for taking corrective action of the control signal during saturation, that is when $u_m = \text{sat}(u) \neq u$. Informally [1], the objective of the AW compensator $\Theta(s)$ is to ([52]):

i) ensure that stability is maintained during and after a saturation event; and

ii) to limit the performance degradation over this period

Much of the remainder of the thesis will attempt to discuss these objectives (and how to achieve them formally) and to give algorithms which can be used to synthesize appropriate

[1] Formal statements will be given later

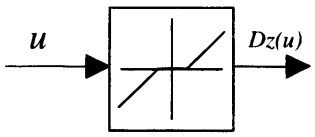

Figure 3.2: Block representation of the *deadzone* function

AW compensators; for the moment it should simply be understood that these are the goals of the designer.

Remark 3.1: Notice that when $sat(u) \neq u$ the saturated plant output $y = Gu_m$ is conditioned before being used for feedback purposes (see Figure 3.1). This is in contrast to some schemes (see for example [105]) where the states of the controller are conditioned directly; this type of AW scheme has been branded "full authority compensaion". As it may not always be possible to access the controller states directly, conditioning may be done on the controller input instead. □

The anti-windup compensator, $\Theta(s)$, is driven by the difference between the *real* saturated and unsaturated control signals

$$\tilde{u} := u - \text{sat}(u) =: \text{Dz}(u) \tag{3.4}$$

This is the well-known nonlinear dead-zone operator (see Figure 3.2). Notice that $\text{Dz}(u) = 0$ $\forall u \in \mathcal{U}$, thereby implying that the anti-windup compensator does not become active until saturation occurs, that is $u \notin \mathcal{U}$. This feature is distinctive among AW compensators and implies that *nominal (small signal) controller behaviour* is preserved unless saturation is encountered. This distinguishes AW compensators from other "saturation controllers" such as model predictive controllers (MPC) ([62, 10]) and saturated linear controllers (proposed by, for example [55, 97]). Note that if the *real* saturated control signal is not available, a synthetic saturation can be placed in the control software to artificially generate this signal. During saturation, and immediately after, the AW compensator produces two signals, $\Theta_1(t)$ and $\Theta_2(t)$, which influence the behaviour of the closed-loop. Roughly speaking $\Theta_2(t)$ helps to stabilise the controller during saturation and $\Theta_1(t)$ enables the AW controller to have a quick impact on the current control signal, as the signal does not have to pass through the dynamics of the controller $K(s)$.

From the above it is clear that AW must operate under the fundamental assumption that the *nominal linear system* (closed-loop system with no saturation present) is stable and well-behaved. This implies that the controller $K(s)$, has been designed to ensure closed-loop stability and that nominal performance specifications are met when $\text{sat}(u) = u$ (i.e. $u \in \mathcal{U}$). If the latter statement were not true, it would be pointless to use anti-windup compensation; good small-

signal linear behaviour is a requirement of AW design in general. In fact, throughout this thesis, a stronger assumption is often stipulated; linear behaviour represents, in some way, "ideal behaviour" and the goal of anti-windup design is to return to linear dynamics. Such an objective will be made more concrete later in the thesis. Conversely, no initial assumption is made on the controller's behaviour during saturation, $\text{sat}(u) \neq u$ $(u \notin \mathcal{U})$, and it is usually the case that the controller $K(s)$ has been designed in ignorance of the saturation limits.

Thus the subject matter of the thesis is the design of the anti-windup compensator, $\Theta(s)$, *not* the design of the linear controller $K(s)$. It is important to point out that although $\Theta(s)$ in no way restricts the local linear behaviour of the controller $K(s)$ (as it is only active for large enough u), the choice of controller $K(s)$ may restrict the type of AW compensator which can be applied. Put another way, for arbitrary $G(s)$ and $K(s)$, there may not exist an AW compensator of a given type which yields closed-loop stability. This will become clear in the next sections.

3.2 A decoupled formulation

Although the architecture portrayed in Figure 3.1 is fairly generic as it can be used to represent almost any linear anti-windup compensator, because the overall system is nonlinear and because no structure is imposed upon the AW compensator $\Theta(s)$, this setup is not particularly convenient for analysis or design of AW schemes. This section will introduce the *M parametrisation* of AW compensators which was first proposed in [116] (see also [118]); the advantage of such parametrisation is that it enables the nonlinear stability and performance AW problems to be more clearly elucidated.

3.2.1 Equivalent representations

Consider Figure 3.3 below, in which a structure has been given to our AW compensator [116, 118], viz

$$\begin{bmatrix} \Theta_1 \\ \Theta_2 \end{bmatrix} = \begin{bmatrix} M - I \\ GM \end{bmatrix} \tag{3.5}$$

The AW compensator is now described in terms of a copy of the nominal plant model, $G(s)$, and a free parameter $M(s) \in \mathcal{RH}_\infty$. This parametrisation is significant as it enables Figure 3.3 to be re-drawn as Figure 3.4 where the closed-loop AW compensated system is decoupled into three distinct parts: *nominal linear loop, nonlinear loop* and *disturbance filter.* The three parts play an important role in AW compensation. Firstly note that now the "disturbance" on

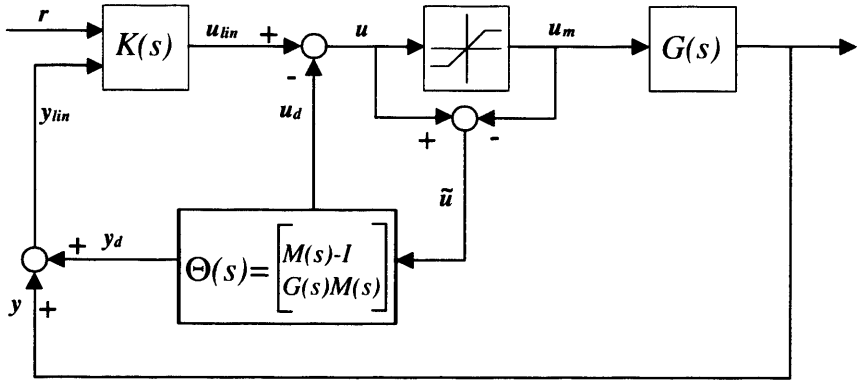

Figure 3.3: Conditioning with $M(s)$

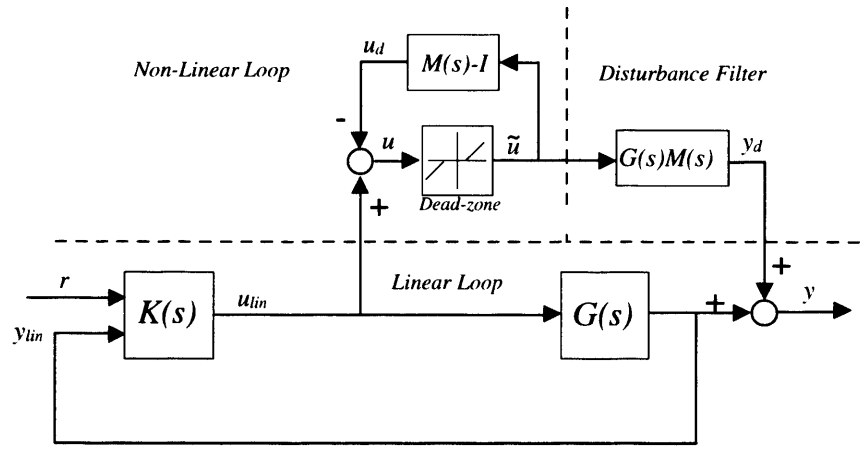

Figure 3.4: Decoupled structure

the system output due to input saturation is represented additively as y_d; thus the total output can be represented as the sum of signal y_{lin}, which is generated by a purely *linear* system, and a signal y_d which only results if input saturation occurs. Note that under the assumption that the linear closed-loop is asymptotically stable (a reasonable practical assumption) and that the open-loop linear plant is *bounded real*, the stability problem is reduced to ensuring that the nonlinear loop is asymptotically stable. Furthermore, note that the disturbance filter provides information about how the system recovers from saturation, i.e. the decay rate of the disturbance filter's states is important in determining the system's time to recover from saturation.

Note that the decoupled structure in Figure 3.4 cannot be implemented because the disturbance filter has a copy of the plant. Instead, it can be used for analysis and design purposes. As mentioned above, the decoupled structure consists of three systems which define three distinct stages of operation [116, 118]:

Stage I The first stage is nominal linear operation, for which the control signal is sufficiently small, i.e $u \in \mathcal{U}$, such that the saturation nonlinearity behaves linearly (Figure 3.3) and the output of the dead-zone nonlinearity, $\tilde{u}$ (Figure 3.4) is zero.

Stage II Once u_{lin} is large enough as to cause $u \notin \mathcal{U}$, the saturation operator will behave nonlinearly (Figure 3.3) and the dead-zone will emit a signal $\tilde{u} \neq 0$ (Figure 3.4) causing the *nonlinear loop* to become active. The nonlinear behaviour will sustain operation until the control signal u re-enters the set $\mathcal{U}$, at which point, as the dead-zone is a static map, $\tilde{u}$ will return to zero.

Stage III Recovery of linear behaviour. Once $u \in \mathcal{U}$ again, and assuming that G, $M \in \mathcal{RH}_\infty$, the system will return asymptotically to linear behaviour in a manner governed by the dynamics of GM (i.e. the *disturbance filter*). Even though the disturbance filter is no longer being forced by u_{lin}, full return to linear operation is only achieved once any transient dynamics decay completely.

Another notable aspect of this parametrisation is that most existing (linear) anti-windup compensators can be interpreted as particular choices of $M(s)$, thus making the decoupled scheme a useful tool for comparing stability and performance properties of different AW techniques. Note that the stability problem is now much simpler and, as will be seen later, the map $\mathcal{T}_p : u_{lin} \mapsto y_d$ provides information on how the saturated behaviour of the system will differ from nominal linear dynamics. As the time spent in *Stage III* varies according to the choice of M, the length of this transient operation mode may be a good way of comparing different compensation schemes. In [118] it was suggested that a good choice of $M(s)$ is given by the coprime factorisation of the plant (i.e. $G = NM^{-1}$), providing a dual parametrisation of anti-windup compensators to that given by [52] (also used by [65] and [16]). This choice of $M(s)$ reduces the disturbance filter to $N(s)$ (one of the coprime factors), where both transfer functions may share the same state space; a *Full Order* AW compensation scheme is generated as a result. The anti-windup problem is then reduced to that of finding the optimal *state feedback* matrix gain F such that $(A + BF)$ is Hurwitz, the nonlinear loop is stable and the map $\mathcal{T}_p$ is small in some sense. Much of the remainder of the thesis will be concerned with formulating and solving this problem rigorously.

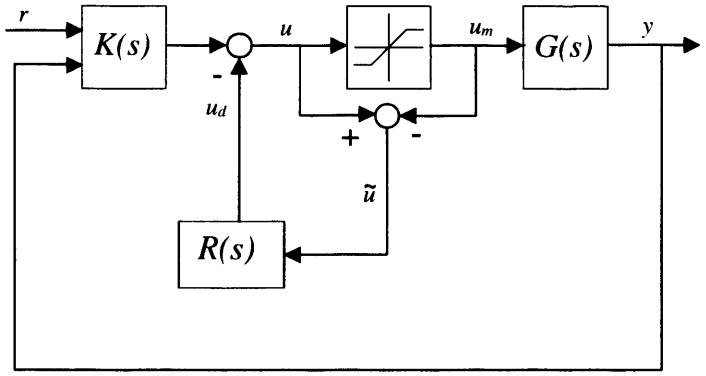

Figure 3.5: Generic AW scheme for a 2 D.o.F. controller

3.3 Relationship with the generic anti-windup scheme

As mentioned at the start of this chapter, due to the various ways of designing and implementing AW compensators, many attempts have been made to unify these architectures. This enables insights to be drawn and comparisons to be made. A particularly useful architecture, which will be referred to as the Θ *approach*, was discussed earlier. Another approach, as suggested in [21] - the so-called "generic AW" scheme (GAW) - may also be useful for such purposes. Although this is a popular setup, it can be shown that it is actually not as generic a representation as the Θ scheme (Figure 3.1). The GAW scheme is shown in Figure 3.5, where the signals have the same meaning and dimensions as before; this time $R(s)$ represents the anti-windup compensator, and again, $K(s)$ and $G(s)$ are the controller and nominal linear plant respectively.

In fact, many of the early AW schemes were formulated using, or can easily be translated to, the R-structure presented in Figure 3.5, where only the output of the controller is conditioned. In general this compensation structure is more compact in the sense that it is represented by a single transfer function $R(s)$, although if the controller is unstable, this structure is not suitable for implementation and may yield compensators of higher order than necessary.

In the "more generic" Θ structure presented in Figure 3.1, the AW compensator is given by a set of two transfer functions, Θ_1 and Θ_2. This is arguably "more generic" because it enables controllers with marginally stable (such as those with integrators) or unstable modes to be treated easily and is also suitable for implementation. Note that the so-called *generic AW scheme* in Figure 3.5 can be interpreted in terms of the scheme described in Figure 3.1 using different values of Θ_1 and Θ_2. In fact, any scheme developed using $R(s)$ can be represented by a family of compensators parametrised by the given transfer function $R(s)$ and a free parameter $\Theta(s)$.

In order for the two compensation structures to be equivalent, the conditioned control signals must be the same. In the so-called GAW scheme (Figure 3.5), which uses $R(s)$ as the AW parameter, the compensated signal u, for a 2-D.o.F controller, is

$$u = K_1 r + K_2 y + R\tilde{u} \tag{3.6}$$

For the block diagram in Figure 3.1, where $\Theta(s)$ is the AW parameter, the compensated control signal u is given by

$$u = K_1 r + K_2(y + \Theta_2\tilde{u}) - \Theta_1\tilde{u} \tag{3.7}$$

By comparing equation (3.6) and (3.7) the following relationship is obtained

$$\Theta_1 = K_2\Theta_2 - R \tag{3.8}$$

Therefore, any compensation scheme given in terms of R has an equivalent representation in terms of Θ, where $\Theta_1(s)$ and $\Theta_2(s)$ are related by equation(3.8). Although this representation is simple, there are many solutions to equation (3.8), providing no clear analytical advantages over the original representation. As discussed earlier, by using a single transfer function M to parametrise the compensator (i.e. $\Theta_1 = M - I$ and $\Theta_2 = GM$), it is possible to expose stability and performance properties which are central to the AW compensation problem. From equation (3.8) and the parametrisation of Θ given in equation (3.5)

$$M = (I - K_2G)^{-1}(I + R) \tag{3.9}$$

This means that most AW schemes can be interpreted as an appropriate choice of M and therefore achieve the decoupled structure proposed by [118]. In this way, it is possible to analyse and compare in a methodical manner the stability and performance properties of existing AW schemes

3.4 Existing AW Schemes

There is a large number of existing AW schemes available for today's practitioner. The most popular and appealing schemes will be briefly reviewed here. Broadly speaking, AW schemes can be separated into two groups, those which we call "traditional" and those which we call "modern", although the distinction is not always clear. This section will discuss a selection of important existing AW schemes and compare them both through the generic structure given in Figures 3.3 and 3.5.

3.4.1 "Traditional" AW schemes

Traditional AW schemes have their roots within industry and were initially thought to be a "practical solution to a practical implementation problem". This being the case, many of them suffer from being *ad hoc* schemes where stability and performance guarantees are not ensured. At the same time they tend to have poor tuning rules which makes their design a trial and error process. A common feature of traditional anti-windup schemes is their general heuristic nature. A further item of commonality is that they are typically based around the controller and do not account for the characteristics of the plant in their design. Several of these schemes are used widely by practitioners due to their simplicity and transparency of implementation. The main negative aspect is that they are rarely accompanied by closed-loop stability guarantees and performance objectives are vague at best.

Most of these schemes are transfer-function based although some have a convenient state-space interpretation. Noting this, it is convenient to introduce the following state-space realisations of the linear controller. Both one-degree-of-freedom (1-D.o.F) and two-degrees-of-freedom (2-D.o.F) controllers will be considered. The 1-D.o.F controller is assigned the following realisation

$$K(s) \sim \left[\begin{array}{c|c} A_c & B_c \\ \hline C_c & D_c \end{array}\right] \tag{3.10}$$

where $u_{lin}(s) = K(s)e(s)$, and $e(s) \in \mathbb{R}^{n_r}$ is the Laplace transform of the error signal $e(t) = r(t) - y(t)$. The 2-D.o.F controller $K(s) = [K_1(s) \quad K_2(s)]$ is assigned the following state-space representation

$$K(s) = [K_1(s)\ K_2(s)] \sim \left[\begin{array}{c|cc} A_c & B_{cr} & B_c \\ \hline C_c & D_{cr} & D_c \end{array}\right] \tag{3.11}$$

The 2-D.o.F controller is driven by the reference signal $r(t)$ and the output $y(t)$ independently, viz $u_{lin}(s) = K(s)[r(s)' \quad y(s)']'$. It is easy to observe that by setting $B_c = -B_{cr}$ and $D_c = -D_{cr}$, the one-degree-of-freedom controller is recovered as a special case of the 2-D.o.F structure.

It is instructive to evaluate classical AW schemes in the context of the generic set-up introduced earlier in Figure 3.3; that is interpreting traditional and modern AW schemes, including the special case of *no compensation*, as certain choices of Θ, and more specifically, a choice of $M(s)$.

No AW Compensation

Although it is probably not correct to class the case of using no compensation as an "AW scheme", it is important to examine this configuration to reveal how a system with no AW may

behave during nonlinear operation. Obviously, in this case both $\Theta_1(s)$ and $\Theta_2(s)$ are identically zero. However, in terms of Figure 3.4, it is possible to find an $M(s)$ that represents the system with no compensation; for a system with a 2-D.o.F. controller, the *no compensation* scheme is parametrised by

$$M = (I - K_2G)^{-1} \tag{3.12}$$

where the disturbance filter is given by

$$GM = G(I - K_2G)^{-1} \tag{3.13}$$

Notice that assuming internal stability of the nominal linear system, the disturbance filter is stable and is given by the linear transfer function from K_1r to y_{lin}. The disturbance filter, and therefore AW performance, are closely related to the *nominal closed-loop*, more specifically its disturbance rejection properties, and provided the nonlinear loop is stable, the closed-loop compensated system is stable.

An obvious necessary condition for global asymptotic stability of the nonlinear loop is that $M(s) - I = (I - K_2G_2)^{-1}K_2G_2 \in \mathcal{RH}_\infty$ (the co-sensitivity function); a necessary condition for global asymptotic stability of the disturbance filter is, again, that the plant be stable and that the sensitivity function $(I - K_2G_2)^{-1} \in \mathcal{RH}_\infty$. A sufficient condition for stability of the nonlinear loop is that the closed loop system is SPR (strictly positive real). Thus without AW compensation necessary conditions are obtained from the two fundamental linear transfer functions: the sensitivity and co-sensitivity functions. Sufficient conditions must be obtained through nonlinear stability tests, and in some cases this may not be easy to establish.

Classical AW

Probably the most intuitive and simple approach is *Classical Anti-Windup*, in which the compensator can be obtained by choosing Θ as

$$\Theta_1(s) = \frac{\alpha}{s}I \tag{3.14}$$

$$\Theta_2(s) = 0 \tag{3.15}$$

or R of Figure 3.5 as $R = \frac{\alpha}{s}$; thus this being the simplest form of interaction between the architectures of Figure 3.1 and Figure 3.5. It follows that the compensated control signal is given by

$$u = \frac{s}{s+\alpha}Ke + \frac{\alpha}{s+\alpha}u_m$$

where $e = r - y$; it is clear from the context that a $1.D.o.F.$ controller has been implemented.

Notice how any integrators present in K are canceled and replaced by first order lags with time constants $\frac{1}{\alpha}$. However, notice that if the controller K has any unstable poles, the transfer function from e to u remains unstable. This limits the application of such a scheme to controllers which are stable except for the presence of integrators. Additional problems may arise when no integrators are present in the controller. If this is the case, observe that a derivative term remains present, generating high overshoots if the reference signal has a step in it. This phenomenon is called *derivative kick* and is undesirable and generally detrimental for the system's initial time response and overall performance.

Classical AW compensation can also be obtained by choosing

$$M(s) = (I + KG)^{-1}(\frac{s+\alpha}{s}) \tag{3.16}$$

where the disturbance filter is then given by

$$GM = G(I + KG)^{-1}\frac{s+\alpha}{s} \tag{3.17}$$

As in the case of no compensation, the disturbance filter is strongly linked to nominal robustness properties of the linear closed-loop, and if the transfer function $G(I + KG)^{-1}$ has a benign frequency response, then the system will recover gracefully after a saturation event has ceased. Observe that the extra term $\frac{s+\alpha}{s}$ can also be used to attenuate unwanted frequencies and enhance the system's recovery from saturation. However, stability is not addressed directly within the design scheme making it necessary to check stability of the system retrospectively. Also note that the only way to enforce nonlinear stability is through the choice of the parameter $\alpha > 0$ which may be restrictive.

Notice that if the controller K has any unstable poles, the transfer function M is not bi-stable and the overall system will not be stable. Again, this limits the application of *Classical AW compensation* to controllers which are stable except for the presence of integrators. Even for stable controllers, it may not always be possible to find an α such that the nonlinear loop is stable.

High Gain AW

High Gain Anti-windup or "Conventional AW" is a technique popular within industry. Good overviews of this technique can be found in [21] and [34] (and references therein). Its popularity may be attributed to the simplicity of its architecture and also to its effectiveness in alleviating windup problems in simple closed-loop systems. In terms of Figure 3.3, this is equivalent to

choosing

$$\Theta_1(s) = -\alpha I \tag{3.18}$$

$$\Theta_2(s) = 0 \tag{3.19}$$

where α is some large scalar - hence the name "high gain" technique. Here the technique is introduced for the general multi-variable scenario, although the high gain technique was originally conceived for single-loop systems. It is perhaps most instructive to examine the high-gain technique in the context of 1-D.o.F control systems (although similar reasoning holds for the more general 2-D.o.F case).

Some simple, although not rigorous reasoning - as described for example in Limebeer [34] - shows that the high gain technique essentially tries to ensure that the control "error" $\tilde{u}$ is as close to zero as possible, i.e. $\text{sat}(u) = u$. This means that during periods of no saturation, no action is taken by the AW compensator; but when control saturation occurs, the compensator tries to ensure that $u \approx \text{sign}(u)\bar{u}$. Note that the reasoning used here is very approximate as no considerations of system dynamics or stability are being made. However, this gives some insight to early ideas and concepts behind AW compensation.

The main problems with the high gain AW technique are that (i) nonlinear stability is not explicitly sought; (ii) no satisfactory allowance for performance is made. Furthermore, if we consider the signal u_m as a "disturbance" on the augmented controller formed by the nominal linear controller and the AW compensator, it is evident that the compensated control signal is therefore given by

$$u = (I + \alpha K)^{-1} K(e + \alpha\tilde{u}) \tag{3.20}$$

From this it is obvious that unless the controller has no zeros (including those at infinity) in the open right half plane, i.e. the controller is minimum phase, linear stability problems will occur; that is, the A-matrix of the augmented controller may not be stable for any value of α. Furthermore, typically large values of α are necessary to ensure good performance in some sense, complicating even more the solution of such AW problem. In terms of the decoupled scheme of Figure 3.4, the relevant generalised parametrisation is easily derived as

$$M = (I + KG)^{-1}(KX + I) \tag{3.21}$$

where the matrix $X = \alpha I$ for some large positive scalar α. The disturbance filter is therefore given by

$$GM = G(I + KG)^{-1}(\alpha K + I) = \alpha G_{cl} + G(I + KG)^{-1} \tag{3.22}$$

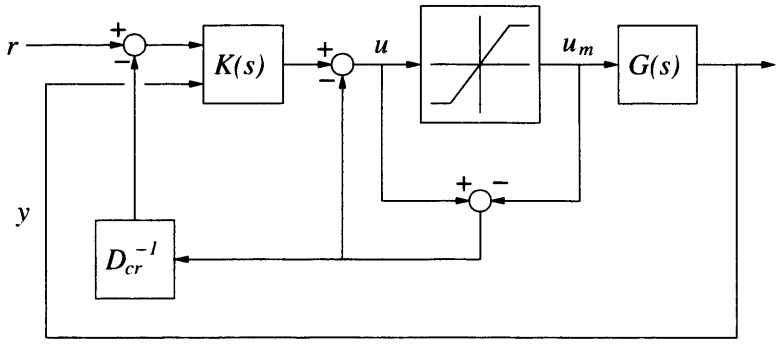

Figure 3.6: Hanus compensation scheme

The disturbance filter is thus represented by the sum of two transfer functions: one representing a scaled version of the nominal linear closed-loop co-sensitivity transfer function $\alpha G_{cl} := \alpha GK(1+GK)^{-1}$, and the other related to the disturbance rejection capabilities of the nominal linear closed-loop. In order for this AW scheme to achieve asymptotic stability, the nonlinear loop must be stable. From equation (3.21), it follows that this requires the transfer function

$$M - I = (I + KG)^{-1}K(X - G) \in \mathcal{RH}_\infty$$

From a purely linear perspective, a necessary condition for stability of the nonlinear loop is that when this transfer function is enclosed within a unity gain feedback loop, the resulting system must also be stable. In this case, choosing $X = \alpha I$ allows the linear stability problem to be posed as a multivariable root-locus problem, which has been suggested in the past [21]. It is important to emphasize again that this would only provide a necessary condition for stability and *does not guarantee* nonlinear stability. In fact, in some cases there will never exist a parameter α which stabilises the system even in a linear sense. This can be overcome by using a variation of the technique based on coprime factorisation [19] but again no guarantees of stability are given.

Hanus Anti-windup

The technique developed by Hanus ([40]) is again a popular choice for practitioners for many of the same reasons as the High-Gain approach. A block diagram of the *Hanus Anti-windup* scheme for a 2-D.o.F controller is shown in Figure 3.6

The idea of the Hanus AW scheme is to calculate (in a static sense) the value of a fictitious reference signal, which Hanus calls the "realisable reference", such that if this reference was applied, no controller saturation would occur. This leads Hanus to suggest partial inversion of

the controller in order to modify the reference such that the saturation limit is not exceeded. Again, giving the state-space realisation of the augmented controller (nominal linear controller plus AW), and assuming that D_{cr}^{-1} exists, we have

$$\begin{aligned} \dot{x} &= (A_c - B_{cr}D_{cr}^{-1}C_c)x + B_{cr}D_{cr}^{-1}u_m + (B_c - B_{cr}D_{cr}^{-1}D_c)y \\ u &= C_c x + D_{cr}r + D_c y \end{aligned} \tag{3.23}$$

The Hanus compensation scheme is equivalently represented by choosing

$$M = (I - K_2G)^{-1}K_1D_{cr}^{-1} \tag{3.24}$$

The disturbance filter is therefore given by

$$GM = G(I - K_2G)^{-1}K_1D_{cr}^{-1} = (I - GK_2)^{-1}GK_1D_{cr}^{-1} = G_{cl}D_{cr}^{-1} \tag{3.25}$$

The poles of the disturbance filter are the same as those of the nominal linear closed-loop, and provided they have been designed in an optimal way, the compensator will have good performance. However, note that there are no free parameters and stability of the nonlinear loop is not always ensured. If the system happens to be stable, then Hanus AW compensation schemes will most likely have good performance.

Note that two key necessary conditions need to be satisfied in order for the Hanus conditioning technique to work: the controller needs to be bi-proper (stable and invertible at infinity); the augmented controller needs to be stable and minimum phase. Note that Hanus compensation scheme is akin to an explicit form of high gain AW, with D_{cr}^{-1} taking the role of α. The explicitness of the formulae may be seen as an advantage but also as a disadvantage, with perhaps more flexibility in the high-gain approach. Although controllers such as PI and PID satisfy the bi-properness requirement of Hanus conditioning, many controllers do not, making this stipulation very restrictive. A convenient way to overcome this is to perform a coprime factorisation of the controller to get

$$K(s) = V(s)^{-1}U(s) \tag{3.26}$$

and, as $V(s)^{-1}$ is by definition invertible and stable (i.e. bi-proper), it is possible to apply Hanus conditioning simply to the $V(s)^{-1}$ term of the controller. Unfortunately, it is not always clear how to choose the coprime factorisation and of course, there is no guarantee of stability (see [117, 19] for reference).

3.4.2 Modern AW Schemes

In order to circumvent the many shortcomings of "traditional" AW (lack of stability guarantees, lack of systematic design and such like) several researchers at around the early 1990's began to bring to light more systematic methods for the construction of anti-windup compensators. Although many different techniques have been proposed, ([31, 67, 37]), some of the more important and popular ones are discussed below.

Observer-based Anti-windup

Arguably, the first "modern" state-space based AW compensation method was proposed by [3] who originally called the scheme the *Generalised Anti-windup Compensator* (GAWC). Given a controller $K(s)$, Åstrom proposed that it be modified to include an observer gain (hence the name) which was driven by the difference between the actual control signal, u and the plant input (the saturated control signal) u_m. The main idea behind Åstrom's proposal was to give the controller information about the saturation level in the system, allowing the controller to adjust its output based on feasible control signal levels. The introduction of the observer gain term also tends to prevent the controller state from "winding up" to excessive values. For a two-degree-of-freedom controller, the observer-based AW compensator is described by the following state-space equations, which represent both the controller and the AW compensator

$$\dot{x}_c = A_c x_c + B_{cr} r + B_c y + H(u_m - u) \tag{3.27}$$

$$u = C_c x_c + D_{cr} r + D_c y \tag{3.28}$$

which can also be written as

$$\dot{x}_c = (A_c - HC_c)x_c + (B_{cr} - HD_{cr})r + (B_c + HD_c)y + Hu_m \tag{3.29}$$

$$u = C_c x_c + D_{cr} r + D_c y \tag{3.30}$$

Note that the a necessary condition for the stability of this AW compensator is that the matrix $A_c - HC_c$ must be Hurwitz, although again note that stability of this matrix alone *does not* guarantee closed-loop stability of the overall nonlinear closed-loop system. In fact the observer-based AW compensator could be considered as something of a generalisation of the Hanus technique (and some other techniques as well).

Although the observer-based technique offers more flexibility than some of the traditional schemes, it is still not sufficiently developed as to provide *nonlinear* closed-loop stability in all circumstances and the placement of the saturated controller poles may not be sufficient to

ensure graceful degradation of performance during saturation. The familiar structure it exhibits may be comforting but no systematic way of choosing the matrix gain H was given in early formulations, although it was clear that different choices of H produce different compensation schemes. Recent work ([12, 33]) has further developed the observer approach to provide systematic ways of synthesising the observer gain such that stability is guaranteed for certain regions of the state-space. However, note that this effectively is still simply *static* anti-windup synthesis.

When viewed through the decoupled M-structure of [118], the transfer function matrix

$$K_H(s) \sim \left[\begin{array}{c|c} A_c & H \\ \hline C_c & 0 \end{array}\right] \tag{3.31}$$

represents the part of the "observer-conditioned" controller driven by the dead-zone function $\tilde{u}$, i.e. $K_H(s)$ is the AW compensator $R(s)$ of Figure 3.5. $M(s)$ can now be represented as

$$M = (1 + KG)^{-1} K_H \tag{3.32}$$

where $M(s)$ has the following state-space representation

$$M = (I - KG)^{-1} \left[\begin{array}{c|c} A_c & H \\ \hline C_c & I \end{array}\right] \tag{3.33}$$

Something similar, although not exactly the same, to the Hanus technique for the 1-D.o.F controller case may be recovered by choosing the observer gain as $H = B_c D_c^{-1}$. This yields a matrix M of the form $M = (I - KG)^{-1} K D_c^{-1}$, where we assume that D_c is nonsingular.

Internal Model Control

Internal model control (IMC) has a rich history in linear systems theory and has often been advocated as a useful control technique. The classical internal model control scheme was appealing because, at least for stable linear plants, the level of feedback used was effectively dependent on the uncertainty present in the system. In [124] it was noted that an IMC structure was also useful for anti-windup compensation and in [107] it was identified as providing an optimally robust anti-windup solution. This property will be re-visited later in the thesis. Figure 3.7 shows the *Internal Model Control Anti-windup* (IMC AW) scheme

Essentially, the AW compensator is a copy of the nominal plant, activated during saturation and driven by the signal $\tilde{u}$. It behaves in such a manner as to ensure that the input which the controller sees during saturation is exactly that of the model of the plant during linear

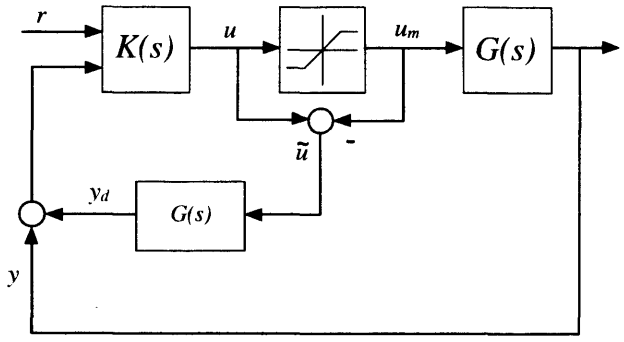

Figure 3.7: IMC Anti-windup scheme

behaviour. Effectively, this means that - for stable plants at least - the IMC AW compensator can preserve closed-loop stability in a *global* sense. In our discussion of AW compensators so far, this is a property that the aforementioned schemes do not have. One of the main criticisms of IMC control, however, is that its performance is heavily dependent on properties of the open-loop plant. Thus if the open-loop plant were to contain lightly damped modes, IMC AW can lead to very poor behaviour during saturation. It should also be mentioned that IMC AW is the only *dynamic* AW scheme considered so far.

It is interesting to give IMC an interpretation in terms of Θ and M. Simply by choosing $\Theta_1(s) \equiv 0$, it yields $\Theta_2(s) = G(s)$ (see Figure 3.7) which represents the IMC scheme in the Θ framework. Similarly, letting $M = I$, the IMC scheme in the framework of [118] is obtained. This latter interpretation provides a particularly lucid view of IMC AW as the nonlinear loop disappears ($M - I = I - I = 0$) which implies that nonlinear stability is unconditionally guaranteed. However, the disturbance filter GM reduces to simply G, implying that recovery from saturation is governed purely by the open-loop plant dynamics. Thus if the open-loop plant has poorly damped poles and such like, poor AW performance is likely to result, explaining the many criticisms leveled at IMC AW.

Kothare's unified coprime factor-based scheme

One of the first *truly modern* AW schemes was proposed in [52]. In this approach the controller is conditioned using two signals which alter the controller's output signal u and the states x_c. These signals are obtained by multiplying the control error (i.e. $u_m - u$) by two free design parameters Λ_1 and Λ_2. It was shown in [52] that most static AW schemes can be interpreted as a coprime factorisation of the controller, $K = V^{-1}U$. Using this structure, [52] proved that the proposed static compensator can be expressed as shown in Figure 3.8 where, for a 1-D.o.F.

control structure, the conditioned control signal is given by

$$u = U(s)e + (I - V(s))u_m \tag{3.34}$$

where V and U share the same state space given by

$$[U(s) \quad V(s)] \sim \left[\begin{array}{c|cc} A_c - H_1C_c & -H_1 & B_c - H_1D \\ \hline H_2C_c & H_2 & H_2D_c \end{array}\right] \tag{3.35}$$

Notice that $A_c - H_1C$ must be stable in order to preserve internal stability of the closed-loop compensated system. The coprime factorisation and the static gains Λ_1 and Λ_2 are related through the following equalities

$$\begin{aligned} H_1 &= \Lambda_1(I + \Lambda_2)^{-1} \\ H_2 &= (I + \Lambda_2)^{-1} \end{aligned} \tag{3.36}$$

It is possible to interpret Kothare's scheme as in [118] by finding a transfer function M which captures the role of V. Combing equations (3.34) and (3.4) we obtain,

$$u = K(s)e + (I - V(s)^{-1})\tilde{u}$$

Equating this with equation (3.7), some simple algebra reveals that

$$M = (I + KG)^{-1}V^{-1} \tag{3.37}$$

Thus Kothare's scheme ([52]) and Weston's scheme ([118]) are similar, except one is interpreted as a coprime factorisation of the controller; the other is interpreted as the choice of a free parameter, M,which may have an interpretation as a coprime factorisation of the plant.

In [52], a design approach for a static anti-windup compensator was suggested; the matrices H_1 and H_2, and thus the AW compensator, were found through an appropriate optimisation problem. Again, it is interesting to notice that particular choices of H_1 and H_2 correspond to some of the popular traditional AW compensators: the Hanus conditioning scheme is obtained when $H_1 = BD_c^{-1}, H_2 = I$; the GAWC method makes the choice $H_2 = I$. In fact, Kothare's scheme is the most general static compensation scheme. They also proposed a design procedure in which dynamic AW compensation is possible using a direct one-step synthesis and then back calculating the AW compensator. This procedure is different from standard linear conditioning as the controller and the AW compensator are synthesised simultaneously. More recently a more rigorous LMI-based method was proposed in [67] - this guaranteed nonlinear stability of the closed-loop system but, as the AW compensators were restricted to being of the static type, for arbitrary plant-controller combinations such compensators may not always exist.

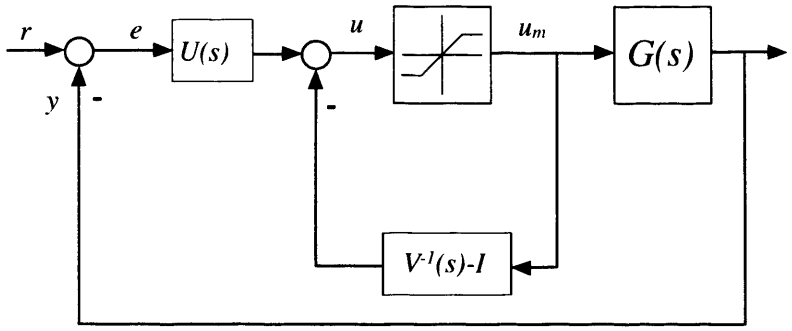

Figure 3.8: Kothare's compensation using coprime factors of the controller

Miyamoto and Vinnecombe's coprime factor-based scheme

The compensators discussed up until this point have not been entirely satisfactory from the perspective of stability and performance: in some methods these concerns have been ignored entirely; in others such as Kothare's ([52, 67]) method, they have only partially been dealt with.

However, [65] extended Kothare's method by allowing the coprime factorisation of the controller to be *non-minimal*; given an initial coprime factorisation, i.e. $K = V_0^{-1}U_0$, the controller can be factored using $U = QU_0$ and $V = QV_0$, where Q is such that Q, $Q^{-1} \in \mathcal{H}^\infty$ and is found by solving an $\mathcal{H}^\infty$ optimisation problem. The closed-loop is guaranteed stable through the small gain theorem and nonlinear performance (see also [16]) is addressed by minimising certain transfer functions that indicate the effects of the saturation on the plant input and output. The system in Figure 3.8 can be seen as the system with a perturbation shown in Figure 3.9 where $\|\Delta\|_\infty \leq 1$. The optimisation problem proposed in [65] is

$$\inf_{Q,Q^{-1}\in H_\infty} \left\| \begin{bmatrix} W_1 G_{u_m d} \\ W_2 G_{yd} \\ G_{ud} \end{bmatrix} \right\|_\infty < 1$$

where G_{ud}, $G_{u_m d}$, and G_{yd} are the transfer functions from the fictitious disturbance signal d to the control action signals u, u_m, and the system output y respectively. One of the main contributions of [65] is that stability is guaranteed if $\|G_{ud}\|_\infty < 1$ (SGT), and a clear performance index is introduced as an essential part of AW design. This is achieved by minimising the weighted induced norms from the disturbance d to y and u_m. Using the Bezout identity i.e. $V_0 M + U_0 N = I$, where M and N are a coprime factorisation of the plant (i.e. $G = NM^{-1}$), it is easy to observe that

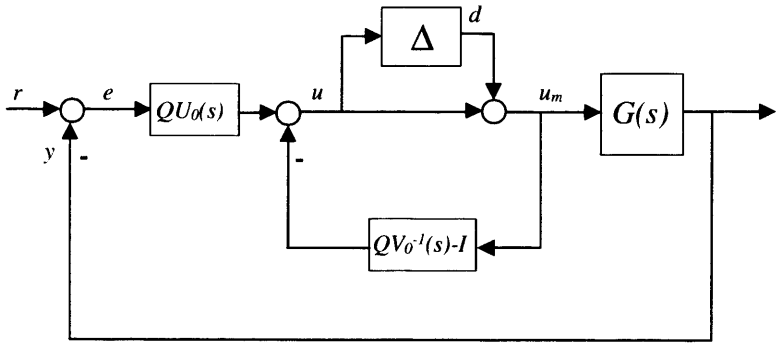

Figure 3.9: Miyimoto & Vinnicombe coprime factor approach

$$\begin{aligned} G_{ud} &= -I + MQ^{-1} \\ G_{yd} &= NQ^{-1} \\ G_{u_m d} &= MQ^{-1} \end{aligned}$$

The formulation shows a very strong link between AW compensation performance and stability, and the coprime factors of the plant.

From equation (3.37) it follows that

$$M = (I + KG)^{-1} V_0^{-1} Q^{-1} \tag{3.38}$$

It is easily shown that M will always be bi-stable, a necessary condition for stability of the nonlinear loop. If $Q = I$, no extra states are added (i.e. static AW compensation) and Kothare's conditioning framework is obtained. This does not always render a stabilising controller and $Q \neq I$ may be required. This will allow for non-minimal coprime factors, introducing extra states to the closed-loop compensated system and generating dynamic (low or full order) AW compensators.

Direct Model Schemes

Until now, most of the compensation schemes (with the exception of the IMC AW) were concerned with acting on the controller irrespective of the nominal plant. The design schemes mentioned tried to reduce the effect of the saturation over some input/output control signal, but took no interest in the plant's behaviour. For example, the Hanus conditioning scheme compensates the original reference signal entering the controller. Alternatively, compensation may be performed on the plant output y before it is used by the controller. [77] develops such a technique and it is termed *model based conditioning.* The scheme is presented in block diagram form in Figure 3.10, where G_m is a user defined transfer function which is usually referred to

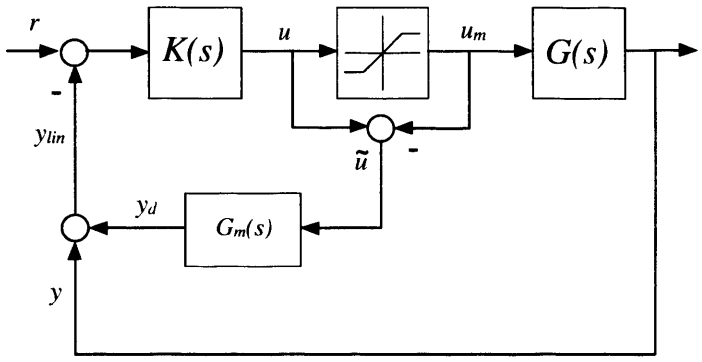

Figure 3.10: IMC like compensation scheme

as the *direct model*. G_m is generally chosen to be an exact copy of the nominal plant model, in which case, and in the absence of plant uncertainty, the input to K_2 is always given by Gu irrespective of the plant input u_m. Notice that in order for the compensation signal to disappear it is necessary for G_m to be stable. It follows that

$$M = (I - K_2G)^{-1}(I - K_2G_m) \tag{3.39}$$

where M is bi-stable only if the nominal closed loop G_{cl}, G_m and $(I - K_2G_m)^{-1}K_2$ are all stable. In addition, and in order to preserve internal stability, $(I - K_2G_m)^{-1}K_1$ must also be stable.

It is clear that if $G_m = G$, the IMC AW scheme is recovered as a special case where $M = I$, making the nonlinear loop completely disappear and providing unconditional nonlinear stability. However, as aforementioned if the open loop nominal plant has any lightly damped poles, the system's performance will normally be unsatisfactory. In this case it is desirable to choose a different transfer function matrix for G_m such that some improvement over the choice of G is made. Although not much work has been done in this respect, the optimisation approach presented by [21] will be described as it gives a novel design procedure for choosing the direct model G_m.

In [21] an $\mathcal{H}^\infty$ optimisation framework was suggested for the purpose of choosing $G_m(s)$. The underlying goal is to choose G_m such that the $\mathcal{H}^\infty$ norm of various transfer functions, thought to capture "good" anti-windup performance, is minimised. The $\mathcal{H}^\infty$ optimisation framework also enabled the controller-AW loop to be guaranteed stable, although no explicit nonlinear stability guarantees were sought. Figure 3.11 shows the subsystem of Figure 3.10 which forms the basis of the $\mathcal{H}^\infty$ optimisation problem proposed. The $\mathcal{L}_2$ gain of the transfer functions relating the signals u_m and e to $\tilde{u} = u - u_m$ and u_d were minimised in order to ensure that good performance during saturation occurs and internal stability of Figure 3.11 results. From

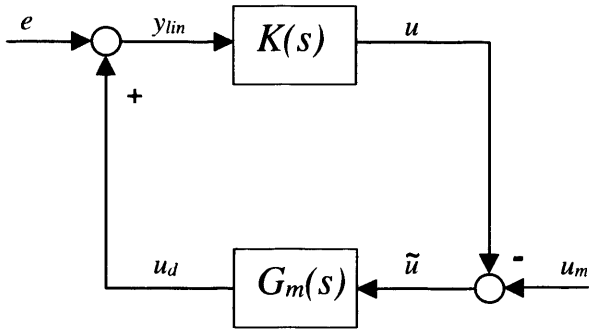

Figure 3.11: Subsystem of an IMC like compensation scheme

Figure 3.11 it follows that

$$u_m - u = Su_m - SKe$$

where $S = (I - KG_m)^{-1}$ is the *sensitivity function.* Notice that the error $u - u_m$ can be made "small" by making G_m "large"; however, this will make the signal leaving G_m "large". These requirements can be captured in a sensible $\mathcal{H}^\infty$ problem formulation where both the error $u - u_m$ and the feedback compensation signal produced by G_m are minimised. The associated *Generalised Regulator Problem* (see [34]) can be expressed as

$$\min_{\text{stab. } G_m} \left\| \begin{array}{cc} W_1 S & -W_1 SK \\ W_2 G_m S & -W_2 G_m^{-1} SK \end{array} \right\|_\infty$$

where W_1 and W_2 are appropriate frequency domain weighting functions used to emphasise the importance of each objective over different frequency ranges. It is worth mentioning that this procedure does not guarantee stability of the nonlinear loop but provides a systematic approach for choosing an appropriate direct model. In other words, if stability is guaranteed *a posteriori*, then the system will have good nonlinear performance.

3.5 Concluding Remarks

This chapter has reviewed many of the existing popular AW methods and has given interpretations of these in terms of the de-coupled representation proposed in [116, 118]. This interpretation is attractive because the properties of the nonlinear saturated system appear as a "disturbance" to the nominal linear system and the stability problem is reduced the the stability of the so-called nonlinear loop. Thus the anti-windup stability and performance properties are easier to interpret and analyse in this framework.

It may be noticed that due to the rather organic emergence of various AW strategies, one can often interpret certain schemes as special cases of others. This may be illuminating in some cases and comforting for the practical engineer, but it should be emphasised that typically these various interpretations do not allow for stability and performance to be captured as conveniently as with the approach of [116, 118].

The schemes reviewed in this chapter are typically those which have some historic importance attached to them; either they are widely used in practice (e.g. [40]) or they are landmarks in the history of AW compensators (e.g. [52]). Since the work on this thesis began, a number of AW compensation schemes which guarantee stability with more rigour have recently emerged. The work of Teel and coworkers should particularly be mentioned and the interested author is referred to [105, 122, 35] for this work. However some of Teel's work can be interpreted in the framework of Weston ([116, 118]), so we do not devote much attention to this.

Other important work can be found in the area of anti-windup for exponentially unstable systems, where stability can only be guaranteed for certain regions of the state-space (or equivalently certain sizes of reference/disturbance). Pioneers in this area are Tarbouriech and co-authors, Gomes da Silva and co-authors, Lin and co-authors. The construction of AW compensators for systems with exponentially unstable modes is considerably harder than the construction for asymptotically stable systems as it is difficult to find a good estimate of the region of attraction which accompanies the compensator. Although this topic is of some importance, most of the work in this thesis is geared towards AW for asymptotically stable linear systems. The interested reader is encouraged to consult the references [15, 104, 100] for information about AW for exponentially unstable systems.

It is hoped that this chapter has given a broad overview of the most important AW schemes available today and has highlighted much of the informality which currently accompanies their design. In the coming chapter it will be shown how more rigour can be incorporated into the design of AW compensators and how a computationally convenient tool, the Riccati equation, can be used in their synthesis.

Chapter 4

Anti-windup compensation for stable systems with input saturation

Chapter 3 gave an overview of existing compensation schemes which have played important roles in the evolution of modern AW strategies. As mentioned at the end of Chapter 3, recent years have seen a large increase in the number of AW schemes proposed and now many of these recent strategies are able to ensure nonlinear closed-loop stability, although few of these have been implemented ([16, 37, 26, 90, 35, 31, 84]) in practical control applications.

Most of the above schemes concentrate on guaranteeing stability for *stable* plants, i.e. $G(s) \in \mathcal{RH}_\infty$, as it is well known that such plants admit *globally stabilising* control strategies despite the presence of input saturation ([37], [105]). Indeed, it is also the case that there *always exists* an anti-windup compensator which can globally stabilise such systems; this is only guaranteed in general if the AW compensator is of the same order as the plant, i.e. the compensator is full-order [35]. This existence property greatly simplifies the analysis of such systems as there is no need to establish regions in which stability is achieved; it is always possible obtain global stability. Conversely, stability analysis for marginally or exponentially unstable systems becomes more problematic and one may be forced to conduct local or semi-global stability analysis (see [32] for example). This is particularly pertinent for exponentially unstable plants as such systems do not admit a globally stabilising *bounded* control strategy. Therefore, the anti-windup strategy only achieves asymptotic stability within a subset of the state-space. Despite such intricacies, the general success in terms of stability guarantees of AW compensation schemes has galvanised the research community into seeking guarantees beyond those of stability, and has brought to the fore the problem of anti-windup performance.

Research on anti-windup has then, over recent years, attempted to secure performance guarantees [67, 110] in addition to the already established stability guarantees. As a system containing

saturation is inherently nonlinear, it is more difficult to quantify precisely what "performance" means in the context of AW compensation, and few of the usual linear tools shed any light on how the problem may be solved. One of the first attempts to establish this notion in a concrete manner was made in [67], where the $\mathcal{L}_2$ induced norm of a certain system was chosen as an appropriate measure of the AW compensator's performance. It was later shown by [37] that there always exists an AW compensator of order equal or greater to that of the plant such that finite $\mathcal{L}_2$ gain constraints are ensured. This complemented known results (see for example [105], [118], and [65] amongst others) where, as mentioned earlier, global stability for stable nominal plants is shown to always be possible via full-order AW compensation.

In formulations such as [37], [67], and more recently [122], the performance index (or $\mathcal{L}_2$ gain condition) is not directly related with the system's return to linear behaviour, this being the implicit goal of most anti-windup strategies ([52]). In fact, it is difficult to directly capture this notion of performance using the schemes advocated in these papers. Instead these papers seek to minimise an appropriate closed-loop induced norm which is thought to be closely related to the performance of the overall closed-loop system. The general setup of this problem is shown in Figure 4.1 where $T(s)$ is the "generalised plant" formed by the combination of the nominal linear controller $K(s)$, the linear plant $G(s)$ without input saturation, and the linear anti-windup compensator $\Theta(s)$. Here $z \in \mathbb{R}^{n_z}$ is a vector of performance objectives which should be minimised, and $w \in \mathbb{R}^{n_w}$ is a vector of exogenous inputs. The feedback loop contains the dead-zone function which represents the effect of saturation on the system (Recall: $\text{sat}(u) = u - \text{Dz}(u)$). The crucial point here is that [67, 35] did not give guidelines for the choice of the performance objectives and although choosing the control error $z = r - y$ may be useful, it is *not precisely* the objective of AW, which is to minimise the deviation from linear (ideal) performance.

In contrast, the M-parametrisation discussed in the previous chapter (introduced in [118]) proposed a decoupled structure which allowed the problem of anti-windup performance to be captured in a clear and intuitive way, exposing the manner in which a system's saturated dynamics would deviated from the nominal linear dynamics. Works such as [110], [90], [61], have exploited this structure and have posed minimisation problems that ensure both stability and performance for the synthesis of static, low-order and full-order AW compensators. In such a set-up, the obvious choice for minimisation would be the size of the map from u_{lin} to y_d, as depicted in Figure 4.3. This is in agreement with the implicit goal of deviating as little as possible from linear behaviour and is also an obvious choice from the architecture.

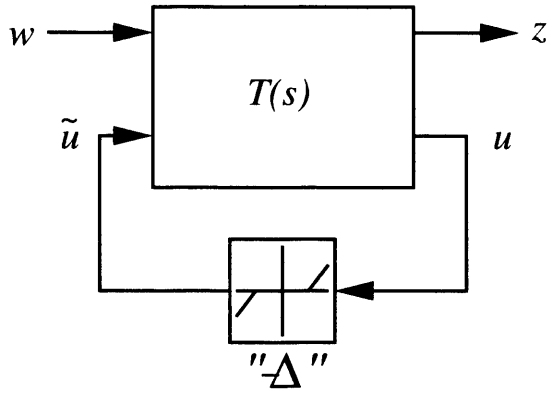

Figure 4.1: Generic AW problem considered in [67]

Another issue that needs to be accounted for when designing AW compensation is robustness to plant uncertainty. Although robustness to uncertainty has been studied in the control literature for many years, it is conspicuously absent from most anti-windup literature. The implicit assumption appears to be that the saturated closed-loop system with anti-windup will inherit similar robustness properties to those of the nominal linear system. As shown in [107], this is not always the case.

This chapter will deal with both the standard (uncertainty free) and robust AW problems and will establish conditions which ensure that the *natural anti-windup problem* is solved - that is, deviation from linear performance is minimal (in the $\mathcal{L}_2$ sense). The problem set-up is essentially the same as in [110, 107] but the synthesis method is novel as the anti-windup compensator is obtained via the solution of a single bounded-real type Riccati equation, offering a numerically superior way of obtaining AW compensators than the "usual" LMI techniques. It is further shown that the synthesis method developed in this thesis gives a *family* of anti-windup compensators which are obtained by adjusting a single diagonal matrix and require no re-solving of the Ricatti equation. This parametrisation is noteworthy as the free matrix W influences the location of the AW compensator poles and also its robustness properties. Much of the work from this chapter has been published in [91] and also in [90].

4.1 Problem Description (no uncertainty)

This section defines in detail the *standard anti-windup problem* considered in the remainder of the thesis. To begin with, the robustness aspects of the problem are ignored; these will be introduced in subsequent sections.

4.1.1 Nominal system description

The open-loop plant $G(s)$ considered is the same as that described in Chapter 3.1. The plant is assumed FDLTI (finite dimensional linear time invariant) with state-space realisation

$$G(s) \sim \begin{cases} \dot{x} &= Ax + Bu_m \\ y &= Cx + Du_m \end{cases} \tag{4.1}$$

where $x \in \mathbb{R}^{n_p}$ is the plant state, $u_m \in \mathbb{R}^m$ is the plant input (saturated control signal) and $y \in \mathbb{R}^q$ is the plant output, which is fed back to the controller. For simplicity disturbances are not considered although they can easily be accounted for (see [118],[110]). The *nominal plant* transfer function is denoted as:

$$G(s) \sim \left[\begin{array}{c|c} A & B \\ \hline C & D \end{array}\right] \tag{4.2}$$

As mentioned earlier, in order for global stability results to be obtained, it is necessary for the plant to be stable; formally the following assumption is made

Assumption 1 *The poles of the nominal plant $G(s)$ are all in the open left-half of the complex plane; equivalently $G(s) \in \mathcal{RH}_\infty$* □

It is assumed that a nominal 2-D.o.F. linear controller $K(s)$ (for the 1-D.o.F. case choose $K_2 = -K_1$), defined by

$$u = \underbrace{[K_1(s) \quad K_2(s)]}_{K(s)} \begin{bmatrix} r \\ y \end{bmatrix}, \tag{4.3}$$

has been designed to meet standard linear performance and robustness specifications. In particular, it is important that the nominal closed-loop system is (internally) stable in the absence of saturation and also that the system is well-posed. Formally this can be stated as requiring that

Assumption 2

$$\begin{bmatrix} I & -K_2(s) \\ -G(s) & I \end{bmatrix}^{-1} \in \mathcal{RH}_\infty \tag{4.4}$$

and

$$\lim_{s \to \infty} K_2(s)G(s) \neq I \tag{4.5}$$

□

4.1.2 Saturation Description

The saturation function, as defined in Section 3.1, is a nonlinear function which has a simple graph but can be complex to handle mathematically due to its non-smooth and non-bijective nature. The interesting feature, which will be repeated here for convenience, is that it satisfies the identity

$$\text{sat}(u) + \text{Dz}(u) = u \tag{4.6}$$

All the following analysis will take place by using the above identity to replace the saturation nonlinearity. In order to accommodate these nonlinearities, the following analysis relies heavily on *sector bounds*, as described in Chapter 2. Both the saturation and deadzone function belong to Sector$[0, I]$, viz

$$\text{sat}(.) \in \text{Sector}[0, I], \quad \text{Dz}(.) \in \text{Sector}[0, I]$$

Formally a decentralised nonlinear element is said to belong to the Sector$[0, I]$ if it satisfies the following definition

Definition 4.1 *The decentralised nonlinearity* $\mathcal{N} = \text{diag}(\eta_1, \ldots, \eta_m)$ *is said to belong to* Sector$[0, I]$ *if the following inequality holds:*

$$\eta_i(u_i)^2 \leq \eta_i(u_i)u_i \leq u_i^2 \quad \forall\, i \in \{1, \ldots, m\} \tag{4.7}$$

□

This definition is a special case of the more general formulation given in Chapter 2 (see also [48]) and initially, a Sector$[0, I]$, is sufficient for our purposes. This will allow us to formulate an $\mathcal{H}^\infty$ -type optimisation problem using the Circle Criterion; one of the resulting feasibility conditions being a Riccati equation of the Bounded Real type.

It must be pointed out that there are more accurate ways of bounding the saturation and dead-zone functions (see [45] for example), although this improved accuracy must be balanced against the extra difficulty in accommodating this within the stability and performance problem to be considered. For instance, in [45], the saturation function is expressed in terms of an $\mathcal{L}_1$ norm bound, i.e. $sat(u) = Hu$ where $\|H\|_1 \leq 1$. Similar approximations can be found in [102].

4.1.3 Anti-windup compensator description

As mentioned in Chapter 3, the plant input $u_m \in \mathbb{R}^m$ is given by the nonlinear saturation function as defined in equation (3.2). If there is no saturation present, $sat(u) = u$ and *nominal*

linear closed-loop dynamics govern the system. One of the central themes in anti-windup conditioning is that the compensator is not active unless saturation occurs, and for this reason the anti-windup compensator is driven by the difference between the unsaturated and saturated control signal, that is

$$\tilde{u} := u - \text{sat}(u) = \text{Dz}(u) \tag{4.8}$$

Effectively this means that assuming saturation never occurred - providing the anti-windup compensator had zero initial conditions - then no corrective action would take place.

In keeping with the architecture described in the previous chapter (and [118]), our anti-windup compensator is parametrised as follows:

$$\begin{bmatrix} \Theta_1 \\ \Theta_2 \end{bmatrix} = \begin{bmatrix} M - I \\ GM \end{bmatrix} \tag{4.9}$$

where $M(s)$ is a stable transfer function matrix. Although this may not be the most general description of an AW compensator, as argued in Chapter 3, this is an attractive architecture due to its decoupling properties. One of the problems with this characterisation is that any compensator designed using this method would potentially be of rather large order, $n_p + n_M$ for example, where n_M is the order of the transfer function matrix $M(s) \in \mathcal{RH}_\infty$. In order for the compensator to have a reduced number of states, some pole-zero cancellations between $G(s)$ and $M(s)$ would be necessary. In fact, in this chapter we accomplish this and insist that $M(s)$ is part of a coprime factorisation of the plant, $G(s) = N(s)M(s)^{-1}$, as suggested by [118]. Using the same architecture and choosing $M(s)$ as some combination of the nominal controller and plant, not as part of this coprime factorisation, [110] and [107] developed methods for static and low order AW compensation based on LMI optimisation. One of the main problems with static and low order conditioning is that there is *no guarantee* that one of these schemes will globally stabilise the system in question. In contrast, there always exists a full-order AW compensator, providing the plant is open-loop stable (see [35]), which globally stabilises a linear control system with saturation, regardless of $K(s)$. Furthermore, as the coprime factor based anti-windup compensator is a type of full order compensator, we can expect that one will always exist providing that Assumption 1 is satisfied. Hence it is this type of compensator which the remainder of the chapter will focus on. Another appealing aspect of making this choice of $M(s)$ is that all coprime factorisations of order equal to the plant can, up to multiplication by

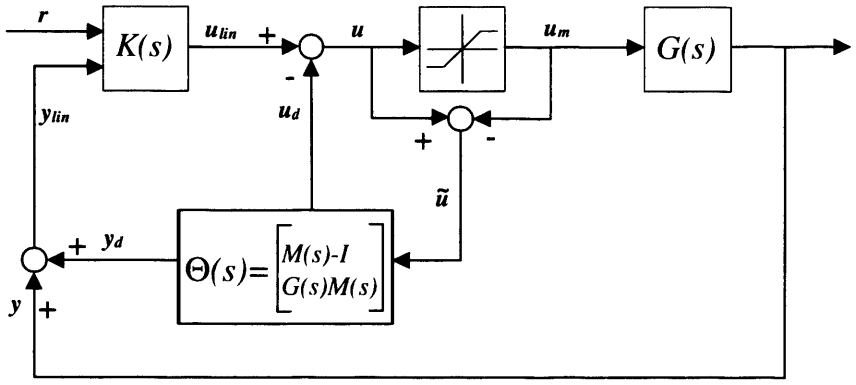

Figure 4.2: Conditioning with $M(s)$

a nonsingular constant matrix, be described by the state-space equations

$$\begin{bmatrix} M-I \\ N \end{bmatrix} = \left\{ \begin{array}{rcl} \dot{x} & = & (A+BF)x + B\tilde{u} \\ u_d & = & Fx \\ y_d & = & (C+DF)x + D\tilde{u} \end{array} \right. \tag{4.10}$$

where F is a free parameter and $A+BF$ must be Hurwitz. Thus, the problem of designing a full-order anti-windup compensator becomes that of choosing an appropriate right coprime factorisation, which in turn reduces to that of choosing an appropriate state-feedback gain matrix F. Therefore, the results of this chapter will offer an alternative synthesis procedure and a simpler insight into full-order anti-windup compensation than the rather involved and unwieldy results in [35].

4.2 Performance AW Problem definition

Characterising the main objective of AW compensation is subjective but the general underlying idea is simple:

We require a fast and smooth return to linear behavior after saturation([52], [105])

We term this objective the *true goal* of anti-windup compensation and this section attempts to define this mathematically. Although many different formulations have arisen (see some of the references given earlier) few have been able to address successfully the *true goal* of AW in a general, systematic and intuitive way.

It is again instructive to consider Figure 4.2, which can be equivalently represented as Figure 4.3. From the latter figure, conditions which ensure the recovery of linear behaviour may be inferred. More specifically, providing that (i) the nonlinear loop is asymptotically stable and (ii) the transfer function $G(s)M(s) = N(s) \in \mathcal{RH}_\infty$, then linear behaviour will eventually

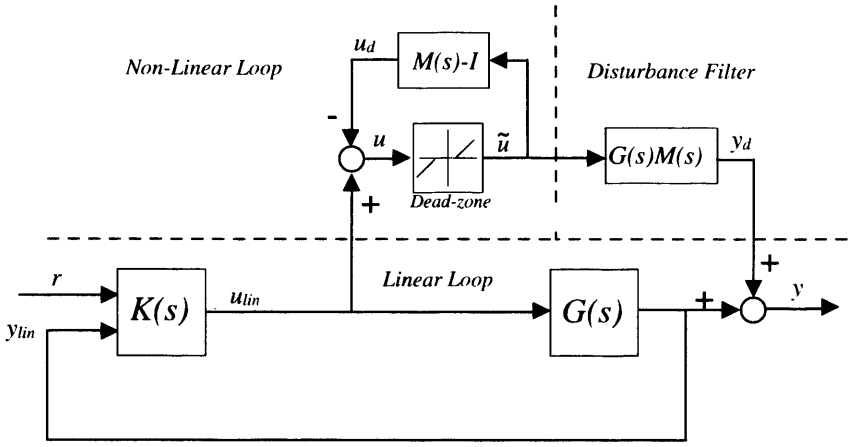

Figure 4.3: Decoupled structure

resume providing the linear control signal u_{lin} falls below the magnitude limits in steady state, that is after some finite time, $T \in (0, \infty)$, $u_{lin} \in \mathcal{U}$ $\forall t > T$. Thus, from a certain perspective, the anti-windup problem could be viewed simply as a nonlinear stability problem. However, from Figure 4.3, observe that our intuitive objectives for good anti-windup performance can be accomplished if the map from u_{lin} to y_d is made "small" in some sense. If this was the case, then the deviation from linear behaviour would be, in some sense, "small". This elevates the anti-windup problem from a pure stability problem into one which also considers performance. Therefore the aim of this chapter will be to give synthesis algorithms for AW compensators which (*iii*) make the $\mathcal{L}_2$ gain of $\mathcal{T}_p : u_{lin} \mapsto y_d$ as small as possible. The clear association between the size of the map $\mathcal{T}_p : u_{lin} \mapsto y_d$ and loss of linear performance will allow us to pose a mathematically rigorous and suitable definition of the problem to be addressed. This is formally encapsulated in the following formulation

Problem 1 *The AW compensator (4.10), is said to solve the anti-windup problem if the closed loop system in Figure 4.3 is stable and well-posed and the following hold:*

1. *If* $\text{dist}(u_{lin}, \mathcal{U}) = 0, \quad \forall t \geq 0$, *then* $y_d = 0, \quad \forall t \geq 0$ *(assuming zero initial conditions for* $M(s)$*).*

2. *If* $\text{dist}(u_{lin}, \mathcal{U}) \in \mathcal{L}_2$, *then* $y_d \in \mathcal{L}_2$.

The AW compensator is said to solve strongly the anti-windup problem *if, in addition, the following condition is satisfied:*

3. *The operator* $\mathcal{T}_p : u_{lin} \mapsto y_d$ *is well-defined and finite gain* $\mathcal{L}_2$ *stable.*

□

The various parts of this problem have the following interpretations:

i) As $\mathcal{U}$ represents the set within which no saturation occurs, or the set in which $\mathrm{Dz}(u) = 0$, if $\mathrm{dist}(u_{lin},\mathcal{U}) = 0, \quad \forall t \geq 0$ then it is implied that u_{lin} has never strayed outside the set $\mathcal{U}$ and hence, the control signal has not saturated. In this case no deviation from linear behaviour is present as $\mathrm{Dz}(u) = 0$, which in turn yields $y_d = 0, \quad \forall t \geq 0$.

ii) If u_{lin} *does* stray outside the set $\mathcal{U}$, and therefore saturation does occur at some point but then in steady state returns to within the saturation bounds, then $\mathrm{dist}(u_{lin},\mathcal{U}) \in \mathcal{L}_2$, assuming $\mathrm{dist}(u_{lin},\mathcal{U})$ is continuous, which is guaranteed provided u_{lin} is piecewise continuous. In this case, it is desirable to eventually recover linear performance and hence the signal $y_d(t)$ to asymptotically to decay to zero. This is ensured if $y_d \in \mathcal{L}_2$, which is guaranteed providing the nonlinear loop was asymptotically stable and $N(s) \in \mathcal{RH}_\infty$.

iii) The amount of deviation from linear performance generated by a given input u_{lin} depends on the size of the resulting signal y_d. Hence minimising the $\mathcal{L}_p$ gain of $\mathcal{T}_p$ is a natural objective to ensure certain level of performance. As the $\mathcal{L}_2$ version of this problem is known to be numerically tractable, this case is considered.

Note the map $\mathcal{T}_p$ is nonlinear and it involves the dynamics of the *nonlinear loop*. It is possible to pose an appropriate optimisation problem consisting of three main parts: a Lyapunov equation guaranteeing stability of the compensators, an $\mathcal{L}_2$ gain minimisation problem and some formulation of the Circle Criterion which guarantees stability of the *nonlinear loop*. The next section of the chapter solves the problem of ensuring

$$\underbrace{\frac{d}{dt}x'Px}_{\dot{V}(x)} + \underbrace{\|y_d\|_2^2 - \gamma^2\|u_{lin}\|_2^2}_{\mathcal{L}_2 \ \ gain} + \underbrace{2\tilde{u}'W(u-\tilde{u})}_{\text{Sector bound}} < 0 \tag{4.11}$$

which ensures asymptotic stability of the nonlinear loop, i.e. $\|\mathcal{T}_p\|_{i,2} < \gamma$.

4.2.1 Solution of the Performance AW Problem

The problem of stability and performance is addressed by minimizing the $\mathcal{L}_2$ gain of $\mathcal{T}_p : u_{lin} \mapsto y_d$, or alternatively finding the minimum $\gamma > 0$ such that $\|\mathcal{T}_p\|_{i,2} < \gamma$, while simultaneously ensuring that the nonlinear loop is stable. The following procedure not only allows the synthesis of an optimal compensator, but also guarantees global asymptotic stability and gives a measure

of global performance provided that the plant $G(s)$ is assumed asymptotically stable. The main result of the section is the following theorem.

Theorem 4.1 *There exists a full order anti-windup compensator* $\Theta = [\theta_1' \quad \theta_2']' \in \mathbb{R}^{(m+q)\times m}$, *as described by equations (4.9) and (4.10), which solves Problem 1 if there exist matrices* $P = P' > 0$, $W = \text{diag}(\omega_1, \ldots, \omega_m) > 0$ *and a positive real scalar* γ *such that the following Riccati equation is satisfied*

$$\tilde{A}'P + P\tilde{A} + PBR^{-1}B'P + \tilde{Q} = 0 \tag{4.12}$$

where

$$\tilde{A} = A + BR^{-1}D'C \tag{4.13}$$

$$\tilde{Q} = C'(I + DR^{-1}D')C \tag{4.14}$$

$$R = (\gamma^2 I - D'D) > 0 \tag{4.15}$$

and the following inequality holds

$$Z = (2W - D'D - \gamma^{-2}W^2) > 0 \tag{4.16}$$

Furthermore, if equation (4.12) and inequality (4.16) are satisfied, a suitable Θ *achieving* $\|\mathcal{T}_p\|_{i,2} < \gamma$ *is obtained by calculating the matrix gain* F *in (4.10) as follows:*

$$F = -\gamma^2(W^{-1} - \gamma^{-2})R^{-1}(B'P + D'C) \tag{4.17}$$

□

Proof: To aid our proof we will need the following identity:

Lemma 4.1 *(Completing the square) Given vectors* $x \in \mathbb{R}^n, y \in \mathbb{R}^m$, *matrices* $X \in \mathbb{R}^{n\times p}, Y \in \mathbb{R}^{p\times m}$ *and scalar* α

$$(\alpha Xx - \alpha^{-1}Yy)'(\alpha Xx - \alpha^{-1}Yy) = \alpha^2 x'X'Xx + \alpha^{-2}y'Y'Yy - x'X'Yy - y'Y'Xx$$

□

In order to solve strongly the AW compensation problem, it is necessary to meet the conditions stated in Problem 1. It is easy to observe that the first two conditions are trivially met if internal stability of the closed-loop compensated system is guaranteed. As will be shown later,

by choosing F as described in Theorem 1, it is possible to guarantee $\|\mathcal{T}_p\|_{i,2} < \gamma$ for any $\gamma > \|G\|_\infty$, therefore solving strongly the AW compensation problem.

For algebraic simplicity, we consider the case where $D = 0$ (the proof when $D \neq 0$ involves much more algebra and hence is solved in appendix A).

Note that as Dz(.) $\in$ Sector[0, I], it follows that for some matrix $W = \text{diag}(\omega_1, \ldots, \omega_m) > 0$

$$\tilde{u}'W(u - \tilde{u}) \geq 0 \tag{4.18}$$

Next assume there exists $V(x) = x'Px > 0$, then if

$$L(x, u_{lin}, \tilde{u}, F, W) \;:=\; \frac{d}{dt}x'Px + \|y_d\|^2 - \gamma^2\|u_{lin}\|^2 + 2\tilde{u}'W(u - \tilde{u}) \tag{4.19}$$

is negative definite, it follows that $\dot{V}(x) < 0$ is a Lyapunov inequality and the closed-loop system is stable. Also notice that if $L(x, u_{lin}, \tilde{u}, F, W) < 0$ and assuming zero initial conditions, integrating $L(.)$ in the time interval from 0 to T and taking the limit $T \to \infty$, yields $\|y_d\|_2 < \gamma\|u_{lin}\|_2$ and hence $\|\mathcal{T}_p\|_{i,2} < \gamma$. Thus, if equation (4.19) is negative definite, the strong anti-windup problem is solved in the $\mathcal{L}_2$ sense.

Expanding (4.19) and substituting $u = u_{lin} - u_d$ gives

$$L = x'C'Cx - \gamma^2 u'_{lin}u_{lin} + \dot{x}'Px + x'P\dot{x} - 2\tilde{u}'Wu_d - 2\tilde{u}'W\tilde{u} + 2\tilde{u}'Wu_{lin} \tag{4.20}$$

This inequality contains several cross-terms in $x, \tilde{u}, u_{lin}$. We now eliminate the cross-product terms in three steps using Lemma 4.1.

(I) The cross-product terms involving u_{lin} and $\tilde{u}$ can be grouped as follows:

$$-\left[\gamma^2 u'_{lin}u_{lin} - 2\tilde{u}'Wu_{lin}\right] = -\|\gamma u_{lin} - \gamma^{-1}W\tilde{u}\|^2 + \gamma^{-2}\tilde{u}'W^2\tilde{u}$$

Combining the above with (4.20), a cost function containing no cross-product terms between u_{lin} and $\tilde{u}$ is obtained. Using equation (4.1) to expand $\dot{x}$ and noticing from equation (4.10) that $u_d = Fx$:

$$L = x'(A'P + PA + 2PBF + C'C)x + 2\tilde{u}'(B'P - WF)x - \tilde{u}'(2W - \gamma^{-2}W^2)\tilde{u} - \|\gamma u_{lin} - \gamma^{-1}W\tilde{u}\|^2$$

(II) The cross-product terms involving $\tilde{u}$ and x can be grouped, including the extra term $\gamma^{-2}\tilde{u}'W^2\tilde{u}$ from **(I)**, as follows:

$$-\left[\tilde{u}'(2W - \gamma^{-2}W^2)\tilde{u} - 2\tilde{u}'(B'P - WF)x\right] =$$
$$-\|Z^{\frac{1}{2}}\tilde{u} - Z^{-\frac{1}{2}}(B'P - WF)x)\|^2 + x'(B'P - WF)'Z^{-1}(B'P - WF)x$$

Note that $Z = (2W - \gamma^{-2}W^2)$ must be positive definite in order to have a well-posed problem, and hence the condition in equation (4.16) is imposed. This condition arises from the necessity to define the real square root term $Z^{\frac{1}{2}}$ which exist in

$$\|Z^{\frac{1}{2}}\tilde{u} - Z^{-\frac{1}{2}}(B'P - WF)x\|^2 \tag{4.21}$$

positive definite for any pair $(\tilde{u}, x)$. It can easily be shown that if $Z \leq 0$, this is not always guaranteed. By replacing this new group of terms, the cost function can be written with no cross-product terms between $\tilde{u}$ and x:

$$\begin{aligned} L = x'(A'P + PA + C'C + 2F'B'P + PBZ^{-1}B'P - 2PBZ^{-1}WF + F'WZ^{-1}WF)x \\ -\|Z^{\frac{1}{2}}\tilde{u} - Z^{-\frac{1}{2}}(B'P - WF)x\|^2 - \|\gamma u_{lin} - \gamma^{-1}W\tilde{u}\|^2 \leq 0 \end{aligned}$$

(III) The terms involving F and $F'F$ can be grouped as follows:

$$\begin{aligned} F'WZ^{-1}WF - 2F'((WZ^{-1}B'P - B'P) = \\ \|Z^{-\frac{1}{2}}WF - Z^{\frac{1}{2}}W^{-1}(WZ^{-1} - I)B'P\|^2 - PB(WZ^{-1} - I)'W^{-1}ZW^{-1}(WZ^{-1} - I)B'P \end{aligned}$$

This last step will yield an expression for the matrix gain F. Finally, by using the results given in **(III)** we obtain an expression for our cost function (4.19) as

$$L(x, u_{lin}, \tilde{u}, F, W) = L_a + L_b + L_c \tag{4.22}$$

where

$$L_a = x'(C'C + A'P + PA + PBZ^{-1}B'P - PB(Z^{-1} - W^{-1})'Z(Z^{-1} - W^{-1})B'P)x \tag{4.23}$$

$$L_b = \|(Z^{-\frac{1}{2}}WF - Z^{\frac{1}{2}}W^{-1}(WZ^{-1} - I)B'P)x\|^2 \tag{4.24}$$

$$L_c = -\|Z^{\frac{1}{2}}\tilde{u} - Z^{-\frac{1}{2}}(B'P - WF)x\|^2 - \|\gamma u_{lin} - \gamma^{-1}W\tilde{u}\|^2 \tag{4.25}$$

Equation (4.22) comprises three terms. A sufficient - and therefore *potentially conservative* - condition for the cost function $L(.)$ to be negative definite is that the first two terms be equal to zero; the last term, L_c, is a negative definite quadratic term and therefore only makes "favorable" contributions to $L(.)$. Setting the second term, L_b, to zero yields a condition for the gain matrix F

$$(Z^{-\frac{1}{2}}WF - Z^{\frac{1}{2}}W^{-1}(WZ^{-1} - I)B'P) = 0 \quad \Leftrightarrow \quad F = (\gamma^{-2}I - W^{-1})B'P \tag{4.26}$$

where $P = P' > 0$ comes from solving the Ricatti equation which makes the first term $L_a = 0$

$$A'P + PA + C'C + PBZ^{-1}B'P - PB(Z^{-1} - W^{-1})'Z(Z^{-1} - W^{-1})B'P = 0 \tag{4.27}$$

which, after some algebraic manipulation, reduces to:

$$A'P + PA + \gamma^{-2}PBB'P + C'C = 0 \tag{4.28}$$

These are exactly the conditions given in Theorem 1 with $D = 0$. Internal stability guarantees that condition (1) of the performance anti-windup problem (Problem 1) is satisfied; the finite $\mathcal{L}_2$ gain of $\mathcal{T}_p$ ensures condition (3) is satisfied, and hence condition (2) is met. Well-posedness of the loop is guaranteed by the lack of direct feedthrough terms, i.e. $M - I$ is strictly proper. □□

Remark 4.1: Notice that the Riccati equation given is of the bounded-real type and only has a solution if $G(s)$ is stable and $\gamma > 0$ is such that $\|G\|_\infty = \gamma_{opt} \leq \gamma$. That is, the performance level of the AW compensator is restricted by the $\mathcal{H}^\infty$ norm of the open-loop plant. This suggests that optimal anti-windup performance is obtained when $\gamma = \gamma_{opt}$, leaving the designer the task of choosing $W > 0$. This freedom in choosing W is absent in [107] and [67] and hence we have recovered freedom in choosing the so-called *stability multiplier.* □

Remark 4.2: The poles of AW compensator (4.10) are the poles of $M(s)$, which are the eigenvalues of the matrix $A + BF$ where F is given by equation (4.17). Note that equation (4.17) contains the "free" parameter $W > 0$, which exerts influence over the location of the AW compensator poles. Thus it can be observed that, providing (A, B) is controllable (it is always stabilisable by virtue of A being Hurwitz), decreasing the size of W will tend to increase the magnitude of the AW compensator's poles. This extra freedom in shaping the AW compensator's poles is useful for discrete-time implementation when careful attention should be paid to their size relative to the sampling rate. In the LMI formulation of [107], W did not appear as a free parameter and hence, there was no such direct control over pole magnitude. Note also that the freedom in choosing W allows one to "transfer" anti-windup action between the compensation signals u_d and y_d. □

Remark 4.3: Apart from being diagonal and positive definite, the only restriction on W is imposed by equation (4.16). When $D = 0$ this reduces to $Z = (2I - \gamma^{-2}W) > 0$ which always holds for small enough W. When $D \neq 0$, the condition on R ensures that $D'D < \gamma^2 I$ which in turn means that inequality (4.16) becomes

$$Z \geq 2W - \gamma^2 I - \gamma^{-2}W^2 > 0 \tag{4.29}$$

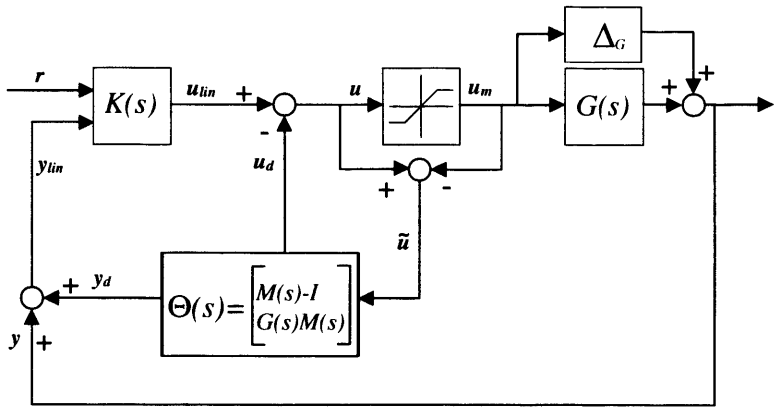

Figure 4.4: Anti-windup scheme with uncertainty

Using the Schur complement this holds if

$$\begin{bmatrix} 2W & W & I \\ W & \gamma^2 & 0 \\ I & 0 & \gamma^{-2} \end{bmatrix} > 0 \tag{4.30}$$

from which W can be determined. In the work carried out so far, it has been straightforward to choose W such that the condition on Z is satisfied. □

4.3 Robust AW Problem

Control engineers rarely have the luxury of dealing with perfect plant models and typically the model $G(s)$ is not a true representation of the real system. A better way of describing the *true linear plant* is

$$\tilde{G} = G + \Delta_G \tag{4.31}$$

where our plant model $G(s)$ is now accompanied by additive uncertainty $\Delta_G \in \mathcal{RH}_\infty$; as we are seeking global results it is necessary to assume stability of the uncertain term Δ_G. It is well known from the robust control literature (see e.g. [88]) that disregard for uncertainty may have serious consequences for the true closed-loop system, and control loops which behave acceptably for the nominal plant may suffer dramatic stability and performance losses when applied to the true uncertain plant. Recent results in the AW literature [99, 26, 107] seem to suggest that obtaining robust performance in the face of saturation may be quite demanding and requires special attention.

Although there are several ways of representing uncertainty, the additive type given in equation (4.31) is appealing as it captures both output-multiplicative and input-multiplicative uncer-

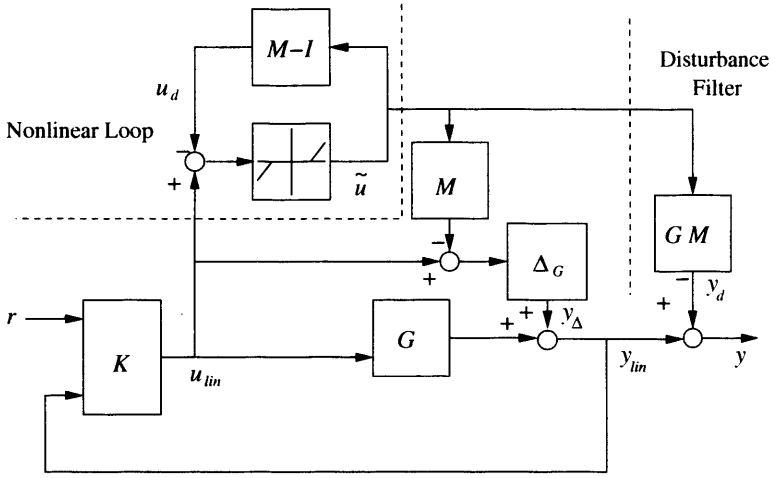

Figure 4.5: Anti-windup scheme with uncertainty

tainties: $\Delta_G = \Delta_0 G$ or $\Delta_G = G\Delta_i$ where Δ_0 and Δ_i are output and input multiplicative uncertainties respectively. The converse is only true if G^{-1} exists.

A key feature of the standard AW problem formulation is that it allows the decoupling of nominal linear dynamics from saturated behavior, allowing Figure 4.2 to be re-drawn as Figure 4.3. The presence of uncertainty destroys this property and, instead, uncertainty-dependent coupling is introduced. Figure 4.4 shows the architecture of an uncertain system $\tilde{G} = G + \Delta_G$ with anti-windup parametrised by $M(s)$. This Figure can be re-drawn as Figure 4.5, but note now that there is coupling between the "linear system" and the *nonlinear loop* through the transfer function matrix $\Delta_G M(s)$. Although it is obvious that sufficiently small Δ_G will not be problematic, for larger uncertainties potential stability issues may arise. Also note that if the map from u_{lin} to $\tilde{u}$ is sufficiently small, similar robustness properties as the linear system can be expected.

Following [107], robustness is tackled via a small gain approach. The following formal assumption is made:

Assumption 3 *The closed-loop linear system is robustly stable; that is* $\|K(I-GK)^{-1}\|_\infty = \beta$ *and* $\Delta_G \in \mathbf{\Delta}$ *where*

$$\mathbf{\Delta} = \left\{ \Delta \in \mathcal{RH}_\infty : \|\Delta\|_\infty < \frac{1}{\beta} \right\} \tag{4.32}$$

□

This assumption guarantees that, in the absence of saturation, the linear system satisfies the small gain condition for stability. From Figure 4.5, note that

$$y_{lin} = Gu_{lin} + \Delta_G[u_{lin} - M\mathcal{F}(u_{lin})] = Gu_{lin} + \tilde{\Delta}_G(u_{lin}) \tag{4.33}$$

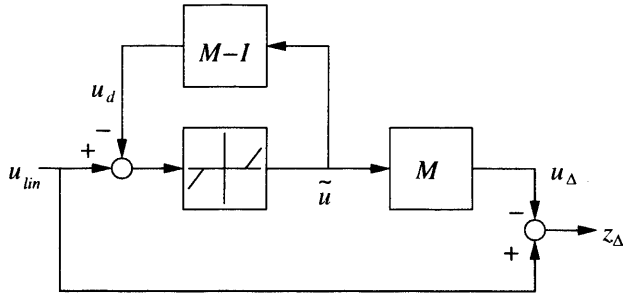

Figure 4.6: Robust stability minimisation problem

where $\mathcal{F}(u_{lin})$ denotes the nonlinear operator from u_{lin} to $\tilde{u}$ and $\tilde{\Delta}_G$ is the "modified" uncertainty representing the effect of saturation on the uncertainty. From the small gain theorem we know that robust stability is obtained if

$$\|\tilde{\Delta}_G\|_{i,2} = \|\Delta_G[I - M\mathcal{F}(.)]\|_{i,2} < \frac{1}{\beta} \tag{4.34}$$

Furthermore the level of robust stability will be equal to or better than that of the linear system if

$$\|\mathcal{T}_r\|_{i,2} = \|I - M\mathcal{F}(.)\|_{i,2} \leq 1 \tag{4.35}$$

It was shown in [107] (see also [108]) that as the nonlinear operator $\mathcal{F}(u_{lin}) = 0$ for sufficiently small u_{lin}, the $\mathcal{L}_2$ gain of $\mathcal{T}_r$ can never be less than unity. Thus nominal robustness is obtained when $\|\mathcal{T}_r\|_{i,2} = 1$ and hence $\|\tilde{\Delta}\|_{i,2} = \|\Delta\|_\infty$. Denoting the output of the $M\tilde{u} - u_{lin}$ (see Figures 4.5 and 4.6) block as z_Δ it then follows that for robust stability of our anti-windup system, we should attempt to minimise the $\mathcal{L}_2$ norm of $\mathcal{T}_r : u_{lin} \mapsto z_\Delta$ (as shown in Figure 4.6). This motivates the following problem formulation.

Problem 2 *The anti-windup compensator (4.9)-(4.10) is said to solve the* robust *anti-windup compensator problem with robustness margin* $1/\mu$ *if the closed-loop in Figure 4.5 is well-posed and the following hold:*

1. *If* $\text{sat}(u) \equiv u$, *then the system is robustly stable for all* $\Delta_G \in \mathbf{\Delta}$.
2. *If* $\Delta_G = 0$, *then* $M(s)$ *solves strongly the standard anti-windup problem (Problem 1) for some performance level* γ.
3. *The operator* $\mathcal{T}_r : u_{lin} \mapsto z_\Delta$ *has finite* $\mathcal{L}_2$ *gain, i.e.* $\|\mathcal{T}_r\|_{i,2} < \mu$.

□

Remark 4.4: Obviously, if $\mu = 1$, we have retained the robustness of the linear system. However, this is not always possible if the performance level, γ, is to be minimised simultaneously, and thus it might be appropriate to relax our robustness requirements in order to obtain performance improvement. □

4.3.1 Solution to the Robustness AW problem

Similar to the performance anti-windup problem above, the *robust anti-windup problem*, eventually reduces to choosing an appropriate coprime factorisation of $G(s)$ and hence, to the choice of a stabilising matrix F (with $(A + BF)$ being Hurwitz). From the discussion in Section 4.3 we know that in order to achieve good robustness we need to minimise $\|\mathcal{T}_r\|_{i,2}$, which is the map from u_{lin} to z_Δ. Before the problem is solved formally, it is useful to examine it from a less rigorous perspective, anticipating solutions that might be expected.

Following similar arguments to those in Section 4.2.1, to guarantee that $\|\mathcal{T}_r\|_{i,2} < \mu$, we consider

$$L(x, u_{lin}, \tilde{u}, F, W) := \frac{d}{dt}x'Px + \|z_\Delta\|^2 - \mu^2\|u_{lin}\|^2 + 2\tilde{u}'W(u - \tilde{u}) \tag{4.36}$$

If $L(.) < 0$ it follows that the anti-windup system is internally stable and that $\|\mathcal{T}_r\|_{i,2} < \mu$ holds. For the sake of illustration, let $W = I$. Although this restricts the design freedom, it enables a simple illustration of a class of robust AW compensators (the case when $W \neq I$ will be discussed next). Expanding equation (4.36) and substituting $u = u_{lin} - Fx$ and $z_\Delta = (u_{lin} - Fx - \tilde{u})$ gives

$$L = x'(A'P + PA + 2PBF + F'F)x + 2xPB\tilde{u} - \tilde{u}'\tilde{u} - (\mu^2 - 1)u'_{lin}u_{lin} - 2xF'u'_{lin} \tag{4.37}$$

Eliminating cross-product terms in three steps (as in the proof of Theorem 4.1), it is possible to obtain conditions

$$\tilde{A}'P + P\tilde{A} + \mu^{-2}PBB'P = 0 \tag{4.38}$$

and

$$Z = (1 - \mu^{-2})I > 0 \Leftrightarrow \mu > 1 \tag{4.39}$$

which ensure global stability and some level of robustness. Furthermore, if equations (4.38) and (4.39) are satisfied, a suitable AW compensator achieving $\|\mathcal{T}_r\|_{i,2} < \mu$ is obtained by calculating the matrix gain F as follows:

$$F = -(1 - \mu^{-2})B'P \tag{4.40}$$

Notice that the immediate solution for the Riccati equation in (4.38) is $P = 0$, which yields $F = 0$ and hence our AW compensator takes the form of an internal-model-control (IMC) compensator. Thus for optimal robustness, the Riccati approach agrees with [107] in advocating the IMC scheme as an optimally robust solution as μ is not restricted by equation (4.38)(note that $\mu = 1$ for $P = 0$). However, there is more freedom in equation (4.38) because by redefining $P =: \tilde{P}^{-1} > 0$ we equivalently obtain, from equation (4.38), the Lyapunov equation

$$\tilde{P}A' + A\tilde{P} + \mu^{-2}BB' = 0 \tag{4.41}$$

which has a positive definite solution, and therefore produces a compensator different to the IMC scheme.

In order to solve the robust AW compensation problem, it is necessary to meet the conditions in Problem 2 (and hence Problem 1). It is easy to observe again that the conditions of the standard AW problem are met if internal stability of the closed-loop compensated system is guaranteed (assume zero initial conditions for the AW compensator). By choosing F as described in (4.40), it is possible to guarantee that $\|\mathcal{T}_r\|_{i,2} < \mu$ for some $\mu > 0$, therefore solving the robust AW compensation problem. It can be argued that the the strong AW problem, i.e. $\|T_p\|_2 \leq \gamma$, is better solved when the IMC-like scheme is avoided (see Theorem 2 and proof).

Remark 4.5: More generally (for $W \neq I$), the expression in (4.36) is given as

$$\begin{aligned} L &= x'(A'P + PA + 2PBF + F'F)x + 2x'PB\tilde{u} - \tilde{u}'(2W - I)\tilde{u} - (\mu^2 - 1)u'_{lin}u'_{lin} \\ &\quad -2x'F'u_{lin} + 2u'_{lin}(W - I)\tilde{u} - 2x'F'(W - I)\tilde{u} < 0 \end{aligned} \tag{4.42}$$

Completing the square for terms involving u_{lin}, a condition on Z is derived as

$$Z = 2W - \mu^{-2}W^2 - I > 0 \tag{4.43}$$

As W is diagonal, $Z > 0 \Rightarrow \mu^2 > \frac{w_i^2}{2w_i - 1}$ $\forall i \in \{1 \ldots m\}$. Notice that $\mu > 0 \Rightarrow w_i > 0.5$ and that the $\min_{w_i}\{\mu(w_i) = 1\}$ and occurs at $w_i = 1$ (or $W = I$). This can be verified by equating the derivative of $\mu(w_i)$ to zero and solving for w_i:

$$\frac{d\mu(w_i)}{dw_i} = \frac{2w_i(w_i - 1)}{(2w_i - 1)^2} = 0 \Rightarrow w_i = 1$$

We assume that the solution is a minimum, that is, the second derivative of $\mu(w_i)$ with respect to w_i is positive. Thus $W = I$ is in fact, the optimal choice which maximises robustness margins. This can be seen in Figure 4.7. □.

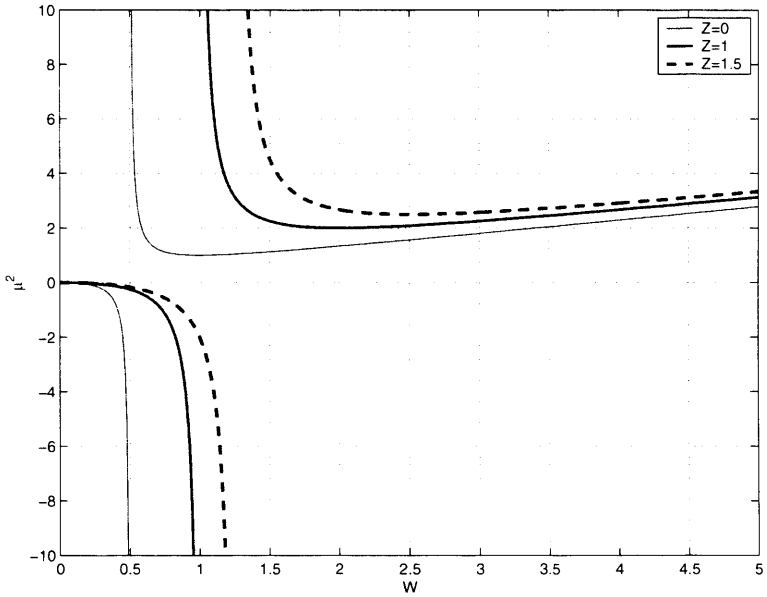

Figure 4.7: μ^2 and w_i such that $Z \geq 0$

The purpose of AW compensation is to improve performance during periods of saturation. Section 4.3 mentioned that the optimal solution (the smallest μ) to the robust AW problem is likely to be IMC-like, which as noted earlier, generally has performance issues. In fact, just considering robustness leads to conditions (4.38) and (4.40) which do not give any explicit performance guarantees, ensuring only robust stability. The real value of conditions (4.38) and (4.40) is when used in conjunction with performance optimization.

Conversely, the AW solutions given in [110] performed well under nominal conditions, but tended to produce AW compensators with large poles and ones which produced large compensation signals. No guarantees about robustness were given until later work [107] which involved computationally expensive LMI optimisation. Furthermore these formulations arguably lacked intuition and some of the features of the full-order AW compensators were clouded by the design method; in particular the "stability multiplier", and its effects on the system, is lost in the optimisation routine.

This section will attempt to show that the Riccati-based work described in the last section (and also in [90, 91]) naturally produces a family of anti-windup compensators where the "stability multiplier" (i.e. W) is a measure of the robustness properties of the system. It will also give a method for the synthesis of robust AW compensators with performance guarantees.

The AW problem of robust stability and performance guarantees involves minimizing a mixed $\mathcal{L}_2$ gain. By combining both objectives, it is possible to pose a sensible $\mathcal{L}_2$ gain optimization

problem which addresses robustness and performance simultaneously. The following theorem gives the solution of such mixed robustness/performance problem.

Theorem 4.2 *Let* Assumption 1 *be satisfied; then there exists a full-order* Robust Anti-windup Compensator $\Theta = [\theta_1' \quad \theta_2']' \in \mathbb{R}^{(m+q)\times m}$, *as described by equations (4.9)-(4.10), which solves* Problem 2 *with robustness margin* $1/\mu$ *if there exist a positive definite matrix* $P = P' > 0$ *and positive real scalars* ω_p *and* γ *such that the following Riccati equation is satisfied*

$$\tilde{A}'P + P\tilde{A} + PBR^{-1}B'P + \tilde{Q} = 0 \tag{4.44}$$

where

$$\tilde{A} = A + BR^{-1}D'C \tag{4.45}$$

$$\tilde{Q} = C'(I + DR^{-1}D')C \tag{4.46}$$

$$R = (\gamma^2 I - D'D) > 0 \tag{4.47}$$

and

$$Z = (\omega_p - \gamma^{-2})(\omega_p^{-1} I - D'D) > 0 \tag{4.48}$$

Furthermore, if equation (4.44) is satisfied, a suitable Θ *is obtained by calculating the matrix gain* F *as:*

$$F = -\gamma^2(\omega_p - \gamma^{-2})R^{-1}(B'P + D'C) \tag{4.49}$$

and the robustness margin is given as $1/\mu = 1/(\gamma\sqrt{\omega_p})$ □

Before giving any formal proof of the theorem, it is instructive to consider the relationship between the standard AW solution and existing robustness properties. For simplicity, assume $G(s)$ is strictly proper (i.e. $D = 0$); then it follows that for simultaneous robustness/performance optimisation we would like to ensure

$$\left\| \begin{array}{c} W_p^{\frac{1}{2}} y_d \\ z_\Delta \end{array} \right\|_2 \leq \mu \|u_{lin}\|_2 \tag{4.50}$$

where $W_p > 0$ is a generally diagonal matrix, which weights the performance variable y_d and allows a trade-off between the different objectives. From the results given earlier in this section, a sufficient condition for this to hold can be easily derived and is given by

$$A'P + PA + \mu^{-2}PBB'P + C'W_pC = 0 \tag{4.51}$$

$$F = -(\hat{W}^{-1} - \mu^{-2})B'P \tag{4.52}$$

which ensures that $\|W_p^{\frac{1}{2}} y_d\|_2 \leq \mu \|u_{lin}\|_2$ and where $\hat{W}$ is the extra parameter introduced by the Circle Criterion formulation and the sector bound definition. Next, assume that W_p is a diagonal scalar matrix, i.e. $W_p = I\omega_p > 0$, and define $P_w := P\omega_p^{-1} > 0$. This allows us to rewrite equation (4.51) as

$$\omega_p(A'P_w + P_wA + \mu^{-2}\omega_p P_w BB'P_w + C'C) = 0 \tag{4.53}$$

Next, defining $\gamma := \mu/\sqrt{\omega_p}$ yields (as $\omega_p > 0$)

$$A'P_w + P_wA + \gamma^{-2}P_w BB'P_w + C'C = 0 \tag{4.54}$$

Similarly we obtain F as

$$F = -(\hat{W}^{-1} - \mu^{-2})B'P_w\omega_p = -(\hat{W}^{-1}\omega_p - \gamma^{-2})B'P_w \tag{4.55}$$

Notice that equations (4.54) and (4.55) are of exactly the same form as (4.12) and (4.17) with P_w playing the role of P, and $\hat{W}^{-1}\omega_p$ that of W^{-1}. The robust stability margin can then be measured using

$$\mu = \gamma\sqrt{\omega_p} \leq \gamma \|\sqrt{W^{-1}\hat{W}}\| \tag{4.56}$$

It is possible to conclude that for small ω_p, or equivalently large W, greater robustness is obtained (small μ corresponds to greater robustness margins, $\frac{1}{\mu}$). Thus in the standard AW problem, the choice of W is directly linked to the robustness of the system and must be chosen large.

Proof:To satisfy the robustness and performance AW problem we need to ensure that both the standard AW problem, i.e. $\|\mathcal{T}_p\|_{i,2} < \gamma$ for some $\gamma > 0$, and the robust AW problem, i.e. $\|\mathcal{T}_r\|_{i,2} < \mu$ for some $\mu > 0$, are satisfied while also requiring internal stability and well-posedness. In order to achieve this we would like to ensure that

$$\left\| \begin{array}{c} \sqrt{\omega_p} y_d \\ z_\Delta \end{array} \right\|_2 \leq \mu \|u_{lin}\|_2 \tag{4.57}$$

If this inequality is satisfied, the maps $\|\mathcal{T}_r\|_{i,2} < \mu$ and $\|\mathcal{T}_p\|_{i,2} < \gamma = \frac{\mu}{\sqrt{\omega_p}}$, i.e. they are finite $\mathcal{L}_2$ gain stable. To guarantee inequality (4.57) holds and to ensure internal stability, as before, it suffices that a certain cost function be negative definite. This cost function is defined as

$$L(x, u_{lin}, \tilde{u}, F, W) := \frac{d}{dt}x'Px + \omega_p y_d'y_d + z_\Delta' z_\Delta - \mu^2 u_{lin}'u_{lin} + 2\tilde{u}'W(u - \tilde{u}) < 0 \tag{4.58}$$

The remainder of the proof is given for the general case when $D \neq 0$. Although it is possible to give a simpler proof when $D = 0$, the simplicity obscures the cross terms which require more care in removing.

First note that we can "absorb" ω_p into the plant's C and D matrices:

$$\|\sqrt{\omega_p} y_d\|^2 = \|\sqrt{\omega_p}[(C + DF)x + D\tilde{u}]\|^2 = \|(C_w + D_w F)x + D_w\tilde{u}\|^2$$

where $C_w = \sqrt{\omega_p} C$ and $D_w = \sqrt{\omega_p} D$.

Expanding (4.58) and substituting $u = u_{lin} - u_d$ and $y_d = (C_w + D_w F)x + D_w\tilde{u}$ gives:

$$\begin{aligned} L &= \dot{x}'Px + x'P\dot{x} + x'(C_w + D_w F)'(C_w + D_w F)x + x'F'Fx \\ &\quad -(\mu^2 - 1)u'_{lin}u_{lin} - \tilde{u}'(2W - I - D'_w D_w)\tilde{u} \\ &\quad -2x'F'u_{lin} + 2\tilde{u}'(W - I)u_{lin} - 2x'F'(W - I)\tilde{u} + 2x'(C_w + D_w F)'D_w\tilde{u} \end{aligned} \quad (4.59)$$

As before, the cross-product terms are eliminated in three steps. **(I)** The cross-product terms involving u_{lin}, $\tilde{u}$ and x are grouped as follows:

$$\begin{aligned} -\left[(\mu^2 - 1)u'_{lin}u_{lin} + 2x'F'u_{lin} - 2\tilde{u}'(W - I)u_{lin}\right] &= -\|(\mu^2 - 1)^{\frac{1}{2}}u_{lin} - (\mu^2 - 1)^{-\frac{1}{2}}((W - I)\tilde{u} - Fx)\|^2 \\ +(\tilde{u}'(W - I) - x'F)(\mu^2 - 1)^{-1}((W - I)\tilde{u} - Fx) & \end{aligned} \quad (4.60)$$

Combining the above with equation (4.59), a cost function containing no cross-product terms between u_{lin}, $\tilde{u}$ and x is obtained:

$$\begin{aligned} L &= x'(A'P + PA + 2PBF + (C_w + D_w F)'(C_w + D_w F) + \tilde{\mu}F'F)x - \tilde{u}'\tilde{\mu}Z\tilde{u} \\ &+ 2x'(C_w + D_w F)'D_w\tilde{u} + 2x'PB\tilde{u} - 2x'F'\tilde{\mu}(W - I)\tilde{u} \\ &- \|(\mu^2 - 1)^{\frac{1}{2}}u_{lin} + (\mu^2 - 1)^{-\frac{1}{2}}((W - I)\tilde{u} - Fx)\|^2 \end{aligned} \quad (4.61)$$

where necessary conditions are obtained [1]as $Z = 2W - W^2\mu^{-2} - I - \tilde{\mu}^{-1}D'_w D_w > 0$ and $\tilde{\mu} = 1 - (\mu^2 - 1)^{-1} = \frac{\mu^2}{\mu^2 - 1}$

(II) The cross-product terms involving $\tilde{u}$ and x are grouped as follows:

$$\begin{aligned} -\left[\tilde{u}'\tilde{\mu}Z\tilde{u} - 2x'(PB + (C_w + D_w F)'D_w - F'\tilde{\mu}(W - I))\tilde{u}\right] = \\ -\|\tilde{\mu}^{\frac{1}{2}}Z^{\frac{1}{2}}\tilde{u} - \tilde{\mu}^{-\frac{1}{2}}Z^{-\frac{1}{2}}(B'P + D'_w(C_w + D_w F) - \tilde{\mu}(W - I)F)x\|^2 \\ +x'(PB + (C_w + D_w F)'D_w - F'\tilde{\mu}(W - I))\tilde{\mu}^{-1}Z^{-1}(B'P + D'_w(C_w + D_w F) - \tilde{\mu}(W - I)F)x \end{aligned}$$

[1]This reduces to the Z given in Theorem 2 when $W = I$ - see later in the proof.

By replacing this group of terms, the cost function can be written with no cross-product terms between $\tilde{u}$ and x, viz:

$$\begin{aligned} L &= x'[A'P + PA + C_w'(I + D_w\tilde{\mu}^{-1}Z^{-1}D_w')C_w + 2C_w'D_w\tilde{\mu}^{-1}Z^{-1}B'P + PB\tilde{\mu}^{-1}Z^{-1}B'P \\ &+ F'(\tilde{\mu} + \tilde{\mu}(W-I)Z^{-1}(W-I) + D_w'(I + D_w\tilde{\mu}^{-1}Z^{-1}D_w')D_w - 2D_w'D_wZ^{-1}(W-I))F \\ &+ 2PB(I + \tilde{\mu}^{-1}Z^{-1}D_w'D_w - Z^{-1}(W-I))F + 2C_w'D_w(I + D_w\tilde{\mu}^{-1}Z^{-1}D_w' - Z^{-1}(W-I))F]x \\ &- \|(\mu^2-1)^{\frac{1}{2}}u_{lin} + (\mu^2-1)^{-\frac{1}{2}}((W-I)\tilde{u} - Fx)\|^2 \\ &- \|Z^{\frac{1}{2}}\tilde{u} - Z^{-\frac{1}{2}}(B'P + D_w'(C_w + D_wF) - \tilde{\mu}(W-I)F)x\|^2 \end{aligned} \tag{4.62}$$

(III) The terms involving F and $F'F$ are grouped. Before going any further, it is possible to write a more compact formulation by using the following identities

$$\tilde{\mu}H = I + \tilde{\mu}^{-1}Z^{-1}D_w'D_w - Z^{-1}(W-I)$$
$$\tilde{\mu}H = Z^{-1}(W - W^2\mu^{-2})\tilde{\mu} + D_w'D_w + \tilde{\mu}(W-I)Z^{-1}(W-I) - 2D_w'D_wZ^{-1}(W-I) + D_w'D_w\tilde{\mu}^{-1}Z^{-1}D_w'D_w$$

where

$$H = W^2\mu^{-2} + (W - W^2\mu^{-2})Z^{-1}(W - W^2\mu^{-2})$$

The problem of grouping terms involving F can be written as:

$$\begin{gathered} F'\tilde{\mu}HF + 2F'(W - W^2\mu^{-2})Z^{-1}(B'P + D_w'C_w) = \\ \|\tilde{\mu}^{\frac{1}{2}}H^{\frac{1}{2}}F + \tilde{\mu}^{-\frac{1}{2}}H^{-\frac{1}{2}}(W - W^2\mu^{-2})(B'P + D_w'C_w)\|^2 \\ -(PB + C_w'D_w)Z^{-1}(W - W^2\mu^{-2})\tilde{\mu}^{-1}H^{-1}(W - W^2\mu^{-2})Z^{-1}(B'P + D_w'C_w) \end{gathered}$$

Using the matrix inversion lemma:

$$H^{-1} = W^{-2}\mu^2 - W^{-2}\mu^2(W - W^2\mu^{-2})\tilde{\mu}R^{-1}(W - W^2\mu^{-2})W^{-2}\mu^2$$

where $R = \mu^2 I - D_w'D_w$. Now define the matrix Q such that

$$Q = Z^{-1}(W - W^2\mu^{-2})\tilde{\mu}^{-1}H^{-1}(W - W^2\mu^{-2})Z^{-1} = R^{-1}(W - W^2\mu^{-2})W^{-2}\mu^2(W - W^2\mu^{-2})Z^{-1} \tag{4.63}$$

The matrix Q is such that the following equality holds:

$$\tilde{\mu}^{-1}Z^{-1} - Q = R^{-1} \tag{4.64}$$

Finally, by using the results given earlier in (**III**), an expression for the cost function (4.58) is given by

$$L(x, u_{lin}, \tilde{u}, F, W) = L_a + L_b + L_c \tag{4.65}$$

where

$$\begin{aligned} L_a &= x'[A'P + PA + PB(\tilde{\mu}^{-1}Z^{-1} - Q)B'P + C_w'(I + D_w(\tilde{\mu}^{-1}Z^{-1} - Q)D_w')C_w \\ &+ 2C_w'D_w(\tilde{\mu}^{-1}Z^{-1} - Q)B'P]x \qquad (4.66) \\ L_b &= x'\|\tilde{\mu}^{\frac{1}{2}}H^{\frac{1}{2}}F + \tilde{\mu}^{-\frac{1}{2}}H^{-\frac{1}{2}}(W - W^2\mu^{-2})Z^{-1}(B'P + D_w'C_w)\|^2x \qquad (4.67) \\ L_c &= -\|(\mu^2 - 1)^{\frac{1}{2}}u_{lin} + (\mu^2 - 1)^{-\frac{1}{2}}((w - I)\tilde{u} - Fx)\|^2 \\ &\quad -\|Z^{\frac{1}{2}}\tilde{u} - Z^{-\frac{1}{2}}(B'P + D_w'(C_w + D_wF) - \tilde{\mu}(W - I)F)x\|^2 \qquad (4.68) \end{aligned}$$

As before the negative quadratic terms, L_c, can be ignored and the second term, L_b, set to zero. This condition allows the designer to obtain a stabilizing matrix gain F as follows

$$\tilde{\mu}^{\frac{1}{2}}H^{\frac{1}{2}}F + \tilde{\mu}^{-\frac{1}{2}}H^{-\frac{1}{2}}(W - W^2\mu^{-2})Z^{-1}(B'P + D_w'C_w) = 0 \qquad (4.69)$$

$$F = -\tilde{\mu}^{-1}H^{-1}(W - W^2\mu^{-2})(B'P + D_w'C_w) \qquad (4.70)$$

which after some simplifications yields:

$$F = -\mu^2(W^{-1} - \mu^{-2})R^{-1}(B'P + D_w'C_w) \qquad (4.71)$$

The positive definite matrix $P = P' > 0$ is obtained by solving the Ricatti equation which makes the first term $L_a = 0$, viz:

$$A'P+PA+C_w'D_wR^{-1}B'P+PBR^{-1}D_w'C_w+PBR^{-1}B'P+C_w'(I+D_wR^{-1}D_w')C_w = 0 \qquad (4.72)$$

Substituting for C_w and D_w transforms equation (4.71) into

$$\begin{aligned} F &= -\mu^2\omega_p^{-1}(W^{-1}\omega_p - \mu^{-2}\omega_p)(\mu^2\omega_p^{-1}I - D'D)^{-1}(B'P_w^{-1} + D'C) \qquad (4.73) \\ &= \gamma^2(W^{-1}\omega_p - \gamma^{-2}I)(\gamma^2I - D'D)(B'P_w + D'C) \qquad (4.74) \end{aligned}$$

where $\gamma = \mu\sqrt{\omega_p^{-1}}$. Re-defining $R = (\gamma^2I - D'D)$ and setting $W = I$ (as it is a free parameter) yields the expressions for F and Z given in Theorem 2. We can apply a similar strategy to equation (4.72) to obtain

$$A'P_w + P_wA + C'DR^{-1}B'P_w + P_wBR^{-1}D'C + P_wBR^{-1}B'P_w + C'(I + DR^{-1}D')C \qquad (4.75)$$

where $P_w = P\omega_p^{-1}$. Note that equation (4.75) has the exact same structure as equation (4.44), but with P re-defined as P_w.

The proof is completed by noting that internal stability - which is guaranteed if the Riccati equation in (4.72) has a solution and F is chosen as stipulated in (4.49) - it ensures conditions

(1) and (3) (and hence condition (2)) of the standard anti-windup problem. This guarantees condition (1) of the robust anti-windup problem, while condition (3) is satisfied through the conditions of Theorem 2. Well-posedness of the system is trivially guaranteed by the absence of direct feed-through terms in the nonlinear loop. □□.

Remark 4.6: As $\mu = \gamma\sqrt{\omega_p}$ it follows that by choosing ω_p small, we have a better robustness margin. Unfortunately, for sufficiently small ω_p, the feedback matrix F also becomes small, leading our AW compensator to approach the IMC solution, which is known to have poor performance. In contrast, a large ω_p creates large compensator poles which may be problematic for practical implementation and are generally linked with small robustness margins. Observe the existing trade-off between robustness and performance and how it is encapsulated in the parameter ω_p: small ω_p yields better robustness margins at the expense of reduced performance. It is interesting to compare the conditions in Theorems 1 and 2. Note that W^{-1} in Theorem 1 is essentially equivalent to ω_p in Theorem 2. Thus the choice of the "stability multiplier", W, plays a central role in the robustness of the anti-windup compensator. Alternatively, in the standard AW solution, W can be seen as the "robustness weighting matrix": choosing W large (equivalent to ω_p small) increases the robustness of the design. This gives some theoretical justification for the robustness of the schemes tested in [41]. □

Remark 4.7: It is not necessary to choose $W_p = \omega_p I$ in robust anti-windup synthesis. We have made this choice in Theorem 2 to enable clear expressions for robustness to be derived, although this is not a requirement in general. With W_p chosen as a more general positive definite (normally diagonal) matrix, it is possible to increase the flexibility in the design and draw the same general conclusions, although the robustness margin will not be as explicit as that given in Theorem 2. □

Remark 4.8: The main difference between the solutions given to the standard and robust AW problems are the conditions imposed by Z in inequalities (4.16) and (4.48). These inequalities impose different conditions on the free parameter, W (alternatively ω_p) giving rise to different extreme solutions. This is perhaps most easily seen for $D = 0$. If this is the case, inequalities (4.16) and (4.48) become

$$Z_{stnd} := 2W - \gamma^{-2}W^2 \Rightarrow 2\gamma^2 I > W \tag{4.76}$$

$$Z_{rob} := (\omega_p - \gamma^{-2})\omega_p^{-1} \Rightarrow \gamma^2 > \omega_p^{-1} \tag{4.77}$$

So when W is as large as possible, that is $W \approx 2\gamma^2 I$, it follows from equation (4.17) that F is nonzero and hence, the compensation scheme is not IMC-like. Conversely, when ω_p is as small

as possible, i.e. $\omega_p^{-1} \approx \gamma^2$, it follows from equation (4.49) that $F \approx 0$ and hence, the IMC solution is recovered as an extreme solution, i.e. the most robust scheme possible. Thus, as expected from the results of [107], one choice for an optimally robust AW scheme (i.e. when ω_p is as small as possible), is simply the IMC scheme. It is also interesting to note that inequality (4.48) ensures that inequality (4.16) holds; the converse is only true if $\|D\|$ is "small". □

4.4 Example

In this section, the effectiveness of the results are shown through an example taken from the literature. This example, that of a missile auto-pilot introduced by [78], was also used in [110] and [79]. The plant is a simplified model of the dynamics of the roll-yaw channels of a bank-to-turn missile:

$$
\begin{aligned}
A_p &= \begin{bmatrix} -0.818 & -0.999 & 0.349 \\ 80.29 & -0.579 & 0.009 \\ -2734 & 0.05621 & -2.10 \end{bmatrix}, \\
B_p &= \begin{bmatrix} 0.147 & 0.012 \\ -194.4 & 37.61 \\ -2716 & -1093 \end{bmatrix}, \quad B_{pd} = \begin{bmatrix} 0 & 0 \\ 0 & 0 \\ 0 & 0 \end{bmatrix} \\
C_p &= \begin{bmatrix} 1 & 0 & 0 \\ 0 & 1 & 0 \end{bmatrix}, \quad D_p = D_{pd} = \begin{bmatrix} 0 & 0 \\ 0 & 0 \end{bmatrix}
\end{aligned}
$$

A nominal linear LQG/LTR controller yields excellent nominal closed-loop time and frequency responses and is given by

$$
\left[\begin{array}{c|c|c} A_c & B_c & B_{cr} \\ \hline C_c & D_c & D_{cr} \end{array}\right] = \left[\begin{array}{cc|c|c} A_{c1} & B_{c1} & 0 & 0 \\ 0 & 0 & -I & I \\ \hline C_{c1} & 0 & 0 & 0 \end{array}\right] \tag{4.78}
$$

where

$$
A_{c1} = \begin{bmatrix} -0.29 & -107.8 & 6.67 & -2.58 & -0.4 \\ 107.68 & -97.81 & 63.95 & -4.52 & -5.35 \\ -6.72 & 64.82 & -54.19 & -40.79 & 5.11 \\ 3.21 & 2.1 & 29.56 & -631.15 & 429.89 \\ 0.36 & -3.39 & 3.09 & -460.03 & -0.74 \end{bmatrix},
$$

$$B_{c1} = \begin{bmatrix} 2.28 & 0.48 \\ -40.75 & 2.13 \\ 18.47 & -0.22 \\ -2.07 & -44.68 \\ -0.98 & -1.18 \end{bmatrix}, C_{c1} = \begin{bmatrix} 0.86 & 8.54 & -1.71 & 43.91 & 1.12 \\ 2.17 & 39.91 & -18.39 & -8.51 & 1.03 \end{bmatrix}$$

The actuators have saturation limits of ± 8 in both channels. Figure 4.8 shows the nominal linear response of the missile for a pulse reference $r = [\ 6 \quad -6\ ]$ applied for 16 seconds. Notice the excellent response and decoupling. However, observe that the control signal strays outside the set $\mathcal{U} = \{(8,8),(-8,8),(-8,-8),(8,-8)\}$ for a considerable period of time. This suggests that the system with saturated actuators might have poor performance and could even become unstable. Figure 4.9 shows the system with saturation (but no AW); clearly the saturation has caused a loss in axis decoupling and gives rise to large overshoots. To limit the degradation caused by saturation, an AW compensator designed using Theorem 1 is introduced. As the anti-windup compensator is designed using the bounded real Riccati equation associated with the open-loop system, the optimal value of γ is $\|G(s)\|_\infty = \gamma \approx 379$, leaving the designer the task of choosing W. Choosing W as $W = 10I_{2\times 2}$ yielded the following value of F:

$$F = \begin{bmatrix} 4.8324 & 31.0935 & 0.9470 \\ -0.1224 & -0.6860 & -0.0004 \end{bmatrix} \tag{4.79}$$

Figure 4.10 shows the missile response with the full order AW compensation proposed in Theorem 1. Notice the improvement over the uncompensated response: the saturated system follows the linear response closely and the return to nominal linear dynamics is swift. Also, observe how the control signal of the compensated system returns to linear behavior faster than the uncompensated system. The system displays additional dynamics introduced by the AW compensator once linear behaviour is resumed. This suggests that the poles of the AW compensator must be fast and well damped in order to reduce the settling times of *post-saturation* transients.

Note that the Riccati based synthesis described in Theorem 1 gives, for a given value of γ (and therefore $P > 0$), a family of gains F, and therefore anti-windup compensators, parameterised by the diagonal matrix $W > 0$. Observe from equation (4.10) that the poles of the anti-windup compensator and the sizes of the compensation signals y_d and u_d are functions of W. Increasing the size of F (and thus decreasing the size of W) leads to larger poles (faster dynamics) and a large compensation signal u_d.

The flexibility in W is useful for implementation as it allows the designer to limit the magnitude

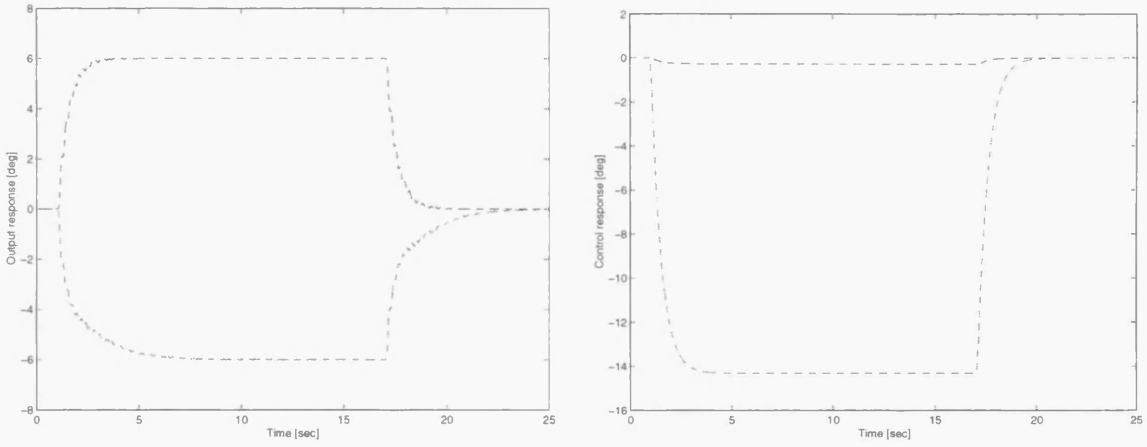

Figure 4.8: Nominal linear response

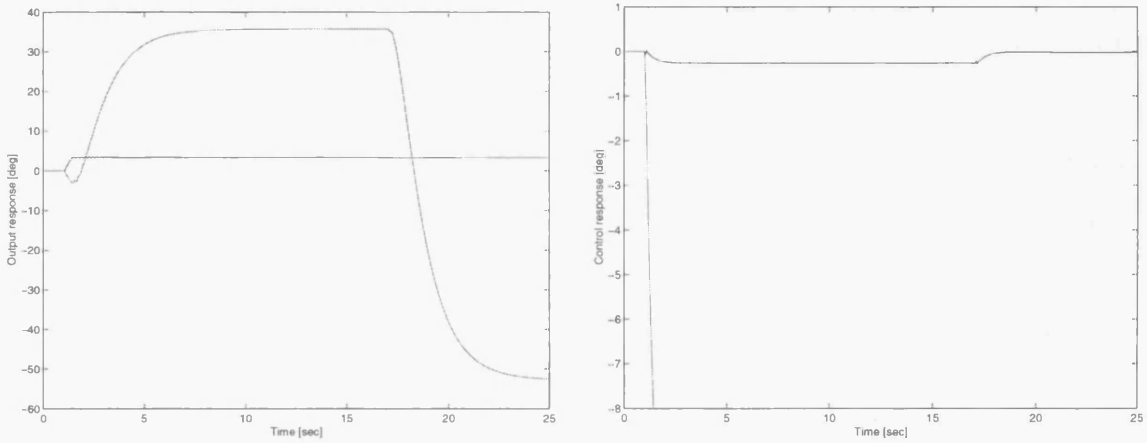

Figure 4.9: Saturated system with no AW compensation

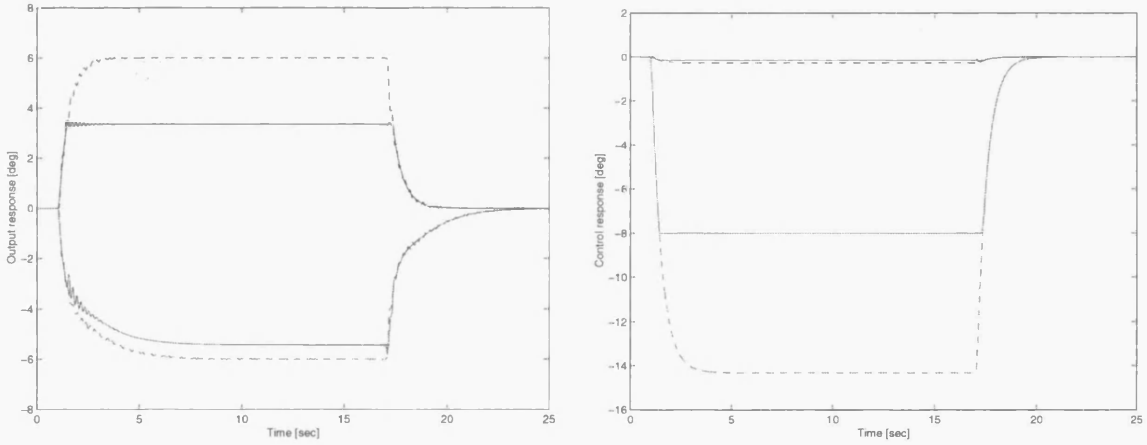

Figure 4.10: Saturated system with full-order AW compensation using Theorem 1

of the compensator poles to ensure that they are compatible with the sampling frequency. The possibility of closely relating the size of the stability multiplier with the systems poles is not present in the various LMI formulations [110, 35] of the AW problem. Figure 4.11 shows time

W	F	Size of poles $spec(A+BF)$
10	$F = \begin{bmatrix} 4.832 & 31.093 & 0.947 \\ -0.122 & -0.686 & -0.000 \end{bmatrix}$	$\mathbf{spec}(A+BF) = 10^3 \times [-8.618 \ -0.013 \pm 0.029i]$
50	$F = \begin{bmatrix} 0.966 & 6.217 & 0.189 \\ -0.024 & -0.137 & -0.000 \end{bmatrix}$	$\mathbf{spec}(A+BF) = 10^3 \times [-1.723 \ -0.004 \pm 0.032i]$
200	$F = \begin{bmatrix} 0.241 & 1.553 & 0.047 \\ -0.006 & -0.034 & 0.000 \end{bmatrix}$	$\mathbf{spec}(A+BF) = 10^2 \times [-4.308 \ -0.021 \pm 0.320i]$

Table 4.1: Variable stability multiplier W for a fixed sampling Rate $\Delta T = 10^{-3}$

simulations for different values of W with a fixed sampling rate of $10^{-3}sec$ (see Table 4.1). Note that, as expected for small W which results in large anti-windup compensator poles, numerical problems occur and the AW compensator does not function well.

Now consider the *real* nominal open-loop plant $\tilde{G}(s) = G(s)\Delta_{act}(s)$ consisting of the nominal plant $G(s)$ plus unmodeled dynamics $\Delta_{act}(s) = \text{diag}(\delta_{act}(s), \delta_{act}(s))$. $\Delta_{act}(s)$ represents unmodeled actuator dynamics of the form:

$$\delta_{act}(s) = \frac{\omega_n^2}{s^2 + 2\zeta\omega_n s + \omega_n^2}$$

where ω_n is the undamped natural frequency and ζ is the damping coefficient. Assuming a "worst case" scenario (from looking at the frequency response of the closed-loop transfer function) and setting these constants to $30rad/sec$ and 0.049 respectively, the actuators have a resonant peak and very large phase shifts near the crossover frequency of the nominal plant. This input-multiplicative uncertainty can be modeled as an additive uncertainty $\Delta_G(s) = G(s)[\Delta_{act}(s) - I]$. It can be verified using the small gain theorem that under this uncertainty the system is robustly stable as $\|K(I-GK)^{-1}\Delta_G\|_\infty < 1$. The nominal (un-saturated) closed-loop response, including uncertainties, is shown in Figure 4.12 and it is clear that stability has been maintained and that linear performance in the face of this uncertainty is remarkably good; the system has good robust stability margins and robust performance properties. However, introducing both saturation and uncertainty leads to the system entering a very high amplitude limit cycle as shown in Figure 4.13.

In order to show the advantages of the Riccati based design method proposed in this paper, it will be compared against the static, low-order and robust full-order LMI methods proposed in [107, 110, 107]. Consider the uncertain, saturated, AW compensated closed-loop system. Firstly, static and low-order compensators are designed using the LMI method described in

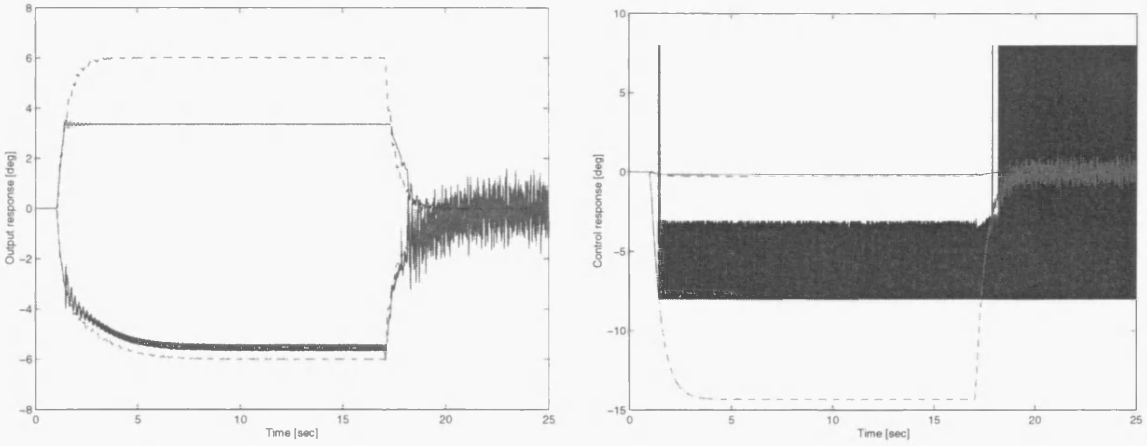

W=$10\times I_2$ and $\Delta T = 10^{-3}$

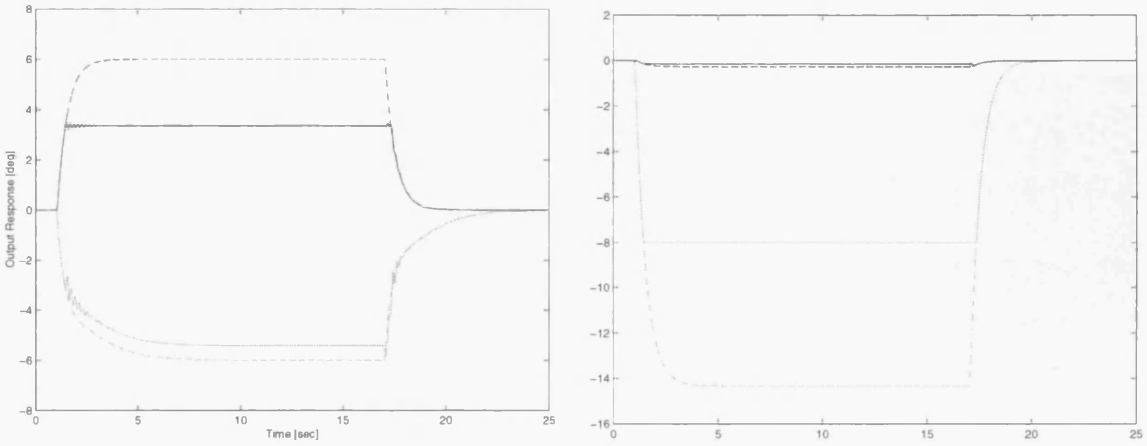

W=$50\times I_2$ and $\Delta T = 10^{-3}$

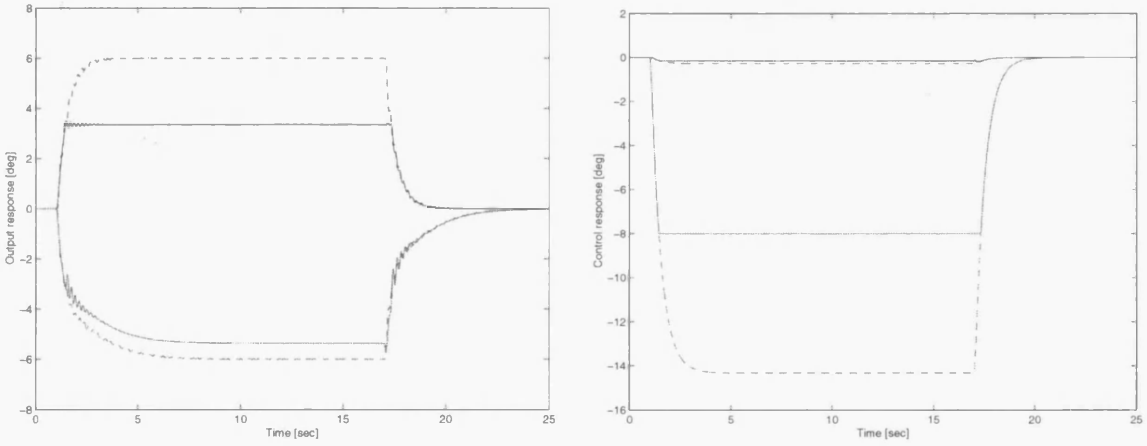

W=$200\times I_2$ and $\Delta T = 10^{-3}$

Figure 4.11: Full order compensation using Theorem 1 for different values of W, $\gamma = 378$ and a sampling rate of $10^{-3}sec$

[110], to give:

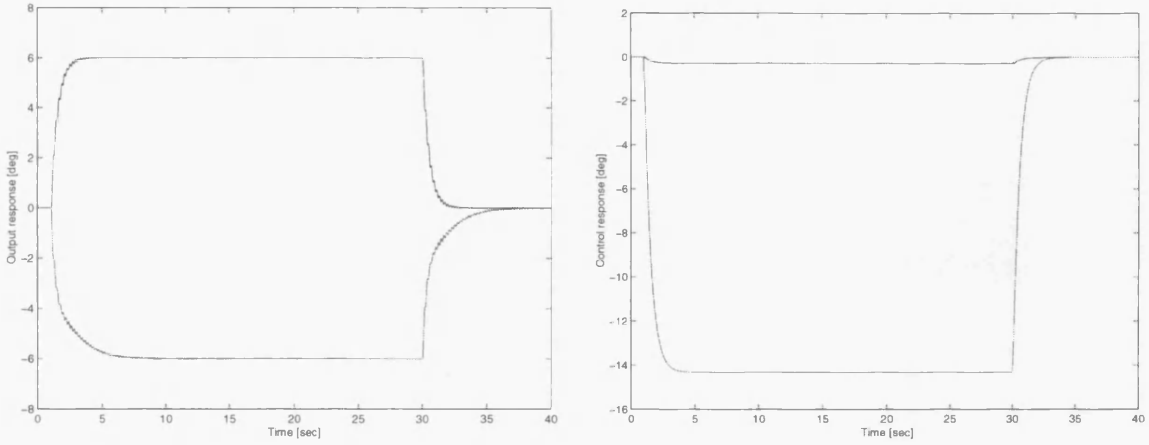

Figure 4.12: Uncertain Unsaturated system

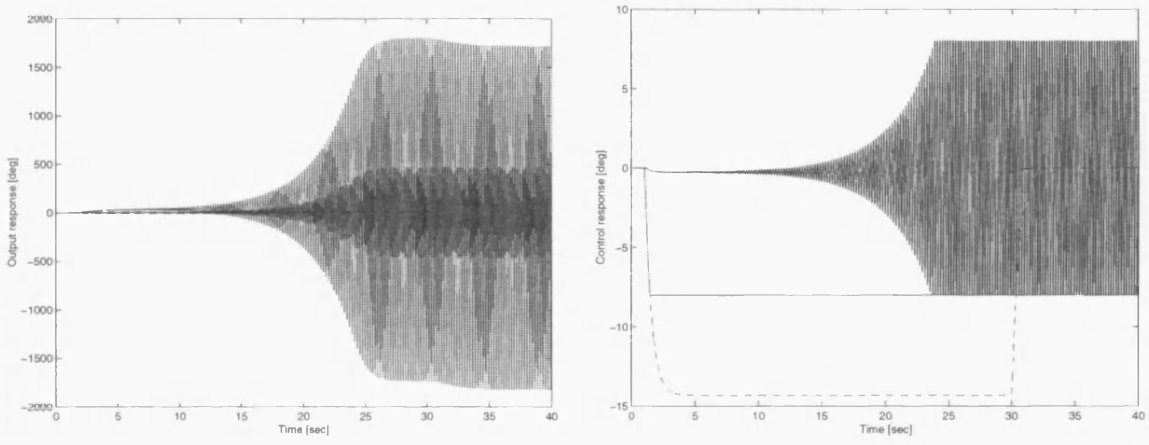

Figure 4.13: Uncertain Saturated system

$$\Theta_{static} = \begin{bmatrix} \Theta_1 \\ \Theta_2 \end{bmatrix} = \begin{bmatrix} -0.9992 & -0.0039 \\ 0.0173 & -0.6921 \\ -0.0112 & -0.5573 \\ -0.2022 & -0.3408 \end{bmatrix}$$

$$\Theta_{loword} = F_1\Theta_1 + F_2\Theta_2 = F_1 \begin{bmatrix} -1.6973 & 5.1136 \\ 3.5044 & 81.5261 \end{bmatrix} + F_2 \begin{bmatrix} -7.2807 & -356.3648 \\ -113.6640 & 53.0146 \end{bmatrix}$$

where the transfer functions $F_1(s)$ and $F_2(s)$ are chosen to be $F_1 = \text{diag}(\frac{2}{s+2}, 1)$ and $F_2 = I_2$

From Figures 4.14 and 4.15 it is evident that both the static and low-order compensators just manage to maintain stability in the presence of uncertainty, but both responses are marked by large amplitude oscillatory responses with long settling times; the tracking and decoupling properties of the system are lost. This reinforces the need for robust AW compensation schemes which can deal with a wide range of uncertainties in a systematic way. Using the approach

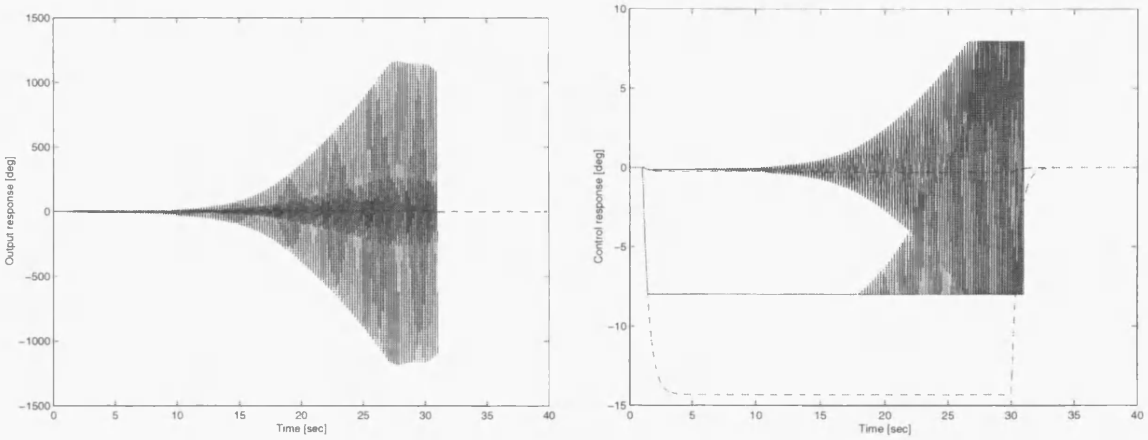

Figure 4.14: Uncertain Saturated system + Static AW compensator

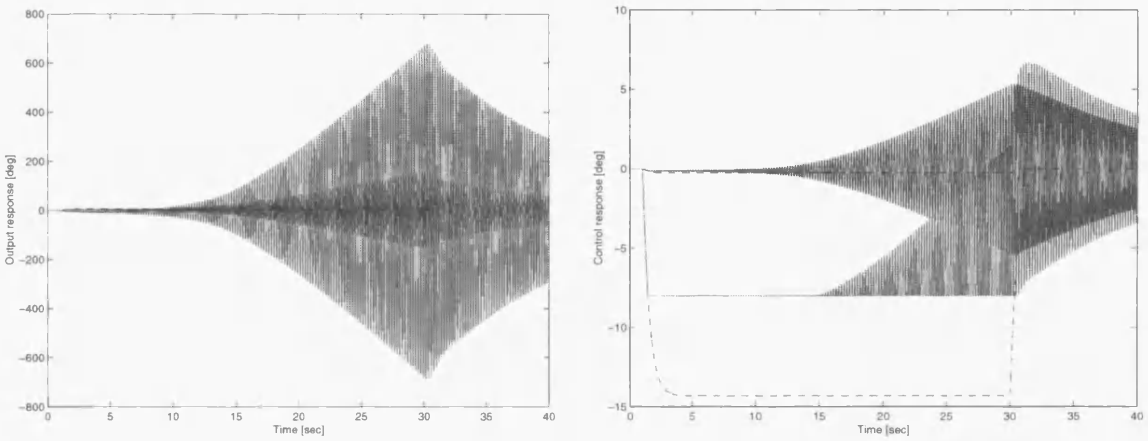

Figure 4.15: Uncertain Saturated system + Low-order AW compensator

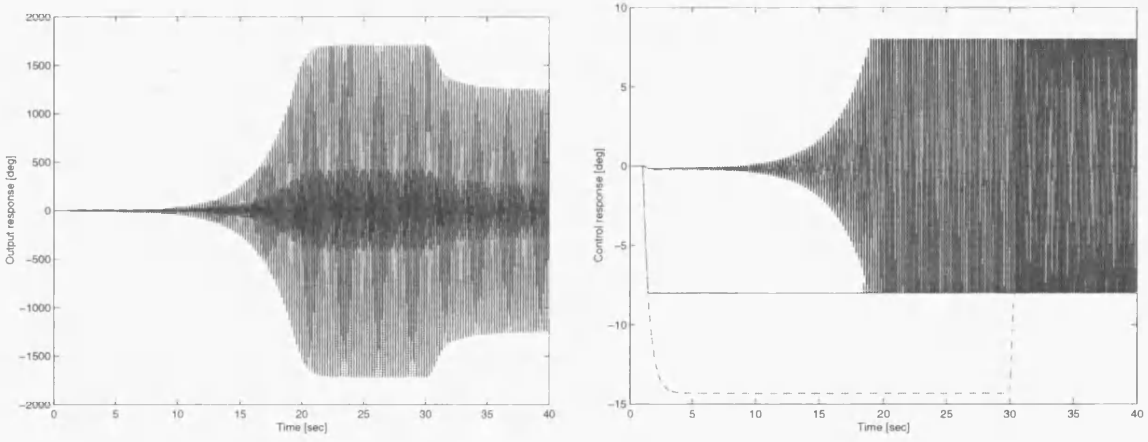

Figure 4.16: Uncertain Saturated system + Full-order LMI based robust AW compensator

of [107], a full-order "robust" LMI-based AW compensator was obtained by choosing weights

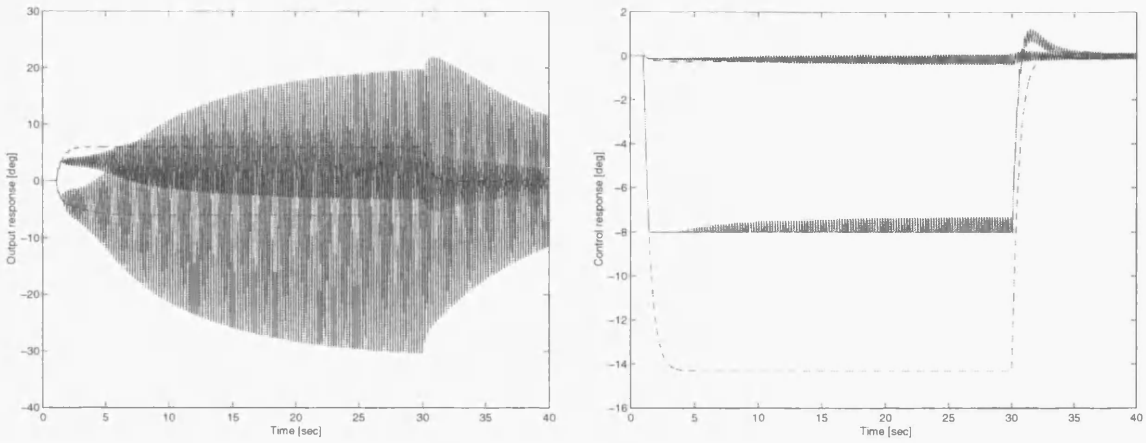

Figure 4.17: Uncertain Saturated system + Full-order Riccati based robust AW compensator

$W_p = I$ (performance) and $W_r = 0.001I$ (robustness) to give the matrix gain:

$$F = \begin{bmatrix} 0.1181 & 0.8070 & 0.0240 \\ -0.0035 & -0.0172 & -0.0002 \end{bmatrix} \tag{4.80}$$

It can be observed that in order to enhance dynamics during nonlinear operation (saturated system) of the overall closed-loop, it is necessary to give more relative importance, via the weight W_p, to performance optimisation. It transpires that with too large a robustness weight, W_r, nominal tracking suffers greatly during saturation.

The robust full-order compensator synthesis of [107] will be compared against the synthesis method proposed in this chapter. Figure 4.16 shows the response of the full-order LMI-based AW compensator proposed in [107]. Surprisingly, its performance is worse than that of the static or low-order compensators. This may be due to the fact that in such a scheme, robustness is achieved by reducing the magnitude of the poles of the compensator. This, in turn, reduces the system's performance. Although this is the ever present trade-off in robust control, the lack of *real* freedom in the LMI synthesis method has a tendency to compromise more performance than necessary.

Figure 4.17 shows the response of the full-order Riccati based AW compensator proposed in Theorem 2. Although the response is far from ideal, it is definitely stable and yields transients around two orders of magnitude lower than the LMI-based compensators. Although the robust Riccati-based compensator has faster dynamics, it is clearly preferable to the LMI based design. This is actually achieved by using Theorem 1, which can be seen as a weighted version of Theorem 2, and setting $W = diag[20, 0.1]$ and $\gamma = 500$. Notice that the freedom in choosing γ and W is especially useful when dealing with robustness issues and is almost absent in the LMI formulations. In other words, the so called stability multiplier (W) and the performance

index γ *efficiently* capture the trade-offs that exist between robustness and performance when designing AW compensators in the presence of uncertainties.

It should be emphasized that the missile example considered here is fairly artificial and the uncertainty is contrived to produce particularly poor responses during saturation. However, it does demonstrate that the problem of uncertainty in anti-windup design is non-trivial and careful attention should be paid to the design of robust anti-windup compensators.

4.5 Conclusions

This chapter has presented an alternative solution to the full-order AW problem with performance and robustness guarantees. The solution given is novel in the sense that the majority of full-order AW design techniques which ensure stability and performance involve LMI's (see [35] for a general treatment): here we simply require the solution to a bounded real type of Riccati equation, reducing the computational burden associated with LMI-based AW synthesis, particularly when dealing with high order systems. The solution proposed, while potentially conservative, is also believed to be more flexible than the LMI solutions as there is a clear link between the free parameter W and the size of the poles of the anti-windup compensator.

The chapter has also suggested a way of accounting for general linear additive uncertainty in a similar way to [107]. The results obtained have uncovered the close relationship between robust stability and the free parameter W, or the "stability multiplier". One of the important features of this perspective on the robustness of an AW compensator is that it enables the designer to trade-off performance and robustness in a more intuitive way than with the LMI based results of [107, 100] and also allows the relative importance of each channel to be captured in the compensator design through the matrix W.

Another important feature is the direct freedom the designer has to choose γ. Although optimal performance is always desired (i.e. $\gamma = \|G\|_\infty$) sometimes it is necessary to compromise performance in order to achieve robust stability. In the LMI formulation given in [107] some intuition is lost and not associated as closely with any of the already existing free parameters; instead, extra weights W_p and W_r are introduced to capture this trade-off.

It is interesting to observe how the design of full-order AW compensators, if no uncertainty is present, may be completely independent from the controller $K(s)$. However, when uncertainties are introduced, this is no longer the case and a small adjustment of the linear loop may enhance robustness of the saturated close-loop plant. Recently the *w*eakened AW problem has been proposed in [26] and it attempts to improve robustness at the expense of adjusting the linear

loop, which has the potential to achieve greater robust stability (see also [61]); as a consequence, the AW compensator modifies the controller not only during saturation periods, but also during uncertain behaviour.

Chapter 5

Rate-Limit AW compensation

5.1 Introduction

Much of the constrained input literature addresses the problem of *input saturation* whereby, as discussed earlier in the thesis, the *magnitude* of the control vector is subjected to element-wise limiting. Not surprisingly, researchers have devoted much attention to this problem due to its prevalence in most engineering applications. As discussed in Chapters 3 and 4, the magnitude saturation problem led practitioners and researchers to develop anti-windup schemes and indeed, many synthesis techniques have been proposed (some of the notable examples are [52], [110], [65], but see Chapter 3 and the references therein for more details). It is evident that at present, at least in principle, the control engineer who faces magnitude saturation problems has tools to enable him/her to address the problem, with some of the more modern AW schemes guaranteeing stability and performance.

However, magnitude limits on the control vector are not the only class of input nonlinearity which may be present in an otherwise linear system. Another significant class of nonlinearity which is well known to cause problems is *input rate saturation.* Although there are various ways of modeling this phenomena, in essence, rate saturation (or rate-limiting as it is often called) limits, normally in an element-wise fashion, the *rate of change* of the control vector. This type of nonlinearity is not as wide-spread as the saturation nonlinearity, as, for example, electrical systems typically are less prone to suffer from this problem. Nevertheless, rate-limited actuators can be a significant problem in many systems, particularly those with mechanical actuators, and in some applications rate-limiting can have devastating consequences. Some of the more notorious examples of the catastrophic effects of rate-limiting are the crashes of the SAAB Grippen [2] and Boeing V22 Osprey aircraft [6], and the meltdown of the Chernobyl nuclear power plant [94].

Due to this, efforts have been made to accommodate rate-limits in control systems and several successful methods have been proposed. However, it is important to mention that most of these results have either been effectively "theory only" ([55, 57, 69, 4, 32]) with little insight for the practicing engineer, or, they have been "practice only" ([82, 98]) results with effectively no stability/performance guarantees. Moreover, compared to the literature on amplitude constrained systems, the literature on rate constrained systems is minimal and thinly spread. Some of the methods which are applied in industry have been developed to make aircraft less prone to rate-saturation, phenomenon which can subsequently lead to the onset of so-called pilot-induced-oscillations (PIO's). These methods - often termed "phase compensators" (see for example [82]) - have effectively attempted to tackle the phase-shift which typically occurs during rate-limiting and indeed the name "phase compensators" often refers to an anti-windup type strategy that addresses this shift. None of these phase compensation schemes are accompanied by anything more than *ad hoc* design procedures and engineering insight.

The academic community has also attempted to address the rate-saturation problem. Most notable are the one-step schemes that seek to design single controllers which account for rate-saturation *a priori* and consist of "one-shot" design techniques. Good examples are [55] and [32] which have had some success, from a purely theoretical perspective, in tackling this problem. Further examples can be found in [99] and the references therein. Popular model predictive control (MPC) techniques also enable simple rate-saturation constraints to be incorporated in the controller design optimisation routine in a relatively straightforward manner, but suffer from problems similar to those associated with MPC in magnitude saturation problems (see [10, 62]).

Recently, some attempts at applying anti-windup (AW) schemes to the rate saturation problem have been made ([4, 45, 100]). Although the development of these schemes can be regarded as a step towards bridging the gap between the need to provide rigorous guarantees of the closed-loop system's behaviour during rate-saturation, and the need to develop techniques which are useful in practice, these schemes have tended to be lacking in intuition and have not been developed enough for the practicing engineer. As mentioned earlier one of main advantages of using AW conditioning schemes is that the linear performance (i.e. the performance when rate-saturation does not occur) is not directly restricted by the conditioning method, giving full freedom in the design of the linear controller. Moreover, the AW compensation schemes advocated in [118] which we follow here are designed independently of the linear controller and thus the same AW compensator can be used with multiple controllers. This will have implications for results reported in later chapters of this thesis.

This chapter will give an *intuitive* but rigorous solution to the rate-limit problem using anti-windup techniques. The focus is on developing an anti-windup technique which is easy to compute and satisfies the demands of the practicing engineer, while also guaranteeing stability and performance levels for the overall closed-loop system. For this work, as is common in the literature, rate-limits will be treated as dynamic systems with a *magnitude-limit* embedded within an internal feedback loop. As will be clear later, this representation essentially allows us to convert our rate-limit problem into a magnitude-limit problem at the expense of augmenting our system with *critically stable* poles. This is a crucial technical difference between the results presented in this chapter and those in the previous one. The presence of these critically stable poles means that, in general, it is difficult to guarantee *global stability* of the closed-loop system, even with an appropriate anti-windup scheme in place. However, this problem is partly overcome by using a semi-global approach instead (this approach has often been used in the literature - see [55, 57] for example). The resulting anti-windup design technique is similar to the one proposed in Chapter 4 but this time the Riccati equation has three free parameters. These parameters influence the performance and stability properties of the system and, hence, the chapter also provides insight into how these parameters can be tuned to capture the trade-offs, which may be required in practice, in a clear and intuitive manner.

5.2 Linear systems with rate-limits

Consider the same stabilisable, detectable and finite dimensional linear-time-invariant (FDLTI) plant $G(s)$ as considered in previous chapters (see Section 3.1 and equation (4.1)). Thus the dynamics of the plant remain the same, but instead of input magnitude-saturation, we assume that the plant is subject to input rate-saturation, viz

$$G(s) \sim \begin{cases} \dot{x} &= Ax + Bu_r \\ y &= Cx + Du_r \end{cases} \tag{5.1}$$

with $x \in \mathbb{R}^{n_p}$, $u_r \in \mathbb{R}^m$ and $y \in \mathbb{R}^q$. Again, we have not explicitly accounted for disturbances in this formulation, although as with the magnitude limit problem, disturbances can be incorporated with little extra effort.

Instead of assuming magnitude-saturation, here we assume the plant is driven by $u_r = \Phi(u)$ which is the output of the rate-limit function

$$\Phi(.) : \mathbb{R}^m \mapsto \mathbb{R}^m \tag{5.2}$$

which is a nonlinear *dynamic* system. The task of designing AW compensators is more complex for this type of dynamic nonlinearity as some of the common assumptions made in the AW

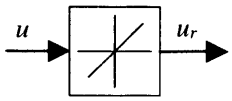

Figure 5.1: Representation of a rate-limit function: $\Phi(.) : \mathbb{R}^m \mapsto \mathbb{R}^m$

literature cannot be made; in particular, the AW community has often used sector bounds to model the saturation nonlinearity (as in Chapter 4, [48]). This has allowed a transparent application of nonlinear stability theory, especially the well known Circle Criteria (see Chapter 2, [48]). Unfortunately, while such an approach is feasible for many *static* nonlinearities, it is not appropriate for a *dynamic* nonlinearity such as rate saturation. In order to address this issue, the rate-limit has been modelled in different ways ([81, 45]), with the objective of allowing the conversion of a rate-limit problem into a problem which can be addressed using standard nonlinear absolute stability tools.

The rate-limit nonlinear function depicted in Figure 5.1 essentially produces an output $u_r(t)$ - the actual plant input - which is a rate-restricted version of the desired control input $u(t) \in \mathbb{R}^m$. In other words, constraint of the input is now on the velocity of the actuator, not its magnitude. Throughout this work we assume, as in the magnitude saturation case, that the nonlinearity $\Phi(.)$ is decentralised, that is

$$\Phi(u) = [\Phi_1(u_1), \ldots, \Phi_m(u_m)] \tag{5.3}$$

Each component $\Phi_i(.) : \mathbb{R} \mapsto \mathbb{R}$ has the following properties for some diagonal constant matrix $H > 0$:

i) if $|\dot{u}_i| < \bar{u}_i$ and $|(u_i - \Phi_i(u_i))| = 0$, then $\Phi_i(u_i) = u_i$

ii) if $|\dot{u}_i| < \bar{u}_i$ and $|H(u_i - \Phi_i(u_i))| \leq \bar{u}_i$, then $\Phi_i(u_i)$ will try to follow u_i with a rate $\dot{u}_{r,i} = \dot{u}_i$

iii) if $|\dot{u}_i| < \bar{u}_i$ and $|H(u_i - \Phi_i(u_i))| > \bar{u}_i$, then $\Phi_i(u_i)$ will try to follow u_i with a rate $\dot{u}_{r,i} = \pm\bar{u}_i$

iv) if $|\dot{u}_i| \geq \bar{u}_i$, then $\dot{u}_{r,i} = \pm\bar{u}_i$; in other words, the output $u_{r,i}$ tries to follow the input u_i with a limited rate

Remark 5.1: The constant matrix H is introduced in order to cover the rate-limit model that will be introduced next. For the case of an ideal RL, this constant matrix takes a value of infinity and the diffrence between properties (ii) and (iii) can not be distinguished. □

The constant rate-limit constraint values are $\bar{u}_i > 0 \; \forall i \in \{1, \ldots, m\}$. If there is no rate-limit present then $\Phi(u) = u$ and *nominal linear closed-loop* dynamics govern the system's behaviour.

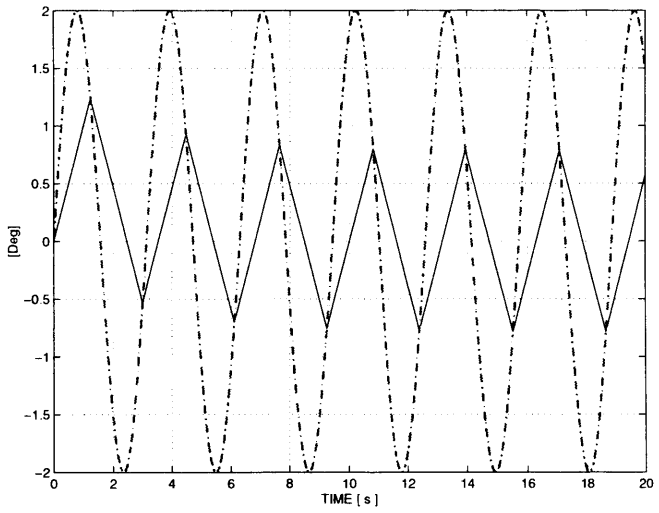

Figure 5.2: Input/Output Characteristics of rate-limits

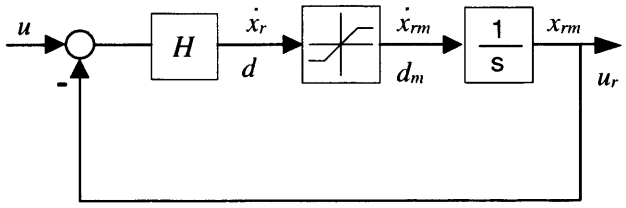

Figure 5.3: Dynamic model of the rate-limit

Thus for inputs $u(t)$ with sufficiently slow rate $\dot{u}(t)$, the rate-limit ideally behaves as the identity operator. For inputs with high enough frequency contents and/or magnitudes, the rate-limit will behave like a dynamical nonlinear operator. For the case where the input is a sine wave with high enough amplitude and frequency, the I/O relationship is shown in figure 5.2.

This *ideal* representation of the rate-limit is not convenient to handle and, furthermore, may not even be an accurate representation of *real* actuator dynamics. An alternative way of representing the rate-limit (see [81]) is as shown in Figure 5.3, where

$$\Phi_{r,i}(.) : \mathbb{R} \mapsto \mathbb{R} \quad i \in \{1, \ldots, m\} \tag{5.4}$$

is an operator mapping the desired control vector $u(t)$ to its rate-limited version $u_r(t)$. This model of the rate-limit features a (decentralised) magnitude saturation in a feedback loop with a set of integrators and a (decentralised) set of gains $H = \text{diag}(h_1, \ldots, h_m)$. Notice that the output u_r tries to track the input u but with its rate limited to $\pm\bar{u}$. To distinguish this problem from the magnitude problem discussed in earlier chapters, the rate-constraint values, which are now interpreted as magnitude saturation constraints in Figure 5.3, are redefined as $\bar{d} = \bar{u}$. The

system's dynamic equations are as follows

$$\Phi_r(u) \sim \begin{cases} \dot{x}_{rm} &= \text{sat}(-Hx_{rm} + Hu) \\ u_r &= x_{rm} \end{cases} \tag{5.5}$$

where the saturation function is the same as defined in Section 3.1, but with the signal $\bar{d}$ (the vector of rate-limits) replacing $\bar{u}$. Essentially, this model allows the rate-limit problem to be transformed into a magnitude limit problem at the expense of augmenting the plant with neutrally stable poles.

Remark 5.2: As illustrated in Figure 5.3, the rate-limit consists of a simple closed-loop system with a saturation function and an integrator. The idea behind this model is that the actuator can be considered to be performing a tracking task - in trying to get the output u_r to follow the input u - subject to a limit on its output rate. Thus $\dot{u}_r = \dot{x}_{rm}$ represents the actuator's actual rate and $\dot{x}_r$ represents the rate it is trying to achieve. □

Remark 5.3: The representation of the rate-limit in Figure 5.3 and equation (5.5) is not identical to that described in equation (5.3). Note that for signals slow enough such that $u(t)$ does not exceed its rate-limits, the representation in equation (5.3) yields $u_r(t) = u(t)$. However, in equation (5.5), the signal $u_r(t)$ is obtained by filtering $u(t)$ through a first order linear system, which in the scalar case, $\Phi_r(.) : \mathbb{R} \mapsto \mathbb{R}$, is given by

$$u_r(s) = \frac{H}{s+H} u(s)$$

Thus in general, by using the representation given in Figure 5.3, $u_r \neq u$ during transient periods. However, it is important to point out that for a large enough choice of H, the two representations, (5.3) and (5.5), are effectively the same. The main difference is that equation (5.5) models, in what is believed to be a more accurate way, the behaviour of a *real* actuator; equation (5.3) does not permit the actuator to have any "linear" dynamics. Thus for the above reasons it is preferable to work with Figure 5.3 (and hence equation (5.5)). □

As mentioned above, to approximate an "ideal" rate-limiter, the gain H must be chosen as a large positive scalar. In practice, this gain reflects other dynamic properties present in the actuator and can be chosen as some value close to its bandwidth. It is important to realise that if H is chosen to be less than the actuators' actual bandwidth, the control signal will present a degraded control action and the system's overall performance may be reduced, even when in linear mode (i.e. no rate-limiting is present). In other words, $H = \text{diag}(h_1, h_2, \ldots, h_m)$ determines the cut-off frequencies of the equivalent linear actuator and the saturation block

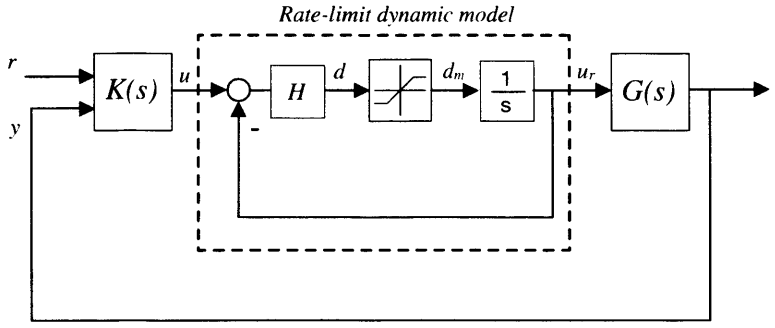

Figure 5.4: Block Diagram of a system with modelled rate-limits

models the velocity limiting. In the limit as $h_i \to \infty \quad i \in \{1, 2, \ldots, m\}$, the "ideal" rate-limit is recovered.

Remark 5.4: The time constant $\frac{1}{H}$ must typically be greater than the dominant frequency components of u in order to prevent the linear dynamics of the actuator from interfering too much with the nominal control system design. This is often a valid practical assumption and if not, some account of these linear dynamics must be taken during nominal linear controller design. □

5.3 Anti-windup compensation for systems with rate-limits

Figure 5.4 shows a block diagram of the closed-loop system with the rate-limit configuration proposed. $G(s)$ is the plant described earlier and $K(s)$ is the 2-degree-of-freedom (2-D.o.F) controller, i.e. $u = [K_1, K_2][r', y']'$. As is typical in the AW literature we assume that $K(s)$ has been designed to stabilise the nominal (not rate-limited) plant $G(s)$ and to achieve nominal performance specifications. The rate-limit model, $\Phi_r(.)$ appears sandwiched between controller and plant. Note that the only nonlinear element in Figure 5.4 is now the saturation nonlinearity which is embedded within the rate-limit model. Thus, defining the "augmented" controller as

$$\tilde{K} = H[K_1 \quad K_2 \quad -I_m] \tag{5.6}$$

and the "augmented" plant as

$$\tilde{G}(s) = \begin{bmatrix} G(s)\frac{1}{s} \\ I\frac{1}{s} \end{bmatrix} \sim \left[\begin{array}{cc|c} A & B & 0 \\ 0 & 0 & I \\ \hline C & D & 0 \\ 0 & I & 0 \end{array}\right] = \left[\begin{array}{c|c} \tilde{A} & \tilde{B} \\ \hline \tilde{C} & 0 \end{array}\right] \tag{5.7}$$

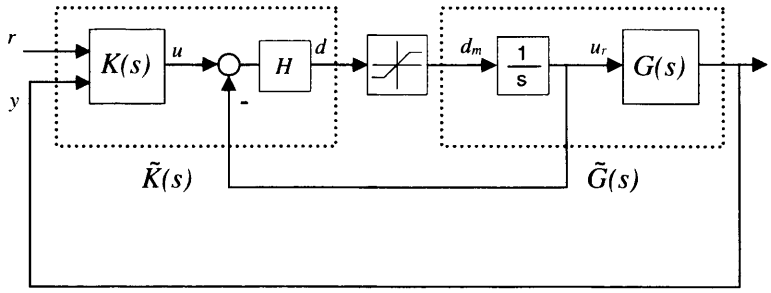

Figure 5.5: Equivalent System with $\tilde{G}(s)$

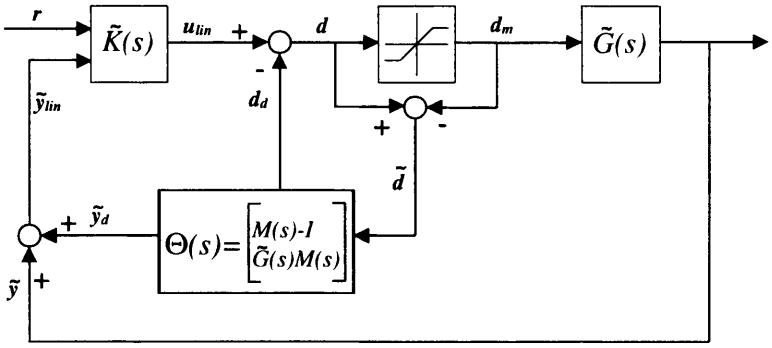

Figure 5.6: Equivalent AW Saturation Problem: replace $G(s)$ with $\tilde{G}(s)$

the system in Figure 5.4 can be represented equivalently as shown in Figure 5.6. The augmented controller, $\tilde{K}(s)$, is now driven by the signals

$$r \in \mathbb{R}^{n_r}, \quad \tilde{y} = \begin{bmatrix} y \\ u_r \end{bmatrix} \in \mathbb{R}^{q+m}$$

and produces the input to the saturation nonlinearity, $d \in \mathbb{R}^m$. The augmented plant, $\tilde{G}(s)$, is driven by the output of the saturation nonlinearity, $d_m = \text{sat}(d) \in \mathbb{R}^m$ and produces the output, $\tilde{y}$. The augmented plant now includes dynamics absorbed from the rate-limit model and thus has a larger state-vector $[x', x'_{rm}]' \in \mathbb{R}^{n_p+m}$; its poles are now those of the plant $G(s)$ plus m poles at the origin.

Note that Figure 5.5 is in the same form as a control system subject to magnitude saturation but with $\tilde{K}(s)$ replacing $K(s)$ and $\tilde{G}(s)$ replacing $G(s)$. Therefore, AW can be introduced in a similar manner to before and is shown in Figure 5.6. The anti-windup compensator $\Theta(s)$ is, again, driven by the difference between the saturated and unsaturated "control" vector $\tilde{d} = d - d_m$ but now it contains a copy of the *augmented* plant dynamics, $\tilde{G}(s)$ and a free parameter $M(s) \in \mathcal{RH}_\infty$. This structure will be described in more detail shortly but for now, simply notice that by using the "augmented" plant and controller, a configuration identical to the magnitude problem has emerged.

5.3.1 Semi-Global Approach

At first glance, the above block diagram manipulation may appear to allow a trivial translation of the rate-limit problem into an equivalent magnitude-limit problem, as depicted in Figure 5.6. It may be incorrectly inferred that a solution of the rate-limit AW problem could be obtained by simple application of the techniques already described in Chapter 4. However, notice that the new plant has poles given by $\mathbf{spec}(\tilde{A})$, consisting of the poles located at $\mathbf{spec}(A)$ and m poles located at zero. Thus even if $G \in \mathcal{RH}_\infty$, it is easy to observe that $\tilde{G} \notin \mathcal{RH}_\infty$, where the new augmented plant is obviously not bounded real. Therefore straightforward application of any of the ideas in Chapter 3 would result in unsuitable problem formulations which *are not solvable* and therefore the methods for magnitude saturation described in Chapter 4 would *fail* for rate saturation if we simply substituted the state-space matrices (A, B, C, D) for $(\tilde{A}, \tilde{B}, \tilde{C}, \tilde{D})$; the resulting Riccati equation would not be of the bounded-real type. However, notice that if $G \in \mathcal{RH}_\infty$, and therefore $\mathbf{spec}(A) \in \mathcal{C}^-$, then $\tilde{G}$ would be stable provided that its zero eigenvalues were perturbed an arbitrarily small amount into the left half complex plane. So although $\tilde{G}$ is not stable, it is *almost* bounded real.

The main technical issue with $\tilde{G}$ is that the imaginary axis poles prevent *true* bounded realness, meaning global stability and finite $\mathcal{L}_2$ gain typically cannot be obtained and often are difficult to address. Therefore, instead of insisting on *global asymptotic stability* and *global finite* $\mathcal{L}_2$ gain - as stipulated for the magnitude-limit problem in Chapter 4 - the aims are relaxed to those of achieving *local* or *semi-global* results instead. Local and semi-global asymptotic stability are defined in Section 2.3 and roughly speaking, the local AW problem aims at finding the lowest possible induced $\mathcal{L}_2$ gain of a certain map (within a certain domain) while maintaining stability of the non-linear loop for the largest domain of attraction possible.

The dead-zone function, defined in equation (3.4), plays a central role in the results derived in this chapter and is key to defining a suitable local AW problem. Note that in terms of the rate-limit problem here proposed, we are interested in the signal $\tilde{d}(t)$ which is generated via

$$\tilde{d}(t) := \mathrm{Dz}(d(t)) \tag{5.8}$$

Thus, as in the definition given in section (4.1.2), we can see that $\mathrm{Dz}(d) = 0 \quad \forall d \in \mathcal{D}$, where the hypercuboid $\mathcal{D}$ is defined as

$$\mathcal{D} = [-\bar{d}_1, \bar{d}_1] \times [-\bar{d}_2, \bar{d}_2] \times \ldots \times [-\bar{d}_m, \bar{d}_m] \tag{5.9}$$

and $\bar{d}_i > 0$, with $i \in \{1, \ldots, m\}$, again represents the rate-limits (which now have the equivalent interpretation as the beginning and end of the i^{th} dead-zone). As before, for any $d \in \mathbb{R}^m$, it

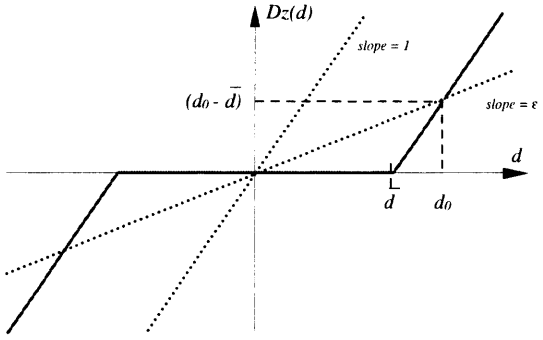

Figure 5.7: Sector bound representation for $Dz(.)$

follows that the dead-zone inhabits, globally, the Sector$[0, I]$

$$Dz(d) \in \text{Sector}[0, I] \quad \forall d \in \mathbb{R}^m \tag{5.10}$$

However, as we will be seeking local (semi-global) results, we shall not consider the case where d inhabits the whole signal space, i.e. $d \in \mathbb{R}^m$; rather we shall consider a subset of $\mathbb{R}^m$. In fact if d is bounded in magnitude, that is if $d_i < d_{0,i}\ \forall i \in \{1, \ldots, m\}$, it is possible to consider a *reduced sector*, as shown in Figure 5.7 for a scalar dead-zone function, which the nonlinearity inhabits locally. This reduced sector notion has been applied several times before in the magnitude saturation context [120, 89, 43] and appears to be a useful way of capturing local stability problems. In summary, the dead-zone function belongs (globally) to Sector$[0, I]$; however, if the input signal to the nonlinearity (i.e. d) is assumed to be below a certain level (i.e. d_0), then the dead-zone function can be said to satisfy a less conservative sector bound Sector$[0, \epsilon I]$, where $\epsilon \in (0, 1)$. It should be noted that assuming a bound on d makes sense for most engineering applications.

Remark 5.5: It is important to notice that if the input signal d exceeds the proposed level of boundedness, d_0, the less conservative sector bound will not hold. In such a case, it is always possible to choose an ϵ closer to unity such that our input signal is always guaranteed to lie within the imposed bound, and therefore, within the proposed Sector$[0, \epsilon I]$; this comes at the expense of reduced allowable performance. □

In order to use our "reduced sector" discovery, we need to define it mathematically. Using the element-wise operator "$\preceq$" introduced in Chapter 2, an alternative and more compact way of defining the set $\mathcal{D}$ is

$$\mathcal{D} = \left\{ d \in \mathbb{R}^m : -\bar{d} \preceq d \preceq \bar{d} \right\} \tag{5.11}$$

Using the same notation, it is convenient to define the set

$$\mathcal{S}(d_0) := \{d \in \mathbb{R}^m : -d_0 \preceq d \preceq d_0\} \tag{5.12}$$

as proposed in [32]. Here, $|d_{0,i}| > \bar{d}_i, \quad \forall i \in \{1, \ldots, m\}$ and hence $\mathcal{D} \subset \mathcal{S}(d_0)$. It is now possible to state that if $d \in \mathcal{S}(d_0)$, then $Dz(d)$ is contained within a narrower and less conservative sector bound. The narrower sector bound is formally defined below

Definition 5.1 *The decentralised static nonlinearity* $\mathcal{N} = \text{diag}(\eta_1, \ldots, \eta_m)$ *is said to belong to* Sector$[0, K_\epsilon]$ *if the following inequality holds:*

$$\eta(d)' W(K_\epsilon d - \eta(d)) \geq 0 \tag{5.13}$$

where $W \in \mathbb{R}^{m \times m}$ *and* $K_\epsilon = diag(\epsilon_1, \ldots, \epsilon_m) \in \mathbb{R}^{m \times m}$ *are positive definite diagonal matrices* □

From Figure 5.7 notice that globally Dz(.) $\in$ Sector$[0, I]$ as the graph of the deadzone never exceeds the unity gradient line; locally it is possible to use tighter approximations and provided $d_i \leq d_{0,i}$ it follows that $\text{Dz}_\text{i}(.) \in$ Sector$[0, \epsilon_\text{i}]$ where

$$d_{0,i} := \frac{\bar{u}_{(i)}}{1 - \epsilon(i)} \tag{5.14}$$

Thus taking $K_\epsilon = \epsilon I$, where $\epsilon = \max_i\{\epsilon_i\}$, it follows that

$$\text{Dz}(d) \in \text{Sector}[0, \epsilon I], \quad \forall |d| \preceq d_0 \tag{5.15}$$

Therefore by restricting our attention to $d \in \mathcal{S}(d_0)$ where $d_0 < \infty$, which in turn implies $\epsilon \in (0, 1)$, the deadzone is guaranteed to inhabit a narrower sector than Sector[0, I] i.e.

$$d \in \mathcal{S}(d_0) \Rightarrow \text{Dz}(d) \in \text{Sector}[0, \epsilon I] \tag{5.16}$$

This reduced sector is crucial for the semi-global results developed in this chapter. Note that for any arbitrary large d_0, then there always exists an $\epsilon \in (0, 1)$ such that Dz$(d) \in$ Sector$[0, \epsilon I]$ (and in fact global results are recovered if $d_{0,i} = \infty \quad \forall i \in \{1, \ldots, m\}$, and hence Dz$(d) \in$ Sector$[0, I]$). It will be shown shortly that the use of this reduced sector allows us to pose an AW problem similar to the magnitude saturation case; the critically stable poles are allowed but at the expense of guaranteeing local asymptotic and small signal $\mathcal{L}_2$ gain properties.

5.3.2 Region of attraction

In AW compensation for systems with magnitude saturation, provided $G(s) \in \mathcal{RH}_\infty$, then a compensator which yielded global stability properties was guaranteed to exist. When $G(s) \notin \mathcal{RH}_\infty$, global stability is not always possible, or convenient, to obtain. Thus many authors ([55, 57]) have relaxed the requirements of stability to being local or semi-global. From a state-space perspective, local stability implies that the system is only asymptotically stable for states within a neighbourhood of the equilibrium point under consideration. The set of all states which converge asymptotically to the equilibrium point is known as the *region of attraction* (ROA). This is defined formally below

Definition 5.2 *Consider a state-space system $\dot{x} = f(x)$, and let $x(t) \in \mathbb{R}^n$, be the solution to this differential equation. Assume that the origin $x = 0$ is an equilibrium point. Then the region of attraction (of the origin) is the set of all points, $\mathcal{A} \subset \mathbb{R}^n$ such that if $x(0) \in \mathcal{A}$ then this implies that $\lim_{t\to\infty} x(t) = 0$.* □

Thus, the region of attraction may be interpreted as the set of all states from which the zero-input solution of a system converges to the equilibrium point. Note that the region of attraction is a positively invariant set (i.e. $x(0) \in \mathcal{A} \Rightarrow x(t) \in \mathcal{A}\ \forall t \geq 0$) and contains the equilibrium point ($x = 0$) in its interior. Hence, if local asymptotic stability is sought, then an accompanying set of initial conditions, $\mathcal{A}$ is also sought. In general, computation of the region of attraction for nonlinear systems is a nontrivial task. Surprisingly, this is also the case with a saturated system, despite the seeming simplicity of the saturation/dead-zone nonlinearity. Over the years many authors ([104, 12, 4, 33, 32, 75, 102]) have proposed methods which can be used to estimate the region of attraction for a saturated system, with these estimates ranging from accurate but difficult to compute [45], to crude but easy to compute, [39, 33].

In our work, as the focus is on semi-global stability, we are content to consider a region of attraction with a crude geometry, but one which, by appropriate choice of AW compensator, can be made arbitrarily large. In the saturated systems literature (as in [56], [33] for example), an ellipsoidal approximation is typically used,

$$\mathcal{E} = \left\{\tilde{x} \in \mathbb{R}^{n_p+m} : \tilde{x}' P \tilde{x} < c\right\}. \tag{5.17}$$

The largest such ellipsoid can be calculated (see for example [96], [109]) using a simple formula which will be given later. The salient feature of this type of representation is that it will allow a transparent relationship between AW design parameters and a subset of the region of

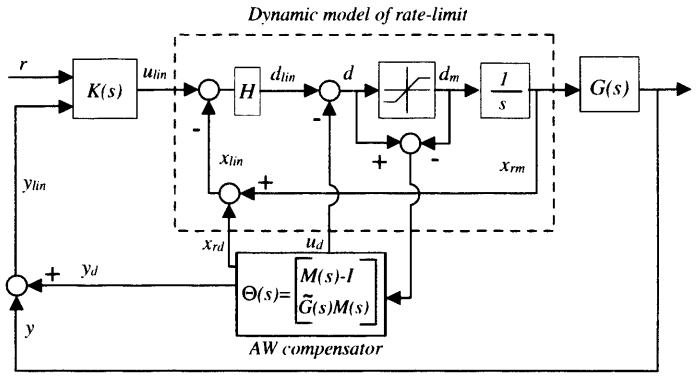

Figure 5.8: Conditioning with $M(s)$

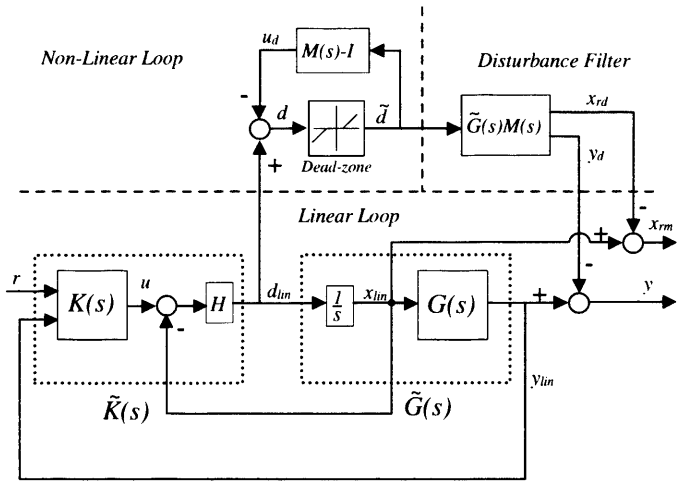

Figure 5.9: Decoupled structure

attraction, $\mathcal{E} \subset \mathcal{X} \subset \mathcal{A}$ to be observed. It must be clarified that the states $\tilde{x}$ are the states of our AW compensator as stability of our linear loop is guaranteed to be global.

5.4 Anti-windup Synthesis

5.4.1 Problem definition

The architecture of our anti-windup compensator is shown in Figure 5.8 where the nominal controller, $K(s)$, plant $G(s)$ as well as the rate-limit dynamics are shown. Θ is the anti-windup compensator, parametrised by $M(s) \in \mathcal{RH}_\infty$ and $\tilde{G}(s)$ as described earlier, which only becomes active once rate saturation has occurred. The compensator has two sets of outputs, $d_d \in \mathbb{R}^m$ and $\tilde{y}_d = [y_d', x_{rd}']' \in \mathbb{R}^{q+m}$, which enter the control signal (the output of the "augmented" controller $\tilde{K}$) and output of the "augmented" plant $\tilde{G}$ respectively.

For magnitude limits, as discussed in Chapter 3 (see also [118]), parametrising Θ by using a

transfer function M and a copy of the plant, which in this case is the augmented plant $\tilde{G}$, yields an appealing decoupling of the closed loop system. Thus choosing

$$\Theta(s) = \begin{bmatrix} M(s) - I \\ \tilde{G}(s)M(s) \end{bmatrix} \tag{5.18}$$

similarly to the results described in Chapter 3, it can be verified that Figure 5.8 can be re-drawn as Figure 5.9 where the closed-loop compensated system with modelled rate-limits is decoupled into *nominal linear system*, *non-linear loop* and *disturbance filter*. Note that in this case the *nominal linear system* consists of the linear controller, the nominal linear plant, and the linear rate-limit dynamics. It is normal for the linear loop to function well without saturation and thus we make the assumption

Assumption 4

$$\begin{bmatrix} I & -\tilde{K}_2(s) \\ -\tilde{G}(s) & I \end{bmatrix}^{-1} \in \mathcal{RH}_\infty \tag{5.19}$$

and

$$\lim_{s\to\infty} \tilde{K}_2(s)\tilde{G}(s) \neq I \tag{5.20}$$

□

The above assumption ensures that the linear loop (including the linear rate-limit dynamics) is internally stable and well-posed. This assumption differs slightly from the magnitude limit case because linear rate-limit dynamics are part of the linear closed-loop. For well-designed linear control loops, this is a valid practical assumption.

Therefore, assuming that the nominal linear system is asymptotically stable, the AW problem can be reduced to that of finding a transfer function $M(s) \in \mathcal{RH}_\infty$ such that the nonlinear loop is zero-input locally asymptotically stable (semi-global asymptotically stable if $G \in \mathcal{RH}_\infty$) and the operator $\mathcal{T}_p : d_{lin} \mapsto \tilde{y}_d$ is well-defined and is small-signal finite gain $\mathcal{L}_2$ stable, i.e. $\|\mathcal{T}_p\|_{i,2} < \gamma$ for some $\gamma > 0$ and some "sufficiently small" input d_{lin}. If such a compensator exists, then we say that it *solves strongly* the *local anti-windup problem.* The following definition will formally describe the AW problem to be considered (based on ideas first appearing in [105]).

Definition 5.3 *The anti-windup, compensator (5.18), is said to solve the rate-limit anti-windup (RLAW) problem within a finite domain, assuming $G \in \mathcal{RH}_\infty$, if the closed-loop system in Figure 5.8 (equivalently Figure 5.9) is well-posed and the following hold:*

1. *The closed-loop AW compensated system is*

a) zero input LAS; and

b) semi-globally asymptotically stabilisable.

2. *If* $\text{dist}(d_{lin}, \mathcal{D}) = 0, \quad \forall t \geq 0$, *then* $\tilde{y}_d = 0, \quad \forall t \geq 0$ *(assuming zero initial conditions for* M*).*

3. *If* $\text{dist}(d_{lin}, \mathcal{D}) \in \mathcal{L}_2 \cap \mathcal{W}$, *where*

$$\mathcal{W} = \{d_{lin} \in \mathbb{R}^m : d \in \mathcal{S}(d_0) \ \forall t \geq 0\} \tag{5.21}$$

then, assuming zero initial conditions, $\tilde{y}_d \in \mathcal{L}_2$.

The compensator $\Theta(s)$ *is said to solve strongly the local anti-windup problem if, in addition, the following condition is satisfied:*

4. *The operator* $\mathcal{T}_p : d_{lin} \mapsto \tilde{y}_d$ *is well-defined and small-signal finite gain* $\mathcal{L}_2$ *stable, or equivalently,* $\|\mathcal{T}\|_{i,2,\mathcal{W}} < \gamma$, *for some* $\gamma > 0$.

□

Observing the decoupled system in Figure 5.9, and as proposed in Definition 5.3, it is clear that the mapping $\mathcal{T}_p : d_{lin} \mapsto \tilde{y}_d$ determines the deviation of the non-linear system's behaviour from nominal. An important feature, inherited from the AW philosophy and the decoupled structure, is that the performance index is purely defined on the saturated system and no constraints are set directly on the controller $\tilde{K}$ (or equivalently on K).

Remark 5.6: As with the magnitude saturation problem, only full-order AW compensators are studied, since for an appropriate choice of $M(s)$ it is possible to design $\Theta(s)$ *independently* of $\tilde{K}(s)$ and more importantly, because a stabilising compensator is always guaranteed to exist either locally or semi-globally. □

In order to achieve full-order compensation, $M \in \mathcal{RH}_\infty$ is chosen as part of a right coprime factorisation of the augmented plant; $\tilde{G} = NM^{-1}$. The disturbance filter will then be reduced to N and the AW compensator is parametrised by the matrix gain F, where $\tilde{A} + \tilde{B}F$ must be Hurwitz. It follows that, in a similar way as for the saturation AW problem, a state-space realisation of such an AW compensator is given by

$$\Theta = \begin{bmatrix} M(s) - I \\ N(s) \end{bmatrix} \sim \left[\begin{array}{c|c} \tilde{A} + \tilde{B}F & \tilde{B} \\ \hline F & 0 \\ \tilde{C} + \tilde{D}F & \tilde{D} \end{array}\right] \tag{5.22}$$

However, as $\tilde{D} \equiv 0$ for any plant G, then

$$\Theta = \begin{bmatrix} M(s) - I \\ N(s) \end{bmatrix} \sim \left[\begin{array}{c|c} \tilde{A} + \tilde{B}F & \tilde{B} \\ \hline F & 0 \\ \tilde{C} & 0 \end{array}\right] \tag{5.23}$$

where $\tilde{x} \in \mathbb{R}^{n_p+m}$ is defined as the AW state vector.

In this case a state-space realisation for our nonlinear operator $\mathcal{T}_p$ is

$$\mathcal{T}_p \sim \begin{cases} \dot{\tilde{x}} &= (\tilde{A} + \tilde{B}F)\tilde{x} + \tilde{B}\tilde{d} \\ d_d &= F\tilde{x} \\ \tilde{y}_d &= \tilde{C}\tilde{x} \\ \tilde{d} &= \mathrm{Dz}(u_{lin} - d_d) \end{cases} \tag{5.24}$$

Thus for "good" anti-windup performance we must choose F (and hence M, N) to guarantee asymptotic stability (within some domain $\mathcal{X} \subset \mathbb{R}^{n_p+m}$) of the nonlinear loop and to minimise the $\mathcal{L}_2$ gain of the map $\mathcal{T}_p$ in a local sense. As mentioned earlier if $G \in \mathcal{RH}_\infty$ it is possible to choose the ROA $\mathcal{X} \subset \mathcal{A}$ arbitrarily large, making it possible to ensure semi-global asymptotic stability. The following lemma, which is fairly obvious from Figure 5.9, enables us to state the RLAW in a slightly more compact form to that given in Definition 5.3.

Lemma 5.1 *The AW compensator (5.23) solves strongly the RLAW problem if Assumption 4 is satisfied and the nonlinear operator $\mathcal{T}_p$ defined in equation (5.24) is zero input LAS and semi-globally stabilisable, and locally finite $\mathcal{L}_2$ gain stable.*

Proof: Consider Figure 5.9 and note that if Assumption 4 is satisfied, then zero input LAS (and semi-global stabilisability of the closed-loop) is ensured if the operator $\mathcal{T}_p$ is itself zero input LAS (and semi-global stabilisable). This implies Condition 1 of the RLAW problem is satisfied. To see that Condition 2 is satisfied, note from Figure 5.9 or equation (5.24) that if $\mathrm{dist}(d, \mathcal{D}) = 0 \ \forall \ t \geq 0$, then assuming zero initial conditions, $\tilde{x}(0) = 0$, it follows that $\tilde{x} = 0 \ \forall t \ \geq 0$ and hence by equation (5.24) that $\tilde{y}_d = 0 \ \forall t \ \geq 0$. Furthermore note that if $\|\mathcal{T}_p\|_{i,2,\mathcal{W}} < \gamma$ for some $\gamma > 0$, then this implies Condition 4 of the RLAW problem is satisfied and hence Condition 3 is also satisfied. Well-posedness of the system in Figure 5.9 follows from Assumption 4 and the fact that the operator $\mathcal{T}_p$ (5.24) contains no direct feed-through terms, meaning all equations are explicit. □□

Thus, as with the magnitude limit AW problem, the RLAW reduces to the study of the nonlinear operator $\mathcal{T}_p$. This will be addressed in the next subsection.

5.4.2 Problem solution

Under the logical conditions of Assumption 4, Lemma 5.1 implies that the nonlinear stability problem contained with the RLAW problem has been transformed into that of guaranteeing local stability of the *nonlinear loop* - see Figure 5.9. Therefore, as with the magnitude case, the problem of ensuring local asymptotic stability of the closed-loop system is equivalent to ensuring zero-input LAS for $\tilde{x} \in \mathcal{X}$ of the nonlinear loop. Moreover, the performance problem is now determined by the mapping $\mathcal{T}_p : d_{lin} \mapsto \tilde{y}_d$ where $\|\mathcal{T}_p\|_{i,2,\mathcal{W}} \leq \gamma$ must be guaranteed.

The following theorem (published in [89]) is the main result of the chapter

Theorem 5.1 *There exists a full order anti-windup compensator* $\Theta = [\Theta_1' \quad \Theta_2']' \in \mathbb{R}^{p+2m\times m}$, *as stated in (5.23), which solves strongly the RLAW problem if there exist matrices* $W = \text{diag}(w_1, \ldots, w_m) > 0$, $P = P^T > 0$, *and positive real scalars* γ *and* ϵ *such that the following Riccati equation is satisfied*

$$\tilde{A}'P + P\tilde{A} + P\tilde{B}(\gamma^{-2}I - 2\tfrac{(1-\epsilon)W^{-1}}{\epsilon^2})\tilde{B}'P + \tilde{C}'\tilde{C} \;=\; 0 \tag{5.25}$$

where the matrix Z *must satisfy the following inequality:*

$$Z = (2W - \gamma^{-2}(\epsilon W)^2) > 2\epsilon W > 0 \tag{5.26}$$

Furthermore, if equation (5.25) is satisfied, a suitable Θ *is obtained by calculating the matrix* F *as*

$$F = -\left(\frac{(2-\epsilon)W^{-1}}{\epsilon^2} - \gamma^{-2}I\right)\tilde{B}'P \tag{5.27}$$

An ellipsoidal estimate of $\mathcal{X}$, *the region of attraction (ROA), is given by*

$$\bar{\mathcal{E}} = \left\{\tilde{x} \in \mathbb{R}^{n_p+m} : \tilde{x}'P\tilde{x} < c_{max}\right\} \tag{5.28}$$

where

$$c_{max} \;=\; \min_i \frac{\bar{d}_i^2 w_i^2}{(1-\epsilon)^2(\frac{(2-\epsilon)}{\epsilon^2} - \gamma^{-2}w_i)^2 B_i'PB_i} \tag{5.29}$$

and w_i *is the* i^{th} *diagonal component of* W *and* B_i *is the* i^{th} *column vector component of* B, *for some* $i \in [1, \ldots, m]$. □□

Proof: A slightly different proof to that in [89] will be given for Theorem 5.1 and will be constructed in several stages as detailed below.

i) The main inequality Consider the function

$$L := \frac{d}{dt}\tilde{x}'P\tilde{x} + \|\tilde{C}\tilde{x}\|_2^2 - \gamma^2\|d_{lin}\|_2^2 + 2\tilde{d}'W(\epsilon d - \tilde{d}) < 0 \tag{5.30}$$

The final term $2\tilde{d}'W(\epsilon d - \tilde{d})$ arises from using the reduced sector defined in Definition 5.1 and if $d \in \mathcal{S}(d, d_0)$ $\forall t \geq 0$ it follows that $2\tilde{d}'W(\epsilon d - \tilde{d}) \geq 0$. Now consider two cases

1. Assume that $\tilde{x}(0) = 0$ and $d_{lin} \in \mathcal{W}$. This implies that $d \in \mathcal{S}(d_0)$ $\forall t \geq 0$ and thus if inequality (5.30) holds then this implies

$$\frac{d}{dt}\tilde{x}'P\tilde{x} + \|\tilde{C}\tilde{x}\|_2^2 - \gamma^2\|d_{lin}\|^2 < 0 \tag{5.31}$$

Integration with respect to time from $t = 0$ to $t = \infty$ gives

$$x(\infty)'Px(\infty) - x(0)'Px(0) + \|\tilde{y}_d\|_2^2 - \gamma^2\|d_{lin}\|_2^2 < 0 \tag{5.32}$$

which in turn implies that $\|\tilde{y}_d\|_2 - \gamma\|d_{lin}\|_2 < 0$ and hence that $\|\mathcal{T}\|_{i,2,W} < \gamma$. Therefore if inequality (5.30) holds, Condition 4, and hence Condition 3, of the RLAW problem are satisfied.

2. Next assume that $d_{lin} = 0$ $\forall\, t \geq 0$ and that $\tilde{x}(0) \in \mathcal{E}$ where

$$\mathcal{E} = \{\tilde{x} \in \mathbb{R}^{n_p+m} : \tilde{x}'P\tilde{x} \leq c\} \tag{5.33}$$

for some $c > 0$. Furthermore let c be sufficiently small to ensure that $d \in \mathcal{S}(d_0)$. Then it follows that $2\tilde{d}'W(\epsilon d - \tilde{d}) \geq 0$ and inequality (5.30) implies that

$$\frac{d}{dt}\tilde{x}'P\tilde{x} + \|\tilde{C}\tilde{x}\|_2^2 < 0 \tag{5.34}$$

This implies that

$$\frac{d}{dt}\tilde{x}'P\tilde{x} = \dot{V}(\tilde{x}) < 0 \tag{5.35}$$

and thus $V(\tilde{x})$ is a Lyapunov function for the nonlinear loop in Figure 5.9), which ensures local asymptotic stability for all $\tilde{x}(0) \in \mathcal{E}$; c must be sufficiently small to ensure $d \in \mathcal{S}(d_0)$. Thus the system is locally asymptotically stable and hence, if inequality (5.30) holds, Condition 1a of the RLAW problem is satisfied.

Thus, it remains for us to prove that satisfaction of inequality (5.30) is equivalent to the expressions given in the Theorem and that Condition 1b is also satisfied.

ii) Evaluation of the main inequality. The remainder of the proof shows how we can re-write the cost function L, equation (5.30), as the conditions given in Theorem 5.1. Evaluating

equation (5.30) results in an inequality containing several cross terms in $\tilde{d}$, d_{lin}, and $\tilde{x}$. Using similar ideas to those proposed in [90], it is possible to address this issue and avoid an LMI formulations.

Expanding (5.30) and substituting $d = d_{lin} - d_d$ gives

$$L = \tilde{x}'\tilde{C}'\tilde{C}\tilde{x} - \gamma^2 d'_{lin}d_{lin} + \dot{\tilde{x}}'P\tilde{x} + \tilde{x}'P\dot{\tilde{x}} - 2\tilde{d}'\epsilon W d_d - 2\tilde{d}'W\tilde{d} + 2\tilde{d}'\epsilon W d_{lin} < 0 \quad (5.36)$$

We now group the cross-product terms in three steps:

(I) Cross-product terms involving d_{lin} and $\tilde{d}$ are grouped as follows:

$$-\left[\gamma^2 d'_{lin}d_{lin} - 2\tilde{d}'\epsilon W d_{lin}\right] = -\|(\gamma d_{lin} - \gamma^{-1}W\epsilon\tilde{d})\|^2 + \gamma^{-2}\tilde{d}'\epsilon^2 W^2\tilde{d} \quad (5.37)$$

Combining the above with (5.36), a cost function containing no cross-product terms between d_{lin} and $\tilde{d}$ is obtained. Using equation (5.23) to expand $\dot{\tilde{x}}$ and noticing that $d_d = F\tilde{x}$:

$$\begin{aligned} L &= \tilde{x}'(\tilde{C}'\tilde{C} + \tilde{A}'P + P\tilde{A} + 2F'\tilde{B}'P)\tilde{x} + \\ &\quad +2\tilde{x}'(P\tilde{B} - \epsilon F'W)\tilde{d} - \tilde{d}'(2W - \gamma^{-2}\epsilon^2 W^2)\tilde{d} - \|\gamma d_{lin} - \gamma^{-1}W\epsilon\tilde{d}\|^2 \end{aligned}$$

(II) Cross-Product terms involving $\tilde{d}$ and $\tilde{x}$ are grouped as follows:

$$\begin{aligned} -\left[\tilde{d}'(2W - \gamma^{-2}\epsilon^2 W^2)\tilde{d} - 2\tilde{x}'(\tilde{B}'P - \epsilon WF)'\tilde{d}\right] &= -\|(Z^{\frac{1}{2}}\tilde{d} - Z^{-\frac{1}{2}}(\tilde{B}'P - \epsilon WF)\tilde{x})\|^2 \\ &+ \tilde{x}'(\tilde{B}'P - WF)'Z^{-1}(\tilde{B}'P - WF)\tilde{x} \quad (5.38) \end{aligned}$$

Note that $Z = (2W - \gamma^{-2}\epsilon^2 W^2)$ must be positive definite in order to have a well posed problem. This condition arises from the necessity of making the quadratic term

$$-\|(Z^{\frac{1}{2}}\tilde{d} - Z^{-\frac{1}{2}}(\tilde{B}'P - \epsilon WF)\tilde{x})\|^2$$

negative for any pair $(\tilde{d}, \tilde{x})$. It can easily be shown that if $Z < 0$, this is not always guaranteed. By replacing this new group of terms, a new cost function is obtained. This cost function has no cross-product terms between $\tilde{d}$ and $\tilde{x}$.

$$L \leq \tilde{x}'(\tilde{C}'\tilde{C} + \tilde{A}'P + P\tilde{A} + 2F'\tilde{B}'P + P\tilde{B}Z^{-1}\tilde{B}'P - 2F'W\epsilon Z^{-1}\tilde{B}'P + F'W\epsilon Z^{-1}\epsilon WF)\tilde{x}$$

(III) Terms involving F and $F'F$ are grouped:

$$\begin{aligned} F'W\epsilon Z^{-1}\epsilon WF + 2P\tilde{B}(I - Z^{-1}\epsilon W)F &= \|Z^{-\frac{1}{2}}(\epsilon WF - (Z\epsilon^{-1}W^{-1} - I)\tilde{B}'P)\|^2 \\ &- P\tilde{B}(Z\epsilon^{-1}W^{-1} - I)'Z^{-1}(Z\epsilon^{-1}W^{-1} - I)\tilde{B}'P \quad (5.39) \end{aligned}$$

This last step will yield an expression for the matrix gain F.

Finally, by using results stated in **(III)** we obtain an expression for our cost function (5.30) as

$$L = L_a + L_b + L_c \tag{5.40}$$

where

$$\begin{aligned} L_a &= \tilde{x}'(\tilde{C}'\tilde{C} + \tilde{A}'P + P\tilde{A} + P\tilde{B}Z^{-1}\tilde{B}'P - \\ &\quad P\tilde{B}(Z\epsilon^{-1}W^{-1} - I)'Z^{-1}(Z\epsilon^{-1}W^{-1} - I)\tilde{B}'P)\tilde{x} \qquad (5.41) \\ L_b &= \|Z^{-\frac{1}{2}}(\epsilon WF - (Z\epsilon^{-1}W^{-1} - I)\tilde{B}'P)\tilde{x}\|^2 \qquad (5.42) \\ L_c &= -\|Z^{\frac{1}{2}}\tilde{d} - Z^{-\frac{1}{2}}(\tilde{B}'P - \epsilon WF)\tilde{x}\|^2 \\ &\quad -\|\gamma d_{lin} - \gamma^{-1}W\epsilon\tilde{d}\|^2 \qquad (5.43) \end{aligned}$$

Equation (5.40) comprises three terms; the last, L_c, is a negative definite quadratic term. Therefore if the first two terms can be set to zero, then $L(.) < 0$. Setting the second term, L_b, to zero yields a condition for the gain matrix F

$$(\epsilon WF - (Z\epsilon^{-1}W^{-1} - I)\tilde{B}'P) = 0 \tag{5.44}$$

$$F = -(\frac{(2-\epsilon)W^{-1}}{\epsilon^2} - \gamma^{-2})\tilde{B}'P \tag{5.45}$$

where $P = P^T > 0$ comes from solving the Ricatti equation which makes $L_a = 0$:

$$\begin{aligned} &C'C + \tilde{A}'P + P\tilde{A} + P\tilde{B}Z^{-1}\tilde{B}'P - \\ &P\tilde{B}(Z\epsilon^{-1}W^{-1} - I)'Z^{-1}(Z\epsilon^{-1}W^{-1} - I)\tilde{B}'P = 0 \end{aligned} \tag{5.46}$$

which, after some algebraic manipulation, reduces to the Riccati equation given in the theorem.

iii) Calculation of the region of attraction. In part i) it was shown that the system is locally asymptotically stable in a set $\mathcal{E} \subset \mathcal{X}$ where $\mathcal{X}$ is a subset of the region of attraction. Here we derive an expression for a $\mathcal{E}$ and also show that it can be made arbitrarily large (and hence that Condition 1b of the RLAW problem is satisfied). As mentioned earlier, we estimate ellipsoidal subsets of the region of attraction and in particular are interested in calculating the largest such ellipsoid, $\bar{\mathcal{E}}$ which has the following form

$$\bar{\mathcal{E}} = \left\{\tilde{x} \in \mathbb{R}^{n_p+m} : \tilde{x}'P\tilde{x} < c_{max}\right\}. \tag{5.47}$$

For the estimation of the region of attraction it is assumed that $d_{lin} = 0$ and, to ensure that the deadzone is within a reduced sector, that the states $\tilde{x}$ belong to the set

$$\mathcal{X} = \left\{\tilde{x} \in \mathbb{R}^{n_p+m} : d \in \mathcal{S}(d_0)\ \forall t\ \geq 0\right\} \subset \mathcal{A} \tag{5.48}$$

Thus to calculate an ellipsoidal region of attraction we seek the largest set such that

$$\tilde{x} \in \bar{\mathcal{E}} \Rightarrow \tilde{x} \in \mathcal{S}(d_0)\ \forall t\ \geq 0 \tag{5.49}$$

or equivalently we seek the largest set

$$\bar{\mathcal{E}} = \left\{\tilde{x} \in \mathbb{R}^{n_p+m} : \tilde{x}'P\tilde{x} < c_{max},\quad |d| = |F\tilde{x}| \preceq d_0\right\} \tag{5.50}$$

Thus if $\tilde{x} \in \bar{\mathcal{E}}$ it follows that $d \in \mathcal{S}(d_0)$ and $\mathrm{Dz}(d) \in \mathrm{Sector}[0, \epsilon I]$; hence the system is locally stable. To calculate $\bar{\mathcal{E}}$, we follow a method used in, for example, [96], [109]. The largest ellipsoid region of attraction can be posed a maximisation problem:

$$\max_{\tilde{x}} \tilde{x}'P\tilde{x} \quad \text{s.t.} \quad |F\tilde{x}| \preceq d_0 \tag{5.51}$$

which is equivalent to

$$\max_{\tilde{x}} \tilde{x}'P\tilde{x} \quad \text{s.t.} \quad |F_i\tilde{x}| < d_{0,i}\ \forall i \in \{1, \ldots, m\} \tag{5.52}$$

where, F_i is the i^{th} row of F. The largest such ellipsoid can then be calculated using

$$c_{max} = \min_i \frac{d_{0,i}^2}{F_i P^{-1} F_i'} \tag{5.53}$$

Substituting for F yields

$$c_{max} = \frac{\bar{d}_i^2 w_i^2}{(1-\epsilon)^2(\frac{(2-\epsilon)}{\epsilon^2} - \gamma^{-2}w_i^2)B_i'PB_i} \tag{5.54}$$

Note that as ϵ can be made arbitrarily close to unity, c_{max} can be made arbitarily large and thus the ellipsoid $\bar{\mathcal{E}}$ can be made arbitrarily large, thus satisfying Condition 1 of the RLAW problem. For a more detailed of the derivation of c_{max}, please refer to Appendix B. □□

Remark 5.7:

a) It is interesting to contrast the rate-limit results with the magnitude-limit results obtained in Chapter 4 (see also[90]). Essentially the main difference is that if $\tilde{G}$ were to be stable i.e. it had no poles at the origin, then ϵ could be set to unity as $\tilde{G}(s)$ would be bounded real (i.e. $S(d, \infty) = \mathbb{R}^m$); hence global results could be obtained as in the magnitude limit problem. This is not possible for the RLAW case as without the term in ϵ, the Riccati equation in the theorem would not be solvable for $P = P' > 0$

b) Unlike the magnitude limit solution, the rate-limit solution is somewhat more intricate. The Riccati equation which results is a function of three "free" parameters: γ, ϵ and the diagonal matrix $W > 0$. In the magnitude case the Riccati equation was independent of W (by virtue of ϵ being chosen to be one), making it easy to change the feedback matrix F independently of the Riccati equation. This is not possible with the rate-limit solution, making it more difficult to tune.

c) It can be seen that as ϵ gets close to unity, the size of c_{max}, and hence the size of $\bar{\mathcal{E}}$ increases, for fixed γ and W. Thus by making ϵ arbitrarily close to unity, the size of the region of attraction can be made *arbitrarily* large for some appropriate choice of γ and W. □

5.5 Tuning the compensator

In the previous section it was possible to pose the RLAW problem as a relaxed version of the magnitude AW problem where asymptotic stability was only guaranteed locally within a domain of attraction $\mathcal{X}$. This was achieved using the concept of a "reduced sector" which was a locally accurate bound of the deadzone nonlinear static function. While this enables local solutions of the RLAW problem to be obtained, a new parameter ϵ was added to the design procedure. Thus, unlike the magnitude limit problem where the only truly free parameter was the diagonal matrix $W > 0$, it is evident that Theorem 5.1 now contains three "free parameters" which can be used for tuning the compensators, viz:

- γ - dictates the local performance of the system
- $\epsilon \in (0, 1)$ - determines the local accuracy of the sector bound on the deadzone
- W - a free parameter which influences both the performance level and the size of the region of attraction.

Although equations (5.25)-(5.27) give a computationally simple way to generate AW compensators, the tuning of the three free parameters, γ, ϵ and W becomes tedious due to the interplay between them and their mutual influence on the solution of the Riccati equation (5.25) such that $P(\gamma, \epsilon, W) > 0$. Furthermore, for each choice of the triplet (γ, ϵ, W), condition (5.26) must be checked to ensure $Z > 0$. Thus in some sense, the formulation looses its simplicity. Two similar algorithms for the tuning of the compensator are now suggested, a noteworthy feature of both being that the bounded-real type Riccati equation associated with the "standard" AW

problem is replaced by a standard LQR-type Riccati equation which, under mild assumptions of stabilisability and detectability of $(\tilde{A}, \tilde{B}, \tilde{C})$, is always solvable for some $P = P' > 0$

5.5.1 Tuning procedure I

Using equation (5.26), which imposes the inequality constraint $Z > 0$, it is possible re-write Theorem 5.1 in a manner where a solution to the Riccati equation (5.25) is always guaranteed. Thus we have the following corollary.

Corollary 1 *There exists a full order anti-windup compensator* $\Theta = [\Theta_1' \quad \Theta_2']' \in \mathbb{R}^{(q+2m)\times m}$ *which solves strongly the anti-windup problem if there exists a matrix* $P = P' > 0$, *and positive real scalars* $\epsilon \in (0,1)$, $k \in (0,2)$ *and* $\rho > 0$ *such that the following Riccati equation is satisfied*

$$\tilde{A}'P + P\tilde{A} - \rho P\tilde{B}\tilde{B}'P + \tilde{C}'\tilde{C} = 0 \tag{5.55}$$

Furthermore, if equation (5.55) is satisfied, a suitable Θ *achieving* $\|T\|_{i,2,\mathcal{W}} < \gamma$ *is obtained by calculating the matrix gain* F *as follows:*

$$F = -(1-\epsilon)^{-1}(1 + \frac{(k-1)\epsilon}{2-k})\rho\tilde{B}'P \tag{5.56}$$

where

$$\gamma = \sqrt{\frac{2-k}{\rho k}} \tag{5.57}$$

An estimate the region of attraction is given by the ellipsoid

$$\bar{\mathcal{E}} = \{\tilde{x} : \tilde{x}'P\tilde{x} \leq c_{max}\} \tag{5.58}$$

where

$$c_{max} = \max_i \left\{ \frac{\bar{d}_i^2}{\rho^2(1 + \frac{(k-1)\epsilon}{2-k})^2 \tilde{B}_i' P \tilde{B}_i} \right\} \tag{5.59}$$

□

Proof: The proof will show how, by re-defining certain parameters, the expressions in Theorem 5.1 can be re-written as those in Corollary 1. First note that using inequality (5.26), we obtain a bound on γ^{-2} as

$$\gamma^{-2} < 2\frac{(1-\epsilon)}{\epsilon^2}W^{-1} \tag{5.60}$$

Introducing $k \in (0,2)$, this can be re-written as the equality

$$\gamma^{-2} = k\frac{(1-\epsilon)}{\epsilon^2}W^{-1} \tag{5.61}$$

Substituting this into equation (5.25) yields the Riccati equation

$$\tilde{A}'P + P\tilde{A} - P\tilde{B}R\tilde{B}'P + \tilde{C}'\tilde{C} = 0 \tag{5.62}$$

where R is defined as

$$R = (2-k)\frac{(1-\epsilon)}{\epsilon^2}W^{-1} \tag{5.63}$$

Choosing $W = \omega I$, allows us to replace R by the scalar expression

$$\rho = (2-k)\frac{(1-\epsilon)}{\epsilon^2}\omega^{-1} \tag{5.64}$$

which yields Riccati equation (5.55) in Corollary 1. Similarly using the expressions for ρ and γ^{-2} in equation (5.27) allows us to write

$$F = -(R + \frac{W^{-1}}{\epsilon})\tilde{B}'P \tag{5.65}$$

Manipulating this expression yields the expression for F given in the corollary as equation (5.56). In turn substituting this expression for F into equation (5.59) allows a new expression for the region of attraction to be obtained as given in equation (5.58). □□

Remark 5.8:

a) Notice that Corollary 1 still has three parameters which must be chosen appropriately in order for a suitable anti-windup compensator to be synthesised: $k \in (0,2)$, $\rho > 0$ and $\epsilon \in (0,1)$. The advantage of this formulation over that of Theorem 5.1 is that the solution to the Riccati equation is now just dependent on the parameter $\rho > 0$ and, furthermore, it is now an LQR-type Riccati equation, and a solution such that $P = P' > 0$ will always exist (as $(\tilde{A}, \tilde{B}, \tilde{C})$ are assumed stabilisable and detectable). The parameters $\epsilon \in (0,1)$ and $k \in (0,2)$ must still be chosen by the designer, but now their choice has no impact of the solution of the Riccati equation although they do affect the performance level and the size of the region of attraction, as presented in equation (5.58).

b) The local $\mathcal{L}_2$ performance is now given by the expression in (5.61) and it is no longer a free parameter, but one which is fixed by the parameters k, ϵ and ω. Obviously as well as affecting the performance, these parameters will also influence the region of attraction, so care has to be taken when choosing them. □

Although Corollary 1 is simply a restatement of Theorem 5.1, it is believed to give a simpler, more intuitive set of conditions of the same results. In particular the interplay between performance and region of attraction appears more transparent and may allow the designer to

trade-off these conflicting design objectives more intuitively. However, while it is an improvement over Theorem 5.1 it does contain the parameter $k \in (0, 2)$ which influences the region of attraction and level of local $\mathcal{L}_2$ performance simultaneously. Note that in equations (5.61) and (5.56), the effects of k can be offset to a large extent by $W > 0$, although this does not appear explicitly in the tuning procedure. It can be observed that in the limit when $k \to 2$, the region of attraction will shrink considerably, where the only possible way of counteracting this effect is by having extremely small values of ρ. Nonetheless, observe how $k \to 2$, by definition of ρ, has this exact effect on ρ, and after some algebraic manipulations it can be concluded that the effects of k on the size of the region of attraction or performance level can be mirrored by different choices of W; different values of k will yield slightly different formulations of the same problem, none of which present significant improvements over each other as of yet.

Thus the real value of k appears to be that of simplification. The previous paragraph is not trying to categorically state that the choice of k is irrelevant to the solution of the RLAW problem. On the contrary, if appropriately chosen, it may significantly simplify the formulation. One such choice is $k = 1$, where the three free parameters are reduced to just two and the region of attraction is made "independent" of ϵ. In this case, equation (5.56) is reduced to

$$F = -(1 - \epsilon)^{-1} \rho \tilde{B}' P \tag{5.66}$$

and provided (5.55) is satisfied, the system will be guaranteed stable within a domain of attraction which can be estimated using the ellipsoid $\bar{\mathcal{E}}$ defined in (5.58), but this time

$$c_{max} = \min_i \left\{ \frac{\bar{d}^2}{\rho^2 \tilde{B}_i' P \tilde{B}_i} \right\} \tag{5.67}$$

This comes at the expense of having ϵ as the only re-tuning parameter, which may be restrictive and sometimes misleading. The most interesting consequence of choosing $k = 1$ is that our expressions for ρ and γ are reduced to

$$\gamma^{-2} = \frac{(1 - \epsilon)}{\epsilon^2 \omega} = \rho \tag{5.68}$$

This translates into $\gamma = 1/\sqrt{\rho}$, which is appealing because the Riccati equation is purely a function of ρ and an explicit bound on the local $\mathcal{L}_2$ gain is given by γ; for the case of $k = 1$, this performance is directly determined by ρ. The exact behaviour of the region of attraction as a function of $P(\rho)$ is not always clear and is rather obscure; nonetheless some basic properties and analysis can shed some light on this matter. This will be discussed later in the section.

One of the interesting features of this new simplified strategy is that it allows *precise* mathematical conclusions to be drawn about the trade-off between the local performance level and

the region of attraction. Under the assumption that $k = 1$, it follows from equations (5.68) and (5.67) that

$$\gamma = \frac{1}{\sqrt{\rho}} \tag{5.69}$$

and

$$c_{max} = \min_i \left\{ \frac{\bar{d}^2}{\rho^2 \tilde{B}_i' P \tilde{B}_i} \right\} \tag{5.70}$$

These equations embody the trade-off between performance and region of attraction as they both involve ρ. In particular it is interesting to see how the region of attraction's size alters as a function of ρ. Note that the region of attraction could equivalently be expressed as

$$\bar{\mathcal{E}} = \left\{ \tilde{x} \in \mathbb{R}^{n_p+m} : \tilde{x}' \rho E(\rho) \tilde{x} \leq 1 \right\}, \tag{5.71}$$

$$E(\rho) := \min_i \rho P(\rho) \frac{\rho \tilde{B}_i' P(\rho) \tilde{B}_i}{\bar{d}_i^2}. \tag{5.72}$$

It is difficult to characterise the size of this ellipsoid, but one way of doing so is by the sum of the length of its semi-axes, which is equal to the trace of $E^{-1}(\rho)$, which can be written as

$$\mathbf{tr}[E^{-1}(\rho)] = \mathbf{tr} \left\{ \max_i (\rho P(\rho))^{-2} \bar{d}_i^2 / \tilde{B}_i' \tilde{B}_i \right\} \tag{5.73}$$

$$= \max_i \bar{d}_i^2 \mathbf{tr} \left\{ [\rho P(\rho)]^{-1} [\rho P_{ii}(\rho)]^{-1} \right\} \tag{5.74}$$

So the key parameter which determines the "size" of the region of attraction is the matrix $\rho P(\rho)$. We will establish how this varies as a function of ρ. First, multiply equation (5.55) by ρ to get

$$\tilde{A}' P \rho + \rho P \tilde{A} - \rho P \tilde{B} \tilde{B}' P \rho + \rho \tilde{C}' \tilde{C} = 0. \tag{5.75}$$

Defining $Q(\rho) := P(\rho)\rho > 0$ we now have

$$\tilde{A}' Q(\rho) + Q(\rho) \tilde{A} - Q(\rho) \tilde{B} \tilde{B}' Q(\rho) + \rho \tilde{C}' \tilde{C} = 0. \tag{5.76}$$

Now if $(\rho^{\frac{1}{2}} \tilde{C}, \tilde{A})$ is detectable, it follows [83, 104, 45] that

$$\frac{dQ(\rho)}{d\rho} > 0, \quad \lim_{\rho \to 0} Q(\rho) = 0. \tag{5.77}$$

From this it also follows that $dQ_{ii}(\rho)/d\rho > 0$. Thus $P(\rho)\rho = Q(\rho)$ and $\rho P_{ii}(\rho) = Q_{ii}(\rho)$ are monotonically increasing functions of ρ. Hence $\mathbf{tr}[E^{-1}(\rho)] = \max_i d_i^2 \mathbf{tr}[Q(\rho) Q_{ii}(\rho)]$, is a monotonically decreasing function of ρ which implies that as ρ increases, the "size" of the region of attraction decreases. Furthermore, in the limit as ρ tends to zero ($\epsilon \to 1$ i.e. global results), the region of attraction be comes the whole state-space.

Note also that we can write F as

$$F = \frac{-1}{1-\epsilon}\tilde{B}'Q(\rho), \tag{5.78}$$

and thus we can see that as ρ becomes smaller, F becomes smaller (in the sense that its norm reduces) and as $\rho \to 0$, $F \to 0$ and we recover the IMC solution; this also corresponds to $\gamma = \infty$. In other words, we have the "worst" performance for the IMC AW case (which is not surprising since $\tilde{G}(s)$ is not bounded real). In conclusion we can see that

$$\gamma \propto \frac{1}{\sqrt{\rho}} \quad \text{and} \quad |\bar{\mathcal{E}}| \propto \frac{1}{\rho}, \tag{5.79}$$

meaning that there is a clear trade-off between minimising the local $\mathcal{L}_2$ gain and maximising the size of the region of attraction.

5.5.2 Tuning Procedure II

Again, this section assumes that $W = \omega I > 0$ is a scalar. From our condition on Z (5.26) we obtain

$$-\rho_2 := \gamma^{-2} - \frac{2(1-\epsilon)\omega^{-1}}{\epsilon^2} < 0 \tag{5.80}$$

From this it follows that our Riccati equation becomes

$$\tilde{A}'P + P\tilde{A} - \rho_2 P\tilde{B}\tilde{B}'P + \tilde{C}'\tilde{C} = 0 \tag{5.81}$$

and that an expression for F is obtained as

$$F = -(\rho_2 + \alpha)\tilde{B}'P \tag{5.82}$$

where $\alpha := \omega/\epsilon$ and ρ_2 are both scalars. Note that as $\rho_2 > 0$, a solution for the LQR-type Riccati equation (5.81) always exists. As before, the solution $P(\rho_2) > 0$ is independent of the other free parameters, in this case, α. This allows α to be used to refine the choice of F. In this case it follows that an estimate of the region of attraction of the system given by equation (5.28) can be rewritten as

$$c_{max} = \min_i \frac{d_{0,i}^2}{F_i P^{-1} F_i'} \tag{5.83}$$

$$= \min_i \frac{\bar{d}_i^2}{(1-\epsilon)^2(\rho_2+\alpha)^2 \tilde{B}_i' P \tilde{B}_i} \tag{5.84}$$

Thus for fixed ϵ the region of attraction can be made larger by choosing $\rho_2 > 0$ and $\alpha > 0$ as small as possible. On the other hand, the local $\mathcal{L}_2$ gain of the system can be found from equation (5.80) as

$$\gamma^2 = \frac{1}{\frac{2(1-\epsilon)\alpha}{\epsilon} - \rho_2} > 0 \tag{5.85}$$

Thus for fixed ϵ choosing, $\alpha > 0$ large compared to $\rho_2 > 0$ yields a smaller $\mathcal{L}_2$ gain. There is a clear trade-off in α: small α implies a large region of attraction, large α implies a small $\mathcal{L}_2$ gain. For both cases a small ρ_2 is desirable. Note that for maximal region of attraction, that is $\alpha << 1$ and $\rho_2 << 1$, we recover something very close to the IMC solution as $F \approx 0$. Note that for equation (5.85) to hold, we must have

$$\alpha > \frac{\epsilon}{2(1-\epsilon)}\rho_2 \tag{5.86}$$

Although this solution may be useful in future work, this thesis has mainly focussed on the first tuning approach as advocated in Section 5.5.1. The alternative tuning procedure described above is given here for completeness and to illustrate how different formulations allow different interactions between parameters to be highlighted. None the less, similar conclusions can always be drawn; there is a trade-off present between the region of attraction and local performance of the system measured as an induced $\mathcal{L}_2$ gain.

5.6 Example

In this section the effectiveness of the results are shown through a known example. The example considered here is that of a missile auto-pilot, the same one used in section 4.4, which is a two-input-two-output third order dynamic linear system. The usual assumptions of stability and good performance are made on the linear closed-loop. This time the actuators have rate constraints of $\pm 7 rad/sec$ imposed in both channels

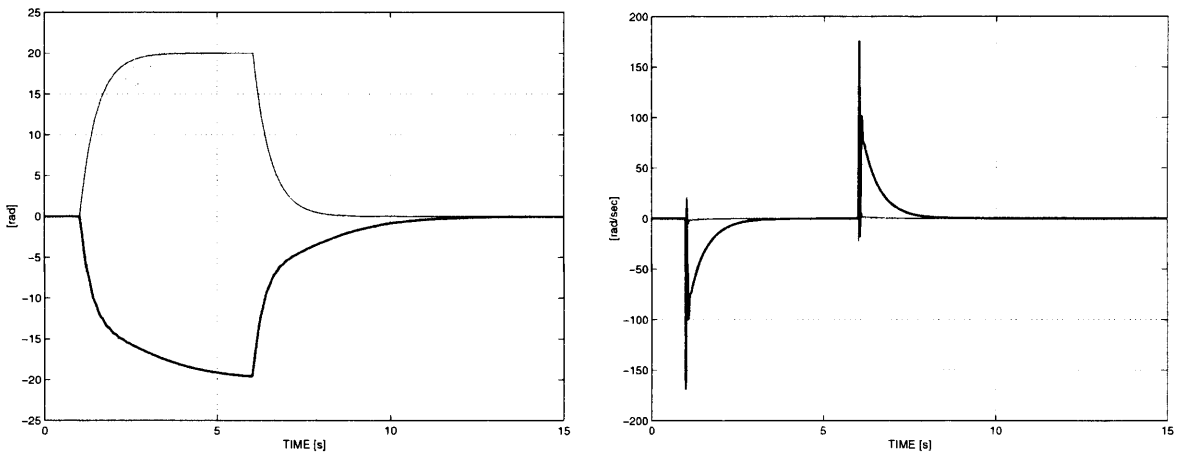

Output $y(t)$ Control signal rate

Figure 5.10: Nominal linear response of missile

Figure 5.10 shows the nominal linear response of the missile for a pulse $r = [\ 20\ \ -20\ ]$. Notice how the system has an excellent response and the outputs are decoupled. However, observe

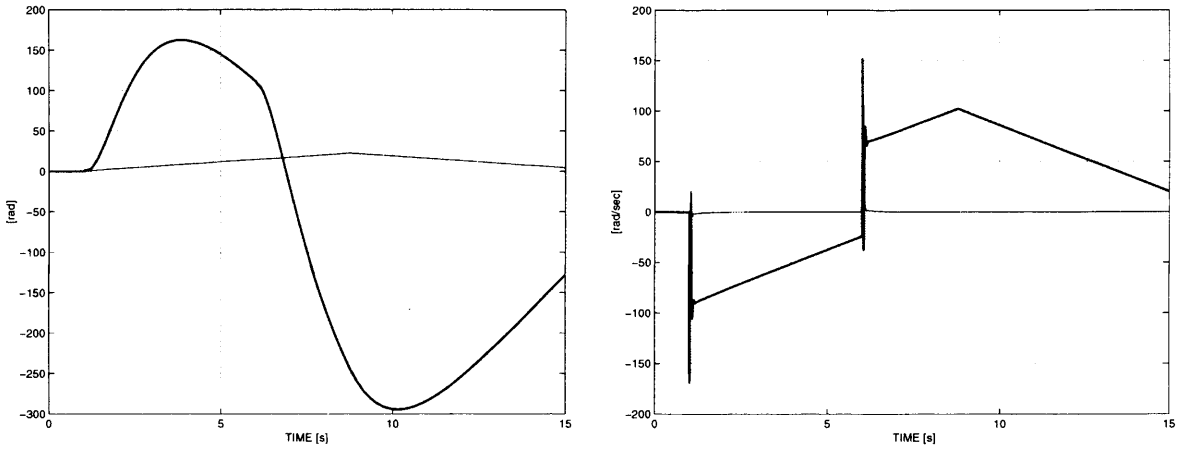

Output $y(t)$ Control signal rate

Figure 5.11: Rate-limited response of missile (no AW)

how the rate of the control signal is outside the set $\mathcal{D} = \{(7,7),(-7,7),(-7,-7),(7,-7)\}$ for some time. This suggest that the system with actuators reaching the rate-limit bounds might have poor performance and may even be unstable. Figure 5.11 confirms this intuitive fact and shows clearly how the system loses its decoupling and tracking properties.

Figure 5.12 shows the missile response with the full order AW compensation proposed in this paper, initially using Theorem 5.1 with parameters chosen as $\epsilon = 0.9$, $\gamma = 8$, and $W = 8$. This yields a matrix F of the form

$$F = \begin{bmatrix} -0.0119 & 0.9613 & 0.0297 & -73.1313 & 1.4744 \\ -0.0831 & -0.0264 & -0.0008 & 1.4744 & -1.4109 \end{bmatrix} \tag{5.87}$$

Notice the improvement over the uncompensated response: the saturated system now tends to follow the linear response closely and the return to nominal linear dynamics is swift.

Observe from equation (5.22) that $M(s) - I$ is a function of F, and consequently the size of the control signal d_d and the compensator dynamics are affected by this parameter. The poles of the AW compensator, i.e. $\mathbf{spec}(\tilde{A} + \tilde{B}F)$, are also a function of F and therefore increasing the size of F, increases the control signal d_d and yields a compensator with faster dynamics. The task of choosing appropriate values of the design parameters is not as simple as in [90], but the approach is still intuitive. The designer's task can be simplified by using the tuning algorithm proposed in section 5.5.1 and will be discussed next.

Tuning algorithm I provides a simple way of characterising the performance level and stability region of the AW compensator. Notice that the available parameters are ρ and ϵ (the parameter k is fixed and has a value of one), where ρ gives a measure of nonlinear performance and ϵ defines the polyhedral set of allowed signals d, i.e. $\mathcal{S}(d_0) = \{d : -d_0 \preceq d \preceq d_0\}$. It was mentioned

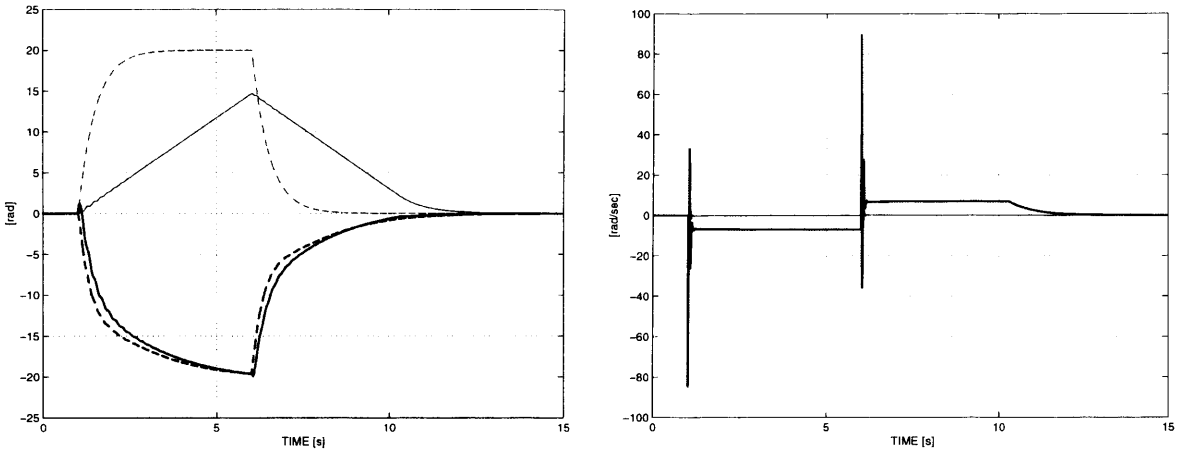

Output $y(t)$ Control signal rate

Figure 5.12: Rate-limited response of missile: − rl + full-order AW; −− nominal linear

that choosing the parameter k equal to unity yields $\gamma = 1/\sqrt{\rho}$, so in order to achieve good performance (i.e. $\|\mathcal{T}_p\|_{i,2,\mathcal{W}}$ small), it is desirable to choose ρ large. From equation (5.67) and the analysis of section 5.5.1 it can be concluded that for an enlarged region of attraction ρ must be small. To illustrate this trade-off two compensators are designed: $\epsilon = 0.9$ is fixed and ρ takes a values of $\rho_{low} = 10^{-4}$ and $\rho_{high} = 10$ for the low and high performance compensators respectively. This yields the following matrix gains

$$F_{low} = \begin{bmatrix} 0.0040 & 0.0511 & 0.0015 & -16.7553 & 0.3411 \\ -0.0006 & -0.0011 & -0.0000 & 0.3411 & -0.1156 \end{bmatrix} \tag{5.88}$$

$$F_{high} = \begin{bmatrix} 36.4902 & 26.6139 & 1.2098 & -411.9622 & 19.2397 \\ -29.9905 & -4.8707 & -0.0962 & 19.2397 & -46.8843 \end{bmatrix} \tag{5.89}$$

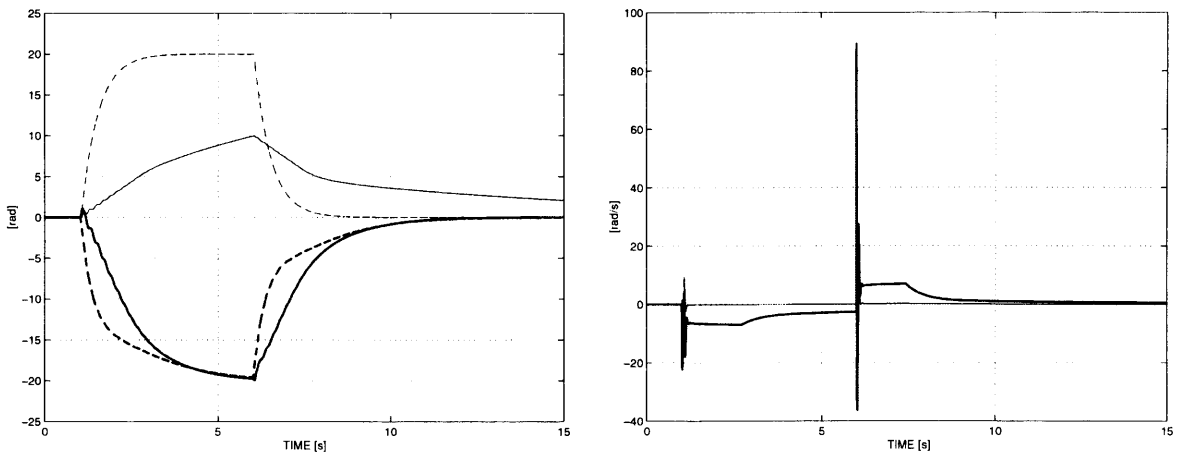

Output $y(t)$ Control signal rate

Figure 5.13: Rate-limited response of missile: − rl + full-order AW; −− nominal linear: ρ_{low}

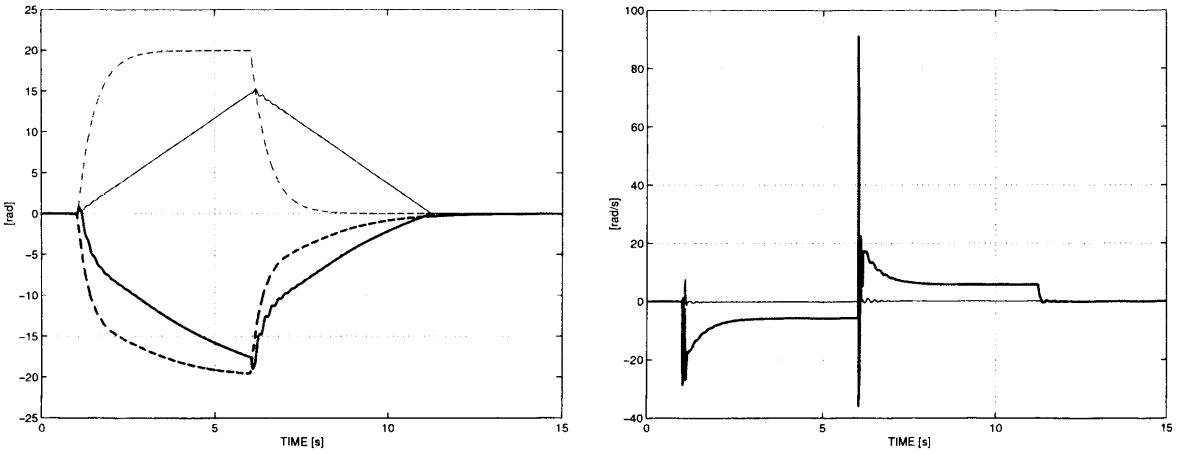

Output $y(t)$ Control signal rate

Figure 5.14: Rate-limited response of missile: $-$ rl + full-order AW; $--$ nominal linear: ρ_{high}

The missile's response due to an input pulse $r = [\ 20 \quad -20\ ]$ is shown in Figure 5.13 and 5.14 which depict the responses obtained with the ρ_{low} and ρ_{high} AW compensators respectively. Clearly in both cases the system's response is enhanced by the use of AW compensation: rate saturation levels are reduced, tracking properties are retained (with the usual constraint on the admissible reference) and return to linear behaviour is well behaved. It is somewhat more difficult to conclude which compensator delivers the best performance; in Figure 5.13, the second channel exhibits fast tracking performance while the first channel is sluggish. In Figure 5.14 the second channel is more sluggish than before, but the response of the first channel is improved. Note however, that the local $\mathcal{L}_2$ gain is simply a bound on the performance measured by "energy" gain and is not as precise as many classical "linear" measures. Consequently, designs may be conservative and the value of γ may not always be an accurate indication of the system's true performance.

5.7 Conclusions

This chapter has addressed the problem of designing anti-windup compensators for systems with rate-constrained inputs. The solution method proposed takes as its inspiration the results of Chapter 4, but relaxes the global stability criteria to local and semi-global in order to obtain computable results. In particular, by modeling the rate-limit as a first order dynamic system with saturated states, it was possible to augment the plant and controller and pose an equivalent magnitude limit problem. From section 4.2.1, equation (4.12), it is clear that a necessary condition for a globally stabilizing compensator to exist is that the plant G is bounded real. As this is not the case for the augmented plant $\tilde{G}$ (even though $G \in \mathcal{RH}^\infty$),

it was necessary to use a reduced sector condition on the deadzone non-linearity in order to address the problem locally.

Theorem 5.1 of this chapter shows how the rate-limit problem can be tackled by solving a single Riccati equation which is a function of several free parameters. Although this method of solving the rate-limit problem is useful in its own right, the tuning of the compensators using the parameters γ, ϵ and $W > 0$ is not straightforward. The results of Section 5.5.1 show how the solution to the rate-limit problem can be re-stated and that this version of the solution provides more insight into tuning the compensator. Clear relationships between the estimate size of the region of attraction and the local $\mathcal{L}_2$ gain were given and can be traded-off against each other.

Although implicitly it is desirable to obtain $\epsilon \approx 1$ in order to obtain a larger region of attraction, this will produce high compensation signals and fast poles. The estimated region of stability $\bar{\mathcal{E}} = \{\tilde{x} \in \mathbb{R}^n : \tilde{x}' P \tilde{x} \leq c_{max}\}$ depends not only on ϵ, but also on W and P, making it desirable to make this goal more explicit in the optimization problem. Noting the recent work of [33], this could be included in future work.

A simple example has showed the effectiveness of the proposed techniques but there is an obvious need for a more significant practical example. The next chapters in the thesis will provide more detailed results of the application of these results to a real world problem: rate-limiting in an experimental aircraft.

Chapter 6

PIO avoidance in an experimental aircraft: design and desktop simulation

6.1 Introduction

Actuators with strict limits on their magnitude or rate have been identified, throughout the thesis, as a cause of problematic behaviour for systems which are otherwise linear. Simple examples have shown how linear behaviour can degrade sharply when actuator nonlinearities are encountered. The same examples have also shown how this degradation can be limited, and performance recovered to some extent, through the use of AW compensation.

One of the application areas in which magnitude and rate limits can be particularly problematic is that of flight control. Over recent years numerous problems have been caused due to actuator rate, and to some extent magnitude, limits and a significant number of papers and reports have now documented the evidence for this ([2, 94, 82, 18, 6]). In particular it appears that, as flight control systems have become more advanced and have the ability to bestow what are deemed to be more desirable performance characteristics on the aircraft, the appearance of "strange" phenomena in aircraft control loops are becoming more common.

One of the most interesting and prevalent of these phenomena is that of pilot-induced-oscillations (PIO's), where magnitude and rate saturation have been implicated in the occurrence of a sub-class of this phenomenon. In particular, rate-limiting has long been linked with destabilising effects and performance degradation in aircraft systems, with PIO behaviour being recorded for both civilian and military aircraft. Perhaps the most notable accidents happened during the development phase of FBW, 4^{th} generation fighter aircraft, such as the JAS-39 Gripen and the YF-22. In both cases the aircraft became unstable as severe actuator rate-limiting was encountered and the aircraft were either lost or heavily damaged during crash landing manoeuvres. Attention to the effects of rate-limiting and other actuator nonlinearities became

a priority and a large number of research initiatives, which emphasized the comprehension, prevention, and alleviation of the nonlinear effects of rate-limiting, sprouted.

In fact, the literature on the subject of PIO problems due to magnitude and rate saturation problems is now very large and a classification system exists; PIO's due to nonlinear actuators, i.e. rate/magnitude saturation, are known as Category II PIO's. This class of PIO has been particularly troublesome and numerous aircraft have suffered as a result. Perhaps the most notorious example is the SAAB JAS-39 Grippen crashes [2] which led to SAAB developing its so-called "phase compensator" [81, 44, 82] to alleviate this effect. This and other similar events paved the way for the development of programs such as US Air Force program [29, 14], and the European GARTEUR Action Groups 12 and 15.

Despite this however, the number of useful, rigorous and systematic techniques available to deal with this problem is relatively limited. Much of the work in the literature has a strong experimental bias with many practitioners concentrating on predicting and categorising PIO events ([64, 51, 50, 20, 29]). While this is useful and certainly equips the control system designer with methods to *a posteriori* test control systems against susceptibility to PIO's, much of the results to date are empirically based and rely on a great deal of engineering insight. Due to the complex and elusive nature of the PIO phenomenon, there are few techniques which address this in a practical way with a satisfactory theoretical basis.

In contrast, the solutions to the rate-limit problem suggested by the control community have tended to be too technical, and lacking in intuition, for practitioners to apply these methods. Furthermore many of these techniques are effectively one-stage design techniques (see for example [55],[32],[95]) which therefore do not sit well with existing legacy controllers which may have been extensively flight tested and which may work admirably in most situations, save that of severe rate-limiting.

With this background, the aim of the chapter is to describe the application of the rate-limit AW techniques introduced in Chapter 5 to a realistic flight control system where PIO behaviour is likely to occur. The chapter will begin with a review of PIO's in general and briefly examine techniques which are already available to deal with this phenomena. The design and extensive nonlinear simulation of the techniques advocated in Chapter 5 will then be described. It should be mentioned that the process described in this chapter was part of the preparation for flight tests performed as part of a GARTEUR AG-15 Action Group, an alliance of European institutions formed to study the prediction and prevention of PIO's. The flight test results are described and analysed in the next chapter.

6.2 Pilot-induced-oscillations

6.2.1 Background

The acronym PIO stands for "pilot induced oscillation", "pilot involved oscillation" or "pilot in-the-loop oscillation". Neither of the three terms has been universally adopted but roughly speaking a PIO refers to an oscillation or an oscillatory tendency in an aircraft in which the pilot plays an active part: he/she is in the feedback loop. Likewise, no universally acceptable definition of a PIO is available although the one given below ([29, 1]) is appealing. In [1] a PIO is defined as a

"*sustained or uncontrollable oscillation resulting from efforts of the pilot to control the aircraft.*"

It can also be described as "*rare, unexpected, and unintended excursions in aircraft attitude and flight path caused by anomalous interactions between the aircraft and pilot.*" ([64])

Some care is required when interpreting oscillatory events in aircraft and it should be noted that not every oscillatory event is a PIO, and, further, that not every PIO will involve actuator magnitude or rate-limits. It is important to emphasize that the distinguishing factor in PIO's, as opposed to other oscillatory events, is that a PIO develops from the efforts of the pilot to control the system and such an event will normally be sustained over several seconds. In order to characterise PIO's some informal checklists have been proposed e.g. *(i)* there must be an oscillation, *(ii)* the aircraft must be out of phase with the pilot, *(iii)* the frequency of the oscillation must be within a frequency range which the pilot could induce, and *(vi)* the amplitude of control inputs, aircraft responses, or both, must be sufficiently large to be of concern. Therefore, not every "strange" aircraft phenomenon can be classified as a PIO.

For some time now ([49]), PIO's have been divided into several categories which are distinguished by their underlying cause; essentially the degree of nonlinearity involved in the event. The three most common categories are thus:

- **Category I:** Linear pilot-vehicle system oscillations. These PIO's are the result of linear effects such as time delay, phase loss due to filters and highly sensitivity systems. Due to their linear nature, these are perhaps the simplest type of PIO to model, understand, and prevent. They are also the least common in flight control applications perhaps because they are usually a consequence of poorly designed baseline control schemes.

- **Category II:** Quasi-linear events where the only nonlinear contributions come from the actuator in the form of rate or position limits. These PIO's have an identifiable nonlinear

contribution which may be accounted for separately; otherwise, the system is assumed linear, stable and well behaved. The nonlinearity most commonly linked to PIO events is the rate-limiting of servo-hydraulic actuators.

- **Category III:** Essentially non-linear pilot-vehicle system oscillations with transients. Such PIO events are rare and extremely difficult to recognize. In the case such an event occurs, its effects are usually severe. Mode switching in the flight control system, or pilot behaviour, that cannot be represented by a quasi-linear equivalent is the most common trigger.

Several researchers have suggested that there may be other types of PIO's which may not be classified in any of the categories defined above and a "Category IV" PIO, which deals with interactions between the pilot and the aircraft's structural modes, has also been suggested.

CAT I PIO's are easily identified and are mainly caused by lags in the system, which in turn, are due to time delays and filters which are sometimes present in fly-by-wire control applications. These are now relatively well understood and by correct adjustment of an aircraft's linear control system, they can be prevented. Cat II PIO's, those in which rate-limiting plays a prominent role, are the category of most importance in this thesis. They are arguably the most troublesome and have led to a number of aircraft crashes and incidents ([18]). Cat III PIO's are much more difficult to deal with and research into such types of PIO is currently still in its infancy. This thesis will concentrate on the prevention of Cat II PIO's.

6.2.2 Factors in Category II PIO events

A simple schematic of the control loops in a standard fly-by-wire aircraft control system is shown in Figure 6.1. This schematic depicts the so-called *pilot-vehicle-system (PVS)* which consists of the raw aircraft dynamics, $G(s)$, the baseline controller, $K(s)$, and the nonlinear actuators, $\Psi(.)$, which represented the saturation and rate-limits. These components are connected through an inner feedback loop and, for many tasks, this system alone dictates the aircraft behaviour. However, when the pilot becomes sufficiently engaged within a task, he/she enters the loop and thus the outer feedback loop, represented by the dashed line, becomes connected to the inner loop by way of the pilot dynamics $K_p(.)$. This second biomechanical feedback loop is created when the pilot observes the aircraft's response (visually, haptically) and reacts by altering his inceptor input in a manner he sees fit, thus closing the loop. Category II PIO's therefore arise due to the interaction of the various components of the PVS, and necessarily the nonlinear behaviour of the actuators.

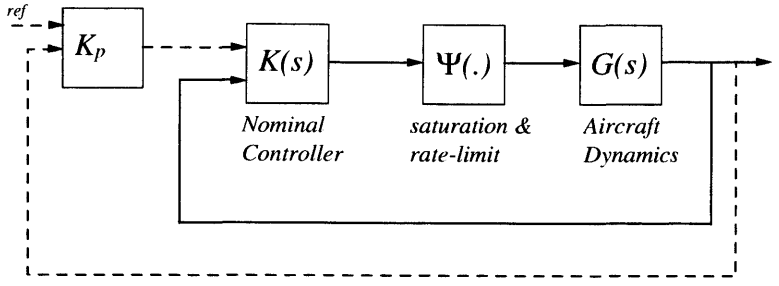

Figure 6.1: Pilot Vehicle System (PVS)

As mentioned in Section 6.2.1, the presence of the pilot within the feedback loop is an important distinguishing factor from other oscillatory events which may occur in the aircraft. However, it is normally the case that, in most recorded PIO events, the aircraft's susceptibility to such unnatural behaviour is not noticeable in normal flying and that PIO-proneness of an aircraft may vary from pilot to pilot. This suggests that in order for a PIO to occur, some other factors must be present, and normally a PIO is due to a number of factors occurring simultaneously. In general, a PIO is initiated by what is called a "trigger" event which can include changes in flight conditions, wind gusts, or highly demanding tracking tasks. It is important to remark that not all trigger events cause a PIO, but all PIO's are initiated by the presence of some trigger. Typical triggers may include uncommon or difficult pilot demands, changes in vehicle or controller dynamics (perhaps due to controller switching or aircraft damage), or disturbances altering the pilot-vehicle coupling. Triggers may come from the environment, the vehicle, or the pilot, with the common feature that they put extra demand on the pilot's ability to concentrate. It may be argued that, while prediction of PIO's is important and research into PIO triggers is worthwhile, it is inevitable that triggers will always be part of the pilot's uncertain environment and that it is difficult, if not impossible, to eliminate all possible triggers. One of the interesting aspects of PIO research was that, during the 1990s, rate-limiting was uncovered as an important aspect of some PIO's, initiating extensive, often experimental, research on addressing this issue.

While a trigger is necessary for PIO type behaviour to occur, it is not the only factor involved and three interacting components can be mentioned: the trigger, which has just been discussed; the controlled aircraft dynamics, which are normally set by an appropriate baseline controller design; and the pilot. The system characteristics are of great importance in assessing an aircraft's susceptibility to PIO's: slow and lightly damped poles, excessive phase lag or time delays may make a given aircraft significantly more PIO prone. Luckily, reasonably good models tend to exist for the controller and aircraft dynamics, making off-line simulation and prediction possible.

The third component of a PIO, the pilot, is perhaps the most complex to deal with and becomes a major issue when simulating the system. In order to obtain simulation results of PIO events, some *pilot model* has to be used to mimic, to some extent, real pilot behaviour. There has been extensive research on pilot models and a range of options are now available ([64, 50] and references therein). Pilot modeling is non-trivial and a full discussion of pilot models is beyond the scope of this thesis; the interested reader is referred to [49, 22, 68, 20]. It suffices to say that any simulation results which purport to represent PIO-type events need to be interpreted with care as they have necessarily been produced with some pilot model which is sometimes a poor approximation to a real pilot.

Notwithstanding the above, it is appropriate to discuss some simple pilot models which are appropriate for the simulation results given there. As will become clear in the next chapter, although the simulation results are based on simple pilot models, they appear to be "good enough" for broad conclusions about the behaviour of the real piloted system to be made. Pilot behaviour, in relation to PIO, can be divided into two types: *compensatory* and *precognitive.* In the case of *compensatory* control, the pilot attempts to minimize a displayed error, generally adding lead compensation to achieve this results. This translates into time delays which often, in high gain closed-loop control applications, yield systems with reduced phase margins. The system then becomes sensitive to phase shifts and in the event of experiencing pronounced rate limiting, a PIO may develop. For *precognitive* control, the pilot's learning curve changes the way he interacts with the aircraft. It has been observed that for such precognitive control strategies, the pilot can be said to behave as a pure gain if the system undergoes demanding tracking tasks. The choice for the pilot model in this thesis was determined using the *open-loop onset point* (OLOP) criterion and assumed *precognitive*; this choice will be discussed shortly.

6.3 Tools for the prediction of pilot-induced oscillations

It has already been mentioned that, in certain aircraft and under certain circumstances, the interconnection of nonlinear actuators, vehicle dynamics, control system dynamics, and the pilot, may give rise to PIO situations. However, this does not imply that for a given interconnection, PIO type events will result and thus there is an obvious need for tools to predict, in a reasonably reliable way, how likely a certain aircraft is to encounter a PIO.

One of the main outcomes of much of the existing PIO literature is a range of methods for predicting different types of PIO. These methods were first developed for the prediction of linear Cat I PIO's and have generally been successful in this regard; some are now often used

in the aerospace industry. A good summary may be found in [64, 63].

A number of techniques are also available for Cat II PIO prediction, although it must be remembered that accurate prediction of such events is somewhat more difficult due to the nonlinear nature of the behaviour. The chief difficulty is finding a technique which is sufficiently precise and non-conservative as to not label an aircraft PIO prone unless it really is, but sufficiently rigorous to identify all PIO behaviour. Philosophically this is quite difficult as nonlinear stability tools tend to be conservative or approximate. Despite this a number of methods have emerged with notable techniques being: Bandwidth/pitch-rate overshoot, Open Loop Onset Point, Pilot Vehicle Dynamics Nonlinear (PVDNL) and the Time Domain Neal Smith (see [64, 63]). Most of these methods have had some success but most are based on practical engineering considerations and arguably have little supporting rigorous theory.

6.3.1 The OLOP Criterion

The method used in this thesis for predicting the PIO susceptibility of an aircraft is the so-called *OLOP Criterion.* This is perhaps one of the most effective criteria for Cat II PIO prediction and has had a number of studies devoted to it ([20, 29]). One of the appealing features of the OLOP criterion is that it combines underlying theory with empirical engineering knowledge; this has been deeply welcomed by many flight-test engineers. Thus, while the OLOP criterion cannot categorically determine whether or not a certain aircraft is PIO prone, it has generally been found to provide useful, indicative results. The OLOP criterion was developed at DLR (Deutsche Zentrum fur Luft und Raumfahrt) using ideas based on "harmonic balance" or describing functions. It was developed to enable flight test engineers to determine how prone aircraft were to Cat II PIO in a simple but accurate way. This thesis does not attempt to develop the OLOP criterion but a brief discussion on its derivation and application is believed to be useful.

Open-Loop-Onset-Point

The OLOP criterion takes its name from the term "Open Loop Onset Point" which is, rather confusingly, defined as the frequency response value (i.e. gain and phase) of the open-loop system (i.e. the system from the rate-limit output to the rate-limit input) at the closed-loop "onset" frequency, ω_{onset}, which is the frequency for which the rate-limit first becomes active for full stick input. The idea behind the OLOP criterion is similar to that of describing function analysis, in that it uses the frequency domain properties of the linear part of the system to

obtain stability criteria. It does not however require explicit computation of the describing function in order to assess stability.

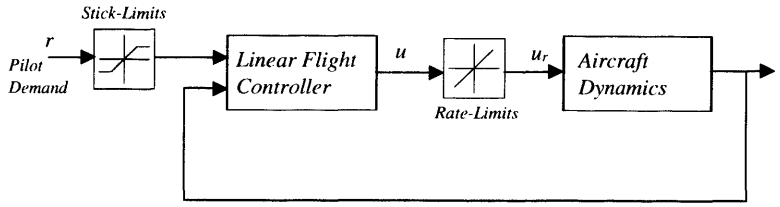

Figure 6.2: Determination of ω_{onset}

The OLOP criterion is currently a single-input-single-output technique and therefore each axis of the aircraft is handled separately. This has so far proved to be adequate although it obviously does not make it appropriate for predicting multi-axis PIO's which might occur at high angles of attack due to coupling. As mentioned above, the onset frequency, ω_{onset}, is defined as the frequency at which the rate-limit first becomes active. It is useful to refer to Figure 6.2 where $u(t)$, which represents the desired control input, and $r(t)$, which represents the pilot demand, are both scalar signals. If the rate-limit nonlinearity is replaced with the identity operator and we represent the maximum demand fed into the control signal (dictated by the stick limits) as $\bar{r} > 0$, then the ω_{onset} can be determined from the equation (see for example [20, 29, 119]) as

$$\bar{r} \, \|T_{u,r}(j\omega_{onset})\| = \frac{\bar{d}}{\omega_{onset}} \tag{6.1}$$

where $T_{u,r}(s)$ is the closed-loop transfer function from the pilot reference demand r to the nominal control demand u, $\bar{r}$ is the maximum stick input and $\bar{d} > 0$ is the maximum rate-limit. Note that $T_{u,r}(s)$ is the transfer function from pilot stick input to control signal in one axis only. Thus for the pitch axis it would be the transfer function from longitudinal stick command to elevator deflection; for the lateral axis it would be lateral stick command to aileron deflection. Note that equation (6.1) can be solved graphically using a Bode plot to determine the intersection of the frequency response of $|T_{u,r}(j\omega)|$ with $\bar{d}/j\omega$: ω_{onset} is the frequency at which the two lines intersect.

Pilot gain determination

The main use of the OLOP criterion in the work described here is that it allows the determination of a suitable pilot model which exposes PIO behavoiur. In the OLOP criterion a simple gain, K_p, is used to model the pilot; although this model is crude, it seems to be adequate for

rough prediction of PIO tendency. In the OLOP criterion, the pilot model is chosen such that the gain of the open-loop pilot-plus-aircraft system, as depicted in Figure 6.3, is such that phase cross-over angle is close to the critical -1 point. Thus K_p is chosen such that the cross-over phase of the transfer function $K_p T_{\phi/\theta,r}(s)$ is $\Phi_c \in [-90, -130]$ degrees for the longitudinal axis and $\Phi_c \in [-110, -160]$ for the lateral axis. In this notation $T_{\phi/\theta,r}(s)$ represents the transfer function from the pilot stick demand to either roll attitude, ϕ, or pitch attitude, θ (depending on whether the pitch or roll axis is under consideration).

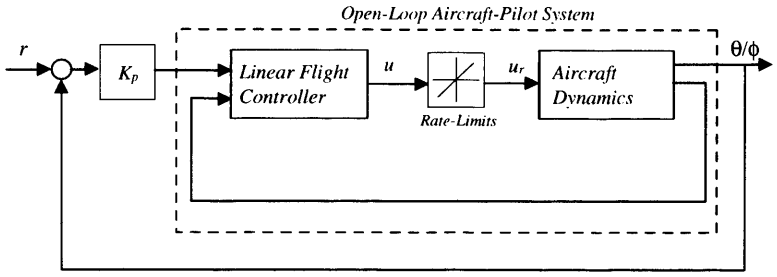

Figure 6.3: Pilot vehicle system: Open and Closed-Loop

Determining PIO susceptibility

The final stage of the OLOP criterion is to use the frequency response of the nominal linear part of the system to determine the aircraft's susceptibility to PIO for the given pilot gains. It is instructive to consider Figure 6.4 . Note that the stability of the system may be determined by breaking the loop either side of the rate-limit, and calculating the transfer function of the linear part of the loop. Nonlinear stability can be (and normally is) assessed by either using describing function techniques or by using tools such as the Circle or Popov criteria. The OLOP criterion takes a different approach as suggested in [98, 20], where the "open-loop" frequency response - gain and phase - is plotted on the Nichols chart. In addition the so-called OLOP boundary, which can be interpreted as something akin to an empirical describing function, is also plotted. The aircraft is then said to be PIO free if the OLOP point (value of the open-loop at frequency ω_{onset}) lies below the boundary and PIO prone if it lies above the boundary. A sample OLOP plot is shown in Figure 6.5. It is emphasised that the OLOP boundary has been determined empirically and does not have much underlying theory associated with it. Nonetheless, it does appear to be useful for predicting single-axis PIO's in aircraft.

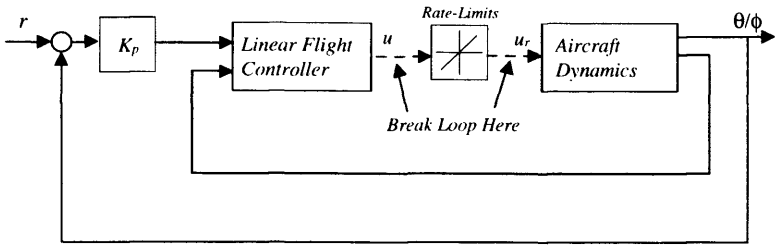

Figure 6.4: Transfer function for OLOP graph

Summary of OLOP

In summary, the OLOP criterion thus consists of three stages:

1. Determine the closed-loop onset frequency, ω_{onset}, by solving equation (6.1) using maximum stick amplitude.

2. Calculate the required open-loop frequency response and find the set of pilot gains (K_p) such that the cross-over phase angle (Φ_c)

$$\begin{aligned} \text{-130deg} \quad &\leq \Phi_c \leq \quad \text{-90 deg} \quad \text{(longitudinal)} \\ \text{-160deg} \quad &\leq \Phi_c \leq \quad \text{-110 deg} \quad \text{(lateral)} \end{aligned}$$

3. Calculate the transfer function around the rate-limit and plot the frequency value at the onset frequency.

Such analysis and its success depends greatly on the fidelity of pilot behavior models, especially during demanding tasks where rate-limiting often presents severe complications. Often simple gain or first-order models are employed, with the overall piloted aircraft system being represented as in Figure 6.1. As the accuracy of the pilot model is always questionable, high fidelity simulation analysis of piloted-aircraft behaviour is a difficult task. However, existing analysis techniques such as OLOP and other more recent derivatives have been found to give a good indication of PIO tendencies [64]. Other pilot models like the Neal-Smith, and its subsequent modifications, have been argued to be more accurate, but a full discussion of these falls beyond the scope of this thesis. The interested reader is referred to [123, 53] for a more complete discussion of this topic. Figure 6.5 shows graphically PIO analysis of a system via the OLOP criterion. In this case, the system is PIO prone as the OLOP point (square marker) lies above the OLOP boundary [1]; if the OLOP point were to lie below this bound, then the system would be deemed free of PIO's.

[1] It is worth mentioning that this bound has been obtained experimentally

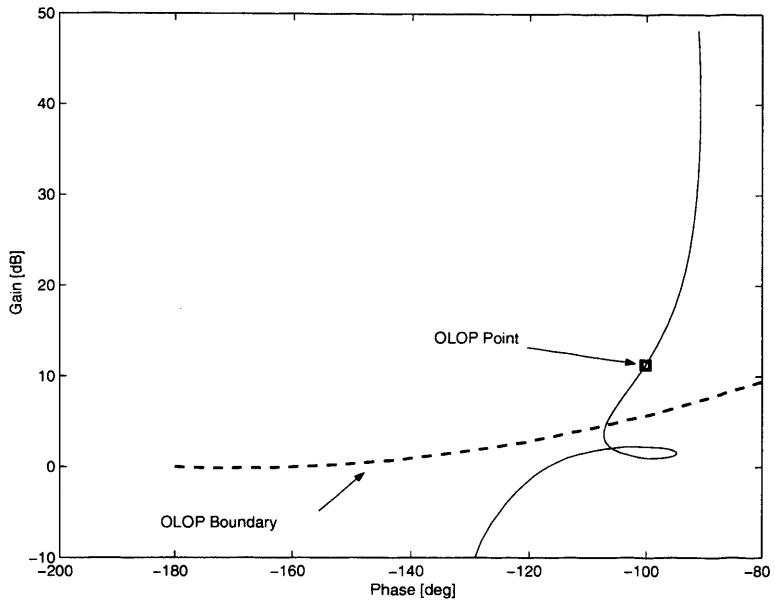

Figure 6.5: PIO determination via the OLOP Criterion

Although some of the predictions may be slightly inaccurate due to pilot-model mismatch, such procedure provides some theoretical insight into some of the troubled regions where PIO's may develop. It also provides a baseline pilot-plus-vehicle model on which different AW strategies may be tested for performance and stability, this being the basis for our desktop simulations.

6.4 Tools for PIO suppression

Despite the vast literature on PIO's, the number of tried-and-tested useful methods to deal with Category II PIO's is relatively limited. By and large, "robustness" to rate-limited actuators can be improved in one of three ways: a complete controller re-design, pilot command shaping, or augmenting the existing controller with an extra element active only during saturation. There are advantages and disadvantages to each method, as discussed below.

Controller re-design. Although such an approach is possible in principle, and indeed there have been many theoretical studies on the design of one-stage controllers to handle actuator rate-limits (see for example [55], [32], [95]), the general feeling in the aerospace community is that such an approach is impractical. A baseline controller re-design is expensive and time consuming, and may even require re-certification by the relevant aviation authorities. Furthermore, although such an approach may allow PIO-free control systems to be developed, such techniques may restrict performance during small-signal operation in order to deliver acceptable performance during large signal operation.

Pilot command shaping. This is commonly used in many aircraft to eliminate undesirable pilot commands and/or to make the aircraft handling qualities different depending on whether coarse or precise maneuvers are being performed. The basic idea is to leave the main feedback control loop intact and only alter the feed-forward path. However, when the pilot is engaged within the outer feedback loop, stability problems can still result and there are no reported methods which address this problem rigorously. While the usefulness of such shaping filters is acknowledged, it is again stressed that, to completely eliminate large or undesirable pilot inputs, an unacceptable compromise of the small-signal performance of the system may be required. Some examples of pilot command shaping are the PIO suppression filters developed by NASA [85] and the DLR phase compensation filter [98]. In both cases, the pilot's input is shaped to reduce the amount of rate limiting and time delay present in the closed-loop system.

Baseline control system augmentation. The third approach to reducing an aircraft's susceptibility to PIO behaviour is to "retro-fit" an additional compensator to the baseline controller. It is assumed that linear control dynamics deliver acceptable performance and stability margins, but when severe rate-limiting situations arise, an additional control element is introduced to reduce the likelihood of PIO behaviour. There are fewer reports on this approach in the literature, although some techniques have emerged, mainly from industry and research establishments (see [81, 44, 73]). Perhaps the best known approach is the "phase-compensation" approach advocated by SAAB [81]. This is essentially a form of AW compensation whereby the controller is augmented with an extra element and, indeed, the name "phase compensators" often refers to an AW-type strategy to address the phase-shift between commanded and actual actuator signal which often occurs during rate-limiting. One of the problems with such methods is that they concentrate on eliminating the phase shift induced by the rate-limit, but do not directly account for stability [2] and performance of the complete nonlinear closed-loop system.

6.4.1 The anti-windup approach and its advantages

Although some attempts at applying modern anti-windup (AW) schemes to flight control problems have been reported(for example in [4, 60]), the systems on which they have been assessed have been grossly simplified, linear, low-order approximations of the true aircraft. Other potential techniques are those of [102] or [120]. However, both schemes involve LMI optimisation, which may suffer from initialisation problems and numerical errors, especially when dealing

[2] Even if phase shifts are eliminated, a divergent in-phase oscillation may still develop

with large, complicated systems. Thus there is a lack of scientific assessment of modern anti-windup techniques in real flight control situations.

This chapter describes the simulation studies which were conducted in preparation for the flight tests that took place in July 2006 as part of the GARTEUR AG-15 activities. The results reported here make use of the results in Chapter 5 (see also [92, 89]) where an intuitive but rigorous solution to the rate-limit problem was given; this combination appears rare in the study of PIO problems. At this stage, it is useful to note that although aircraft actuators are both position and rate-limited, position saturation is encountered much less frequently in flight control, making it desirable to concentrate on the rate saturation problem. There are several notable advantages to using the AW results given in Chapter 5 which make them attractive for the flight control setting:

- The AW compensator is only active during and immediately after saturation has occurred. This means that existing legacy controllers, which probably had great effort devoted to it, may later be augmented with an AW compensator without any extra restrictions being imposed.
- The design of the AW compensator is independent of that of the linear controller and thus a *single* AW compensator can be used with *many* different linear controllers (although the transient response will obviously change). This can be useful in flight control systems as controllers sometimes have both attitude-command and rate-command modes.
- The method only requires the solution of a single Riccati equation with three free parameters (later reduced to two as discussed in Section 5.5.1); thus it is relatively simple to construct an anti-windup compensator which guarantees stability and performance.

One of the interesting features of the work in Chapter 5 is that it is local in nature, with one of the main trade-offs being that between performance (measured as an $\mathcal{L}_2$ gain) and the size of the region of attraction [3]. The tuning framework introduced in Section 5.5.1 allows a reasonably transparent and intuitive trade-off between these two conflicting goals, which is vital for practical implementation.

6.5 The ATTAS aircraft

The ATTAS (Advanced Technologies Testing Aircraft System) is a highly augmented *VFW-614* experimental aircraft operated by DLR (Deutsche Zentrum fur Luft und Raumfahrt) and

[3] A similar trade-off was observed in [102]

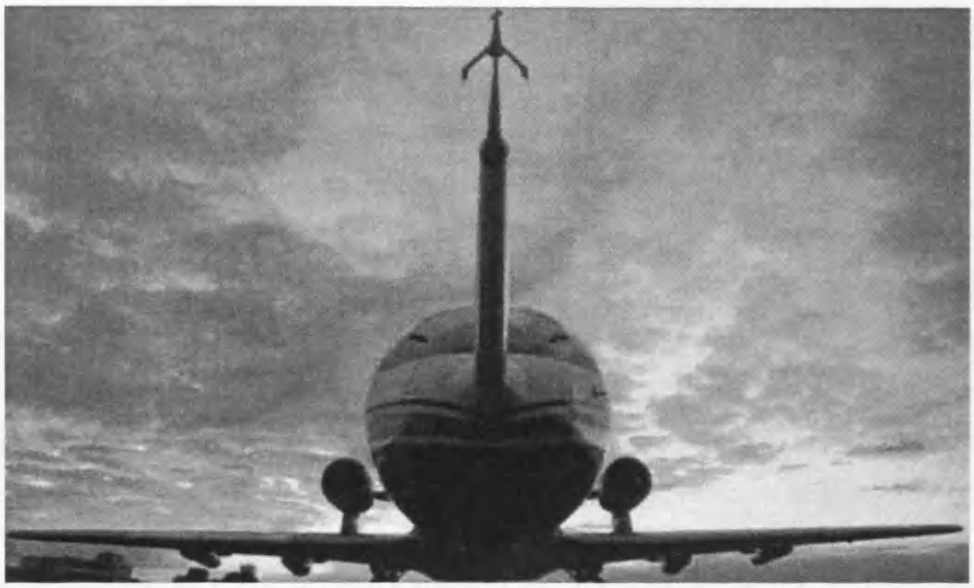

Figure 6.6: Front view of ATTAS aircraft

used to assess flying qualities and flight control laws. It is a medium sized jet aircraft which, before modification was capable of seating approximately 20 passengers, together with a two person flight crew. Since modification, much of the former passenger area is now devoted to computer equipment and instrumentation.

The ATTAS has several customized systems such an adaptive fly-by-wire flight control system capable of hosting different flight control strategies, cockpit display and an extensive set of flight test instrumentation. For the SAIFE campaign the aircraft was fitted with a passive side-stick as the primary control inceptor, allowing the pilot to reach high amplitude/frequency control inputs with relative ease. This also augmented the maneuvering capabilities of ATTAS while reducing the workload on the pilot. Safety of the ATTAS is ensured with a mechanical back-up control system that is activated only in the event that the safety pilot needs to override the experimental control laws. This allows relatively easy and fast clearance procedures, and therefore, experiments can be flight tested without going through the extensive process of flight certification.

The ATTAS dynamics are fairly benign with few stability issues and rate-limits sufficiently high to avoid most PIO type behaviour. ATTAS has a large flight envelope and the dynamics of the aircraft vary with Mach number and altitude. However, for small perturbations about the trim condition, it can be considered as essentially linear and a scheduled "linear" controller can be used to endow the system with adequate stability and performance properties.

Although the ATTAS is typically not prone to unexpected behavior, the objective of the work

was to make the un-augmented system susceptible to PIO's and then to add the AW compensator in order to reduce or eliminate this susceptibility. PIO-type behaviour was therefore induced by applying sufficiently aggressive pilot inputs and using sufficiently low software rate-limit values which can be adjusted using the on-board flight control computer (i.e. software rate-limits were adjusted to half their nominal values). Although such a procedure can be viewed as a little artificial, the outcome from these simulations (and the flight tests which followed) was expected to shed some light on the assessment of the anti-windup techniques developed in Chapter 5. Furthermore, note that an approach using artificially degraded rate-limits is the only safe way of conducting flight tests, as any dangerous rate-limiting can easily be removed by reverting to the standard fly-by-wire configuration, or allowing the safety pilot to take control with the mechanical system.

6.5.1 The ATTAS aircraft and flight control system

A block diagram of the basic ATTAS configuration used in this chapter is depicted in Figure 6.7. It consists of consists of three main parts: the nonlinear flight dynamics, the actuators (including the engine), and the controller. In addition, the "inner" control loop is augmented with an "outer" loop which represents the actions of the pilot. This is the same structure proposed in figure 6.1 and represents the general structure of most flight control systems.

A nonlinear model of the inner loop (the nonlinear plant, actuators and controller) was provided by DLR together with a set of trim points which corresponded to different flight conditions scattered across the flight envelope. The sample period used in the ATTAS on-board FBW system was set to 0.03 seconds; this was imposed on the simulation model too. It is important to have this in mind as to avoid sampling and numerical issues (which manifest themselves as spurious aircraft behaviour), it was necessary that any AW compensators had relatively slow poles.

Nonlinear plant

This is the nonlinear model of the main airframe augmented with the linear portion of the actuator models. The resulting plant is thus a complex high-order nonlinear system with 27 states, 23 inputs (17 are pilot commands and 6 are wind related disturbances) and 32 outputs, although only 12 are used for feedback. For this work, the aircraft dynamics were partitioned into longitudinal and lateral/directional axes (see Table 6.1). The longitudinal channel has the elevator command (for pitch control) and the Power-Lever command (thrust, for airspeed

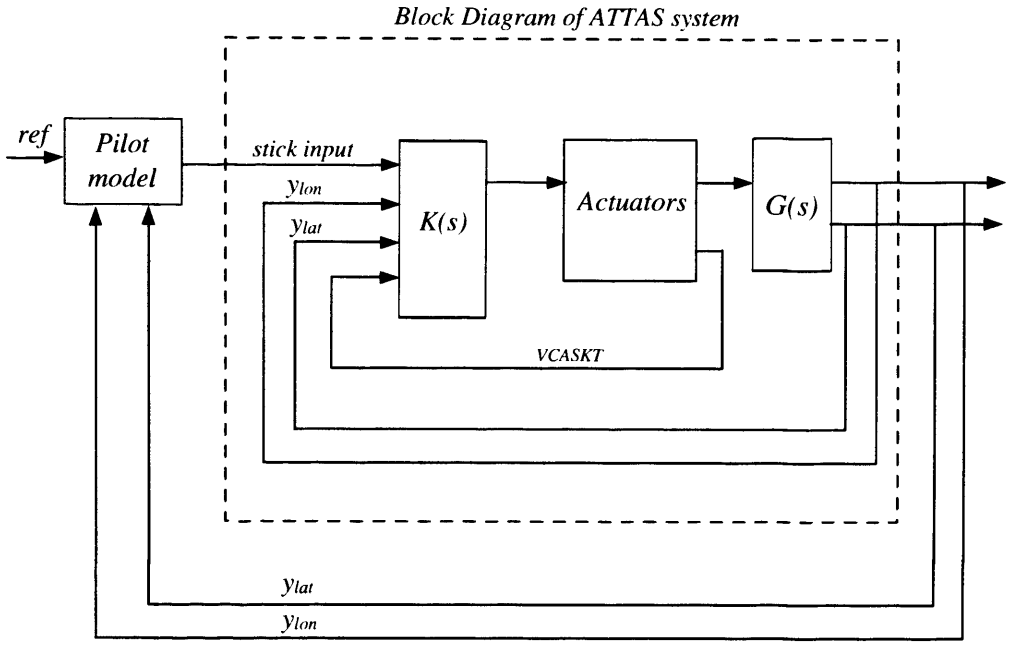

Figure 6.7: Block Diagram of ATTAS aircraft model

control) signals as control inputs, the first of which has strict rate constraints. Measurements of pitch angle $\theta(rad)$, and pitch rate $q(rad/s)$ are the primary variables used for feedback in this axis, with the airspeed being used to schedule the control law.

Input	Symbol	Units
elevator	$\mathbb{X}_i$	radians
power lever	PL	radians
Output	**Symbol**	**Units**
Pitch attitude	θ	radians
Pitch rate	q	radians/s
Angle of attack	α	radians
Flight path angle	γ	radians
True airspeed	VTAS	knots
longitudinal velocity	u_K	m/s
vertical velocity	w_K	m/s

Table 6.1: ATTAS longitudinal input/output information

The lateral channel has the aileron and rudder command signals as control inputs with both channels having strict rate constraints. The primary lateral outputs for feedback are the roll angle $\phi(rad)$, and the roll and yaw rates - $p(rad/s)$ and $r(rad/s)$ respectively. The lateral

input-output structure is summarised in Table 6.2.

Input	Symbol	Units
aileron	η	radians
rudder	ζ	radians
Output	**Symbol**	**Units**
Roll attitude	ϕ	radians
Roll rate	p	radians/s
Yaw angle	ψ	radians
Side-slip angle	β	radians
Yaw rate	r	radian/s
lateral velocity	v_K	m/s

Table 6.2: ATTAS lateral input/output information

As our AW design method requires the plant to be linear, the system was trimmed and linearised using DLR algorithms. This was done around eight distinct flight conditions spread across the FBW envelope. The flight condition initially preferred for anti-windup design was Mach 0.3, 20,000 feet, straight and level flight, which was chosen since simulation revealed that it was one of the most problematic flight conditions; additionally the plant was open-loop stable in both channels. Interestingly, it was observed that the AW compensator designed at this operating point seemed to function successfully at other flight conditions despite the change in aircraft dynamics.

Flight control system

A block diagram of the main ATTAS flight control system is shown in Figure 6.8. The inputs on the left hand side represent the four pilot commands and the feedback signals used in the control laws. Notice that the velocity and the yaw controllers are simply open-loop controllers and effectively only scale the pilot input to yield suitable control signals to the plant. The pitch and roll controllers do, however, use feedback of pitch/roll attitudes and rates respectively, both being scheduled with airspeed.

As the velocity and yaw controllers do not affect the aircraft's proneness to PIO and as they are simply open-loop, they will, by and large, be ignored in much of the subsequent analysis and design. The two important controllers, in terms of PIO and AW implementation, are the pitch and roll controllers. Both of these controllers are rate-command-attitude-hold controllers,

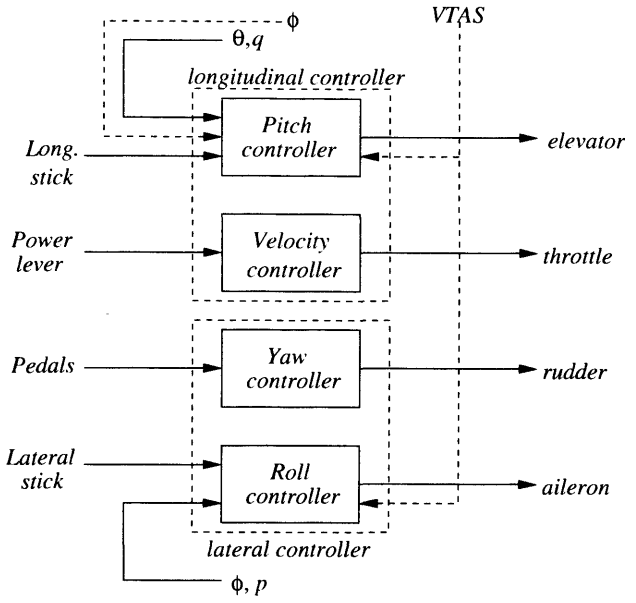

Figure 6.8: Simplified ATTAS flight control system

normally acting as a pure rate command controller unless the pilot stick command is zero. The pitch controller is essentially a proportional rate controller which generates an elevator command from pilot stick force and pitch rate feedback. During zero pilot demand, the controller switches (in a continuous sense) to a PI attitude controller by feeding back θ and its integral. Some decoupling is also achieved through feeding back the square of the roll rate, ϕ, although the gain associated with this is relatively low.

The roll controller behaves similarly, with the controller generating two aileron inputs from the pilot stick force, and the roll angle and rate feedback, with the attitude portion of the controller becoming active during zero pilot demand. There is no decoupling term in this controller and the yaw channel is left open-loop. Both the lateral and longitudinal controller gains are scheduled over the flight envelope by a measurement of the airspeed, VTAS.

The controller has been used on ATTAS for many years and was designed with no performance specifications in mind, but with the sole goal of retaining stability and reducing pilot workload. Initially this controller was intended to help pilots reach trim points with reduced effort and fly for longer hours. This is mentioned as later in the Ground simulation phase it was noticed that the attitude hold portion of the controller could be removed to enhance aircraft sensitivity.

Actuators

The actuator block includes saturation and rate-limiting of the control inputs, and a nonlinear model of the engine. In the longitudinal axis, only the elevator command signal has rate-limit constraints modelled as in Figure 5.3 with $H = 6.7$ and rate saturation of $0.523 rad/sec$. The power lever command signal is not rate-limited and open-loop, therefore it is not included in AW compensator design.

The lateral axis actuators have rate-limits in both the ailerons and rudder signal. The rudder rate-limit is of less importance as the yaw channel is open loop - it is also removed from the design process. The aileron actuators have a bandwidth determined by $H = 6.7$ and rate-limits of $0.47 rad/sec$.

Pilot

For this work it was assumed that the pilot provides an outer-loop of attitude stabilisation, that is, the pilot is a system providing a stick input on the basis of higher-level attitude commands and observed attitudes. For simplicity, the pilot was modelled as a diagonal constant matrix with its two diagonal elements representing the pilot "gain" in the pitch and roll axes:

$$K_p = \text{diag}(K_{plon}, K_{plat})$$

Although crude, there has been some success with such models in the past, and as mentioned earlier, this static model mimics the behavior of a *precognitive* type pilot when he encounters a PIO event. The pilot gains, K_{plon} and K_{plat}, were chosen using the OLOP criterion, rendering an open-loop cross-over phase of about $\Phi_{clon} \approx -130^o$ and $\Phi_{clat} \approx -160^o$ respectively.

Flight Envelope

The flight envelope of the ATTAS in FBW mode is given in Figure 6.9. The linearised ATTAS models provided by DLR, and proposed for the subsequent flight test, where chosen as follows (for more detail see table 6.3):

- Flight conditions 1 to 3 are at $10,000 ft$ with velocities ranging from Mach 0.3 to Mach 0.5
- Flight conditions 4 to 7 are at 20,000 ft with velocities from Mach 0.3 to Mach 0.6

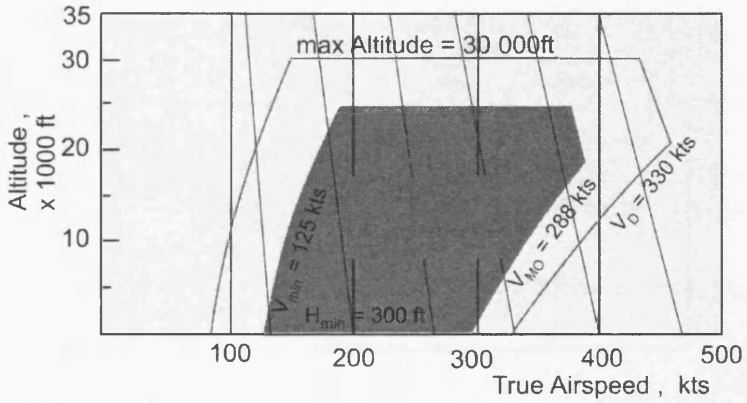

Figure 6.9: ATTAS Flight Envelope

Flight Condition No.	Velocity (VIAS) [kts]	Altitude [ft]	Comments
1	198.44	10000	
2	264.59	10000	
3	330.74	10000	
4	198.44	20000	
5	164.59	20000	
6	330.74	20000	
7	396.88	20000	
8	135	1350	-3deg γ
9	135	20000	-5deg γ

Table 6.3: Up-and-away and lading approach Flight Conditions (FC)

- FC 8 and 9 are landing approach configurations at 1500 ft and 135 knots with flight path angles, of $\gamma = -3$ deg and $\gamma = -5$ deg respectively

Flight conditions are well spread within the flight envelope, touching different types of flight dynamics. At low speed the aircraft becomes less responsive; at high speeds, the maneuverability of the system is increased and noticeable effects may emerge from rate-limiting.

6.6 Anti-windup design and implementation for ATTAS

As mentioned in the previous section, like most fixed-wing aircraft, ATTAS can be naturally decoupled into the longitudinal and lateral/directional dynamics. Likewise, apart from a small

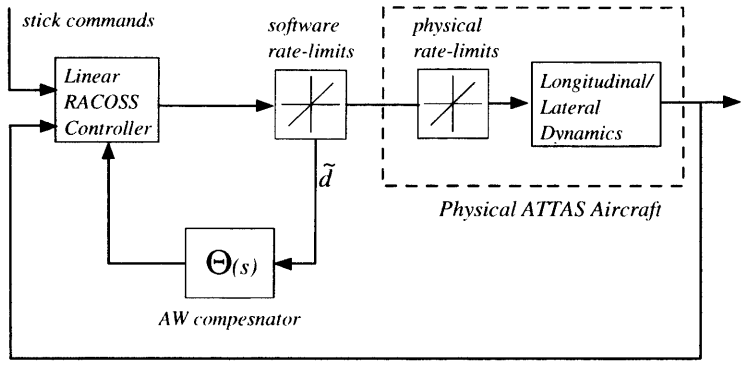

Figure 6.10: Block diagram of the system with added software rate limits

cross-coupling from the lateral dynamics to the longitudinal controller (see Figure 6.8), the control system can also be decoupled into lateral and longitudinal parts. Again, as mentioned before, due to the nonlinear nature of the ATTAS flight dynamics and the scheduled nature of the ATTAS controller (which is known as "RACOSS"), an anti-windup compensator must de designed using a linearisation around a trim point. DLR provided 9 different trim points, all of which could be potential candidates for AW design. However, after some investigation, Flight Condition (FC) 4 was chosen as the point around which the AW compensator would be designed.

At FC4, the aircraft is trimmed at Mach 0.3, 20,000 feet, which is a low speed, high altitude flight condition; at this trim point the aircraft tends to be more difficult for the pilot to control satisfactorily as the aircraft is, in theory, less responsive. During initial simulations of the nonlinear ATTAS model, it was observed that FC4 was perhaps the most problematic of all nine flight conditions and, using suitable pilot gains, it was possible to excite oscillatory behaviour using sufficiently demanding synthetic pilot references. Furthermore at FC4, the linearised ATTAS dynamics were stable in both the lateral and longitudinal axes, making it possible, in principle, to achieve semi-global stability.

It was also discovered that, because ATTAS dynamics do not vary greatly with changes in flight condition, AW compensators designed at FC4 tended to function well when implemented at other trim points. In fact, unlike other more complex aircraft, ATTAS seemed an ideal test-bed for linear AW techniques as, certainly around its trim points, the aircraft behaved in a largely linear manner.

The architecture used for the nonlinear simulation (and also subsequent flight test) is shown in Figure 6.10. The fully coupled lateral/longitindal nonlinear model was used together with the linear RACOSS controller (although this is approximately decoupled as mentioned earlier)

for simulation purposes. The nonlinear simulation features two sets of rate-limit, the first modeling the physical rate-limits in the aircraft; the second modeling the software rate-limits which can be adjusted to any level below the physical rate-limits and to which we have full access. Note that, providing the software rate-limits are set below the physical actuator the physical rate-limits will never enter their nonlinear regime and will behave linearly. The anti-windup compensator shown is actually decoupled into longitudinal and lateral parts, viz $\Theta(s) = \text{diag}(\Theta_{long}(s), \Theta_{lat}(s))$, each element of which was designed for the longitudinal and lateral dynamics respectively. The anti-windup compensator becomes active only when rate-limiting occurs in the software rate-limits.

One of the main features of the scheme is the introduction of an extra *software* rate-limiter with added AW compensation. This approach is closer to real control applications as such "protective" elements are common practice in flight control systems; it is undesirable that the actual control effectors reach their limits, so software limits (either using logic or dynamic filtering) are added.

The protective rate-limiter added to the system is realised as depicted in figure 5.9, where the level of rate saturation and the linear bandwidth (BW) of the added protection are parameters chosen by the designer within the constraints that the rate-limit must be less than the physical limits and the bandwidth must be sufficiently high so not to interfere with the linear controller. One of the advantages of inserting such software limiters is that rate-limit levels can be manipulated via the on-board computer, allowing the assessment of the influence of rate-limit levels on PIO susceptibility. Furthermore, notice that by adding software limits, full availability of the signal $\tilde{d} = d - \text{sat}(d)$, which is required by the AW compensator, is automatically obtained; this would not be the case if using the physical rate-limit. The software rate-limiter has been designed to switch between three different levels of saturation: full rate-limits (i.e. $0.47 rad/sec$ for the lateral channel and $0.523 rad/sec$ for the longitudinal), 60% and 50% of the original value. The linear software rate-limit BW is set by choosing $H = 50$, which is greater than the actual actuator's BW; this reduces the impact that the newly added *linear* dynamics have on "regular" dynamics (i.e. no added software rate limits).

6.6.1 Design parameters

The design method of Section 5.5.1 was used to produce a full-order AW compensator around the design point of Mach 0.3, 20,000 feet [4]. For simplicity, the free parameter k was set to unity, reducing F to equation (5.56). The size of the region of attraction can be enlarged by making c_{max} in equation (5.59) large (which is equivalent to ρ being small). The performance index γ is related to the $\mathcal{L}_2$ gain of the map $\mathcal{T}_p$ (see Chapter 5) and must be made small in order to have good performance. As $\gamma = 1/\sqrt{\rho}$, a trade-off must be made between performance and the size of the region of attraction. The main issues that need to be addressed when designing AW compensation may be summarised as follows:

- Stability of the closed-loop compensated system must be guaranteed for a sufficiently big domain of attraction (i.e. ρ must be small, and consequently c_{max} big)
- As AW performance is of great concern, the map $\|\mathcal{T}_p\|_{i,2,\mathcal{W}} < \gamma$ must be as small as possible, which translates into a small performance index γ (i.e. making ρ big)
- The system must exhibit an improvement in its stability margins and performance

As mentioned above, due to the natural decoupling of the longitudinal and lateral dynamics at the trim point, the longitudinal and lateral AW designs were carried out separately. As k was chosen as unity for both channels, this reduced the design choices to ρ and ϵ in both axes; after several iterations, these were chosen as indicated in Table 6.4, yielding the optimal matrix gains, where $F_lon \in \mathbb{R}^{1\times 14}$ and $F_lat \in \mathbb{R}^{1\times 16}$as

$$F_{lon} = \begin{bmatrix} 0.0655 & -0.0294 & 0.7356 & 4.3948 & 0.0012 & 0 & 0.0012 & \\ & 0 & 0 & 0 & -0.0605 & -0.0008 & -0.0446 & -50.1453 \end{bmatrix} \quad (6.2)$$

$$F_{lat} = \begin{bmatrix} 0.0156 & 2.5669 & 6.6531 & 4.1785 & 0.4310 & -0.0749 & -0.0061 & -0.0533 \\ & 0.0681 & 0.0061 & 0.0595 & -0.0464 & -0.0014 & -0.0657 & -81.1278 & -9.4727 \end{bmatrix} \quad (6.3)$$

Compensator	ρ	ϵ	$\mathcal{L}_2$ gain
$AWC4_{long}$	10^{-8}	0.998	10^4
$AWC4_{lat}$	10^{-6}	0.998	10^3

Table 6.4: Design parameters and $\mathcal{L}_2$ gain for FC4

[4]This flight condition was initially considered but later removed from the actual flight test plan - see next chapter

The parameters values in Table 6.4 were chosen after a process of simulation based tuning. Due to the complexity of the ATTAS model, it was somewhat more difficult to arrive at "optimum" values for ρ and ϵ. It is also important to note that as γ represents the local *nonlinear* $\mathcal{L}_2$ gain of the system, it is a somewhat more vague measure of *actual* system performance; this is in contrast to the linear systems case, where the $\mathcal{L}_2$ gain is equal to the $\mathcal{H}^\infty$ norm, which has a well-defined frequency domain interpretation. As with all nonlinear systems the correspondence between the $\mathcal{L}_2$ gain and the performance of the system as observed due to specific inputs is not always clear. However it did seem to be the case that the system response with AW was significantly better than without AW for most parameter choices.

One of the difficulties in the tuning of the compensator was managing the trade-off between region of attraction and performance: according to the formulae of Section 5.5.1, whatever is gained in performance is paid for in region of attraction size.

However, it must be emphasized that the expression for c_{max} derived in Section 5.5.1 is a bound on the size of an ellipsoid which is contained *within* the region of attraction; the *actual* region of attraction is often larger ([33, 12, 100, 102]). Moreover, as the region of attraction is estimated from the Circle Criterion, it is likely to be much larger than guaranteed by this method: it is guaranteed that $\bar{\mathcal{E}} \subset \mathcal{X}$; the converse is rarely true. Thus there is often conservatism in the estimation of the region of attraction.

It was noticed that for values of ϵ which yielded a very tight sector bound, the system becomes less sensitive to changes in ρ, giving more room for fine tuning. It was also observed that even though performance is not directly dependent on ϵ ($\gamma = 1/\sqrt{\rho}$ for the case of choosing $k = 1$), a degradation of tracking performance was noticed as the reference signal increased (this translates into bigger stability regions of the autonomous system, i.e. $d_{lin} = 0$). This means that ϵ must be chosen large enough as to ensure that $d \in \mathcal{S}(d, d_0)$, but small as to allow for performance enhancement to be noticeable.

6.7 Nonlinear simulations

6.7.1 Desktop Simulation Setup

Nonlinear simulation is used as a tool for the comparison and verification of different AW compensation schemes. The model provided by DLR is an *almost* exact copy of the one existing within the ground simulator; this means that any problems found in desktop simulations will replicate themselves in ground simulations. This was observed by applying "clinical" reference

inputs (with clinical we mean constructed signals such as doublets or 3-2-1 type signals) to the vehicle system and comparing desktop and ground simulation results; this demonstrated that the two where highly correlated. As mentioned earlier the only noticeable source of discrepancy would come from the pilot model and the "real" pilot. As the AW compensator will be implemented on the nonlinear model, there are no guarantees that the closed-loop compensated system will retain stability or performance, nevertheless, if the aircraft remains close enough to trim point, similar dynamics to that of the linearised system can be expected.

It is DLR's policy to reject any control scheme or experiment that has problems during the desktop and ground simulation phase, so it is important to develop accurate, well structured testing procedures in order to avoid future problems. The results obtained during desktop simulation provided valuable information as to how the system is expected to behave when being tested on the ground simulator with a real pilot. Although this will be discussed later, it is important to mention again that the greatest source of mismatch comes from the pilot model, not the vehicle itself, so actual ground tests were expected to be somewhat "unpredictable". This is an aspect that cannot be overlooked as PIO's by definition are only present in a PVS and are due to the interaction existing between the aircraft and the pilot.

Nonlinear simulations were carried out using software rate-limits to generate the signal $\tilde{d}$, which drives the anti-windup compensator. The rate-limit value, as mentioned above, could be set at 50 %, 60 % and 100%, to artificially modify the aircraft's susceptibility to PIO. After some initial simulation studies, it was found that PIO susceptibility was negligible for normal rate-limit values and that a 50 % rate-limit value seemed to make the aircraft noticeably more PIO prone. One of the main concerns about reducing the rate-limits was that pilots could find certain tasks difficult to perform due to a general "sluggish" feel to the aircraft rather than PIO proneness. However with the rate-limits set at 50 %, the chances of encountering PIO events seemed sufficiently increased, without greatly affecting the general "feel" of the system.

It was found, using the OLOP criterion, that pilot gains $K_{plon} = K_{plat} = -1.2$ stabilised the pilot-plus-aircraft system (for the nonlinear plant), yielding well damped dynamics in absence of rate-limits. Note that it is normally possible to achieve stability by lowering the pilot gains; this comes at the expense of having reduced performance. The idea here is to show how AW compensation copes with stability and performance issues that may arise when highly demanding reference signals are combined with "aggressive" pilot models. Figure 6.11 shows the effects of closing the pilot-vehicle loop with an aggressive pilot model, which translate to high gain, pilot control strategy and exposes the theoretical PIO tendencies of the ATTAS.

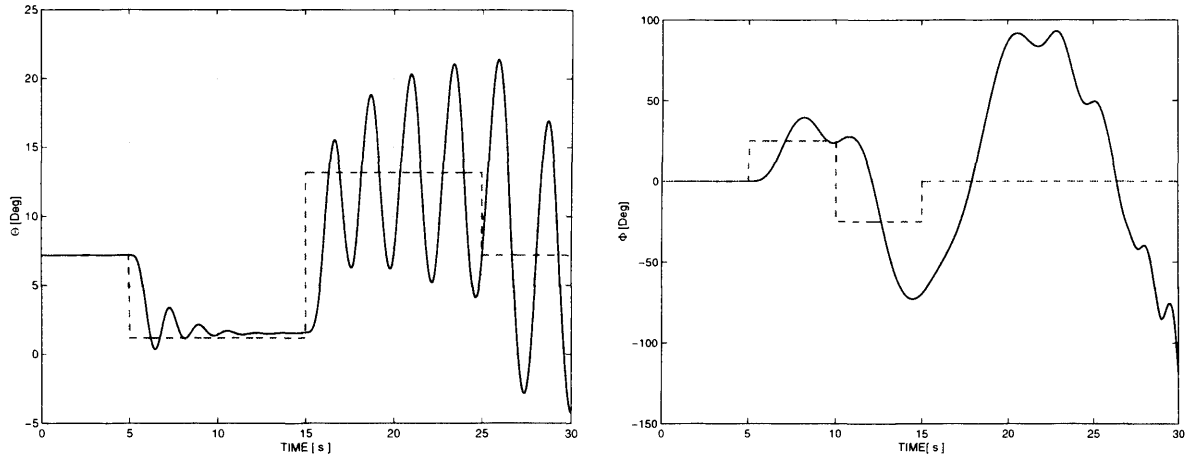

Longitudinal Axis Lateral Axis

Figure 6.11: OLOP analysis for flight condition FC4

6.7.2 Longitudinal Simulation Results

For the longitudinal axis simulations, a pitch-attitude doublet pulse reference (period 20 seconds, duty cycle 50 %, amplitude 6 degrees) was applied. The reference sequence starts at $5sec$ and returns to zero after one cycle (i.e. $25sec$). This type of task is useful as the pilot needs to give aggressive stick commands, exciting the rate limits in such a way that PIO behaviour, if any, is exposed; both gross acquisition and fine tracking can be evaluated by analising this maneuver. The maximum pitch attitude sought was large, but not too close to the aircraft's maximum attainable angle at the flight condition in question. In addition to exciting severe rate-limiting, this caused the aircraft to deviate from its trim point, thus testing the AW compensator non-locally and in a nonlinear regime. This potentially increased the difficulty of the AW compensator's task of maintaining stability as it had to function away from its design point.

Figure 6.12 shows the simulated behaviour of the aircraft for the aforementioned reference demand. When no AW compensation is used, the pitch attitude, θ continues to oscillate long after the reference command has returned to zero value; the system has lost stability and entered a limit cycle consistent with PIO-type behaviour. The same figure shows the pitch attitude response to the same input, but this time with AW protection employed. Although some oscillatory behavior is still present, the AW compensator manages to provide stability and recovers tracking performance swiftly. The initial response of the system is slightly more sluggish with the AW compensator engaged; this is typical of the behaviour induced using AW compensation and appears to be necessary to preserve local stability. In other words, some responsiveness of the aircraft has been sacrificed for greater stability properties.

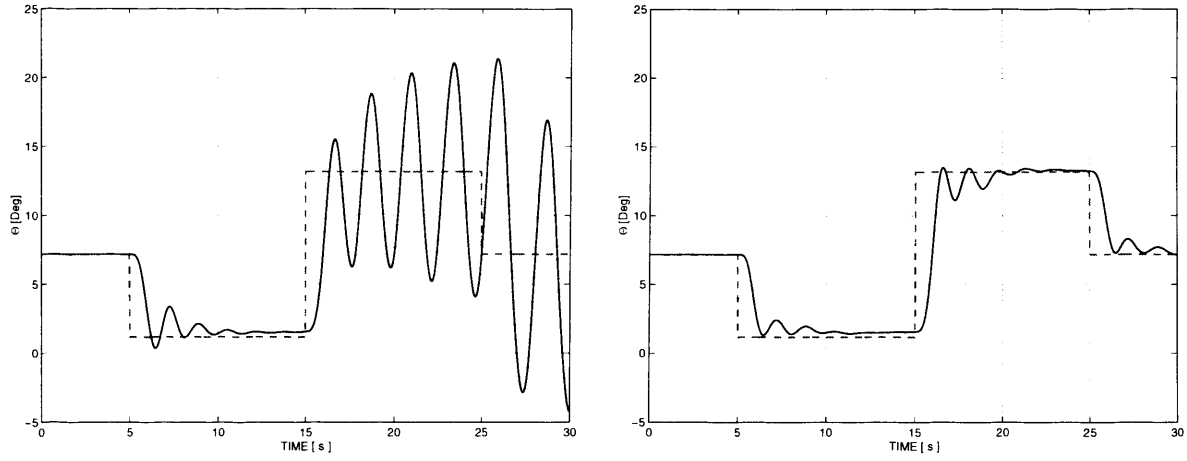

θ [Deg], No AW

θ [Deg] + AW

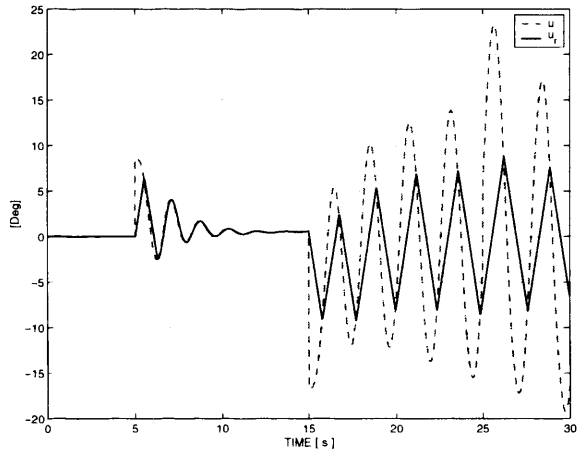

u and u_r [Deg], No AW

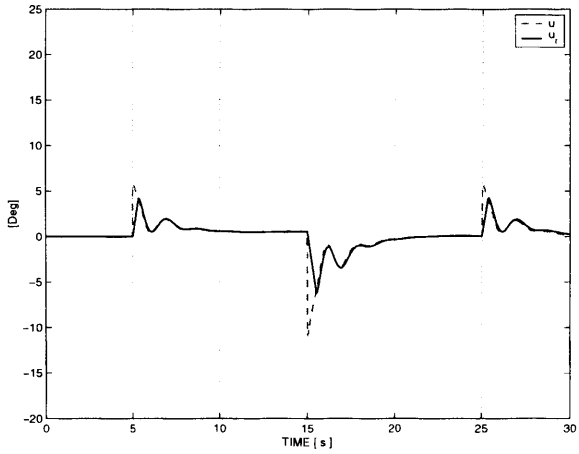

u and u_r [Deg] + AW

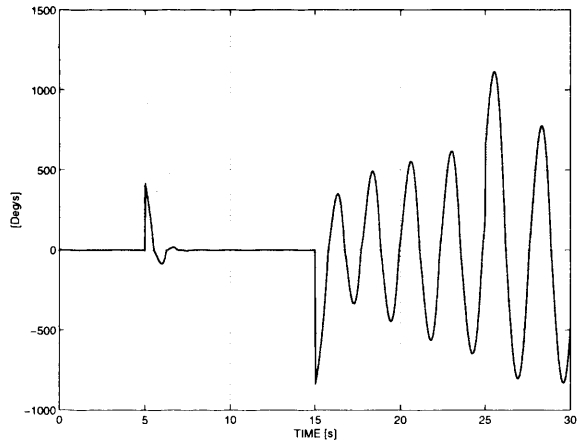

$\tilde{d}$ [Deg/s], No AW

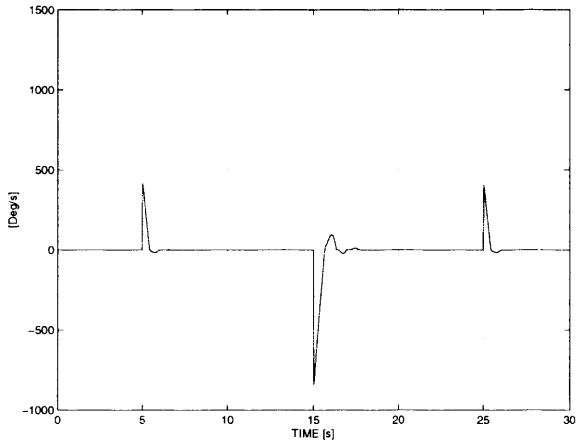

$\tilde{d}$ [Deg/s] + AW

Figure 6.12: Pilot-plus-Aircraft model simulation: Longitudinal channel

Figure 6.12 also shows the signals entering and leaving the software rate limiter, i.e. u and u_r. Both with and without AW compensation, the signal u_r tries to follow the real control signal u but with limited rate, in this way verifying that the software rate-limits are indeed "limiting"

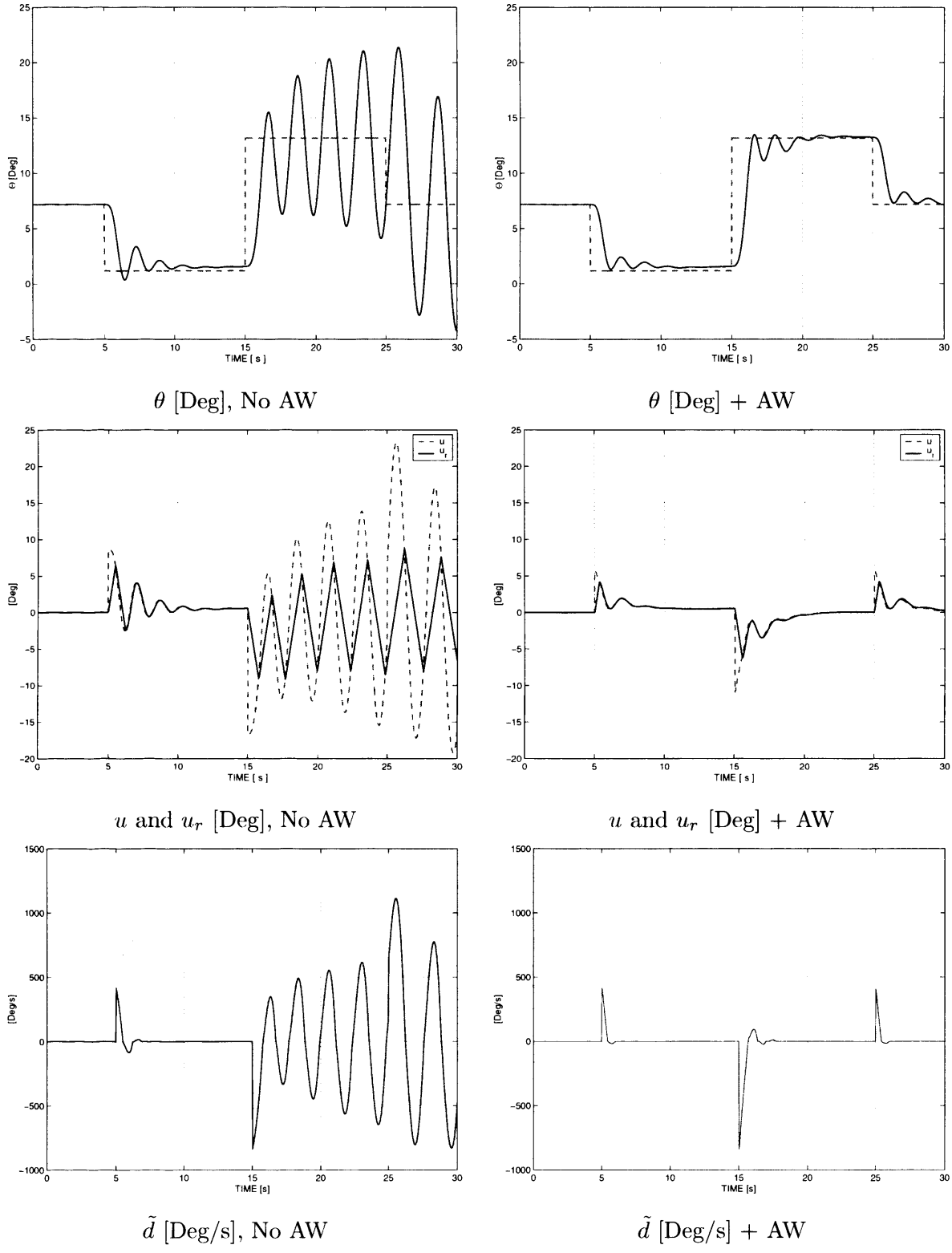

θ [Deg], No AW

θ [Deg] + AW

u and u_r [Deg], No AW

u and u_r [Deg] + AW

$\tilde{d}$ [Deg/s], No AW

$\tilde{d}$ [Deg/s] + AW

Figure 6.12: Pilot-plus-Aircraft model simulation: Longitudinal channel

Figure 6.12 also shows the signals entering and leaving the software rate limiter, i.e. u and u_r. Both with and without AW compensation, the signal u_r tries to follow the real control signal u but with limited rate, in this way verifying that the software rate-limits are indeed "limiting"

the control signal's rate. When no AW is used, the rate limited control signal reaches a state of full saturation similar that exhibited in Figure 5.2. This is to be expected as the system enters a limit cycle that causes it to be "locked" in saturation. When AW compensation is implemented, the system recovers stability and a decrease in the system's rate saturation level is achieved. Observe how the AW compensator avoids severe rate saturation by conditioning the control signal u before it enters the rate limiter, resulting in reduced phase lag between the intended control signal u and the real control command u_r. Note however that a reduction of phase lag is not alone sufficient to prevent PIO's, as is sometimes indicated in the literature; this is an oversimplification of a nonlinear phenomenon and extra care concerning stability issues must be taken.

As the AW compensators were designed using de-coupled linearisations, it is important to take into account the coupling effects that exist in the nonlinear model. It is possible to obtain a general idea of the degree of this coupling by observing how much ϕ drifts from its trim value. As shown in Figure 6.13, when AW is engaged, the roll angle ϕ remains very close to its trim value meaning that there is little coupling from the pitch axis intro roll. Without AW compensation engaged, there is somewhat more coupling and the roll angle appears to be trapped in a low amplitude limit cycle.

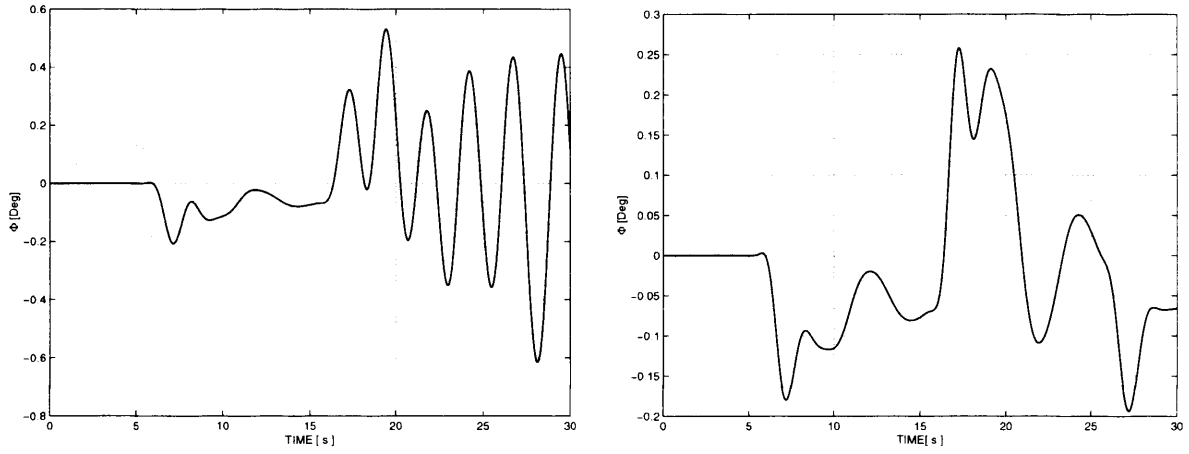

ϕ [Deg], No AW ϕ [Deg] + AW

Figure 6.13: Signal ϕ: Pilot-plus-Aircraft model

Next we will discuss how changes in trim point and pilot gains may affect the overall response. Robustness to plant uncertainty was discussed in Chapter 4, where it was shown that the AW synthesis methods proposed there had some inherent robustness properties that where dictated by the "stability multiplier" W. As the rate limit AW scheme proposed builds on such methods, it may be expected that some of this robustness tolerance permeates to the local AW problem

solution. This is of great importance as uncertainty may come with deviation from trim point, an issue of great interest when dealing with nonlinear systems. If the AW compensator is robust enough, it is expected that it will retain stability for more than one point in the flight envelope. Figures 6.14 and 6.15 show the pitch angle, θ, for flight conditions 2 and 6 respectively. In both cases the AW compensator implemented was designed using the linearised model of FC4 (the same used for simulation of figure 6.12), and, as can be observed, the compensator appears to be reasonably robust to changes in trim point. At FC2 the aircraft with AW engaged is able to avoid PIO behaviour, whereas without AW compensation it is not. At FC6, the aircraft's response becomes oscillatory even with AW engaged, although the amplitude of oscillation is notably lower than when AW is not active. In fact for most operation points, the AW compensated aircraft yields much better responses than when AW is not engaged, and it would perhaps be possible to consider one robust AW compensator to cover the whole of the flight envelope.

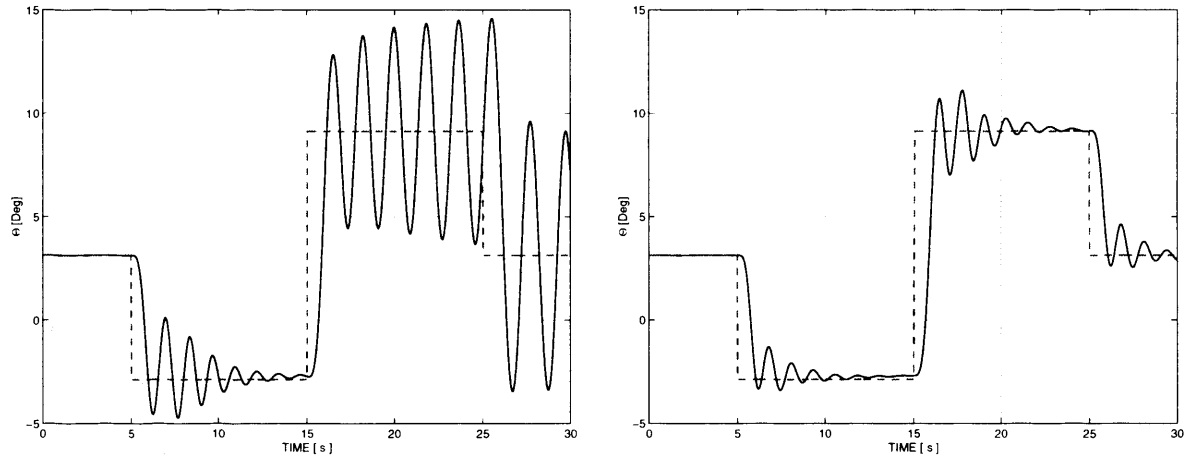

θ [Deg], No AW θ [Deg] + AW

Figure 6.14: Pitch angle θ: Pilot-plus-Aircraft model - FC2

To finalise the analysis of the longitudinal axis, it is worth mentioning that the results obtained in desktop simulation are susceptible to changes in the pilot model. This is demonstrated through simulation (see Figure 6.16) of the closed-loop system with reduced pilot gains (i.e. $|K_{plong}| = 0.8$). Although instability is not encountered using this lower gain, it is still interesting to note the decreased oscillatory behaviour of the system when AW is engaged, although the speed of response is slightly slower.

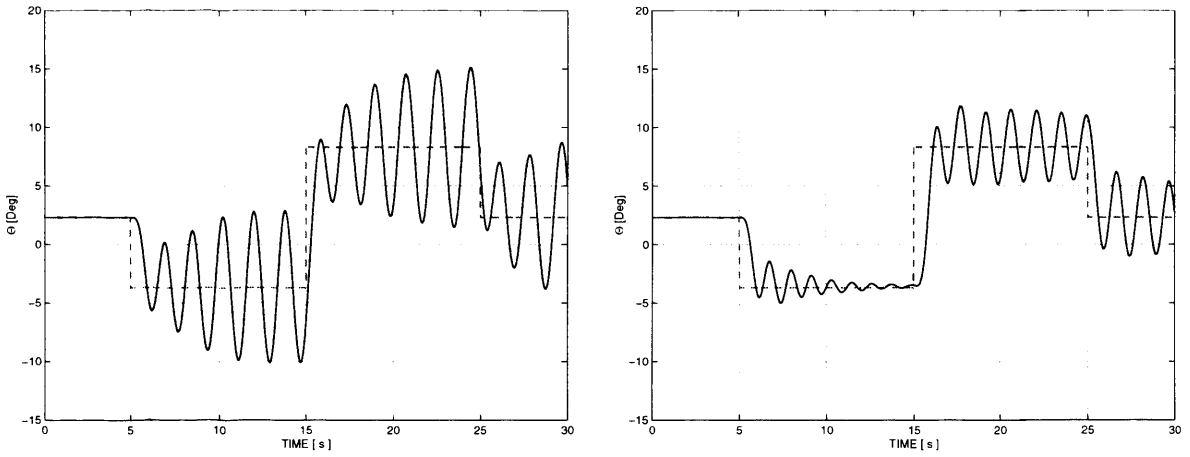

θ [Deg], No AW θ [Deg] + AW

Figure 6.15: Pitch angle θ: Pilot-plus-Aircraft model - FC6

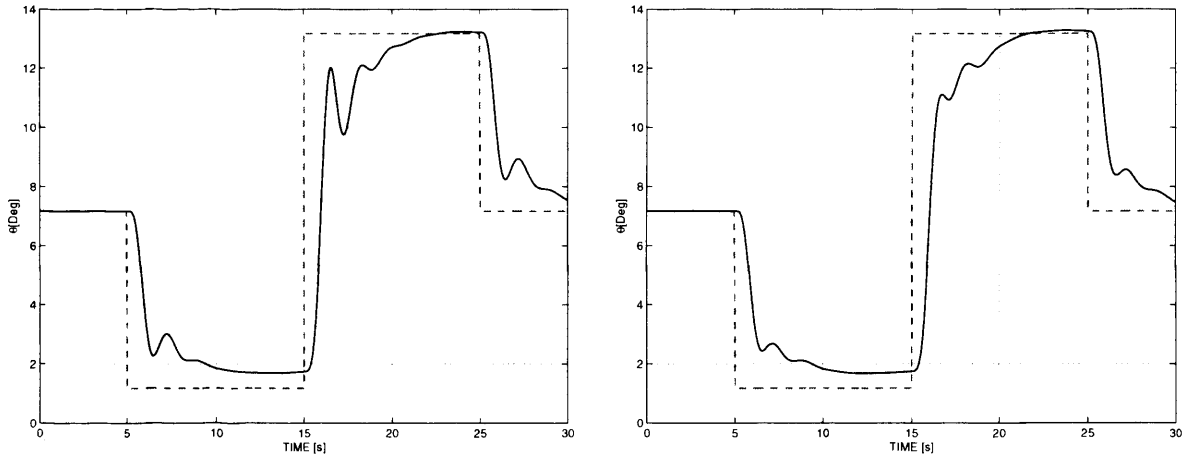

θ [Deg], No AW θ [Deg] + AW

Figure 6.16: Pitch angle θ: Pilot-plus-Aircraft model - $K_{plon} = 0.8$

6.7.3 Lateral Simulation Results

The lateral axis appeared less PIO-prone than the longitudinal axis and, in order to excite PIO-like behavior, roll-attitude references with shorter periods and larger amplitudes were required. Thus, the roll-attitude reference was chosen as a pulse train of period 10 seconds, duty cycle 50% and amplitude 25 degrees. The pulse has a start at $5sec$ and then returns to zero after $15sec$ (i.e. after completing one cycle). Figure 6.17 shows the behaviour of the lateral axis due to the above reference being applied. Without AW compensation, a slow divergent oscillation in roll attitude, ϕ, is evident. With AW compensation, things are different: the response of the system due to the same roll attitude demand converges rapidly to the trim point ($\phi = 0$ degrees) after the demand is removed, with only a residual oscillation slightly tarnishing the system's response.

The tracking performance with AW is still rather sluggish but it is clearly stable. It must be emphasized that anti-windup cannot "remove" the physical rate-limiting but can improve the way the system copes with these limits.

It is useful to observe how the signals around the rate saturation element behave. From Figure (6.17) it is possible to observe that the actual control signal u_r has limited rate. Notice how the system with AW control has a faster and smother return to linear dynamics, that is $u = u_r$. This can essentially translate into a system that is outside linear constraints for shorter periods of time and, therefore, is less prone to performance degradation and PIO events. This is enforced by the extreme reduction obtained in saturation level when using AW. This is measured through the signal $\tilde{u}$ and as shown in Figure (6.17), rate limiting occur less often and with less magnitude when using AW

Once again, it is a good exercise to analyse the coupling existing between lateral and longitudinal axis. In this case we observe the effects that changes in the roll angle have on the pitch angle. As previously discussed for the longitudinal axis, the effects of pitch to roll coupling are tolerably small. However, from Figure 6.18 the converse is not true. The lateral instability which occurs when no AW is present causes large (60 degree) excursions in the pitch attitude θ. When AW is engaged some coupling is still observed, but is an order of magnitude smaller and convergent. While one expects some coupling between lateral and longitudinal axes in nonlinear simulation, it appears that during rate-saturation this coupling can be significant if AW is not used.

The same AW compensator designed for FC4 was tested on FC2 and FC6. Figures (6.19) and (6.20) show that this compensation scheme is robust to deviations from trim point and provides enhanced performance at both FC2 and FC6. At both trim points the use of the AW compensator designed at FC4 prevents the system from becoming unstable. In fact, as FC2 and FC6 seem more PIO prone than FC4, it can be observed that AW is more useful at these flying conditions with very oscillatory responses being observed without AW engaged. Although the AW compensator was not designed specifically for these flight conditions, as it inherently incorporates some robustness, one can expect it to function reasonably well providing the dynamics of the system are not too different at these other trim points.

Figure 6.21 shows the response of the PVS when the pilot gain is reduced ($K_{plat} = 0.8$). As expected, for this lower pilot gain, the aircraft has better stability properties for both cases; with and without AW. The system settles down relatively swiftly after the reference demand is withdrawn. Note that for this case, the rate-limiting is not as severe and thus one would not

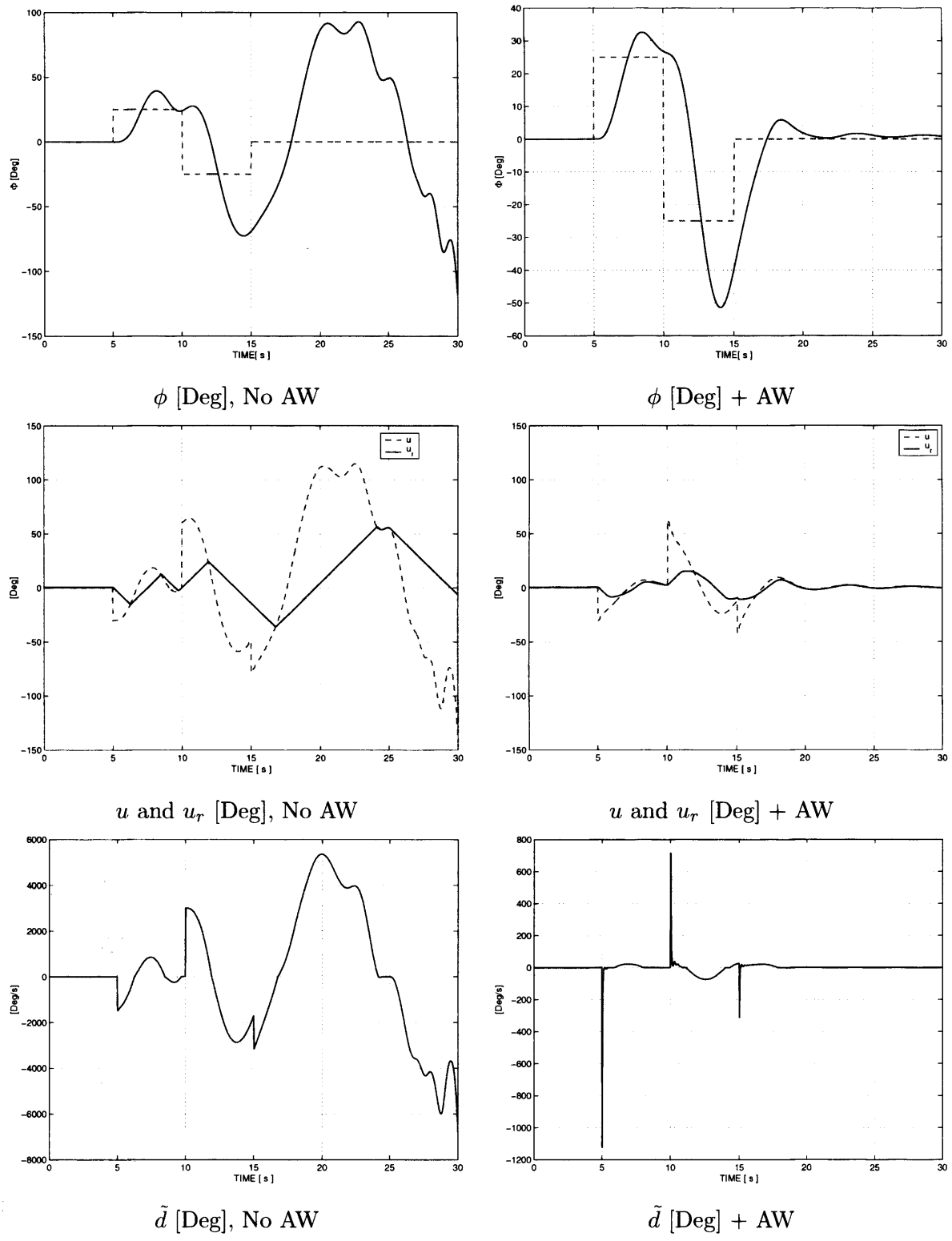

ϕ [Deg], No AW

ϕ [Deg] + AW

u and u_r [Deg], No AW

u and u_r [Deg] + AW

$\tilde{d}$ [Deg], No AW

$\tilde{d}$ [Deg] + AW

Figure 6.17: Pilot-plus-Aircraft model simulation: lateral channel

expect as much of a difference between AW and no AW responses.

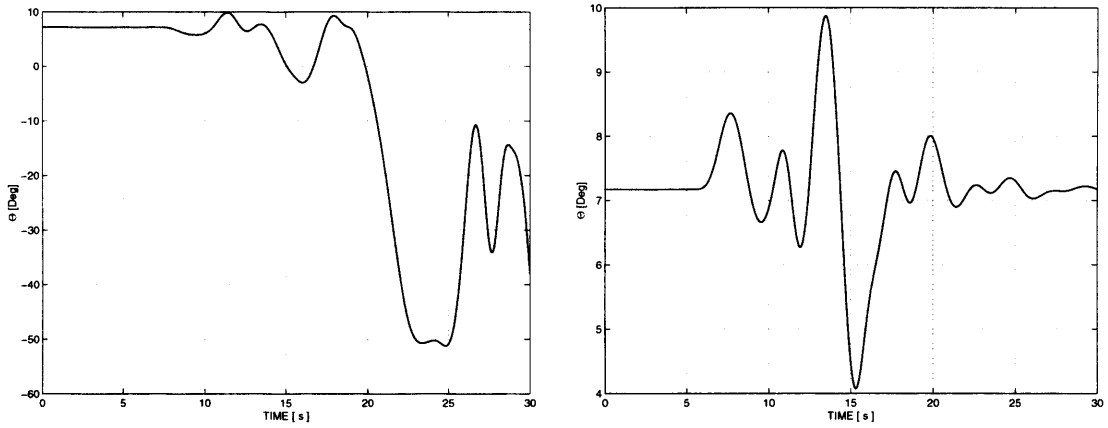

θ [Deg], No AW θ [Deg] + AW

Figure 6.18: Signal θ: Pilot-plus-Aircraft model

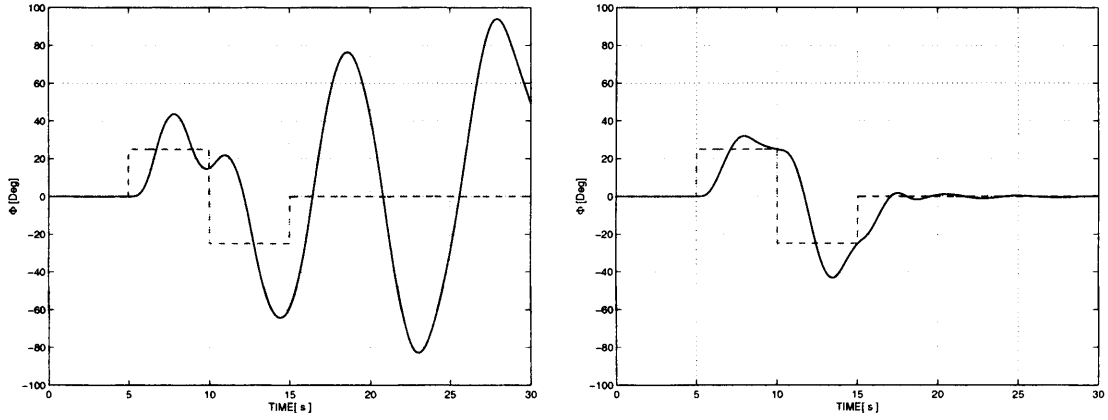

ϕ [Deg], No AW ϕ [Deg] + AW

Figure 6.19: Roll angle ϕ: Pilot-plus-Aircraft model - FC2

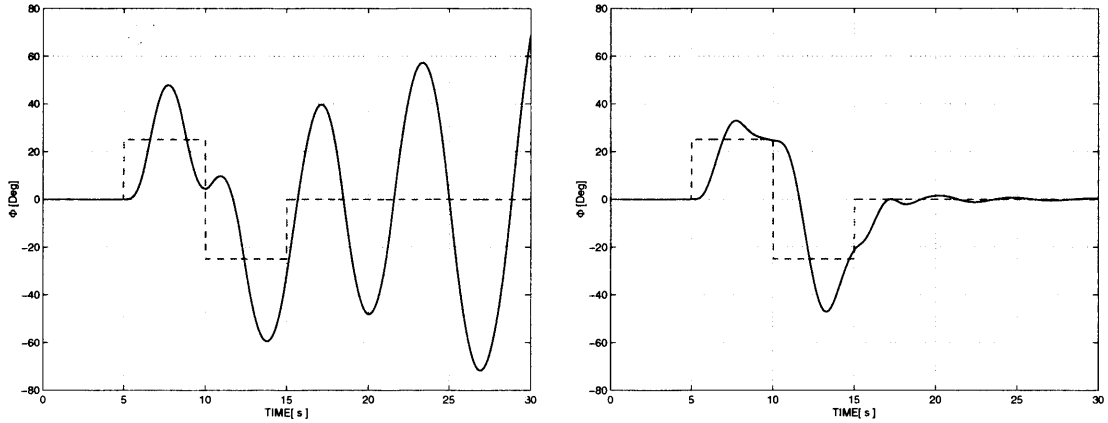

ϕ [Deg], No AW ϕ [Deg] + AW

Figure 6.20: Roll angle ϕ: Pilot-plus-Aircraft model - FC6

6.8 Conclusion

The results obtained in this section have illustrated the advantages of using AW compensation in a realistic flight control application. By reducing the level of rate saturation to 50% of its

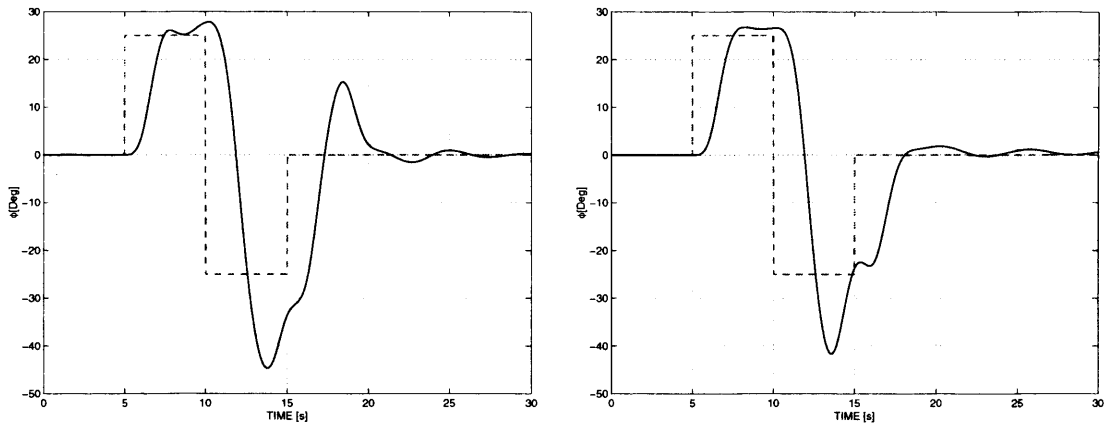

ϕ [Deg], No AW ϕ [Deg] + AW

Figure 6.21: Roll angle ϕ: Pilot-plus-Aircraft model - $K_{plon} = 0.8$

original value, it was possible to degrade the ATTAS performance and induce what may be thought of as Category II PIO's. It may be observed through time domain analysis that AW compensation increases stability margins and reduces the risk of PIO events developing. Such events where present for reference signals that demanded aggressive inputs from the pilot. The reference signals where chosen as to considerably excite the rate limits in such a way that the overall closed-loop compensated system had a clear performance degradation; the reference signal tried to make the pilot use full stick inputs at frequencies near to the system's onset frequency. This was achieved by using the reference signals describe in the previous section and a simple gain pilot model.

It is important to mention that even though the results presented in this chapter where successful in showing the benefits of using AW compensation, the simplicity of the pilot model makes this nonlinear simulation a simple approximation of what *might* happen when a "real" pilot commands the aircraft. Having this in mind (see [64]), any PIO event that may occur during desktop simulations may not necessarily happen during ground simulation, or in real flight. Although this is a great limitation and more complex, accurate pilot models may be desired, this is outside the scope of this research but acknowledged as a fundamental part in obtaining high fidelity results during the design phase of such rate compensation applications.

An advantage of using the algorithms proposed in section 5.5.1 is that the designer may choose how fast the compensator poles are. This is of great importance as a constraint in the sampling rate was imposed by DLR. This means that if compensator poles are sufficiently large, numerical errors may occur and may even be confused with PIO behaviour. Choosing the size of the compensator poles is a characteristic that is not present in similar LMI formulations ([100]).

Chapter 7

PIO avoidance in an experimental aircraft: flight test evaluation

Figure 7.1: Airborne ATTAS aircraft

Previous chapters have described some of the perils of rate and magnitude saturation and have advocated anti-windup solutions to these problems. Chapter 6 described the application of the rate-limit anti-windup compensation results developed in Chapter 5 to a complex flight control problem where it was shown, through nonlinear simulation, that anti-windup techniques had the potential to improve aircraft resilience to Category II PIO's. This chapter describes how the anti-windup compensators discussed in Chapter 6 were applied in practice and the results of their subsequent flight testing.

The flight tests described in this chapter formed the major part of the SAIFE (*Saturation Alleviation In-Flight Experiment*) campaign which was conducted at DLR Braunschweig, Germany, in the summer of 2006. These flight tests were seen as important because they implemented the anti-windup compensators developed in Chapters 5 and 6 on a *real* aircraft and were flown by

a *real pilot*; the latter is particularly difficult to replicate in simulation. It is believed that the anti-windup compensators tested in the SAIFE campaign are the first "advanced" anti-windup compensators to be tested in-flight and mark a significant step forward into the understanding of the design and evaluation of anti-windup compensators for PIO avoidance. In fact, these flight tests were considered so successful that follow-up tests are planned for August 2007.

7.1 The SAIFE Experiment: objectives and preparation

This section will describe the *Saturation Alleviation In-Flight Experiment* (SAIFE) that was conducted in July 2006 at DLR, Braunschweig. The flight tests were conducted on the ATTAS aircraft described in Chapter 6, where the vehicle was operated in "degraded" mode (rate-limits at 50 % of nominal value) in order to increase its susceptibility to PIO behaviour. The flight tests' main objectives were to:

- Quantify, through pilot ratings and time domain analysis, the degree of success that the AW scheme for rate-limits, developed in Chapter 5 and designed in Chapter 6, could have in a real flight control application
- Verify the claims of modern AW techniques: *"Can modern AW compensation schemes deliver in a real industrial environment the saturation alleviation and performance enhancement that they claim?"*
- Increase the involvement of industry in researching and implementing modern AW techniques

Another objective, of less importance, was to collect data of any possible PIO instances of the "degraded" ATTAS; future work may use this flight data to asses the detrimental phase shift associated with rate-limiting and corroborate prediction techniques such as the OLOP criterion. The experiment was conducted in such a way that at each flight condition (see table 6.3) two pilots evaluated a series of tasks (HQDT, the "birdie", off-set landings) for a degraded ATTAS aircraft, providing PIO (on the PIO rating scale) and HQR (on the standard Cooper-Harper rating scale) ratings. This was done for various flight conditions and for both the system with and without AW compensation, providing an extensive set of in-flight data which is one of the highlights of this work.

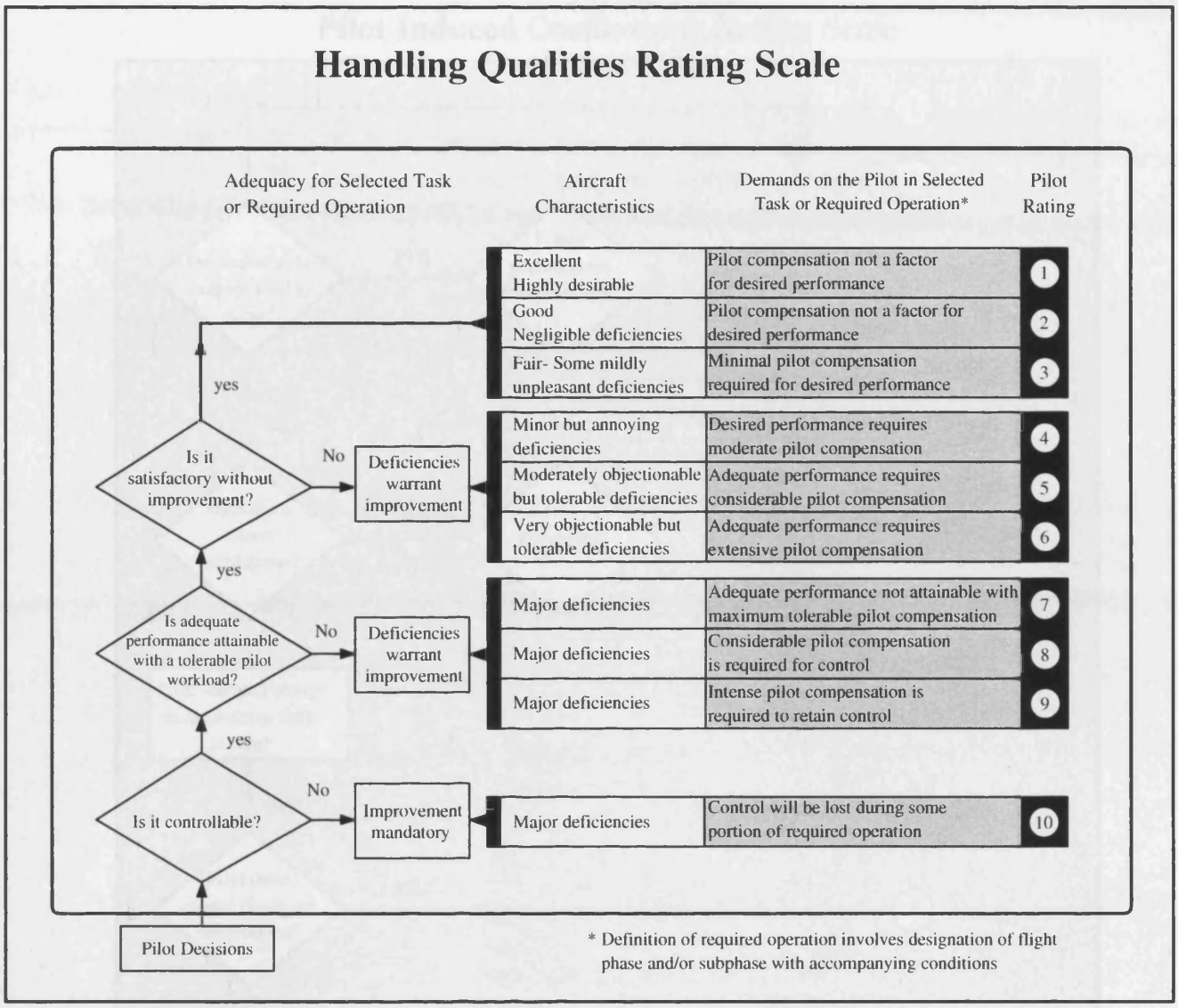

Figure 7.2: Cooper-Harper Handling Qualities Rating Scale

7.1.1 From design to flight test

The SAIFE tests involved flight testing and assessment of very new anti-windup compensators, and it is thought that this is the first practical in-flight application of modern AW schemes. Although tests of similar compensators have been reported in [41, 59], the SAIFE campaign involved pilots, and as such, safety was the priority in these tests, particularly as the aircraft would be flying in a degraded manner with its manouevrability significantly retarded. Therefore in order to ensure the results were conducted under safe and scientific conditions, a somewhat lengthy procedure, starting with AW design and culminating with flight test was followed.

Table 7.1 briefly describes the step-by-step procedure which was followed to enable an AW compensator to be implemented on the ATTAS aircraft. The first few stages are self-explanatory

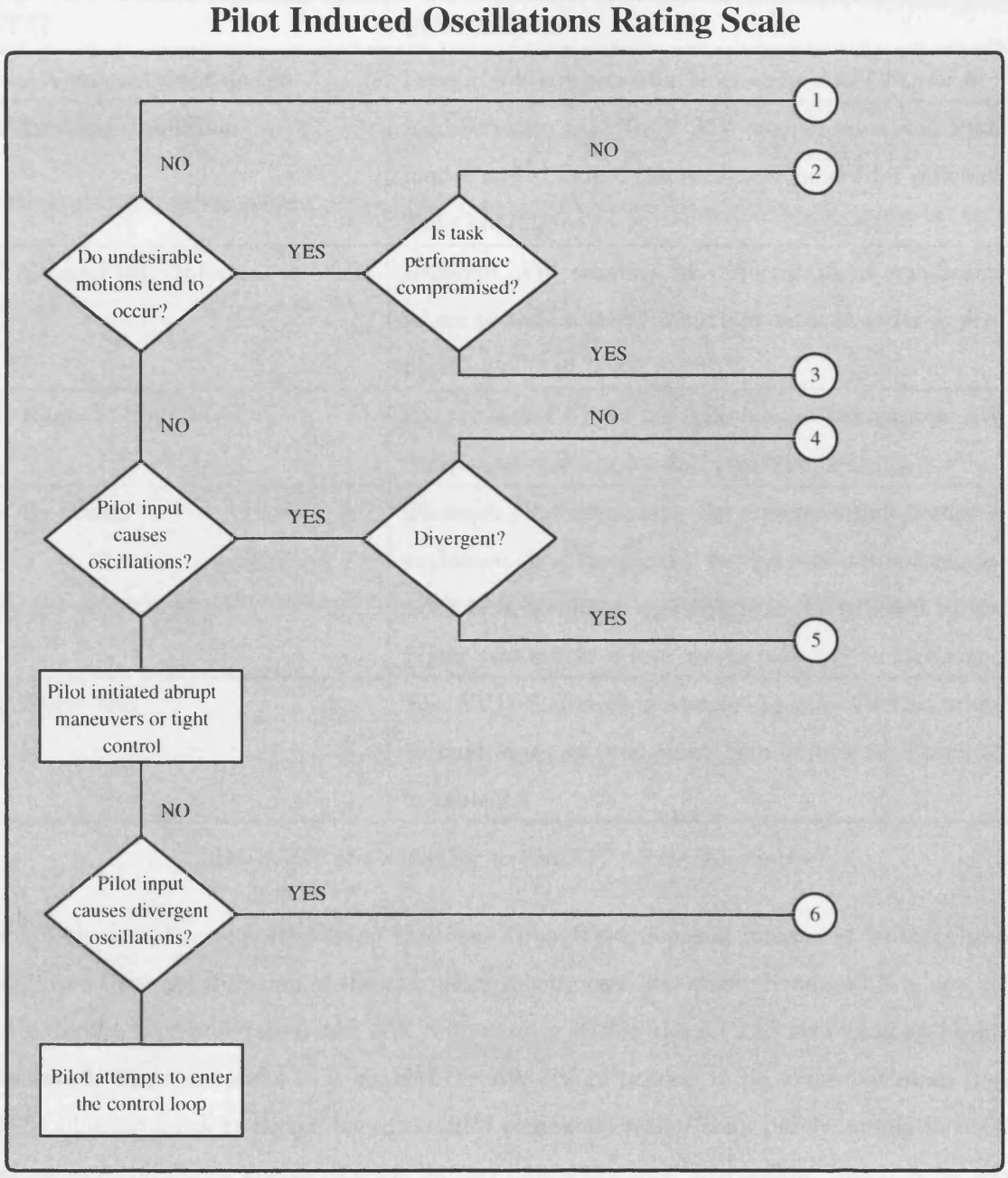

Figure 7.3: PIO Rating Scale

and have been extensively discussed in previous chapters, especially Chapter 6. It is worth mentioning that, in order to have different levels of rate saturation and to accommodate several AW compensators in one flight test, it was necessary to implement a switching strategy using the on-board flight control computer and switch box. This was operated by the flight test engineer present in both ground and flight test. The existing baseline controller (the RACOSS controller) was also implemented in a form which was amenable to anti-windup compensa-

STEP	COMMENTS
1. AW compensator design	Design AW compensator as described in Chapter 6
2. Desktop simulation	Add software rate limit, AW compensator and Pilot model and simulate the nonlinear model for different flight conditions
3. Ground test (informal at DLR)	Different AW schemes at different flight conditions where tested on the Ground simulator in order to prepare for piloted tests
4. Piloted Ground test	Experimental Flight test pilots asses the various AW compensations scheme and give comments
5. Re-design	Through pilot comments the compensation design is evaluated. If it the general feeling is that the compensator is in someway optimal, then we proceed to the Flight test stage. If not, we go back to the first step.
6. Flight test	The ATTAS aircraft is assessed by two different pilots through a set of predefined manoeuvres as described in table 7.3.

Table 7.1: Steps leading to the ATTAS SAIFE tests

tion. This was then exported using the *Real-Time Workshop* and integrated to the Ground simulator. Over the duration of the campaign this process was streamlined and it is now relatively easy to accommodate a new AW compensator within the ATTAS switching and control framework. This was useful as it enables the AW design process to be somewhat more "practical", allowing quick re-design based on pilot comments rather than purely simulations - the designs were produced specifically for human interaction and perception, which is far more complicated than usual time domain criteria (i.e. raise time, overshoot, damping, etc.) used to measure performance of control strategies. Thus the streamlined AW implementation scheme allowed for quick and convenient re-design of compensators allowing more pilot feedback in the understanding and design of the AW strategies.

7.2 Ground Based Simulations

Section 6.7 discussed desktop nonlinear simulations that produced an initial AW scheme and provided a "feel" for AW compensation design for the ATTAS aircraft. Ground-based simula-

tion was the first step beyond this and a necessary evaluation stage before real flight test. The ground tests of the SAIFE campaign were all conducted on the ATTAS Ground simulator at DLR, Braunschweig. The ATTAS simulator provides a convincing replica of the real system, including an ATTAS cockpit, on-board computers and visual systems, and pilot inceptors. It is used to verify the safety of any experiment prior to actual flight. Some of the "head-down" displays were custom-designed for the SAIFE campaign, providing a "birdie" visual tracking cue, the compensator being used, and an ON/OFF flag for rate limit activity.

Figure 7.4: ATTAS Ground Simulator, DLR Website

The initial objective of the ground simulations was to test the software developed for the AW compensators and to ensure that it functioned harmoniously with the existing ATTAS systems. In this aspect the ground tests were useful as the flight-simulator at DLR features an exact copy of the flight control hardware used on the real ATTAS aircraft. Thus satisfactory functionality of the in-flight software could confidently be predicted through ground test.

The second important objective of the ground tests was to provide a preliminary assessment of the anti-windup designs which were obtained through desktop nonlinear simulation. Ground simulation allowed pilot feedback to be obtained and compensators were sometimes re-designed on this basis. Although it was found that the compensators designed using nonlinear simulation were fairly good when tested in the ground simulator, several changes to the flight test campaign were made due to the discoveries made at this stage. The most noteworthy ones are described below.

- The first ground-based tests consisted of "informal" flying in the simulator, viz, no testing of specific manoeuvres but general "flying" of the aircraft in the simulator. For these first few tests, the main pilot pitch and roll inceptor consisted of a heavy yoke (somewhat like a steering wheel which could be pushed forward) which had the characteristics of a highly damped mechanical filter. This effectively added a feed-forward "command shaping" filter to the pilot reference input which prevented the pilot from applying aggressive commands

which could cause severe rate-saturation. In fact, this type of inceptor degraded the linear performance of the aircraft and prevented rate-saturation meaning that the anti-windup compensators never became active. The yoke was then replaced with a passive side-stick (which resembles a "joystick"), allowing the pilots to be more aggressive in their reference commands with reduced workload. This allowed ATTAS manoeuvrability to be more fully exploited and, as no command filtering was present, more rate-saturation was likely to to occur. This uncovered issues that where key to the redesign of the AW compensator and the flight test itself.

- After a few hours of informal flying plus about an hour of formal testing of various manoeuvres it became clear that another change was required for in-flight testing: the reduced rate-constraints were removed from the elevators and it was decided not to test the longitudinal axis in flight. There were several practical reasons for this. Firstly, it was observed that, in order to induce any noticeable degradation of the longitudinal axis, the pilot had to make high pitch angle acquisition manoeuvres, making the aircraft drift rapidly from its trim value. In fact, when the rate-limits were significantly excited, inevitably the system would operate far from its trim value most of the time. This was an issue partly because the AW compensators were designed around a specific trim point, and thus testing far from it would possibly yield unpredictable results, but also because the structural constraints of the aircraft would make the required manouevres difficult to perform in flight. The second reason for excluding the longitudinal axis from flight testing is that the baseline RACOSS controller did not behave as well in the pitch axis and produced reasonably large overshoots, making the recovery of linear performance not entirely desirable.

- The standard baseline (RACOSS) controller for ATTAS' pitch and roll axes has both a rate-command and an attitude hold part. During non-zero stick displacement, the rate-command portion of the controller is active, but when the stick is centred an additional attitude hold (AH) element is also added to the control law. The AH part of the control law was crudely designed and after several hours of ground-based simulation it was noted that there appeared to be no clear advantages of including the AH portion of the controller. Thus the AH element was removed from the RACOSS controller, making the baseline linear controller simply a rate-command type controller. This had the beneficial side effect of reducing the RACOSS controller to a simple gain matrix, which simplified later analysis.

- Section 6.7 and the discussion therein mildly explored the robustness of AW compensators to changes in flight condition. Robustness was not methodically treated for the RLAW problem, but from nonlinear ATTAS desktop simulation and the results of section 4.3, it was expected that a *robust* compensator could be designed and implemented for all FC's. In simulations this appeared to be true, with improved performance being observed across the flight envelope with an AW controller designed at FC 4. However, ground-based tests revealed that the effects of deviating from flight condition appeared to be somewhat more severe than initially thought, and the approach of "one *robust* AW compensator" for the whole of the flight envelope was replaced by the idea of designing a dedicated AW compensator for each flight condition. This posed no computational problems for the on-board computers but required the design of a switching strategy which could select between eight (including the "no AW" case) different AW compensators (see table 7.2). The appropriate compensator had to be switched "in" at a given FC by the flight test engineer in synchronicity with the pilot.

In addition to allowing the various practical issues identified above to be addressed, the ground tests also gave an opportunity to re-design the AW compensators based on pilot comments as well as simulation results. This was particularly important for the SAIFE tests as the pilot is such an important factor in PIO behaviour; it is nearly impossible to replicate human behaviour in a desktop simulation environment. Designing for systems where humans interface with the control strategy is fundamentally complex as it implies addressing issues such as workload and perception, given to us in the form of pilot ratings, and are generally not easy to abstract. The initial designs were lacking this "pilot feedback" and hence, re-designs based on pilot comments were considered prudent. Moreover, during the ground simulations, a few unexpected problems emerged, some of which were solved by retuning the compensator.

The most noticeable, negative comment which was initially made by the pilots was with regard to the aircraft's increased sluggishness when AW was added. This was due to an over cautious conditioning scheme that retained stability for a large set of signals at the expense of degrading the small signal performance of the overall system. Although some improvement was noticed (as commented by the pilots the system was more predictable) it was probably not worth using AW compensation if such a high amount of performance had to be sacrificed. In other words PIO-"resistance" was obtained at the price of sluggish performance.

As mentioned before, the system's performance is strongly related to the value of the parameter ρ, where lager values render better system performance. Initially it was thought that having

a large sector bound, i.e. $\epsilon = 0.998$, would give large regions of attraction and acceptable performance levels. A restriction present throughout is that of the sampling rate, which in this case is set to $0.03sec$, and which in turn restricts the size of the compensator's poles and consequently the achievable performance levels. The issue of acceptable performance levels was addressed and the following steps where taken: (i) the size of the sector bound was reduced by reducing the size of ϵ, (ii) the size of ρ was increased as to enhance local performance of the closed-loop compensated system; this reduced the allowed set of plant states such that $d \in \mathcal{S}(d, d_0)$, reduced the size of the system's poles, and allowed lower $\mathcal{L}_2$ gains to be obtained. In general, choosing a smaller sector bound relaxes the limitations imposed on the allowed small-signal $\mathcal{L}_2$ gain by compromising stability; our system is guaranteed stable within a smaller region of attraction but can achieve better local performance levels (measured as the size of a predefined $\mathcal{L}_2$ induced gain, i.e. $\|\mathcal{T}_p\|_{i,2,\mathcal{W}}$ in Definition 5.3). It is important to highlight that the restriction on the size of ρ comes mainly from the constraints imposed on the sampling rate of the ATTAS on-board computational system. Another source of restriction is having unstable plant dynamics.

Pilot comments enabled an understanding of certain characteristics that were desirable and allowed re-design based on a more *realistic* pilot-plus-aircraft system than was possible in desktop simulation. Some of these comments were not entirely in agreement with conventional control engineering wisdom. In particular, the initial design strategy was to keep overshoot as small as possible and to maintain damping and stability for as large a possible region. The pilots observed that the reduction in overshoot implied a reduced rise time, which in turn translated into a "more sluggish", less responsive system. Thus, with this in mind, the AW compensators were then retuned to retain the aircraft's initial time response as much as possible while still reducing the level of rate saturation and increasing the region of guaranteed performance and stability. The final parameters used for the AW compensators are shown in Table 7.2.

7.3 Flight Plan

It was mentioned in Chapter 6 that nine different flight conditions were used as potential design and test points for the AW compensators. However, during the ground tests it became clear that time would prevent testing at all flight conditions. This was partly due to the time required to re-trim the aircraft at diverse flight conditions and also due to fuel limitations which would require the aircraft to re-fuel before certain conditions were attained; in conclusion, re-trimming is a time consuming process which restricts the allowable test points.

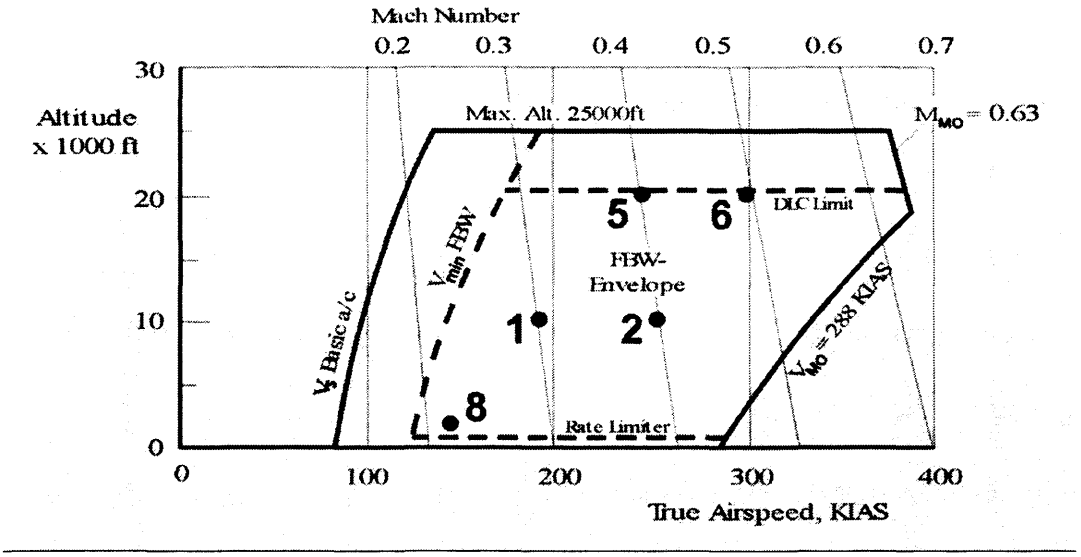

Figure 7.5: Flight Test Trim Points

Therefore, it was decided to select approximately half of the original flight conditions; test points are shown in Figure 7.5. In short, four up-and-away flight conditions, two low speed (FC1 and FC5), two high speed (FC2 and FC6), would be tested; one landing approach would also be included in the experiment (FC8). It should be noted that this flight test plan excludes FC4 which was observed to be one of the most troublesome flight conditions in simulation. Unfortunately this flight condition was located on the edge of the fly-by-wire flight envelope and therefore was considered too risky to assess in real flight. While the flight conditions indicated in Figure 7.5 are obviously a proper subset of those tested in simulation, they do represent a wide range of flying conditions, providing information that can later be extrapolated to other points in the envelope.

As PIO susceptibility is highly dependent of the "type" of pilot, two experimental test pilots from the German Air Force where assigned to the SAIFE campaign. These pilots were both experienced test pilots (actually involved in the Eurofighter programme) with a wide range of flying experience but with no knowledge about the VFW-14 aircraft on which ATTAS is based. Prior to in-flight testing they were familiarised with the aircraft handling and controls in the ATTAS simulator. It was thought advantageous to use very experienced pilots without an intimate knowledge of the ATTAS aircraft so that pilot ratings would not be biased by the "inverse model" which pilots may obtain after flying with a certain aircraft for long periods of time.

Both pilots had very different flying strategies, which must not be confused with experience. Pilot I was known to be a *high gain* pilot while Pilot II was know to be a *low gain* pilot. This differing approach was believed to be appropriate as it would give a more balanced representation of the AW compensators' performance and would allow a comparison of both flying strategies.

AW compensation schemes where designed for each specific flight condition; all compensators were mounted in a "rack" and selected via on-board switching. Seven different compensators where designed (as described in section 6.7): one dedicated compensator for each flight condition, with FC 2 and FC 8 having an extra compensator for comparative purposes. Table 7.2 shows the trim point and design parameters ρ and ϵ for each of the AW compensators.

Compensator No.	Flight Condition No.	(ρ)	ϵ
1	1	10^{-7}	0.96
2	2	10^{-6}	0.96
3	2	10^{-5}	0.96
5	5	10^{-7}	0.96
6	6	10^{-7}	0.96
8	8	10^{-8}	0.96
9	8	10^{-6}	0.96

Table 7.2: AW compensation parameters

A fixed ϵ equal to 0.96 was chosen as it is thought to give a sufficiently large sector condition; the existing trade-off is then captured exclusively by ρ. The compromise between large ROA and closed-loop system performance was observed both in desktop and ground based simulations, and therefore, the parameter ρ must guarantee large stability regions without sacrificing too much system performance. Compensation focused on enlarging the system's region of attraction; this implied choosing ρ as small as possible. For FC2 and FC8 an extra compensator was designed, where ρ was increased as to improve closed-loop performance, but at the expense of decreasing the size of the estimate of the region of attraction [1].

Pilot induced oscillations can cause catastrophic behaviour in aircraft and thus, to guarantee the safe operation of the aircraft and to ensure that these potentially hazardous situations are

[1]Note that only the size of the estimate is reduced; the *actual* region of attraction may stay unchanged

approached safely, it was imperative that PIO situations were approached methodically and safely. Thus the following build-up approach was used at all flight conditions by both pilots.

1. Low Bandwidth Testing
2. High Bandwidth Testing
3. Operational Testing

This was also believed to be advantageous because the very nature of the flight tests was to induce unnatural aircraft behaviour and so, some caution was necessary. The different phases of testing are described below

- *Low Bandwidth Testing* consists of semi closed-loop and closed-loop bank angle capture tasks. This enables the pilot to a have a "feel" for the system and become familiar with ATTAS dynamics. This gives the pilot a general notion of how the system behaves under relatively simple roll commands; this stage may also be referred to as *warm-up* testing.
- *High Bandwidth Testing* employs HQDT (Handling Qualities During Tracking) test techniques, which currently is the only method that allows for systematic, high bandwidth PIO resistance testing, and is therefore sometimes also referred to as handling qualities stress testing. When the pilot is required to perform a tracking task, i.e. an error signal prompts the pilot to close the control loop, he will adopt by nature a low gain flying technique consistent with satisfactory task performance. Interestingly, when pilots experience stress, anxiety or fear they will assume a high gain control strategy which may excite rate-limits quite considerably.

  The aim of HQDT testing is to artificially increase pilot bandwidth, i.e. the frequency and amplitude content, by requiring the pilot to track a point as aggressively and rapidly as possible, correcting even the smallest tracking error. The test is also setup in a build-up approach where initially the pilot is required to track small amplitude and low frequency inputs, progressing to higher frequencies and amplitudes up to the point where the pilot reaches a "bang-bang" control strategy; the pilot behaves like a switching function, reversing the control input as soon as the error signal changes sign. The degree to which an aircraft withstands such violent inputs is quantified using PIO Ratings (PIOR's).

  During the SAIFE campaign the pilot was asked to apply HQDT while capturing a wings level roll attitude from an initial 30 degree offset using the roll attitude indicator in the main head down display (MHDD) as reference.

- *Operational Testing* tries to uncover PIO tendencies in routine tasks such as offset landings and tracking of certain visual cues.

  - The *"Birdie"* Target Tracking Task was used at up-and-away flight conditions and requires the pilot to closely track a generic birdie (aircraft symbol) projected onto the ATTAS head-down-display (HDD) with an aircraft water line symbol. The tracking reference is made up of a set of ramps and steps that are believed to excite the rate-limits and expose PIO tendencies. Once the task has concluded, the pilot gives HQR's for gross acquisition and fine tracking, and PIO ratings for the "birdie" task. Display latency was found to be no factor during the assessment. Figure 7.6 shows the pilot's HDD during a birdie tracking task and also depicts the roll trajectory of the birdie. For each birdie task performed the pilot rated the handling qualities and PIO tendencies of the aircraft.

  - The *Offset Landing Approaches* were conducted at the Schwerin-Parchim airfield, shown in Figure 7.7. For these landing approaches, the aircraft was reconfigured with flaps set to 14 degrees and landing gear extended. As this was considered a demanding task, the rate-limits were increased from 50 % of their nominal values to 60 %, although the pilots still remarked upon the sluggishness of the aircraft dynamics. For this task, the pilots where asked to capture centreline on the active runway from an initial 200 meter lateral offset from the nominal approach path; focus was placed on the centreline capture task. Two different AW compensator designs where tested for this approach/landing task enabling a comparison of performance levels through pilot comments, HQR's, and PIOR's.

To assist and prepare the pilots for flight test, and for reference in-flight, each pilot was given a set of flight test cards which described the sequence of tests to be carried out at each manoeuvre. Table 7.3 gives a summary of the chronological development of the test.

7.4 Flight Test Results

The SAIFE campaign culminated in 6 hours of flight tests which were carried out in two sessions in a single day. As mentioned earlier, each pilot evaluated various manoeuvres in the ATTAS aircraft at all five of the test conditions. At every test condition the aircraft was flown both with and without AW compensation engaged. The improvement in flying qualities was assessed using pilot "questionnaires" in which the pilots assigned ratings for certain manoeuvres and

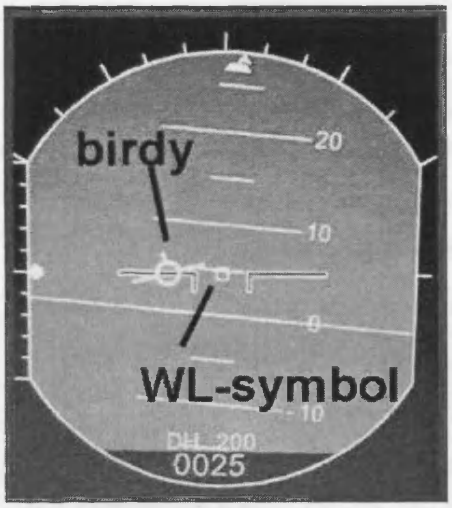

Generic tracking task in MHDD

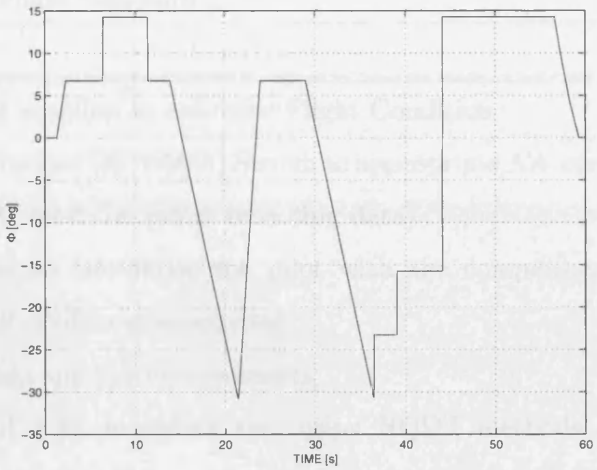

Generic tracking task reference signal

Figure 7.6: Birdie Tracking Task

Figure 7.7: Schwerin-Parchim airfield

made comments on the general feel of the aircraft or any specific incidents; data was also logged for each test point, allowing the assessment of performance improvements, if any, via time data. Thus the results can be divided into two categories: those due to pilot ratings and comments, and the time domain data collected.

7.4.1 Pilot evaluation

As mentioned earlier, at each flight condition the two pilots evaluated a series of tasks. At the up-and-away flight conditions (flight conditions 1,2,5 and 6) these tasks were based on the HQDT technique for bank-angle capture and "birdie" tracking task; for flight condition 8, the

Flight Test card	
STEP No.	
1	Check trim values and stabilise at reference Flight Condition
2	Activate rate-limit reduction (60%-50%),Switch to appropriate AW compensator and turn SIM mode on (start recording data)
3	General discrete tasks to familiarise the pilot with the compensator (bank-to-bank and roll doublet manoeuvres)
4	Recapture FC and make qualitative comments
5	From a bank angle of ± 30, recapture zero using HQDT methods at different levels
6	Re-establish Initial Conditions and give PIO ratings
7	Start "Birdie" task
8	Track visual reference signal in the roll axis until sequence terminates
9	Provide HQR for gross acquisition and fine tracking. Give a general PIO rating for the "birdie "task
10	Turn SIM mode off

Table 7.3: Flight Test Card - overview of the flight plan

pilot was required to perform an offset-landing approach. Again, each pilot performed the same manoeuvres using the degraded rate-limits both with and without AW compensation. For each manoeuvre, the pilots assigned PIO-ratings (measured on the PIO Rating scale [49, 29]) and/or handling qualities ratings (HQR's) based on the standard MIL specifications (as described in [1, 29]). Although a full discussion of these ratings is somewhat beyond the scope of the thesis, for both of these scales lower ratings are better: an aircraft with low PIO and HQR ratings is considered less prone to PIO and to have better handling qualities.

The results for the up-and-away flight conditions are tabulated in Table 7.5 and the results for the offset landing approach are given in Table 7.6. The notation "w/l" indicates that the rating given was due to the workload involved and "n/a" indicates that this rating was not applicable or was not assigned. The key tasks which were rated are summarised in Table 7.4.

From the ratings in the tables it can be inferred - at least as far as PIO ratings and HQR's were concerned - that the presence of AW *did not degrade the aircraft's* performance at any flight condition. For up-and-away flight conditions it appears that, at lower speeds (flight conditions 1 and 5), both pilots found that AW compensation typically bestowed some minor improvement

PIO-c	PIO rating: bank angle capture
HQR-g	HQR: gross acquisition, birdie
HQR-f	HQR: fine tracking, birdie
PIO-b	PIO rating: birdie
HQR-cl	HQR: centreline capture
HQR-t	HQR: touch-down zone
PIO-t	PIO rating: touch-down zone

Table 7.4: Key to HQR/PIO ratings

in aircraft performance. Pilot I (the high gain pilot) gave PIO and HQR ratings which were roughly the same for the aircraft both with and without AW compensation engaged. At FC1 he noted that the gross acquisition of the aircraft with the AW compensator engaged was slightly better than without but otherwise the ratings were identical for FC1 and FC5.

Pilot II (the low gain pilot) seemed to find minor improvements in the low speed behaviour of the aircraft with AW engaged. Although the PIO ratings and HQR's he awarded at FC1 and FC5 were not vastly different comparatively, one can detect frequent instances where either the PIO susceptibility or handling qualities were improved when AW was used. For example at FC5 the pilot awarded an HQR of 7, corresponding to Level 3 flying qualities, for gross acquisition in the birdie task. When the AW compensator was switched in, the HQR fell to 5, corresponding to Level 2 flying qualities, which is a significant improvement.

For the up-and-away flight conditions it seemed that most performance improvement was observed at high speeds (flight conditions 2 and 6). At these flight conditions significant improvements were detected by both pilots. For instance at FC 2, both pilots gave a birdie tracking PIO rating of 4 with no AW; this dropped to a 2 with AW Compensator 3. In fact, at FC 2 AW compensator 3 improved HQR and PIO ratings in all cases. A similar story can be observed at FC6 where AW compensator 6 improved HQR and PIO ratings in all cases except for the PIO rating for the "birdie" task where no PIO rating was assigned when AW was not engaged. One remarkable feature of the flight tests was that improvements were noticed not only on the PIO ratings; the HQR ratings improved as-well.

It is more difficult to interpret the results for the offset landing approach shown in Table 7.6. The presence of AW does, on average, seem to bestow some performance improvement on the aircraft, particularly in the centerline capture task. In this task Pilot II actually awarded the AW compensator an HQR rating of 3 (Level 1 flying qualities) whereas when AW was not

used, this degraded to an HQR of 6 (which is borderline Level 3). However, it must also be noted that several entries in this table were not completed due to the extreme difficulty of this manoeuvre. During the execution of this task, which is considered difficult in the ATTAS aircraft, strong cross-winds were encountered near the airfield, thereby increasing the difficulty even further. Thus, in some cases, the pilot had to either abandon the manoeuvre before its completion, or it was completed with inadequate accuracy preventing the award of an HQR or PIO rating. In addition it must be mentioned that Pilot II did encounter a PIO in the final stages of the landing approach with AW compensator 8 engaged. Although this task was repeated and no PIO occurred, it is not clear why this was the case, although again the difficult weather conditions could be the cause. This is currently the subject of further investigation.

FC No.	Compensator	Pilot 1 (high-gain)				Pilot 2 (low-gain)				Improvement	
		PIO-c	HQR-g	HQR-f	PIO-b	PIO-c	HQR-g	HQR-f	PIO-b	Pilot 1	Pilot 2
1	none	4	6	5	3	4	6	5	4	n/a	n/a
1	1	4	5	5	3	3	5	5	3	slight	minor
2	none	5	6	5	4	4	6	5	4	n/a	n/a
2	2	4	5-6	5(w/l)	3	2	5	4	4	minor	major
2	3	3(good)	5 (w/l)	4	2	2	5(w/l)	4	2	major	major
5	none	5(good)	7	6	5	4	7(w/l)	6	4	n/a	n/a
5	5	5	7	6	5	4	5	5	4	none	minor
6	none	5	6	5	n/a	5	6(w/l)	5	4	n/a	n/a
6	6	3	5 (w/l)	4	3	3	5	4 (w/l)	2	major	major

Table 7.5: Up and away flight conditions

Flight Condition No.	Compensator	Pilot 1 (Q)			Pilot 2 (Markus)			Improvement	
		HQR-cl	HQR-t	PIO-t	HQR-cl	HQR-t	PIO-t	Pilot 1 (high gain)	Pilot 2 (low gain)
8	none	5	6	4	6	n/a	n/a	n/a	n/a
8	8	4	5	3	4	n/a	5	some*	some*
8	9	4	6	4	3	3	n/a	slight*	major*

Table 7.6: Landing approach flight conditions

7.4.2 Time Domain Analysis

Flight test data was gathered for all tasks which were performed and, in total amounted to several hundred megabytes. In this section, certain portions of this flight test data will be presented and analysed. For the up-and-away flight conditions, data is presented for the birdie tracking task only, as this allows the aircraft bank angle to be plotted against the true reference - "the birdie" - which the pilot was attempting to follow. Data collected from the HQDT task is more difficult to analyse as the manner in which the pilot performs it is very dependent on his/her own perception of the bank angle tracking and PIO's can be easily avoided by the pilot lowering his/her gain; the main value of this task is in the ratings which were discussed earlier.

Flight test data is presented for high-speed flight conditions (FC 2 and FC 6), for one low speed flight condition (FC5), and for the landing approach FC8. It is believed that this data gives a complete overview of the data obtained during flight.

When assessing the data it is important to be aware that there is a human element that needs to be taken into account. When pilots first fly an aircraft, they are still adapting to its environment and the capabilities of the vehicle and may, initially, give biased ratings. With time, pilots may become more familiar with the aircraft and confuse this with actual controller action. The tests were spread out in time such that there is some assurance that the *learning factor* will not play such a large role in the pilot's appreciation of the aircraft's manoeuvrability.

Figures 7.8 - 7.13 show experimental time histories for the birdie tracking tasks for the high gain pilot (Pilot I) and the low gain pilot (Pilot II). Time histories are shown with and without AW compensation. The signals shown are roll angle ϕ, pilot stick command, control signal demand$u$ and rate-limited control signal u_r. Although the task is very demanding and generally the steps are not long enough as to analyse the system's characteristics classically, the plots give a rough indication of the aircraft's performance. The following criteria are of particular interest:

- PIO tendency of the pilot-aircraft loop and how hard is it for the pilot to maintain stability.
- Level of rate-limiting present in the system and how far is the system from linear operation.

Pilot I, FC2 (Figure 7.8): High gain pilots have generally been linked to PIO's and are therefore very useful for test purposes. Initially the system with no AW is considered. The roll angle exhibits some oscillatory behaviour and some high overshoots. There are also instances when

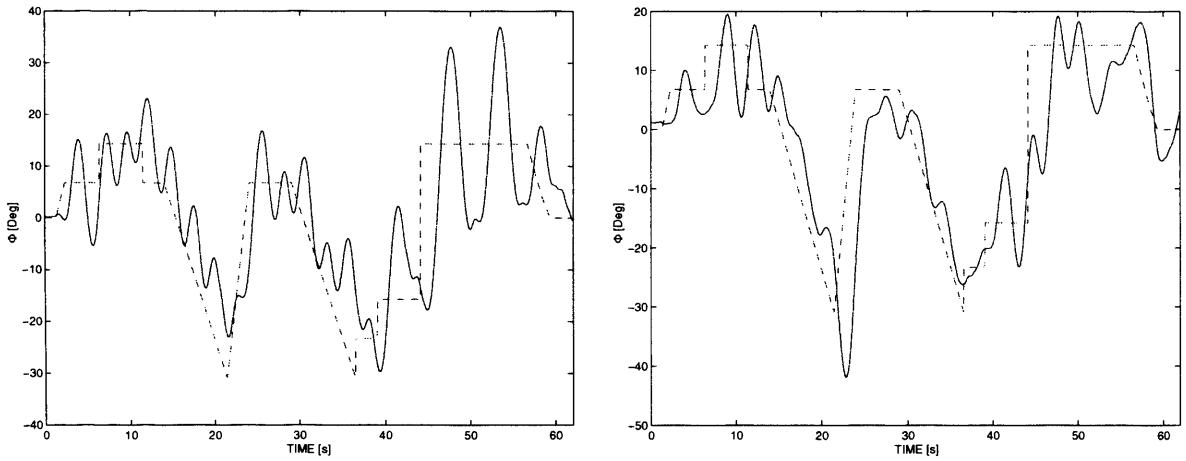

ϕ [Deg], No AW

ϕ [Deg] + AW

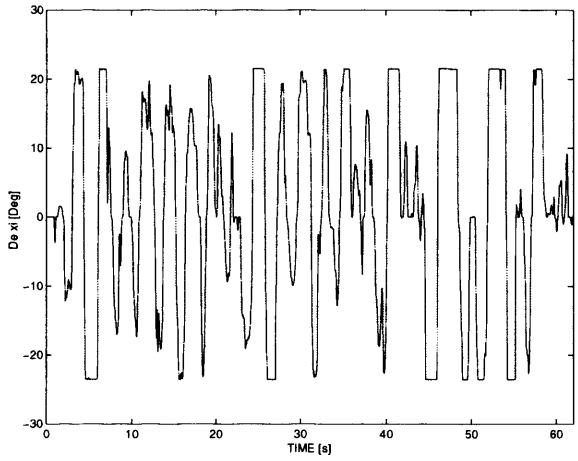

Stick Input Signal [Deg], No AW

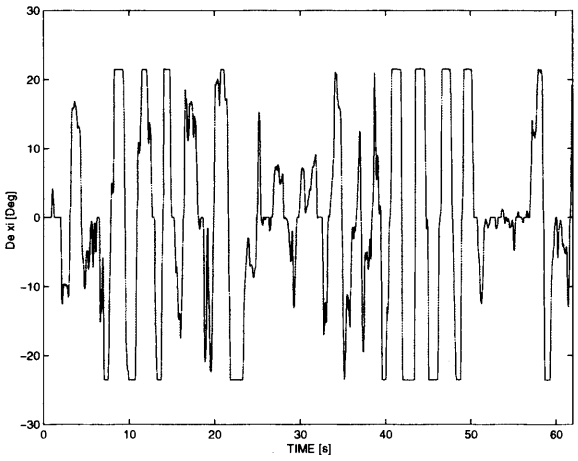

Stick Input signal [Deg] + AW

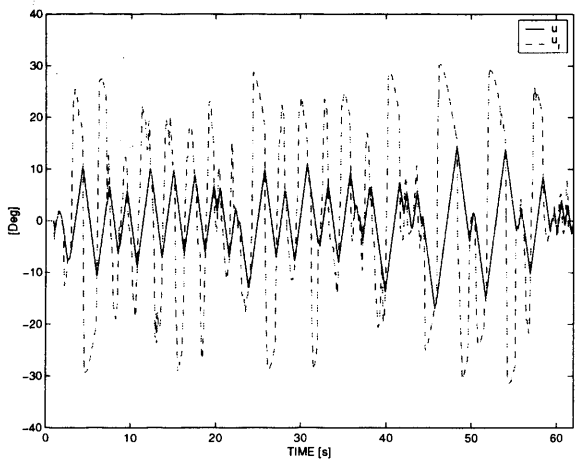

Input d and Output $\bar{d}$ of the RL , No AW

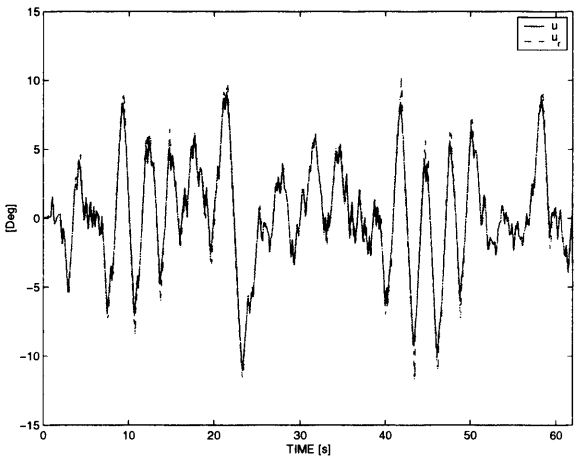

Input d and Output $\bar{d}$ + AW

Figure 7.8: Lateral Tracking Task for Pilot I and FC No. 2 - AW compensation No. 1

it appears that a divergent oscillation may be developing and the pilot is "lowering his gain" to prevent this. Notice that the system has very high levels of rate-limiting and operates outside its linear range most of the time with high levels of control signal phase-shift. Some

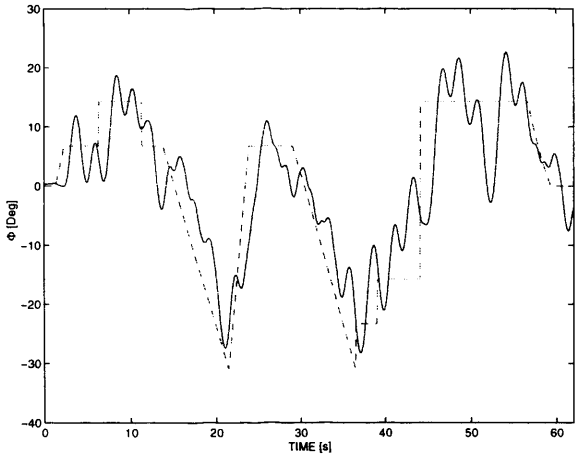

ϕ [Deg], No AW

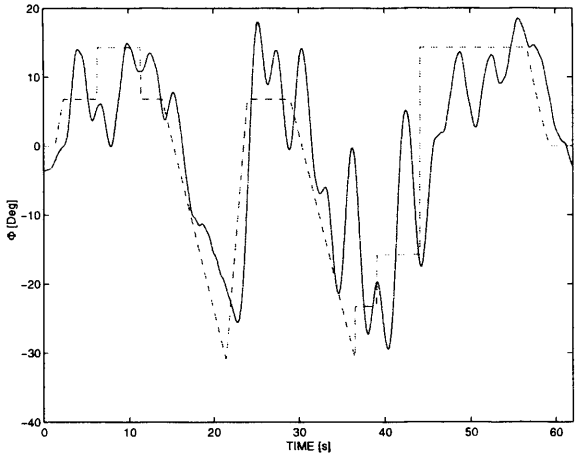

ϕ [Deg] + AW

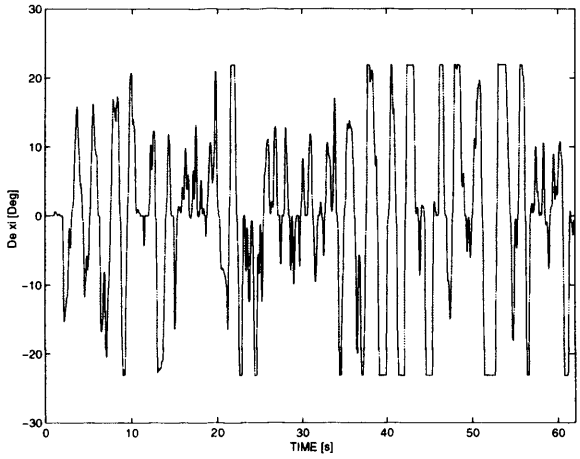

Stick Input Signal [Deg], No AW

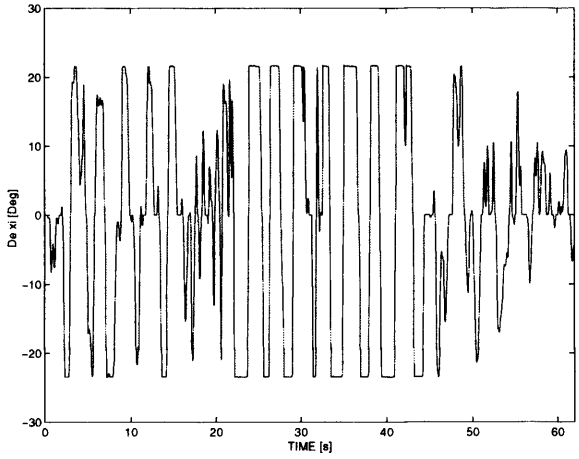

Stick Input signal [Deg] + AW

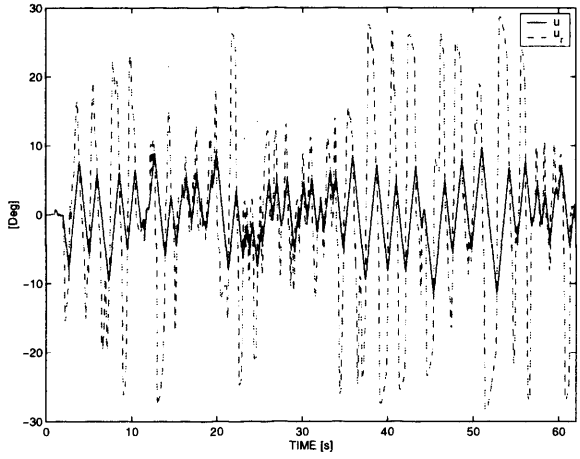

Input d and Output $\bar{d}$ of the RL , No AW

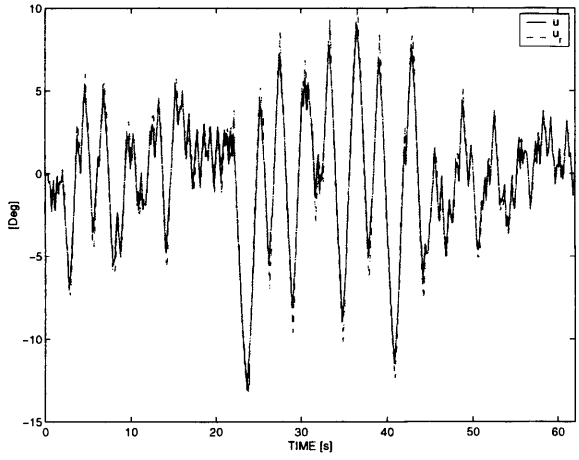

Input d and Output $\bar{d}$ + AW

Figure 7.9: Lateral Tracking Task for Pilot II and FC No. 2 - AW compensation No. 1

improvement in the aircraft behaviour can be observed when using AW compensation, perhaps with finer tracking achievable and slightly less oscillatory behaviour. Note the markedly reduced rate-limiting in the lower graphs, with the rate-limited signal remaining much closer to the

commanded control signal.

Pilot II, FC2 (Figure 7.9): This pilot was inherently lower gain, and less likely to generate PIO events. With no AW compensation, observe that the roll angle has frequent, large overshoots and fine tracking seems poor. Tracking capabilities of the system are deeply affected by rate-limiting; high oscillations develop, especially when the pilot initiates abrupt manoeuvres (i.e. step reference signals). Notice that the pilot uses full stick commands most of the time in order to control the system, increasing the work load and tendency to PIO. In addition, the control signal remains rate-limited for a considerable amount of time and there is a large difference between the commanded and actual control signal (i.e. $\tilde{d}$ is large). When AW is introduced, tracking performance appears to be slightly better and is a little less oscillatory.

Pilot I, FC5 (Figure 7.10): The system with no AW appears to be less PIO prone for this flight condition and performance is not as affected as in the previous data (FC2). The system still exhibits oscillatory behaviour and fine tracking issues. AW compensation does not offer the level of performance enhancement that was expected and time domain data agrees with pilot ratings in that few performance benefits can be observed from looking at the roll angle, ϕ. However, the lower graph does show that rate-saturation is substantially lower when using AW, although it is not clear that this has a major effect on performance. The "failure" of AW to provide much performance improvement can perhaps be attributed to the lack of performance degradation during rate-saturation at FC5; in other words, if deviation from linear dynamics is not detrimental for the closed-loop system, then AW conditioning will probably have little effect on the systems overall performance.

Pilot II,FC5 (Figure 7.11): This time the system with AW seems to have enhanced performance, allowing the pilot to achieve some fine tracking and reduce oscillations considerably. In general, pilot II has been labelled as the low gain pilot, but in this case, Pilot II seems to be slightly more aggressive than Pilot I. This may explain why the benefits of AW compensation may only be noticeable in the time history of Pilot II.

Pilot I, FC6 (Figure 7.12): Again, Pilot I seems to be behaving in quite a conservative manner, not demanding too much from ATTAS. Rate limits are excited less and therefore represent less of a threat for the system. When AW is used, rate saturation levels are, again, reduced but performance in not greatly enhanced. The system exhibits better gross acquisition but more overshoot. It may also be observed that AW compensated system tends to be less PIO prone, (with some slow build oscillatory behaviour observed when the system has no AW).

Pilot II, FC6 (Figure 7.13): This figure perhaps shown the advantages of AW compensation

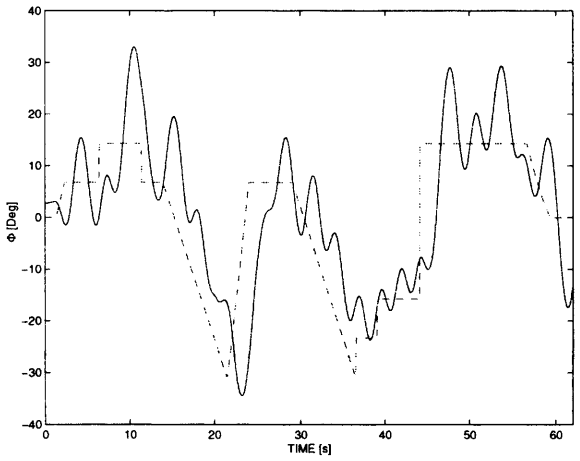

ϕ [Deg], No AW

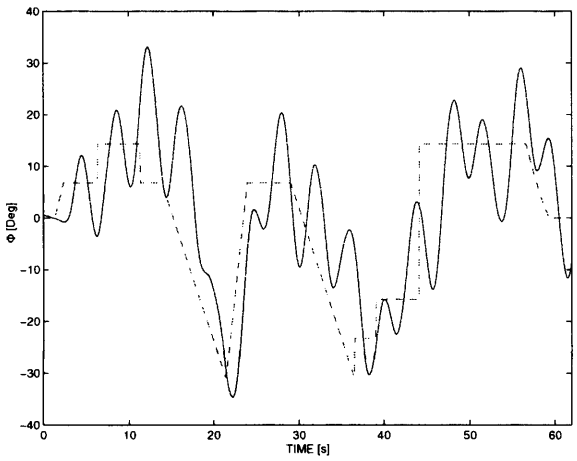

ϕ [Deg] + AW

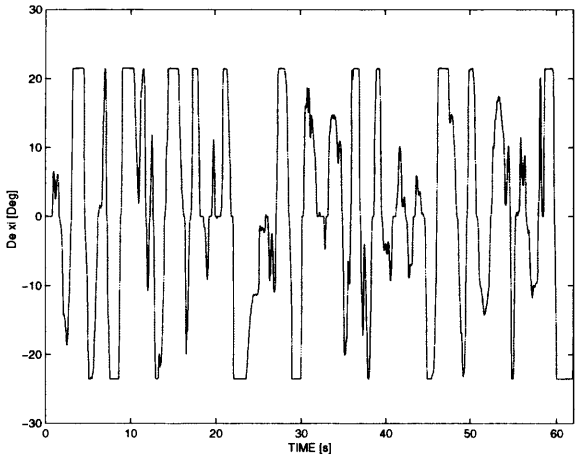

Stick Input Signal [Deg], No AW

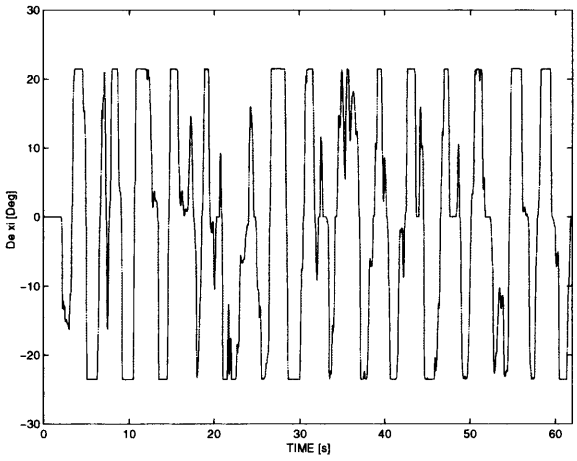

Stick Input signal [Deg] + AW

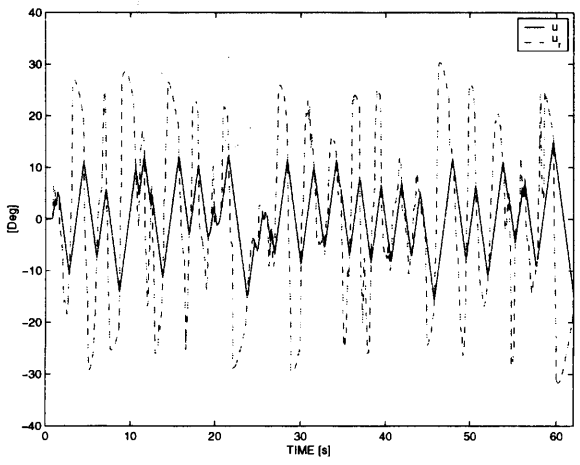

Input d and Output $\bar{d}$ of the RL , No AW

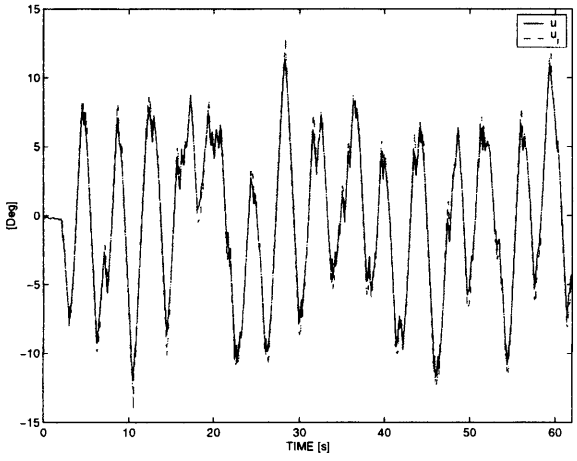

Input d and Output $\bar{d}$ + AW

Figure 7.10: Lateral Tracking Task for Pilot I and FC No. 5 - AW compensation No. 5

most clearly. Without AW compensation the roll attitude response was oscillatory and appeared unpredictable. When AW compensation was introduced, the roll angle had noticeably better tracking properties with overshoot and oscillation dramatically reduced. Although the

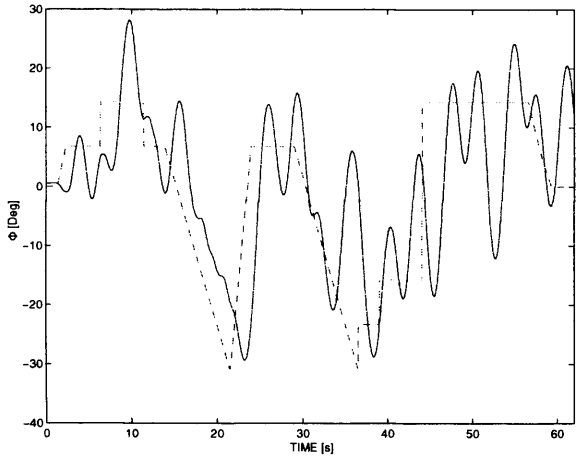

ϕ [Deg], No AW

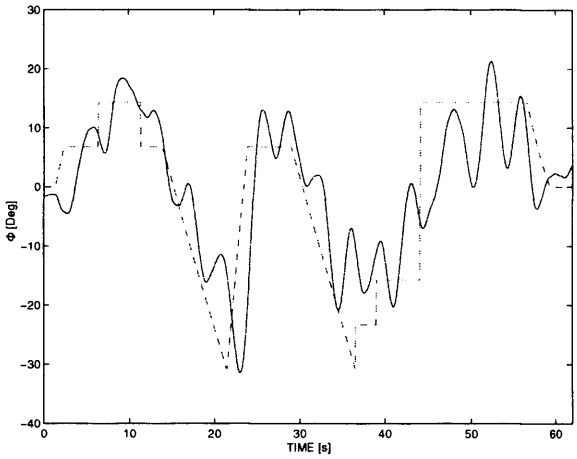

ϕ [Deg] + AW

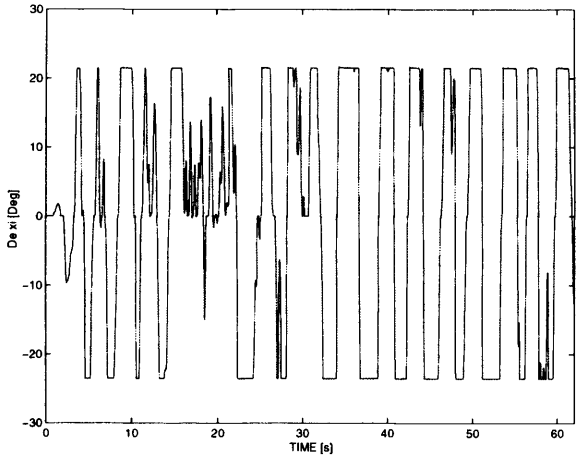

Stick Input Signal [Deg], No AW

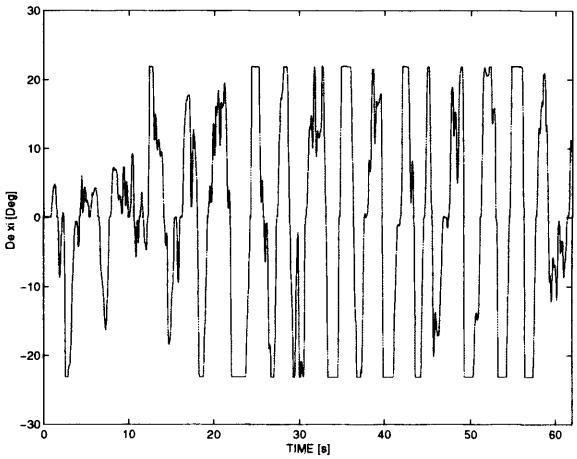

Stick Input signal [Deg] + AW

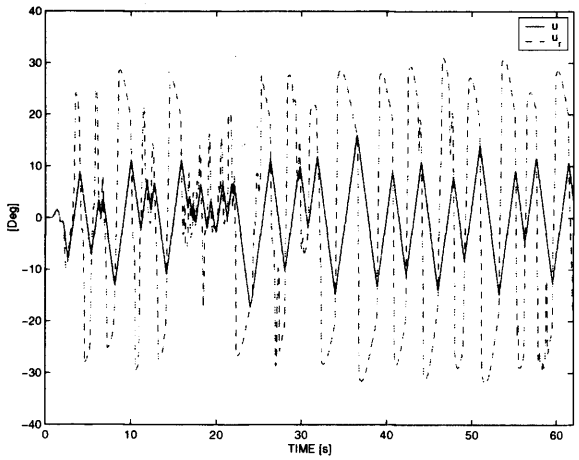

Input d and Output $\bar{d}$ of the RL , No AW

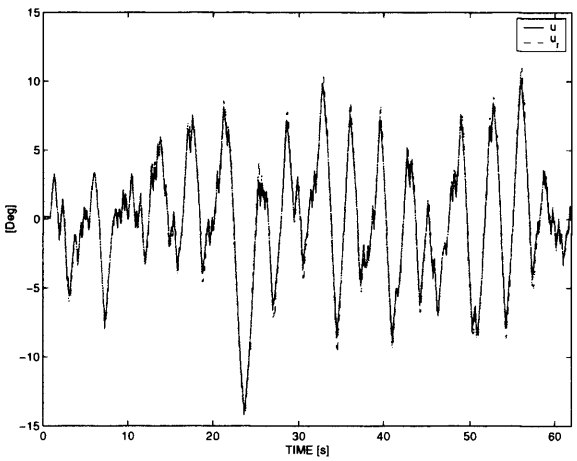

Input d and Output $\bar{d}$ + AW

Figure 7.11: Lateral Tracking Task for Pilot II and FC No. 5 - AW compensation No. 5

aircraft appears to be more sluggish, fine acquisition is possible but with an increase in the workload. It is important to observe that the conditioned control signal is less aggressive, and therefore, the system is outside linear behaviour for shorter periods of time. Pilot stick

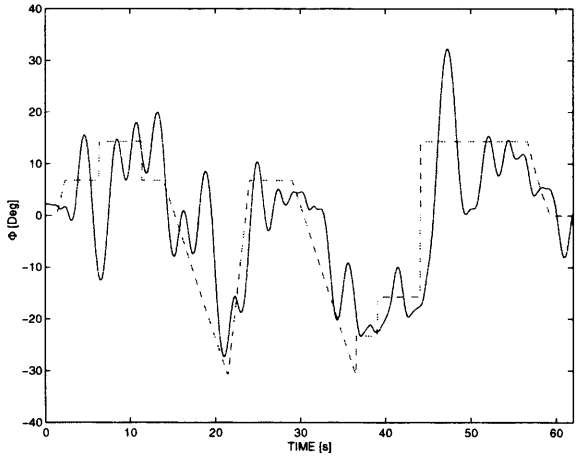

ϕ [Deg], No AW

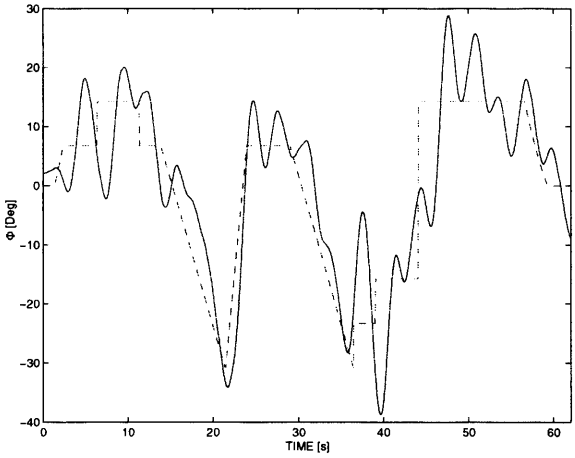

ϕ [Deg] + AW

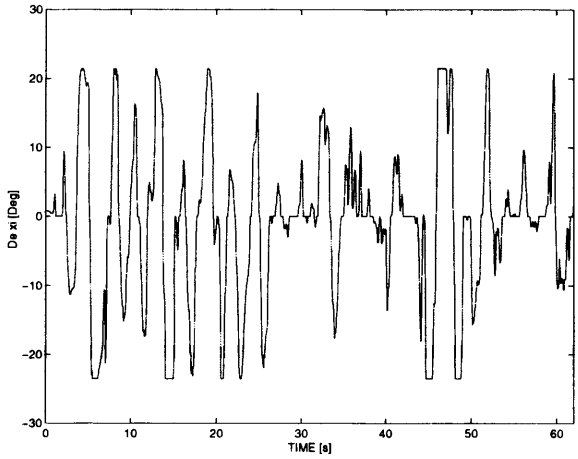

Stick Input Signal [Deg], No AW

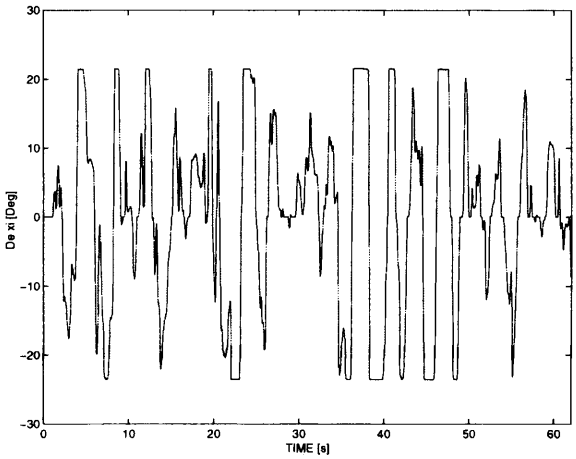

Stick Input signal [Deg] + AW

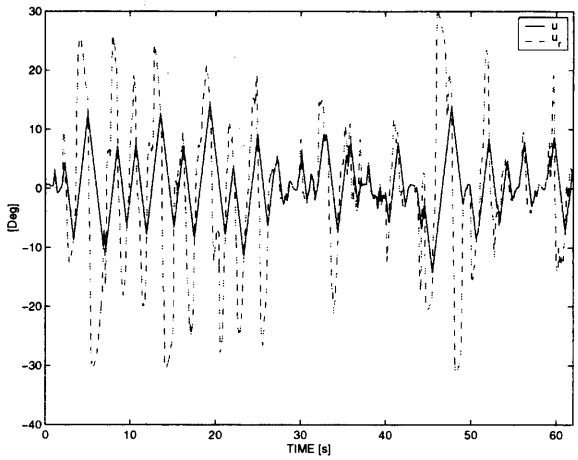

Input d and Output $\bar{d}$ of the RL , No AW

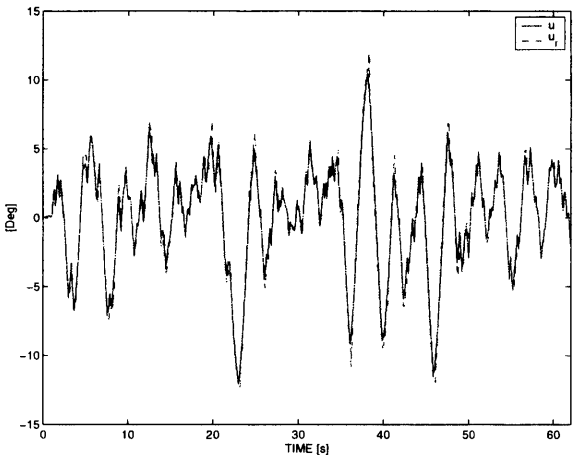

Input d and Output $\bar{d}$ + AW

Figure 7.12: Lateral Tracking Task for Pilot I and FC No. 6 - AW compensation No. 6

commands are reduced and in general, with the exception of fine tracking, the workload is less.

The analysis for up-and-away flight conditions showed great potential, especially for high speed flight conditions, improving pilot ratings in general. Although it is always difficult to corrob-

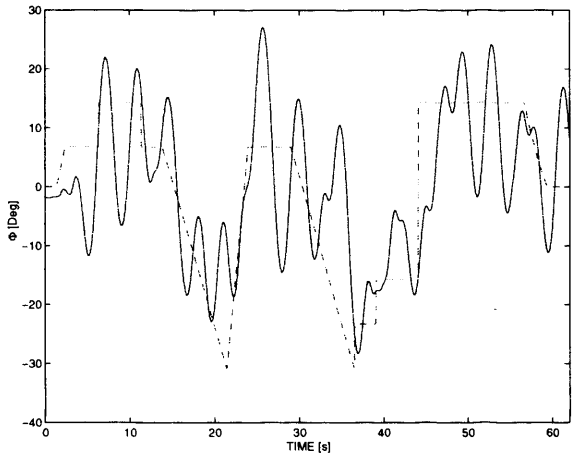

ϕ [Deg], No AW

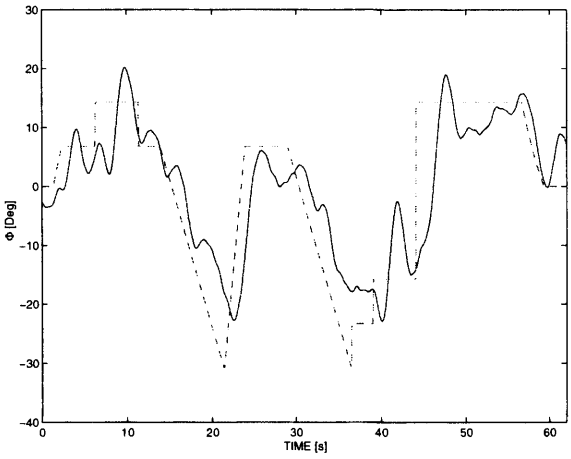

ϕ [Deg] + AW

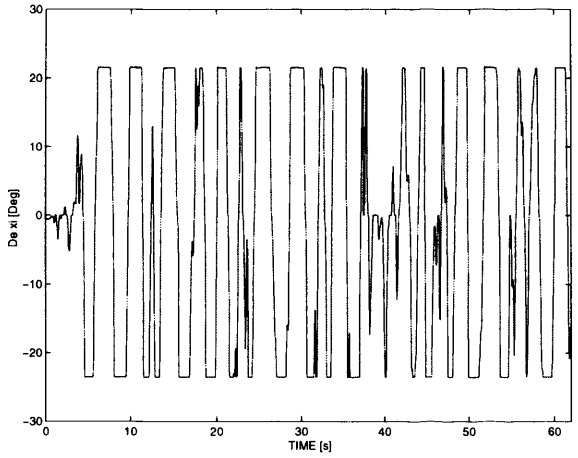

Stick Input Signal [Deg], No AW

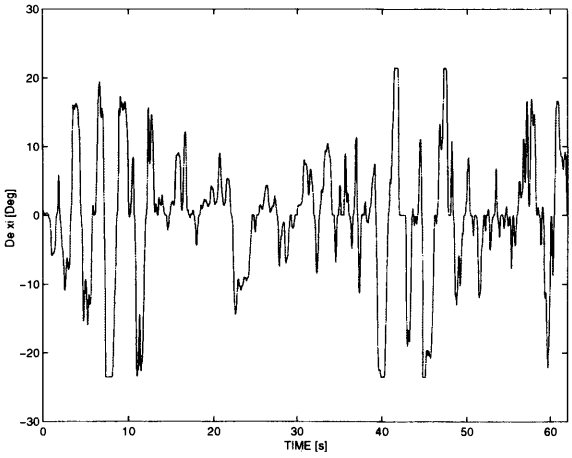

Stick Input signal [Deg] + AW

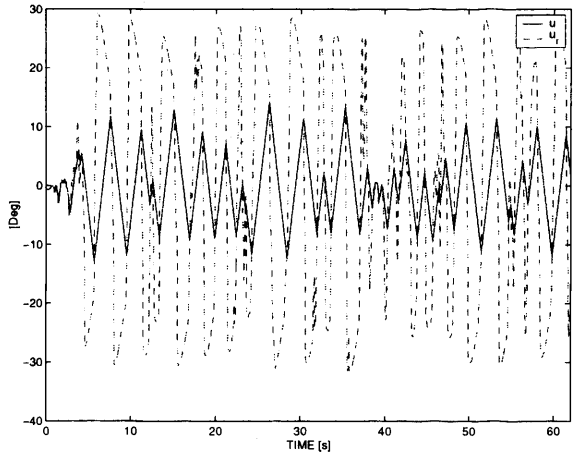

Input d and Output $\bar{d}$ of the RL , No AW

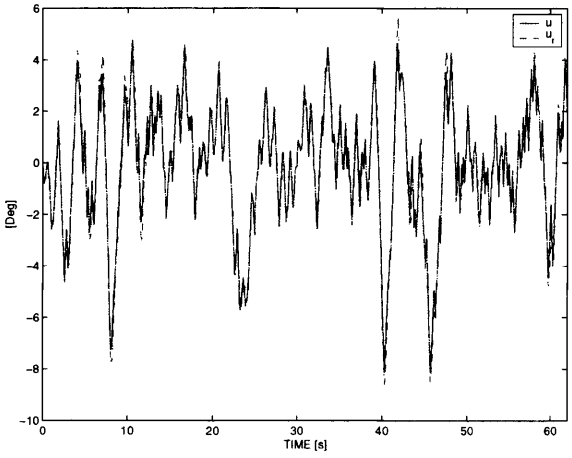

Input d and Output $\bar{d}$ + AW

Figure 7.13: Lateral Tracking Task for Pilot II and FC No. 6 - AW compensation No. 6

orate exactly what the pilot comments with both time histories and pilot ratings, we may say that the three where quite congruent.

Now landing approach FC's will be analysed in a similar way. Note that the landing approach

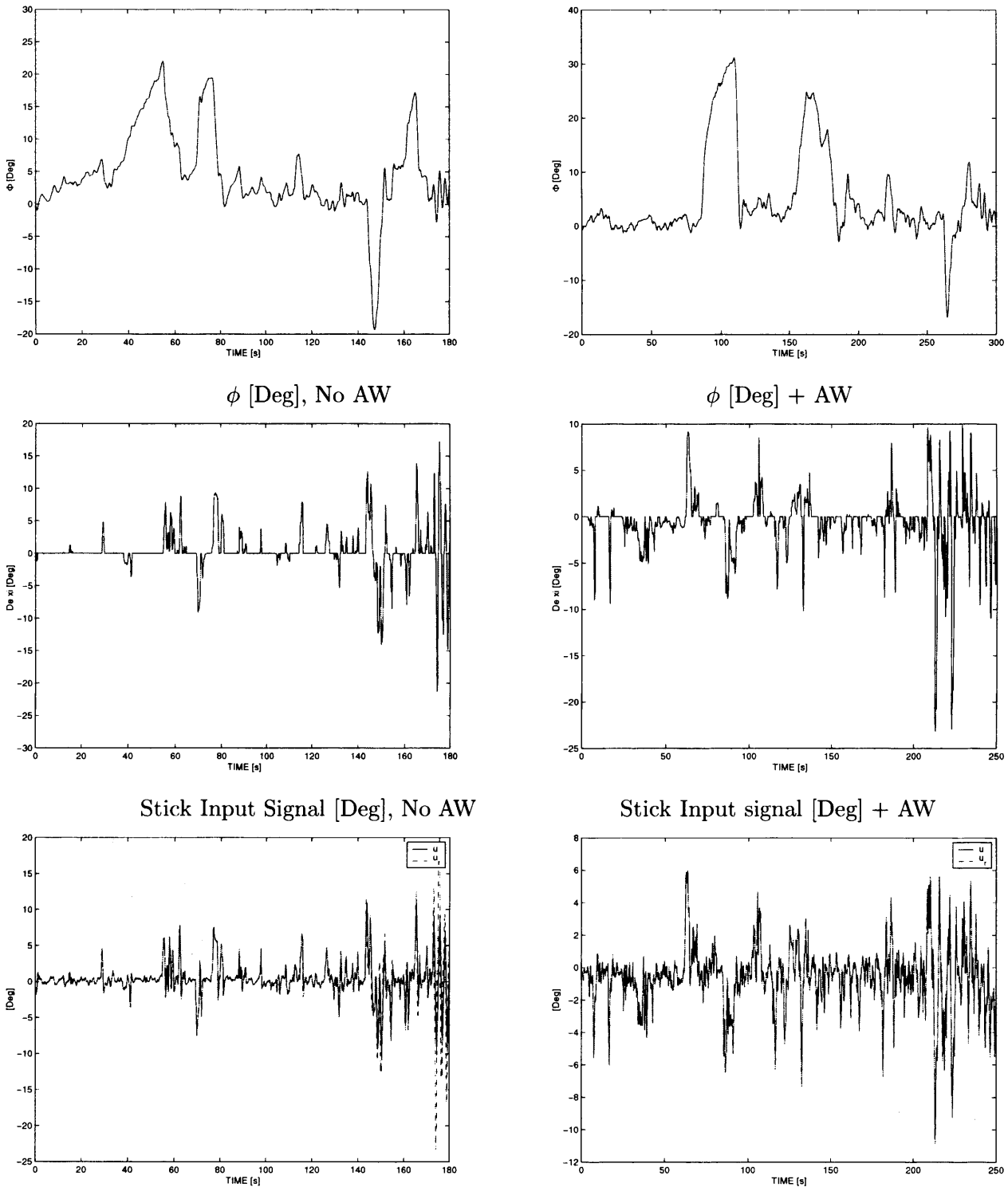

ϕ [Deg], No AW

ϕ [Deg] + AW

Stick Input Signal [Deg], No AW

Stick Input signal [Deg] + AW

Input d and Output $\bar{d}$ of the RL , No AW

Input d and Output $\bar{d}$ + AW

Figure 7.14: Landing Approach task for Pilot I and FC No. 8 - AW compensation No. 9

was considered an extremely demanding manoeuvre by the pilots - for the ATTAS aircraft at least. It is something of a multi-axis manoeuvre too with the pilot exerting a lot of effort in the yaw channel as well as the roll channel. For this and the associated safety issues, the pilots seemed to be less aggressive and therefore a milder rate-limit excitation seemed to cause

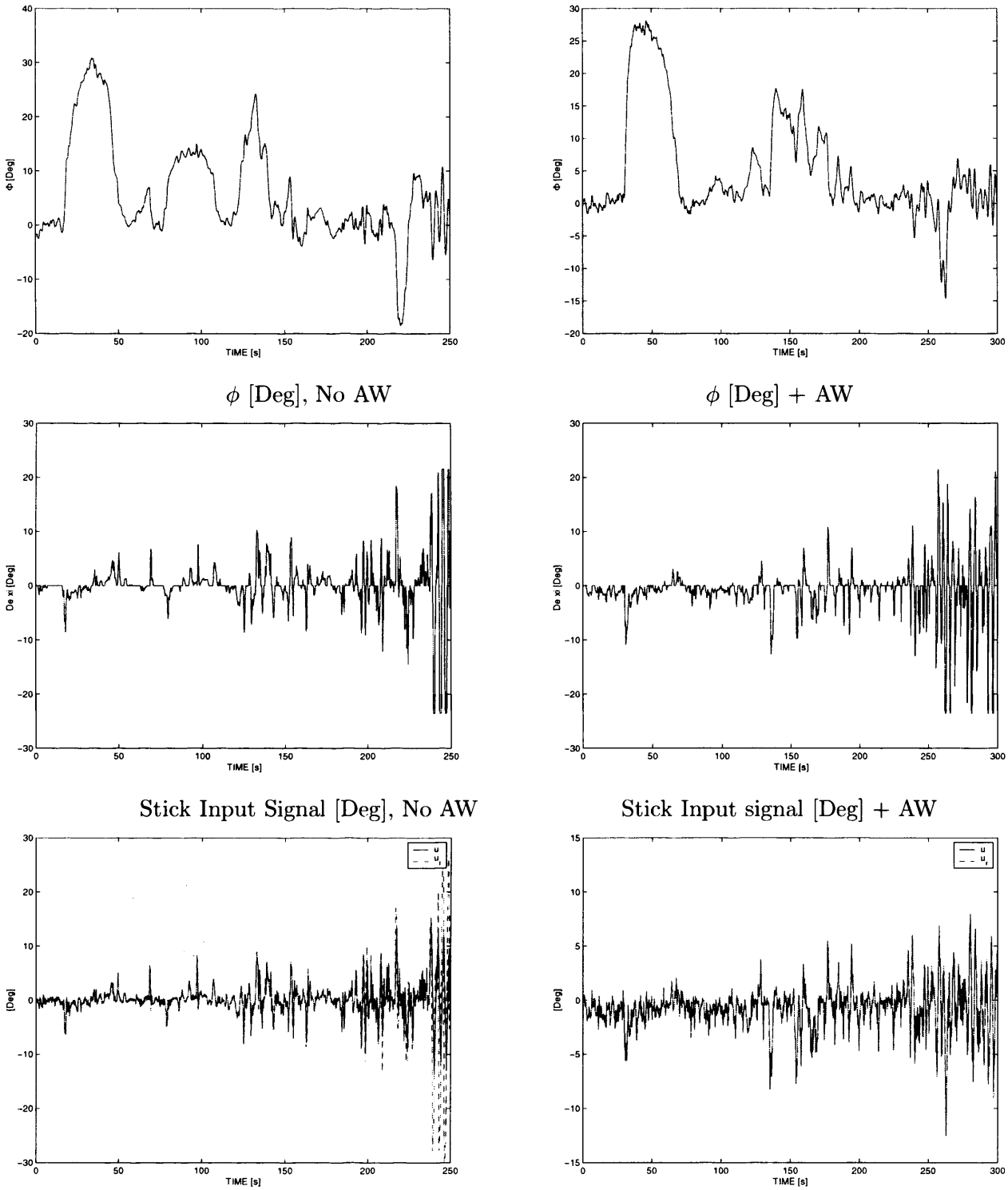

ϕ [Deg], No AW

ϕ [Deg] + AW

Stick Input Signal [Deg], No AW

Stick Input signal [Deg] + AW

Input d and Output $\bar{d}$ of the RL , No AW

Input d and Output $\bar{d}$ + AW

Figure 7.15: Landing Approach Task for Pilot II and FC No. 8 - AW compensation No. 9

sufficient problems. It is also very important to notice that at this particular trim point, the aircraft is more susceptible to outside disturbances such as wind gusts, allowing for extra sources that may trigger a PIO.

Pilot I, FC8 (Figure 7.14): It is possible to observe that centre line capture is slightly easier when using AW compensation. The pilot comments mentioned that the aircraft felt more predictable and had acceptable performance. This is also reflected on the ratings (see Table 7.6) given by the pilot, where HQ and PIO ratings improved. Although most of the time the system appears to be within acceptable limits of linear behaviour, once close to the ground, the pilot seems to enter a state of alert (the pilot is approaching the ground) and the system exhibits higher rate-limiting action. This is reduced when using AW compensation, minimising the risk of PIO occurrences.

Pilot II, FC8 (Figure 7.15): Most of the comments of Pilot I seem to be corroborated by Pilot II; predictability, enhanced fine tracking and less PIO tendencies. This is true for most of the task, but the pilot mentioned that at the end of the task, that instant before touching ground, undesirable dynamics developed and the pilot had to reduce the gain drastically in order to recover. Although the precise nature of these dynamics is still under scrutiny, it may be difficult to target the cause of this "PIO" as factors such as wind and pilot's lack of practice play important roles.

7.4.3 Discussion

The qualitative pilot ratings clearly show the advantage of adding anti-windup compensation for the degraded aircraft with rate-limiting. This seems to be true for all flight conditions, although the advantages of anti-windup are most striking at higher speeds (FC2 and FC6) where Table 7.5 indicates PIO rating improvements by two points in some cases and often HQR improvements too. The time-histories most clearly show the improvement due to anti-windup for the case of the *low-gain* pilot (II) where a clear reduction in pilot workload and oscillatory response can be observed (see Figure 7.13) when AW is present. It is thus not surprising that Pilot II records some of his best PIO/HQR ratings for AW compensations at this flight condition (FC6) and these ratings are substantially better than those with no AW.

Correspondence between time-domain data and the results given in Table 7.5 is less clear for the *high gain* pilot (I). Although Table 7.5 shows that this pilot preferred the response of the aircraft with AW (with ratings given being similar to Pilot II), it is less evident how this is manifested within the time-domain data. While some mild improvement in tracking, together with a reduction in rate-limiting may be observed in Figure 7.12, the improvement is not striking. However, it should be pointed out that the pilots may consciously or unconsciously adjust their "gain" and piloting technique as the task progresses. Indeed, close inspection of

Figure 7.12 reveals that the pilot stick command is zero for short periods, perhaps as the pilot removes himself from the loop to prevent oscillations building up (the pilot remarked on this during the flight).

Both pilots remarked that they felt that AW improved the predictability of the aircraft response, although mentioned that the aircraft also felt more "sluggish". On the basis of these flight tests, it is not clear yet how AW compensators affect sluggishness and how this can be avoided; an investigation into this aspect would be desirable, requiring further flight testing.

7.5 Conclusion

This chapter has presented results from a flight test at DLR Braunschweig which were conducted using the RLAW scheme developed earlier in the thesis. Pilot ratings and inspection of recorded time-domain data clearly show the nonlinear (rate saturated) performance improvement attainable with anti-windup compensation, particularly at high-speed, up-and-away flight conditions. An important characteristic, and one that was expected, is the reduction in the level of rate-limiting of the control signal when AW is present, reducing deviation from linear dynamics and probably increasing the life of the actuator.

However, it must be said that the difference between the AW-free and the AW-engaged responses were not as marked as initially expected; PIO tendency and performance degradation where not as high as in desktop simulation. This may be the cause of pilot model mismatch; the simulated pilot gains may have been chosen too large. It was observed that our *high gain* pilot, Pilot I, did not deliver the aggressive manoeuvres that were necessary to make the loss in tracking and stability properties clearly visible; in fact, the *low gain* pilot exploited more of the ATTAS capabilities, driving the system to more difficult regions, this being the case where AW proves to be beneficial. Another source of discrepancy, as highlighted by the pilots, is the fact that in-flight testing always tends to be more cautious as the pilot knows and *feels* that this is *real* and that any mistake may develop into severe, even deadly, consequences.

While there seemed to be broad correspondence between the choice of AW tuning parameters and the performance observed in-flight, the *precise* effects of changing these parameters could not be determined from the flight tests and further investigation is required to obtain clearer tuning guidelines.

Overall, the SAIFE tests were considered very encouraging and the results should aid the development of PIO-free aircraft. The results obtained from the SAIFE tests were well-received by the European Aerospace community, particularly the GARTEUR AG-15 action group and

several papers have resulted from this research: [9, 92]. Based on the success of these flight tests another set of tests is planned for August 2007 where a clearer picture of the tuning parameters' effects is sought and a more detailed investigation into the AW compensators' robustness will be carried out.

Chapter 8

Conclusions

The main goal of this thesis was to present a "novel" way of synthesising plant-order AW compensators and their application to the Category II PIO problem. The reader has been introduced to some of the most important AW schemes, "traditional" and "modern" compensation are considered, in order to set the "mood" for the work later developed. The AW compensation methods developed have addressed the following questions

(i) Is it possible to guarantee stability of the closed-loop saturated system?

(ii) Is it possible to enforce performance guarantees? How much does the system diverge from linear dynamics?

Traditional compensation schemes are deeply rooted in industry, where no stability or performance guarantees are given and design is usually fairly ad hoc. Many *modern* AW techniques have been successful at guaranteeing stability but have not been able to satisfactorily address performance. This thesis has attempted to improve on these stability results by proposing compensators that guarantee performance in an intuitive way and in a way which is of central interest to the practising control engineer. Thus, in a certain sense, this thesis has tried to blend the aspirations of traditional AW with the rigour of modern AW.

Throughout this thesis, the control input saturation problem has been addressed using full-order AW compensation and the Weston-Postlethwaite AW configuration. In early work [37, 36], the problem had been formulated and solved using LMI optimisation techniques where a clear performance index (the map from u_{lin} to y_d) was minimised. This procedure was used to design suboptimal compensators, i.e. static and low-order, as well as full-order compensators. The work in [110] was based on LMI methods however and, while useful, these have two distinct disadvantages: (i) their computational cost is high, and problematic for high-order plants; and

(ii) the role of some parameters is clouded by the optimisation process. The methods proposed in this thesis improve upon this by replacing the LMI optimisation with a Riccati equation, thus lowering the computational burden, and also providing a *family* of optimal compensators parametrised by the so-called "stability multiplier", giving more flexibility to the designer.

The main contributions of the thesis can thus be summarised as

- The development of Riccati-based AW synthesis techniques. As mentioned above, these lessen the computational burden and provide increased flexibility to the designer. These properties are thought to be useful in practice, particularly when the control engineer is faced with large, complex systems. The *robust* AW problem is naturally addressed by this method and an important link between the stability multiplier and the robustness of the overall system was uncovered. Thus, the robust anti-windup problem can be solved using the Riccati framework with little extra effort. This is important as we may capture the design trade-offs without adding any extra weighting matrices in more transparent intuitive manner. As an aside, it was also noted that an optimally robust AW compensator - the IMC compensator - appears as a special case of the results here described, which is in agreement with the literature.

- The development of Riccati-based AW synthesis techniques for systems with rate-limits. This problem is a natural extension of the magnitude limit problem but features several technical difficulties, notably lack of bounded realness, which complicate the problem. It was shown how the global anti-windup problem could be relaxed to a semi-global/local anti-windup problem when rate-constraints were present and a solution obtained using similar Riccati machinery to those developed for the magnitude problem. Due to a more complicated interaction of design parameters in the rate-saturation case, a tuning technique was then devised which enabled the designer to trade-off performance against the size of the region of attraction bestowed by the anti-windup compensator. In particular it was shown that the system's local $\mathcal{L}_2$ gain had to be traded-off against the size of an ellipsoidal estimate of the region of attraction.

- The application of Riccati-based techniques to a realistic Cat II PIO alleviation problem. The Riccati-based rate-limit anti-windup techniques were applied to a simulation of the ATTAS aircraft for which the actuator rate-limits where artificially degraded to make the aircraft PIO prone. Extensive nonlinear simulation showed that when the Riccati-based AW techniques were applied, the system was substantially less PIO prone than with no AW tested. Moreover, the presence of the AW compensators often prevented divergent

behaviour which would have occurred otherwise.

- The implementation and flight test of Riccati-based AW techniques on a real aircraft.

  The highlight of this thesis was the testing of the AW design techniques developed here in a real flight environment, where its performance was quantified by pilot ratings for both handling qualities and PIO tendency. It is thought that this is the *first in-flight assessment of a modern AW compensation scheme.* Flight tests were made possible thanks to the GARTEUR AG-15 group, and more specifically thanks to DLR and its Advanced Testing Technologies Aircraft System. The aim of this test was to prove that modern AW compensation schemes, more specifically the scheme proposed here, may deliver stability and performance enhancements in highly demanding environments, reducing the PIO tendencies of highly agile aircraft.

  The test was carried out by two test-pilots from the German air-force, making their comments and ratings reliable and valuable. The results demonstrated that PIO tendencies in aircraft can be substantially reduced by using AW compensation. The most dramatic improvements were observed for the flight conditions when the aircraft was most agile, auguring well for the use of such techniques in the aerospace industry. The tests were considered so successful that more are being planned for late 2007.

While the findings of the thesis were considered fairly successful, there remains more research to be conducted in AW compensation. Some particularly important avenues for future research are

- More robustness analysis of the AW compensators. Although attention to robust *stability* was given in Chapter 4, the treatment there effectively uncovered the robustness properties which the Riccati approach yielded "for free". Future research could concentrate on incorporating robust performance directly in the optimisation process, in the spirit of [61]

- Further flight testing of the AW compensators. Of particular interest is the robust performance of the compensators in different flight conditions. For the flight tests described, an AW compensator was designed for each different flight condition. A subsequent analysis revealed that the compensators had broadly the same frequency response but it would be interesting to discover how significant this was and whether a single compensator could function throughout the entire flight envelope or whether some form of scheduling was necessary. A potential problem with the AW compensators tested was that, as they were

full-order, they had rather large state dimension. In practice, something of much lower order would be preferred and research on how the order can be reduced while guaranteeing the AW compensator properties is required.

- Extension of the AW techniques to nonlinear systems. All the techniques developed here assumed that the system was linear apart from actuator magnitude and rate-limits. Although such a simplification is often a good engineering approximation, it is well known that some systems, such as highly agile aircraft have dynamics which are more nonlinear. An obvious avenue of future research is to try to extend these AW techniques to nonlinear systems using either linear parameter varying (LPV) techniques or state-dependent-Riccati equation (SDRE) techniques. An obvious difficulty with this extension is that the Weston-Postlethwaite scheme depends heavily upon the superposition principle which would not be valid in the nonlinear scenario.

In conclusion, the methods of AW compensation have developed greatly over the last two decades, progressing from ad hoc modifications to systematic design routines. This thesis has presented an AW scheme which is thought to make the anti-windup synthesis problem rigourous yet intuitive, making it useful for complex practical applications.

Appendix A

Proof of Theorem 4.1 for $D \neq 0$

Consider the formulation of the standard AW problem given in chapter 4, and assume $D \neq 0$. Using the same problem formulation of equation (4.11)

$$\boxed{L = \dot{x}'Px + x'P\dot{x} + y'y - \gamma^2 u'_{lin}u_{lin} + 2\tilde{u}'W(u - \tilde{u}) < 0} \tag{A.1}$$

where $u = u_{lin} - Fx$, and for the case of $D \neq 0$, $y = (C+DF)x + D\tilde{u}$. Using the same technique of completing squares in order to reduce the original equation, it is possible to pose a simple set of constraints that guarantee stability (L is negative definite) and a certain performance level. Substituting u and expanding equation (A.1)

$$L = \dot{x}'Px + x'P\dot{x} + y'y - 2\tilde{u}'WFx - 2\tilde{u}'W\tilde{u} - \gamma^2 u'_{lin}u_{lin} + 2\tilde{u}'Wu_{lin}$$

Cross terms in u_{lin} and $\tilde{u}$ are reduced in the same manner as in step one of the proof give for the case of strictly proper systems, i.e $D \neq 0$. This reduces the above equation to

$$L = \dot{x}'Px + x'P\dot{x} + y'y - 2\tilde{u}'WFx - \tilde{u}'(2W - \gamma^{-2}W^2)\tilde{u} - \|\gamma u_{lin} - \gamma^{-1}Wu_{lin}\|^2$$

Noting the quadratic term is negative definite, this implies

$$L \leq \dot{x}'Px + x'P\dot{x} + x'(C+DF)'(C+DF)x + 2x'(C+DF)'D\tilde{u} - 2\tilde{u}'WFx - \tilde{u}'Z\tilde{u}$$

where

$$\boxed{Z = 2W - \gamma^{-2}W^2 - D'D > 0} \tag{A.2}$$

As before Z must be positive definite in order to guarantee a well-posedness of the problem. We now proceed to substitute $\dot{x}$ (see equation 4.1) and expand (and group) as follows:

$$L \leq x'[A'P+PA+2PBF+(C+DF)'(C+DF)]x+2x'PB\tilde{u}+2x'(C+DF)'D\tilde{u}-2\tilde{u}'WFx-\tilde{u}'Z\tilde{u}$$

Terms involving $\tilde{u}$ and x, are grouped as follows:

$$\begin{aligned} -\tilde{u}'Z\tilde{u} + 2x'[C'D + F'(D'D - W) + PB]\tilde{u} = \\ -\|Z\tilde{u} - Z^{-1/2}[B'P + D'C + (D'D - W)'F]\|^2 \\ +x'[C'D + F'(D'D - W) + PB]Z^{-1}[D'C + (D'D - W)F + B'P]x \end{aligned}$$

This reduces our main inequality to

$$\begin{aligned} L \leq\ & x'\left(A'P + PA + 2PBF + (C + DF)'(C + DF) + \right. \\ & \left. [C'D + F'(D'D - W) + PB]Z^{-1}[D'C + (D'D - W)F + B'P]\right)x \end{aligned}$$

Expanding and grouping terms in F, it is possible to reduce even further our inequality and obtain a condition that allow us to guarantee that L is negative definite. We now have,

$$L \leq x'[A'P+PA+C'C+(PB+C'D)Z^{-1}(B'P+D'C)+F'HF+2(PB+C'D)(I+Z^{-1}D'D-Z^{-1}W)F]x$$

where the matrix H is defined as

$$H = (D'D - W)Z^{-1}(D'D - W) + D'D \tag{A.3}$$

We now reduce the terms containing F in order to find an expression for the matrix gain. The terms can be grouped as

$$\begin{aligned} F'HF + 2(PB + C'D)(I + Z^{-1}D'D - Z^{-1}W)F = \\ \|H^{1/2}F + H^{-1/2}(I + D'DZ^{-1} - WZ^{-1})(B'P + D'C)\| \\ -(PB + C'D)(I + Z^{-1}D'D - Z^{-1}W)H^{-1}(I + D'DZ^{-1} - WZ^{-1})(B'P + D'C) \end{aligned}$$

We can make our problem less mathematically exhausting by using the matrix inversion lemma, where

$$H^{-1} = \gamma^2 W^{-1}ZR^{-1}W^{-1}$$

and $R = \gamma^2 - D'D > 0$. It is easy to observe that $L \leq 0$ if the group of terms

$$\begin{aligned} & A'P + PA + C'C + (PB + C'D)[Z^{-1} - Z^{-1}(W - \gamma^{-2}W^2)H^{-1}(W - \gamma^{-2}W^2)Z^{-1}](B'P + D'C) \\ & +\|H^{1/2}F + H^{-1/2}(I + D'DZ^{-1} - WZ^{-1})(B'P + D'C)\| \leq 0 \end{aligned}$$

is guaranteed negative definite. After some algebraic manipulations, and assuming $D'D \neq 0$, it can be proved that we have stability if

$$\begin{aligned} L \leq\ & A'P + PA + C'C + (PB + C'D)R^{-1}(B'P + D'C) \\ & \|H^{1/2}F + H^{-1/2}(I + D'DZ^{-1} - WZ^{-1})(B'P + D'C)\|^2 \leq 0 \end{aligned} \tag{A.4}$$

A sufficient condition for this to be the case is then

i) $A'P + PA + C'C + (PB + C'D)R^{-1}(B'P + D'C) = 0$

ii) $\|H^{1/2}F + H^{-1/2}(I + D'DZ^{-1} - WZ^{-1})(B'P + D'C)\|^2 = 0$

Thus, negative definiteness of $L(.)$ can be guaranteed if the Riccati equation in (i) has a positive definite solution $P' = P > 0$ and the term F is chosen such that the expression (ii) holds. To complete the proof, we will reduce the remaining quadratic term to the conditions give in Theorem 4.1. First notice that the quadratic term can be made zero by virtue of the free parameter F. Equating this term to zero we obtain

$$\begin{aligned} F &= H^{-1}(W - \gamma^{-2}W^2)Z^{-1}((B'P + D'C) \\ &= \gamma^2 W^{-1}ZR^{-1}W^{-1}(W - \gamma^{-2}W^2)Z^{-1}(B'P + D'C) \\ F &= \gamma^2(W^{-1} - \gamma^{-2})R^{-1}(B'P + D'C) \end{aligned} \tag{A.5}$$

The previous equation shows how the matrix gain F is obtained by properly adjusting the free parameters in order to guarantee inequality (A.2). We now proceed to reduce equation (A.4) to obtain the conditions of theorem 4.1. Thus expanding equation (i) and grouping the terms in P yields

$$\boxed{(A + BR^{-1}D'C)'P + P(A + BR^{-1}D'C) + C'(I + DR^{-1}D')C + PBR^{-1}B'P \leq 0} \tag{A.6}$$

Therefore we an conclude that if the Riccati equation (A.6) has a solution for $P = P' > 0$, the there exists a full-order AW compensator that guarantees stability of the saturated closed-loop. The free parameters W and γ must be chosen as to guarantee inequality (A.2), but at the same time can be used obtain a family of stabilising compensators parametrised by W (shown in equation (A.5)); the designer has the freedom to choose the one that delivers the best performance for the specific application.

Appendix B

Proof of Estimate of Region of Attraction

As discussed in Chapter 5, a key objective of the AW problem is to maximise the size of the ellipsoid estimation of the region of attraction, which requires a bound on the size of the signal d entering the deadzone function. As the region of attraction is to be estimated, it is assumed that $d_{lin} \equiv 0$ and hence it is required that $|d| \preceq d_0$. Thus, we want to find the largest scalar, c_{max} such that

$$\max_{\tilde{x}} \tilde{x}' P \tilde{x} \leq c_{max} \quad \text{s.t. } |d| \preceq d_0 \tag{B.1}$$

As $d_{lin} \equiv 0$, then $d = -F\tilde{x}$ and it follows that

$$|F\tilde{x}| \preceq d_0 \quad \Leftrightarrow \quad -d_{0,i} \leq F_i \tilde{x} \leq d_{0,i} \quad \forall i \in \{1, \ldots, m\} \tag{B.2}$$

where F_i is the i^{th} row vector of the matrix F. As we are interested in the largest ellipsoid $\tilde{x}' P \tilde{x}$ (such that $|d| \preceq d_0$), our objective is to find the maximum values of AW states $\tilde{x}$ such that equation (B.2) is satisfied. For simplicity, and without any loss of generality, only the positive values will be used in the proof; as we are trying to maximise the size of a quadratic function of $\tilde{x}$, the sign of this signal is of no concern. In this way the maximum $\tilde{x}$ such the equality $F_i \tilde{x} = d_0$ holds is given by

$$\tilde{x} = F_i^{\dagger} d_{0,i} \tag{B.3}$$

where $\dagger$ denotes the *right* pseudo-inverse. Now define

$$\tilde{x}_{opt} := \min_i F_i^{\dagger} d_{0,i} \tag{B.4}$$

and also

$$\tilde{x}'_{opt} P \tilde{x}_{opt} = \min_i d_{0,i}^2 (F_i^{\dagger})' P (F_i^{\dagger}) =: c_{max} \tag{B.5}$$

Then it follows that for all $x \in \mathcal{E}$ where

$$\mathcal{E} := \left\{ \tilde{x} \in \mathbb{R}^{n+m} : \tilde{x}' P \tilde{x} \leq c_{max} \right\} \tag{B.6}$$

that $|d| \preceq d_0$ and, furthermore, that this is the largest ellipsoid in which this holds. Defining the diagonal matrix K as

$$K = -\left(\frac{(2-\epsilon)W^{-1}}{\epsilon^2} - \gamma^{-2} I \right) \tag{B.7}$$

it follows that F can be written as $F = KB'P$ and that $F_i = k_i B_i' P$ where k_i is the i^{th} diagonal element of K and B_i is the i^{th} column of the matrix B. Using this definition, the right pseudo inverse of F_i can be written as

$$F_i^{\dagger} = k_i^{-1} B_i (B_i' P B_i)^{-1} \tag{B.8}$$

The term $(B_i' P B_i)$ is always guaranteed nonsingular as B_i has full column rank and P is positive definite. The expresion for the ellipsoid c_{max} in equation (B.6) can thus be written as

$$c_{max} = \min_i d_{0,i}^2 (F_i^{\dagger})' P (F_i^{\dagger}) = \min_i (\frac{d_{0,i}}{k_i})^2 (B_i' P B_i)^{-1} B_i' P B_i (B_i' P B_i)^{-1} \tag{B.9}$$

As the term $B_i' P B_i$ is a scalar, it is easy to observe that

$$c_{max} = \min_i \frac{d_{0,i}^2}{k_i^2 B_i' P B_i} \tag{B.10}$$

After some algebraic manipulations, the expresion given in equation (B.10) can be reduced to that given in Theorem 5.1, thus completing the proof.

References

[1] Anon. Flying qualities of piloted vehicles. Technical Report MIL-STD-1797, U.S. Military Standard, March 1987.

[2] Anon. Why the grippen crashed. *Aerospace America*, page 11, 1994.

[3] K.J. Astrom and L. Rundqwist. Integrator windup and how to avoid it. *Proc. American Control Conf.*, 2:1693–1698, 1989.

[4] C. Barbu, R. Reginatto, A.R. Teel, and L. Zaccarian. Anti-windup design for manual flight control. *Proc. American Control Conference*, pages 3186–3190, 1999.

[5] D.P. Bohn, C. Atherton. An analysis package comparing PID anti-windup strategies. *IEEE Control Systems*, 15(2):34–40, 1995.

[6] C. Bolkcom. V-22 osprey tilt-rotor aircraft. *CRS Report for Congress*, page Code RL31384, 2005.

[7] S. Boyd, L. El Ghaoui, E. Feron, and V. Balakrishnan. *Linear Matrix Inequalities in System and Control Theory.* siam, 1994.

[8] R. Bracewell. *The Fourier Transform and Its Applications.* McGraw-Hill, 1965.

[9] O. Brieger, M. Kerr, D. Leissling, I. Postlethwaite, J. Sofrony, and M.C. Turner. Flight testing of a rate-compensation scheme on the ATTAS aircraft. *Proc. DGLR Conference*, 2006.

[10] E. Camacho and C. Bordons. *Model Predictive Control.* Springer-Verlag, 2004.

[11] Y.Y. Cao and Z. Lin. An anti-windup design for polytopic systems by a parameter-dependent lyapunov function approach. *International Journal of Systems and Science*, 37(2):129–139, 2006.

[12] Y.Y. Cao, Z. Lin, and D.G. Ward. An anti-windup approach to enlarging the domain of attraction for linear systems subject to input sauration. *IEEE Trans. Automatic Cotrol*, 47(1):140–145, 2002.

[13] T. Chen and B. Francis. *Optimal Sampled-Data Control Systems.* Springer-Verlag, London, 1995.

[14] National Research Council. *Aviation Safety And Pilot Control: Understanding and Preventing Unfavorable Pilot-Vehicle Interactions.* NATIONAL ACADEMY PRESS, Washington, D.C., 1997.

[15] S. Crawshaw. Global and local analysis of coprime-factor based anti-windup for stable and unstable plants. *Proc. European Control Conference*, 2003.

[16] S. Crawshaw and G. Vinnicombe. Anti-windup synthesis for guaranteed $\mathcal{L}_2$ performance. *Proc. IEEE Conf. on Decision and Control*, 2000.

[17] J.A. De Dona, S.O.R. Moheimani, and G.C. Goodwin. Robust combined PLC/LHG controller with allowed over-saturation of the input signal. *Proc. American Control Conf.*, pages 750–751, 2000.

[18] M.A. Dornheim. Report pinpoints factors leading to YF-22 crash. *Aviation Week and Space Technology*, 137(19):53–54, 1992.

[19] J.C. Doyle, D.F. Enns, and R.S. Smith. Control of plants with input saturation nonlinearities. *Proc. American Control Conf.*, pages 2147–2152, 1987.

[20] H. Duda. Prediction of pilot-int-the-loop osciallations due to rate saturation. *Journal of Guidance, Control and Dynamics*, 20(3):581–587, 1997.

[21] C. Edwards and I. Postlethwaite. Anti-windup and bumpless transfer schemes. *Automatica*, 34(2):199–210, 1998.

[22] Johnson E.N. and Pritchett A.R. Generic pilot and flight control model for use in simulation studies. *AIAA Modeling and Simulation Technologies Conference and Exhibit*, 2002.

[23] A.T. Fuller. In-the-large stability of relay and saturating control systems with linear controllers. *International Journal of Control*, 10(4):457–480, 1969.

[24] P. Gahinet and P. Apkarian. A linear matrix inequality approach to $\mathcal{H}_\infty$ control. *ijrnc*, 4:421–448, 1994.

[25] P. Gahinet, A. Nemirovski, A.J. Laub, and M. Chilali. *LMI Control Toolbox.* The MathWorks Inc., 1995.

[26] S. Galeani, S. Nicosa, A.R. Teel, and L. Zaccarian. Output feedback compensators for weakened anti-windup of additively perturbed systems. *Proc. of the IFAC World Congress*, 2005.

[27] G. Garcia, S. Tarbouriech, R. Suarez, and J. Alvarez-Ramirez. Nonlinear bounded control for norm-bounded uncertain systems. *IEEE Transactions on Automatic Control*, 44(8):1254–1258, 1999.

[28] S.L. Gatley, M.C. Turner, I. Postlethwaite, and A. Kumar. A comparison of rate-limit compensation schemes for pilot-induced-oscillation aviodance. *Aerospace Science and Technology*, 10:37–47, 2006.

[29] G.P. Gilbreath. Prediction of pilot-induced-oscillations due to actuator rate-limiting using the open-loop-onset-criterion. Master's thesis, US Airforce Institute of Technology, 2001.

[30] A. H. Glattfelder and W. Schaufelberger. Stability of discrete override and cascade-limiter single-loop control systems. *IEEE Transactions on Automatic Control*, 33(6):532–540, 1988.

[31] A.H. Glattfelder and W. Schaufelberger. *Control Systems with Input and Output Constraints.* Springer-Verlag, London, 2003.

[32] J.M. Gomes da Silva Jr., S. Tarbouriech, and G. Garcia. Local stabilisation of linear systems under amplitude and rate saturating actuators. *IEEE Transactions on Automatic Control*, 48(5):842–847, 2003.

[33] J.M. Gomes da Silva Jr., S. Tarbouriech, and R. Reginatto. Analysis of regions of stability for linear systems with saturating inputs through an anti-windup scheme. *Proc. IEEE Conference on Control Applications*, 2002.

[34] M. Green and D.J.N. Limebeer. *Linear Robust Control.* Prentice Hall, New Jersey, 1996.

[35] G. Grimm, J. Hatfield, I. Postlethwaite, A.R. Teel, M.C. Turner, and L. Zaccarian. Anti-windup for stable linear systems with input saturation: an LMI based synthesis. *IEEE Transactions on Automatic Control*, 48(9):1509–1525, 2003.

[36] G. Grimm, I. Postlethwaite, A.R. Teel, M.C. Turner, and L. Zaccarian. Case studies using linear matrix inequalities for optimal anti-windup compensator synthesis. *Proc. European Control Conf.*, 2001.

[37] G. Grimm, I. Postlethwaite, A.R. Teel, M.C. Turner, and L. Zaccarian. Linear matrix inequalities for full and reduced order anti-windup synthesis. *Proc. American Control Conf.*, 2001.

[38] G. Grimm, A.R. Teel, and L. Zaccarian. The l_2 anti-windup problem for discrete-time linear systems: definition and solutions. *Proc. American Control Conference*, 2003.

[39] P. Gutman and P. Hagander. A new design of constrained controllers for linear systems. *IEEE Transactions on Automatic Control*, 30:22–33, 1985.

[40] R. Hanus, M. Kinnaert, and J. L. Henrotte. Conditioning technique, a general antiwindup and bumpless transfer method. *Automatica*, 23:729–739, 1987.

[41] G. Herrmann, M.C. Turner, and I. Postlethwaite. Pratical implementation of a novel anti-windup scheme in a hdd-dual-stage servo-system. *IEEE/ASME Transactions on Mechatronics*, 9(3):580–592, 2004.

[42] G. Herrmann, M.C. Turner, I. Postlethwaite, and G. Guo. Application of a novel anti-windup scheme to a hdd-dual-stage actuator. *Proc. American Control Conference*, 2003.

[43] H. Hindi and S. Boyd. Analysis of linear systems with saturation using convex optimization. In *37th IEEE Conference on Decision and Control*, pages 903–908, Tampa, Florida, USA, 1998.

[44] G. Hovmark and G. Duus. Experimental evaluation of phase compensating rate limiters in an aircraft's lateral flight control system. Technical Report TP-120-04, GARTEUR, August 2000.

[45] T. Hu, A.R. Teel, and L. Zaccarian. Regional anti-windup compensation for linear systems with input saturation. *In American Control Conference, Portland (OR), USA*, pages 3397–3402, 2005.

[46] P. Kapasouris, M. Athans, and G. Stein. Design of feedback control systems for stable plants with saturating actuators. *Proc. IEEE Conf. on Decision and Control*, 1988.

[47] N. Kapoor, A.R. Teel, and P. Daoutidis. An anti-windup design for linear systems with input saturation. *Automatica*, 34(5):559–574, 1998.

[48] H.K. Khalil. *Nonlinear Systems.* Prentice Hall, New Jersey, 1996.

[49] D. H. Klyde, D.T. McRuer, and T.T. Myers. Unified pilot-inducedoscillation theory, volume i: Pio analysis with linear and nonlinear effective vehicle characteristics, including rate limiting. Technical Report Contract F33615-94-C-3613, Flight Dynamics Directorate, Wright Laboratory, Wright-PattersonAFB OH, December 1995.

[50] D.H. Klyde, D.T. McRuer, and T.T. Myers. Pilot-induced oscillation analysis and prediction with actuator rate limiting. *Journal of Guidance, Control and Dynamics*, 20(1):81–89, 1997.

[51] D.H. Klyde, D.M. Smith, and C. Harris. Describing functions for higher order actuator models with rate limiting. *AIAA Atmospheric Flight Mechanics Conference and Exhibit*, 2002.

[52] M.V. Kothare, P.J. Campo, M. Morari, and C.N. Nett. A unified framework for the study of anti-windup designs. *Automatica*, 30(12):1869–1883, 1994.

[53] Foringer L.A. and Leggett D.B. An analysis of the time-domain neal-smith criterion. *AIAA Atmospheric Flight Mechanics Conference and Exhibit*, pages 154–162, 1998.

[54] P. Lancaster and M. Tismenesky. *The theory of matrices.* Ac. Press, Orlando, 2nd Ed., 1985.

[55] Z. Lin. Semi-global stabilisation of linear systems with position and rate-limited actuators. *Systems and Control letters*, 30:1–11, 1997.

[56] Z. Lin, R. Mantri, and A. Saberi. Semi-global output regulation for linear systems subject to input saturation - a low and high gain design. *Control Theory and Advanced Technology*, 10(4):2209–2232, 1998.

[57] Z. Lin and A. Saberi. A semi-global low and high gain design technique for linear systems with input saturation - Stabilisation and Disturbance rejection. *International Journal of Robust and Nonlinear Control*, 5:381–398, 1995.

[58] J.C. Lozier. A steady-state approach to the theory of saturable servo systems. *IRE Transactions on Automatic Control*, 1:19–39, 1956.

[59] P. March and M.C. Turner. Anti-windup compensator designs for permanent magnet synchronous motor speed regulation. In *Proc. of the IEEE International Electric Machines and Drives Conference*, Antalya, Turkey, 2007.

[60] V.R. Marcopoli and S.M. Phillips. Analysis and synthesis tools for a class of actuator-limited multivariable control systems: a linear matrix inequality approach. *International Journal of Robust and Nonlinear Control*, 6(9-10):1045–1063, 1996.

[61] A. Marcos, M.C. Turner, D.G. Bates, and I. Postlethwaite. Robustification of static and low-order anti-windup designs. *IFAC Symposium on Robust Controller Design*, 2006.

[62] P. Mhaskar, N. El-Farra, and P. Christofides. Stabilization of nonlinear systems with state and control constraints using lyapunov-based predictive control. *System and Control Letters, in press*, 2006.

[63] D.G. Mitchell and D.H. Klyde. Investigating the role of rate limiting in pilot-induced oscillations. *JOURNAL OF GUIDANCE, CONTROL, AND DYNAMICS*, 27(5), 2004.

[64] D.G. Mitchell and D.H. Klyde. Recommended practices for exposing pilot-induced oscillations or tendencies in the development process. *USAF Development Test and Evaluation Summit*, 2004.

[65] S. Miyamoto and G. Vinnicombe. Robust control of plants with saturation nonlinearity based on comprime factor representations. *Proc. IEEE Conf. on Decision and Control*, pages 2838–2840, 1996.

[66] E.F. Mulder and M.V. Kothare. Synthesis of stabilising anti-windup controllers using piecewise quadratic Lyapunov functions. *Proc. American Control Conf.*, pages 3239–3243, 2000.

[67] E.F. Mulder, M.V. Kothare, and M. Morari. Multivariable anti-windup controller synthesis using linear matrix inequalities. *Automatica*, 37(9):1407–1416, 2001.

[68] M. Mulder, W.J. Kaljouw, and M.M. van Paassen. Parameterized multi-loop model of pilots use of central and peripheral visual motion cues. *AIAA Modeling and Simulation Technologies Conference and Exhibit*, 2005.

[69] T. Nguyen and F. Jabbari. Disturbance attenuation for systems with input saturation: an LMI approach. *IEEE Trans. Automatic Control*, 44(4):852–857, 1999.

[70] Alan V. Oppenheim and Alan S. Willsky. *Signals and Systems.* Prentice Hall, New Jersey, 1996.

[71] Hippe P. and Wurmthaler Ch. Systematic closed loop design in the presence of input saturation. *Automatica*, 35:689–695, 1999.

[72] C. Pittet, S. Tarbouriech, and C. Burgat. Stability regions for linear systems with saturating control via Circle and Popov criteria. *Proc. IEEE Conference on Decision and Control*, 5:4518–4523, 1997.

[73] I. Postlethwaite, M.C. Turner, and E. Prempain. An $\mathcal{H}^\infty$ approach to rate-limit compensation for pilot-induced-oscillation avoidance: concept, demonstration and comparison (preliminary version). *GARTEUR technical report*, TP-120-06, 2001.

[74] F. Potre, R. Sheng, and N. Brixius. SDPHA: A code for semidefinite programming. *http://www.math.uiowa.edu/ rsheng/SDPHA/sdpha.html*, 1997.

[75] I. Queinnec, S. Tarbouriech, and G. Garcia. Anti-windup design for aircraft flight control. *IEEE Conference on Control Applications*, 2006.

[76] Hanus R. The conditioned control: a new technique for preventing windup nuisances. *Proceedings of the International Federation for Information Processing - Automation for Safety in Shipping and Offshore Petroleum Operation*, 21(1):221–224, 1980.

[77] Hanus R. A new technique for preventing control windup. *Automatica*, 21(1):15–20, 1980.

[78] A.A. Rodriguez and J. R. Cloutier. Control of a bank-to-turn missile with saturating actuators. *Proc. American Control Conference*, 1994.

[79] B.G. Romanchuk. Some comments on anti-windup synthesis using LMI's. *International Journal of Robust and Nonlinear Control*, 9(10):717–734, 1999.

[80] W. Rudin. *Functional analysis.* McGraw-Hill, 1991.

[81] L. Rundquist and K. Stahl-Gunnarsson. Phase compensation of rate-limiters in unstable aircraft. *Proc. IEEE Conference on Control Applications*, 1996.

[82] L. Rundqwist and R. Hillgren. Phase compensation of rate limiters in jas 39 gripen. *AIAA-96-3368-CP*, 1996.

[83] A. Saberi, Z. Lin, and A.R. Teel. Control of linear systems with saturating actuators. *IEEE Trans. on Automatic Control*, 41(3):368–378, 1996.

[84] M. Saeki and N. Wada. Synthesis of a static anti-windup compensator via linear matrix inequalities. *International Journal of Robust and Nonlinear Control*, 12:927–953, 2002.

[85] M.F. Shafer, R.E. Smith, J. F. Stewart, and R.E. Bailey. Flight test experience with pilot-induced oscillation suppression filters. Technical report, NASA, January 1984.

[86] G. Shi, A. Saberi, and A.A. Stoorvogel. On the $\mathcal{L}_p$ (l_p) stablisation of open-loop neutrally stable linear plants with input subject to amplitude saturation. *International Journal of Robust and Nonlinear Control*, 13:735–754, 2003.

[87] S. Skogestad and I. Postlethwaite. *Multivariable Feedback Control - Analysis and Design.* Wiley, Chichester, 2005.

[88] S. Skogstad and I. Postlethwaite. *Multivariable feedback control: analysis and design.* Wiley, Chichester, England, 2nd edition, 2006.

[89] J. Sofrony, M.C. Turner, and I. Postlethwaite. Anti-windup synthesis for systems with rate-limits: a Riccati equation approach. *Proc. SICE Annual Conference*, 2005.

[90] J. Sofrony, M.C. Turner, and I. Postlethwaite. Anti-windup synthesis using Riccati equations. *Proc. IFAC World Congress*, 2005.

[91] J. Sofrony, M.C. Turner, and I. Postlethwaite. Anti-windup synthesis using Riccati equations. *International Journal of Control*, 80(1):112–128, 2007.

[92] J. Sofrony, M.C. Turner, I. Postlethwaite, O.M. Brieger, and D. Leissling. Anti-windup synthesis for PIO aviodance in an experimental aircraft. *IEEE Conference on Decision and Control*, 2006.

[93] M. Soroush, N. Mehranbod, and S. Mehdi-Alaie. Directionality in input-constrained systems: its definition and optimal compensation. *Proc. American Control Conference*, pages 2002–2006, 1999.

[94] G. Stein. Respect the unstable. *IEEE Control Systems Magazine*, pages 12–25, 2003.

[95] A.A. Stoorvogel and A. Saberi. Output regulation of linear plants with actuators subject to amplitude and rate constraints. *International Journal of Robust and Nonlinear Control*, 9(10):631–657, 1999.

[96] R. Suarez, J. Alvaerz-Ramirez, and J. Solis-Daun. Linear systems with bounded inputs: global stabilisation with eigenvalue placement. *International Journal of Robust and Nonlinear Control*, 7:835–845, 1997.

[97] H.J. Sussmann, E.D. Sontag, and Y. Yang. A general result on the stabilisation of linear systems using bounded controls. *IEEE Transactions on Automatic Control*, 39(12):2411–2425, 1994.

[98] Wilmes T. and Duda H. Investigation of electronic filters to prevent aircraft-pilot-coupling. Technical Report ISBN 111-98/29, Institut fur Flugmechanik, Braunschweig, November 1998.

[99] S. Tarbouriech and G. Garcia. *Control of Uncertain Systems with Bounded Inputs.* Springer-Verlag, London, 1997.

[100] S. Tarbouriech, G. Garcia, and A.H. Glattfelder. *Advanced Strategies in Control Systems with input and Output Constraints.* Springer-Verlag, London, 2006.

[101] S. Tarbouriech, J.M. Gomes da Silva Jr., and G. Garcia. Delay-dependent anti-windup strategy for linear systems with saturating inputs and delayed outputs. *International Journal of Robust and Nonlinear Control*, 14(7):665–82, 2004.

[102] S. Tarbouriech, I. Queinnec, and G. Garcia. Stability region enlargement through anti-windup strategy for linear systems with dynamics restricted actuator. *International Journal of Systems Science*, 37(2):79–90, 2006.

[103] A.R. Teel. A nonlinear small gain theorem for the analysis of control systems with saturation. *IEEE Transactions on Automatic Control*, 41(9):1256–1270, 1996.

[104] A.R. Teel. Anti-windup for exponentially unstable linear systems. *international Journal of Robust Nonlinear Control*, pages 701–716, 1999.

[105] A.R. Teel and N. Kapoor. The $\mathcal{L}_2$ anti-windup problem: Its definition and solution. *Proc. European Cont. Conf.*, 1997.

[106] M.C. Turner, G. Herrmann, and I. Postlethwaite. Discrete-time anti-windup: Part 1 - stability and performance. *Proc. European Control Conference*, 2003.

[107] M.C. Turner, G. Herrmann, and I. Postlethwaite. Accounting for robustness in anti-windup synthesis. *Proc. American Control Conference*, 2004.

[108] M.C. Turner, G. Herrmann, and I. Postlethwaite. Improving robustness in anti-windup synthesis. *IEEE Transactions on Automatic Control, to appear*, 2007.

[109] M.C. Turner and I. Postlethwaite. Guaranteed stability regions of linear systems subject to actuator saturation using the low-and-high gain technique. *International Journal of Control*, 74(14):1425–1434, 2001.

[110] M.C. Turner and I. Postlethwaite. A new perspective on static and low order anti-windup synthesis. *International Journal of Control*, 77(1):27–44, 2004.

[111] M.C. Turner, I. Postlethwaite, and D.J. Walker. Nonlinear tracking control for multivariable constrained input linear systems. *International Journal of Control*, 73(12):1160–1172, 2000.

[112] F. Tyan and D.S. Bernstein. Anti-windup compensator synthesis for systems with saturating actuators. *International Journal of Robust and Nonlinear Control*, 5(5):521–537, 1995.

[113] E. Villota, M. Kerr, and S. Jayasuriah. A study of configurations for anti-windup control of uncertain systems. *IEEE Conference on Decision and Control*, 2006.

[114] N. Wada and M. Saeki. Design of a static anti-windup compensator which guarantees robust stability. *Transactions of the Institute of Systems, Control and Instrumentation Enigneers*, 12(11):664–670, 1999.

[115] K.S. Walgama and J. Sternby. Conditioning technique for multiinput multioutput processes with input saturation. *IEE Proceedings D*, 140(4):231–241, 1993.

[116] P.F. Weston and I Postlethwaite. Analysis and design of linear conditioning schemes for systems containing saturating actuators. *IFAC Nonlinear Control System Design Symposium*, 1998.

[117] P.F. Weston and I Postlethwaite. Analysis and design of linear conditioning schemes for systems with nonlinear actuators. *Internal Report, Dept. of Engineering, Leicester Univ.*, 98-6, 1998.

[118] P.F. Weston and I Postlethwaite. Linear conditioning for systems containing saturating actuators. *Automatica*, 36(9):1347–1354, 2000.

[119] J.B. Witte. An investigation relating longitudinal pilot-induced oscillation tendency rating to describing function predictions for rate-limited actuators. Master's thesis, US Airforce Institute of Technology, 2004.

[120] F. Wu and M. Soto. Extended anti-windup control schemes for LTI and LFT systems with actuator saturations. *International Journal of Robust and Nonlinear Control*, 14(15):1255–1281, 2004.

[121] J.-S. Yee, J.L. Wang, and Sundararajan. Robust sampled data $\mathcal{H}^\infty$ flight controller design for high α stability-axis roll manoeuver. *Control Enigneering Practice*, 8:735–747, 2001.

[122] L. Zaccarian and A.R. Teel. A common framework for anti-windup, bumpless transfer and reliable designs. *Automatica*, 38:1735–1744, 2002.

[123] Y. Zeyada, R.A. Hess, and W. Siwakosit. Analysis of aircraft handling qualities and pilot-induced oscillation tendencies with actuator saturation. *AIAA Atmospheric Flight Mechanics Conference and Exhibit*, pages 401–414, 1998.

[124] A. Zheng and M. Morari. Anti-windup using internal model control. *Interntional Journal of Control*, 1994.